MDI-2

T. Tauchi, KEK

10th International Accelerator School for Linear Colliders,
December 8-19, 2016, Mt.Fuji, Japan

1. Introduction

Characteristics of e^+e^- collisions

The total energy is used in an elementary process.

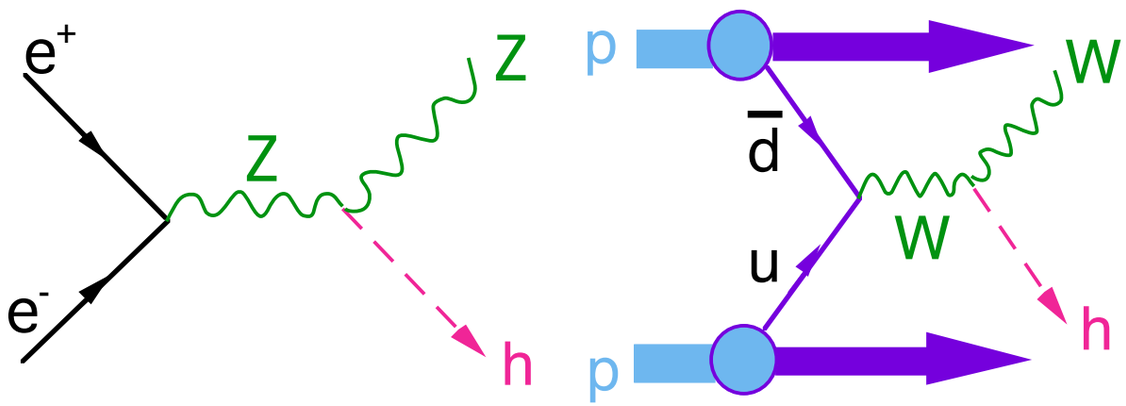

e.g. Higgs production at LC LHC

(dominant process is gg→h)

Their cleanness are certainly seen in simulations.

(1) Clear identification of the final state

(2) Precision measurements

Caveat : There could be “un-expected backgrounds” at Linear colliders for frontier machines as well as experiments.

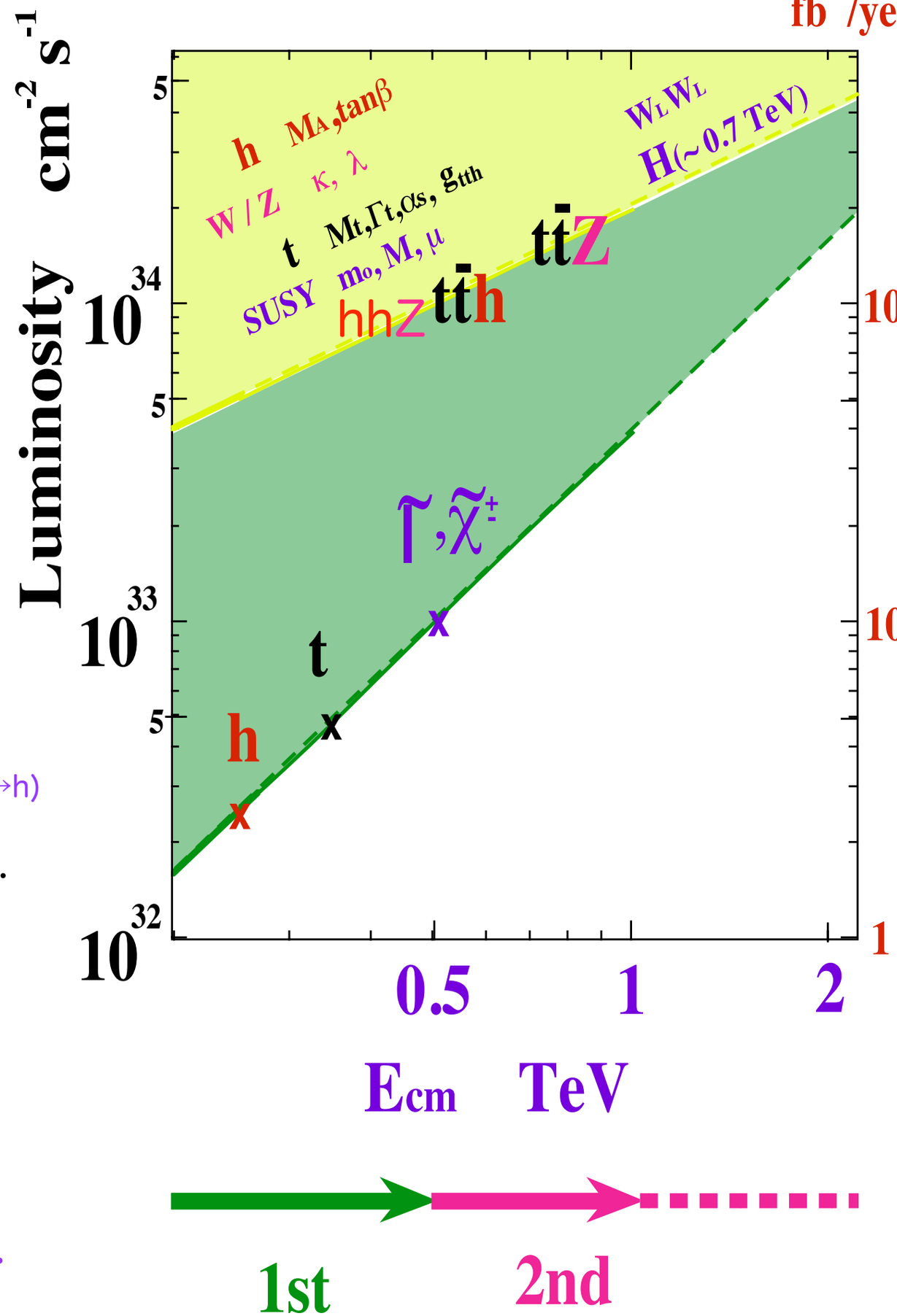

M.Lindner, ZPC31,295(1986)

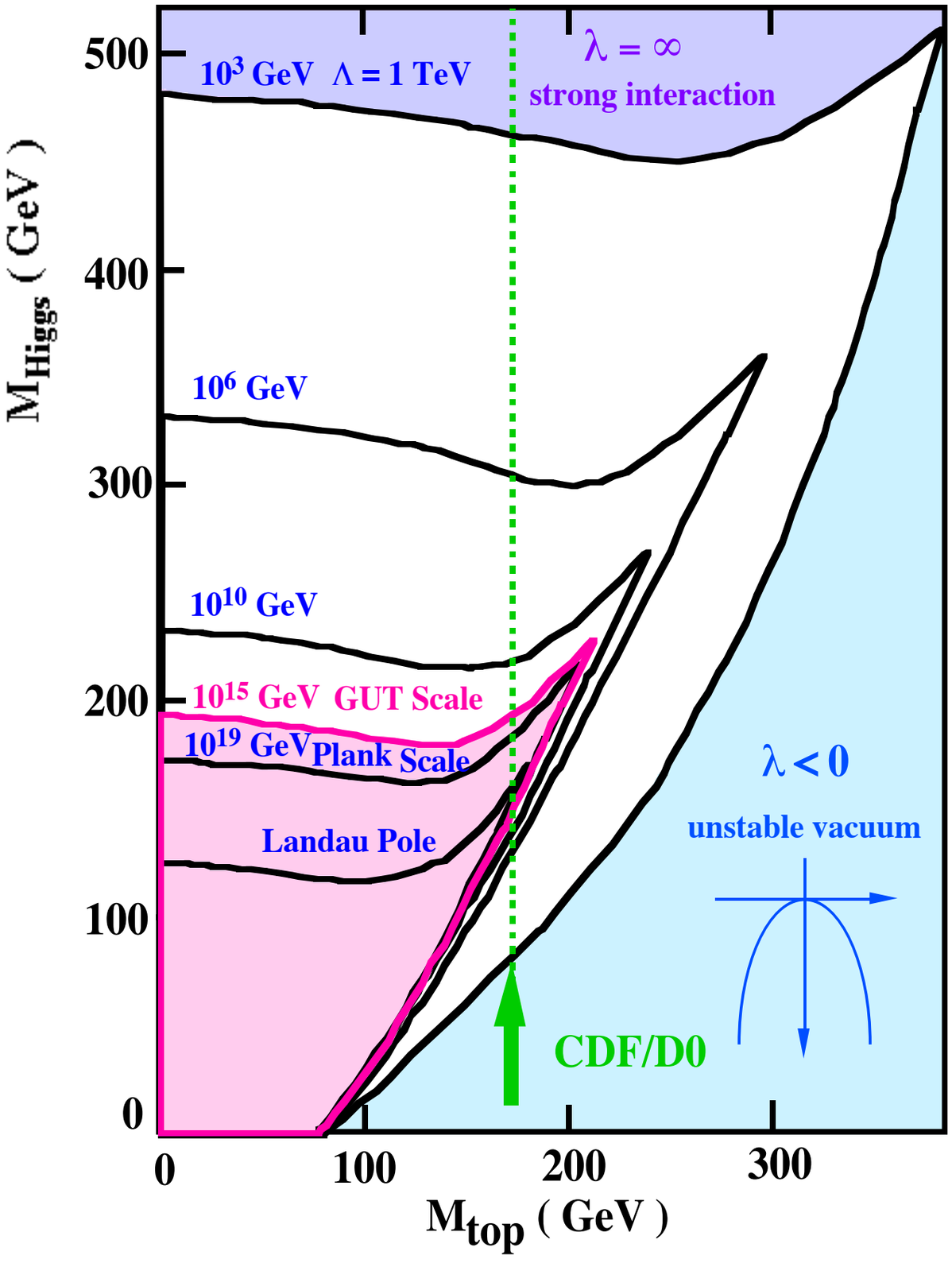

Upper Bound of Lightest SUSY-Higgs Mass

ref. T.Moroi, Y.Okada, Physics Letters B**295**(1992)73-78

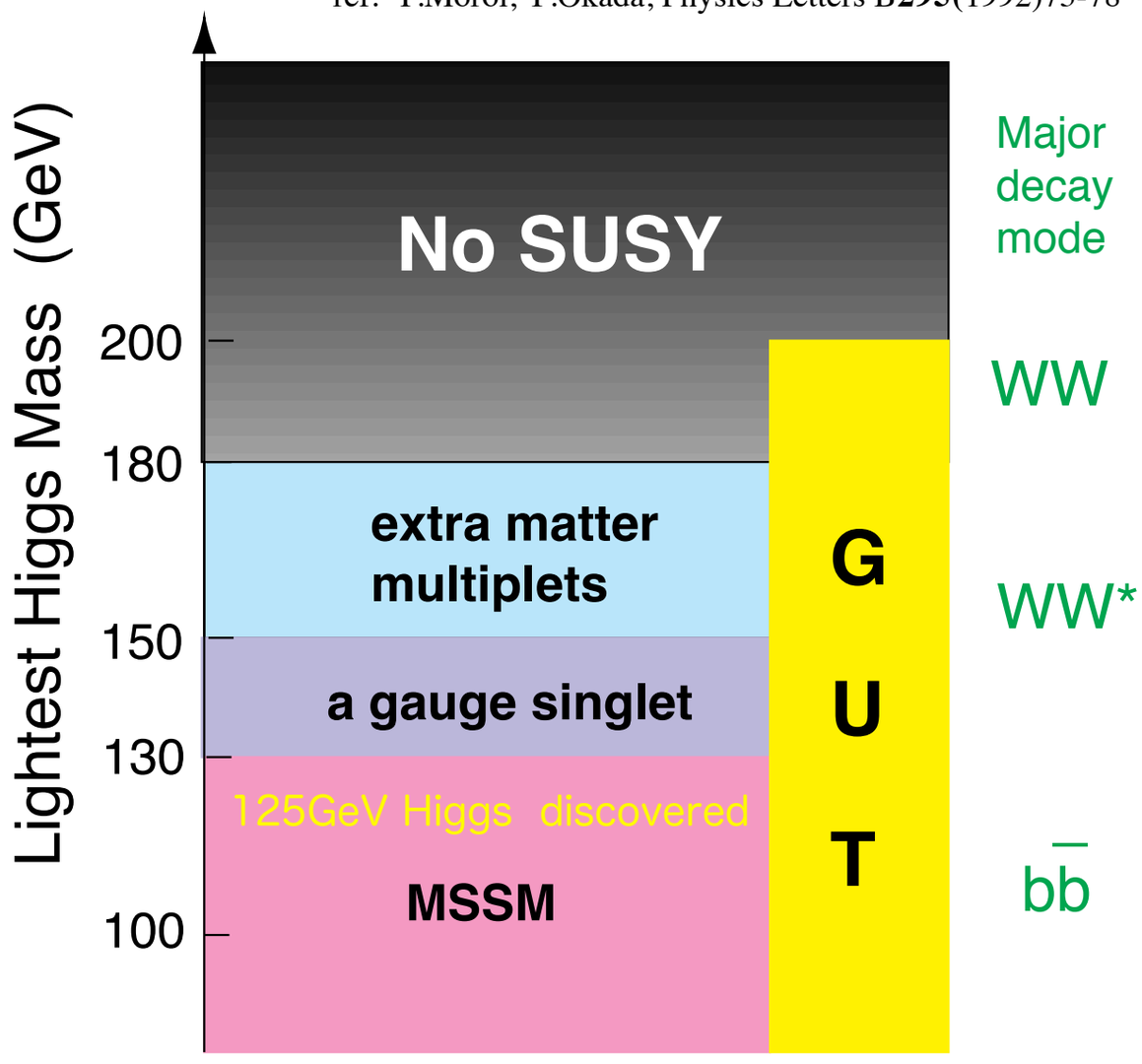

M_{top} = 175 GeV

ICHEP2012 : m_t=173.18±0.94GeV by CDF,D0

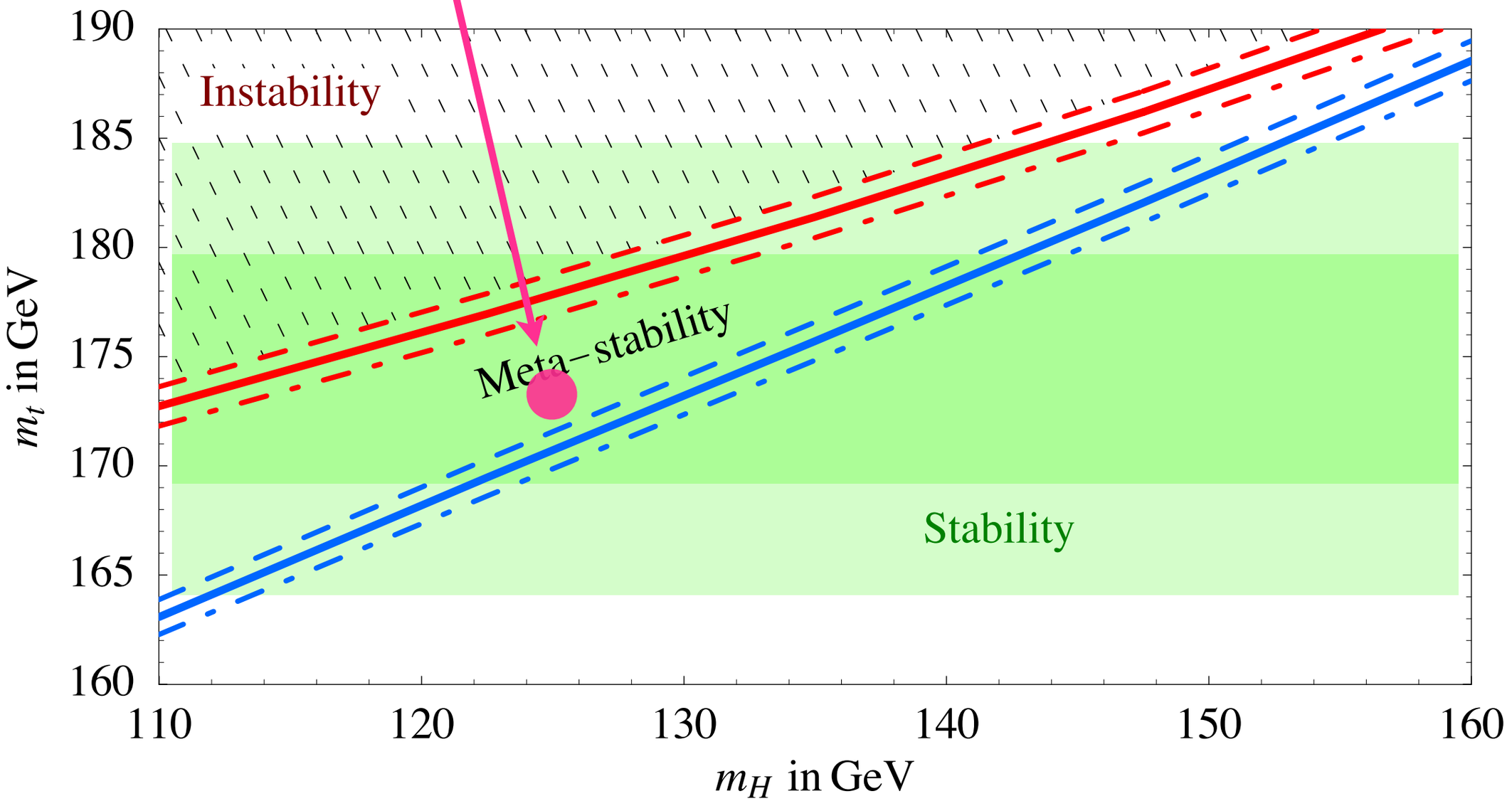

Figure 4: *Metastability region of the Standard Model vacuum in the* (m_H, m_t) *plane, for* $\alpha_s(m_Z) = 0.118$ *(solid curves). Dashed and dot-dashed curves are obtained for* $\alpha_s(m_Z) = 0.118 \pm 0.002$. *The shaded area indicates the experimental range for* m_t. *Sub-leading effects could shift the bounds by* ± 2 GeV *in* m_t.

G. Isidori, G.Ridolfi and A.Strumia, On the metastability of the Standard Model vacuum, hep-ph/0104016

R.B. Palmer, "Prospects for high energy e^+e^- linear colliders", Annu. Rev. Nucl. Part. Sci. 1990. 40: 529-92

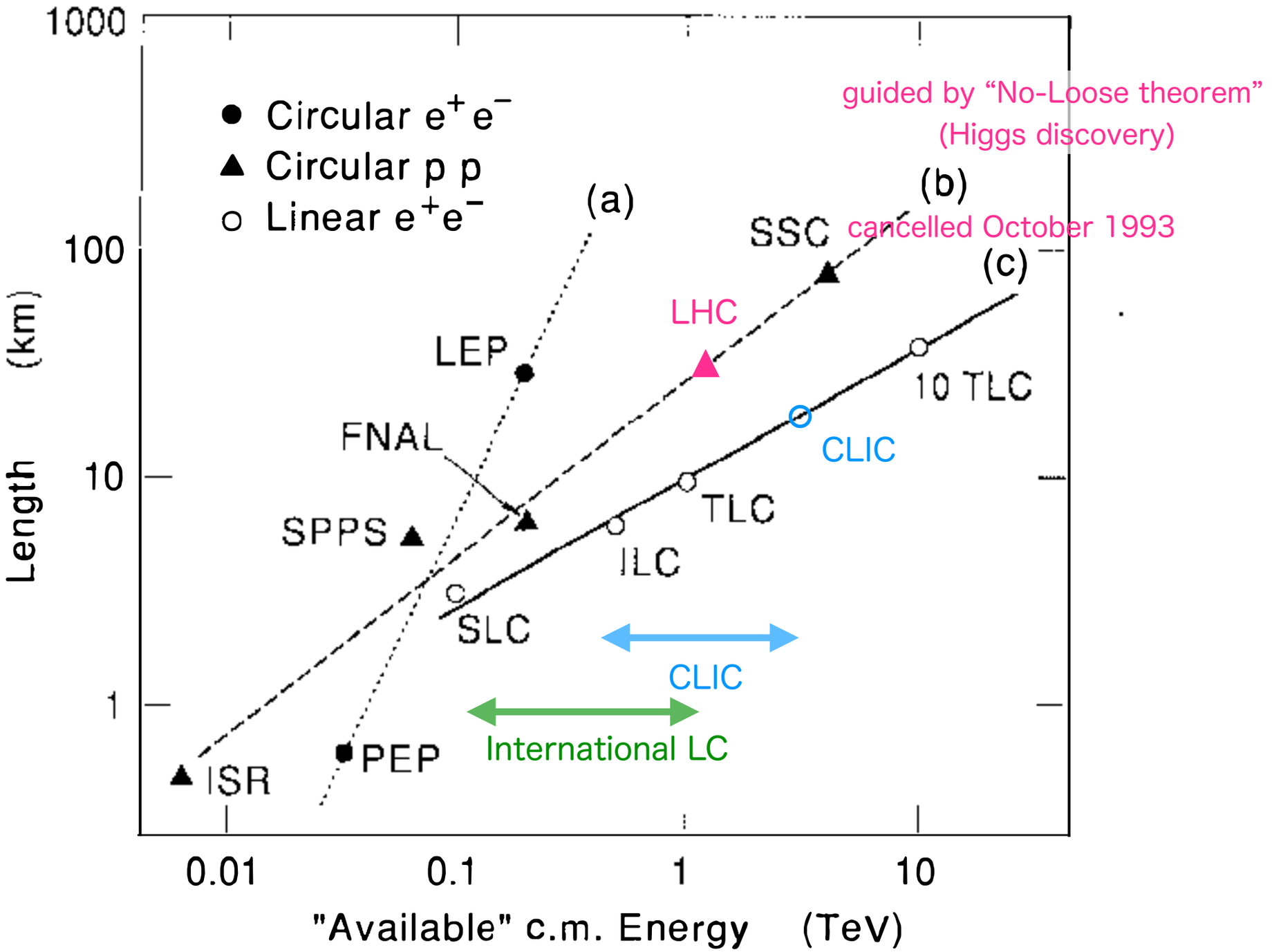

Figure 2 The “available” center-of-mass energy of various colliders, plotted against the circumference or total length of each machine. The available energy for proton or antiproton machines is taken to be one tenth of the total energy. For (*a*) circular electron-positron machines; (*b*) circular proton or antiproton machines; and (*c*) linear electron-positron machines.

ILC

as an example

International Linear Collider(ILC)

31km long Linear accelerator based on the SC-RF

Aug. 2004　Choice of the COLD technology (ICFA)

Mar. 2005　ILC GDE (Global Design Effort) organized

Barry Barish is the GDE director

Mar. 2006　BCD (Baseline Configuration Document)

Aug. 2007　RDR(Reference Design Report) completed

with the cost estimations, R&D test facilities

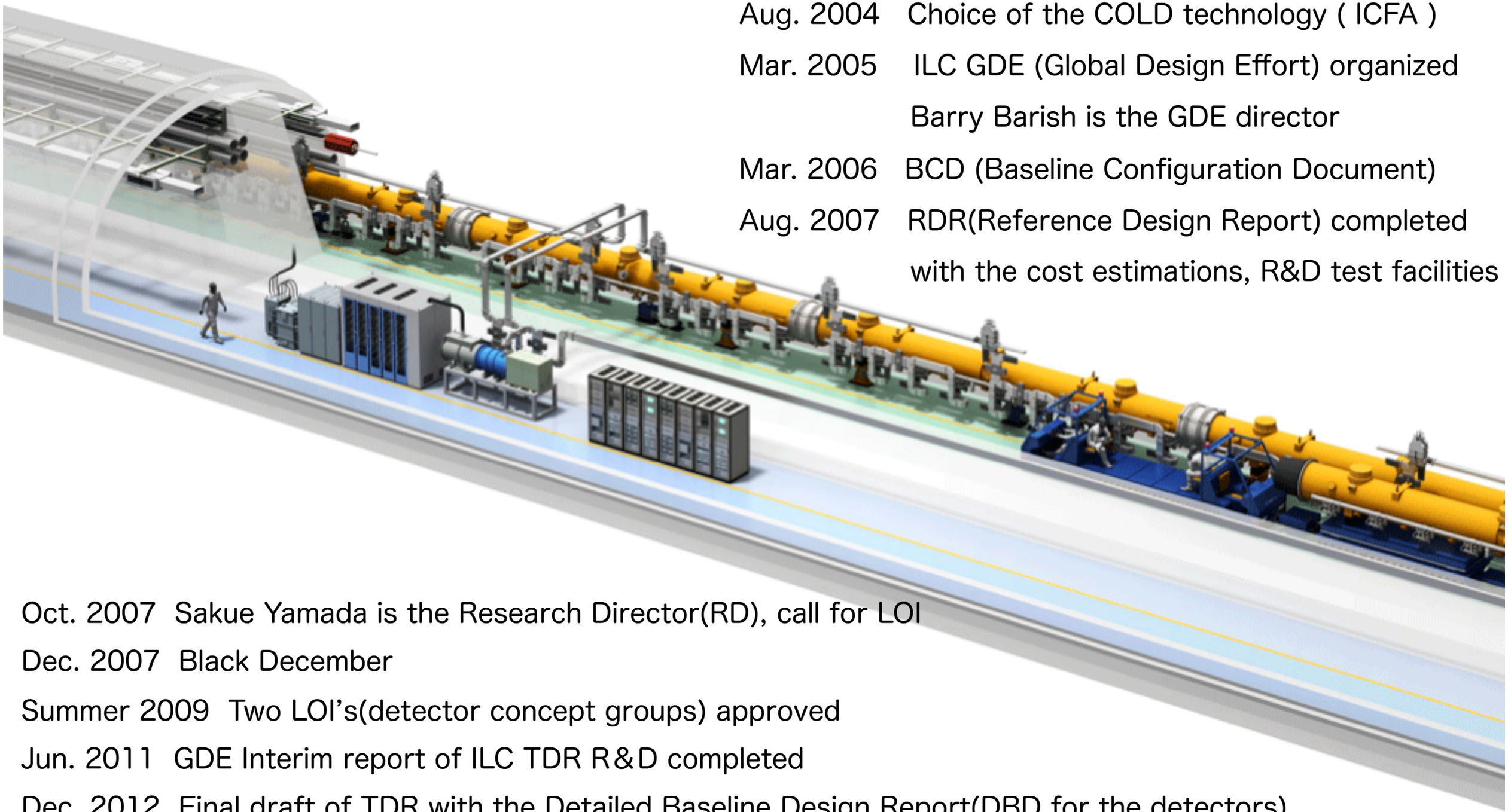

©Rey.Hori/KEK

Oct. 2007　Sakue Yamada is the Research Director(RD), call for LOI

Dec. 2007　Black December

Summer 2009　Two LOI's(detector concept groups) approved

Jun. 2011　GDE Interim report of ILC TDR R&D completed

Dec. 2012　Final draft of TDR with the Detailed Baseline Design Report(DBD for the detectors)

Feb. 2013　GDE resolved and Linear Collider Collaboration (LCC) organized, Lyn Evans is the LCC director

Jun. 2013　TDR completed

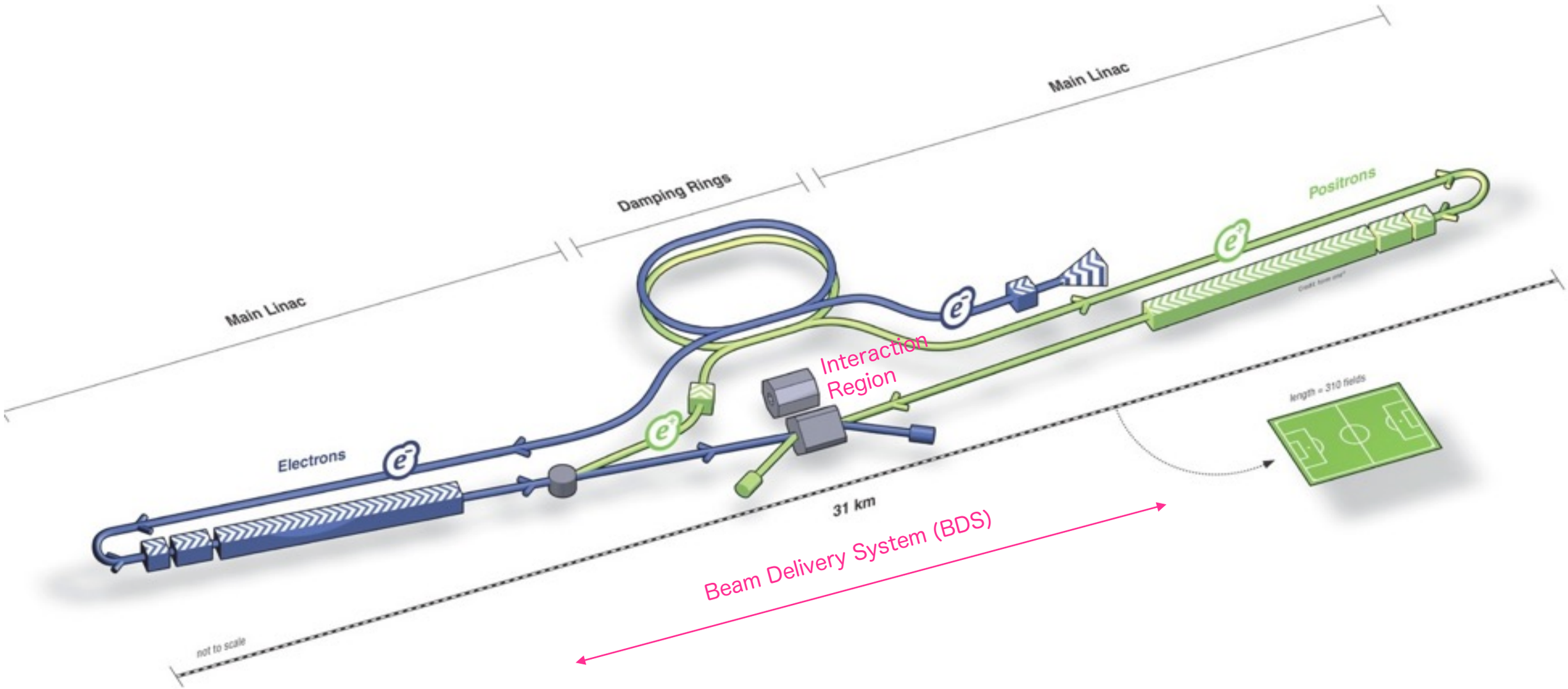

ILC Scheme | © www.form-one.de

What is MDI ?

MDI is Machine Detector Interface

Machine : Beam Delivery System (BDS)

from LINAC-end to beam dump

collimation, energy/polarization, final focus,
extraction (energy/polarization) and beam dump

Detector : Interaction Region

experiment (physics; Higgs, Top, W/Z, SUSY, extra-D ...)

luminosity, background and minimum veto-angle

International Linear Colliders
ILC and CLIC

Detector /Physics

LCC-physics

Common task groups :MDI

MDI

collective view of requirements from detector /physics

Machine

LCC - Accelerator

Systems :BDS

Characteristics of beams at ILC

(1) Beam sizes and shape at the beam energy of 250GeV, i.e. very flat

vertical beam size : σ_y^*=5.9nm

horizontal beam size : σ_x^*=474nm

bunch length : σ_z^*= 300μm

beam focussed with β_x^*=1.1cm, β_y^*=480μm and the distance of final Q from IP L*=4.1m

(2) Beam polarization

80% for electron beam and 30% for positron beam

(3) Beam intensity

number of electrons (positrons) = 2 x 10^{10} / bunch

(4) Collision frequency

The two beams collide with a train of 1,312 bunches separating by 554 ns at the repetition rate of 5Hz and the horizontal crossing angle of 14 mradian.

upgrade option with 2,625 bunches/train, 366 ns of bunch interval at 5Hz

(5) Horizontal crossing

The crossing angle is needed for the extraction of beams down to the beam dump

The 14m radian was chosen in the optimization with the physics performances.

First the luminosity reduction by the horizontal crossing and the recover by the crab crossing

$$L \equiv L_0 \times \eta = \frac{N^2}{4\pi\sigma_x\sigma_y} \times \eta(\phi_c, \sigma_x/\sigma_z), \text{ where } \phi_c = \text{crossing angle}$$

Approximation for the geometric reduction

$$\eta \approx \frac{4}{\pi}\frac{1}{\phi_c}\left(\frac{\sigma_x}{\sigma_z}\right) \text{ for } 1 \gg \phi_c > \frac{\sigma_x}{\sigma_z}$$ assuming rigid elliptical beams

$$\therefore \eta \approx 0.14 \text{ with } \sigma_x/\sigma_z = 0.0016, \phi_c = 14\text{mrad at ILC, which is fully recovered by the Crab crossing}$$

It is in good agreement with the CAIN results : η = 0.15 and the full recovery is confirmed.

Estimation of the geometric reduction

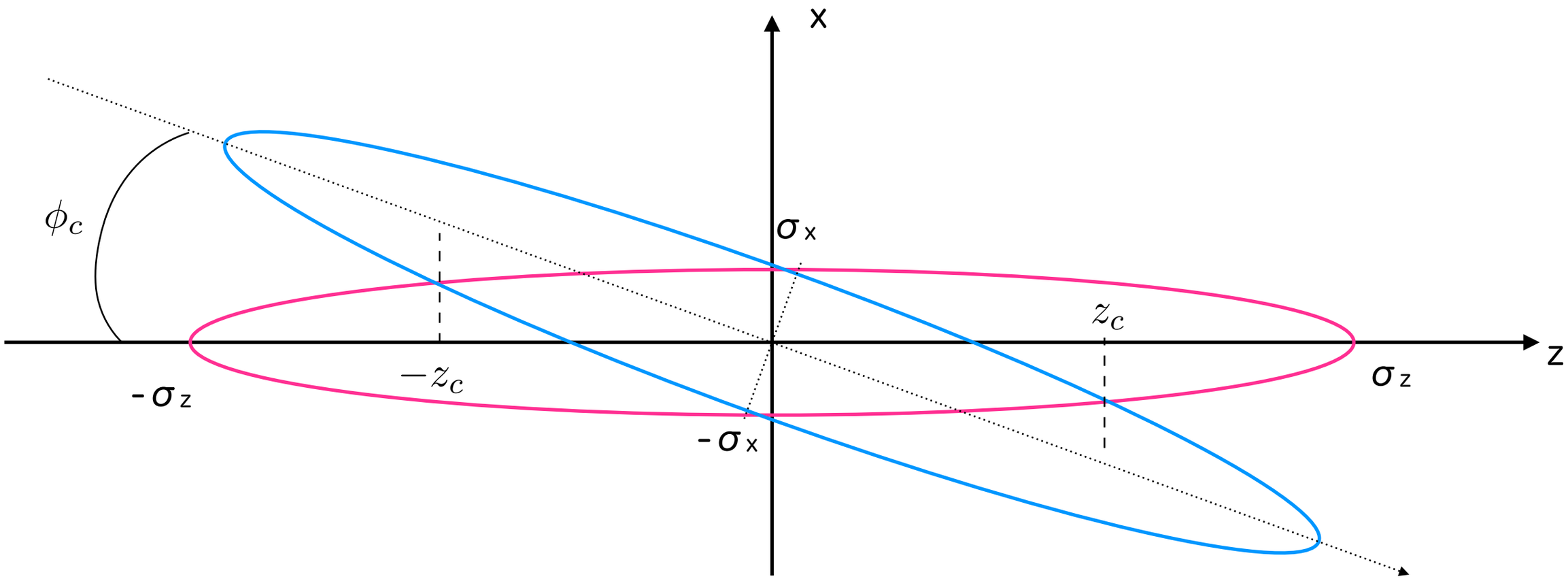

$$z_c \approx \frac{1+\cos\phi_c}{\sin\phi_c}\sigma_x \qquad \text{the overlapping area } A_{ovr} \approx 2z_c\sigma_x$$

$$\therefore \eta \approx \frac{A_{ovr}}{\pi\sigma_x\sigma_z} \approx \frac{4}{\pi}\frac{1}{\phi_c}\frac{\sigma_x}{\sigma_z} \qquad \sigma_x/\sigma_z = 0.0016 \text{ at ILC}$$

The other approximation is,

$$\eta \approx \frac{1}{\sqrt{1+\left(\frac{\sigma_z}{\sigma_x}\tan\frac{\phi_c}{2}\right)^2}}$$

assuming rigid elliptical beams

,which is better for $\phi_c \sim \sigma_x/\sigma_z$, e.g. 2mrad crossing

Crab Crossing Scheme

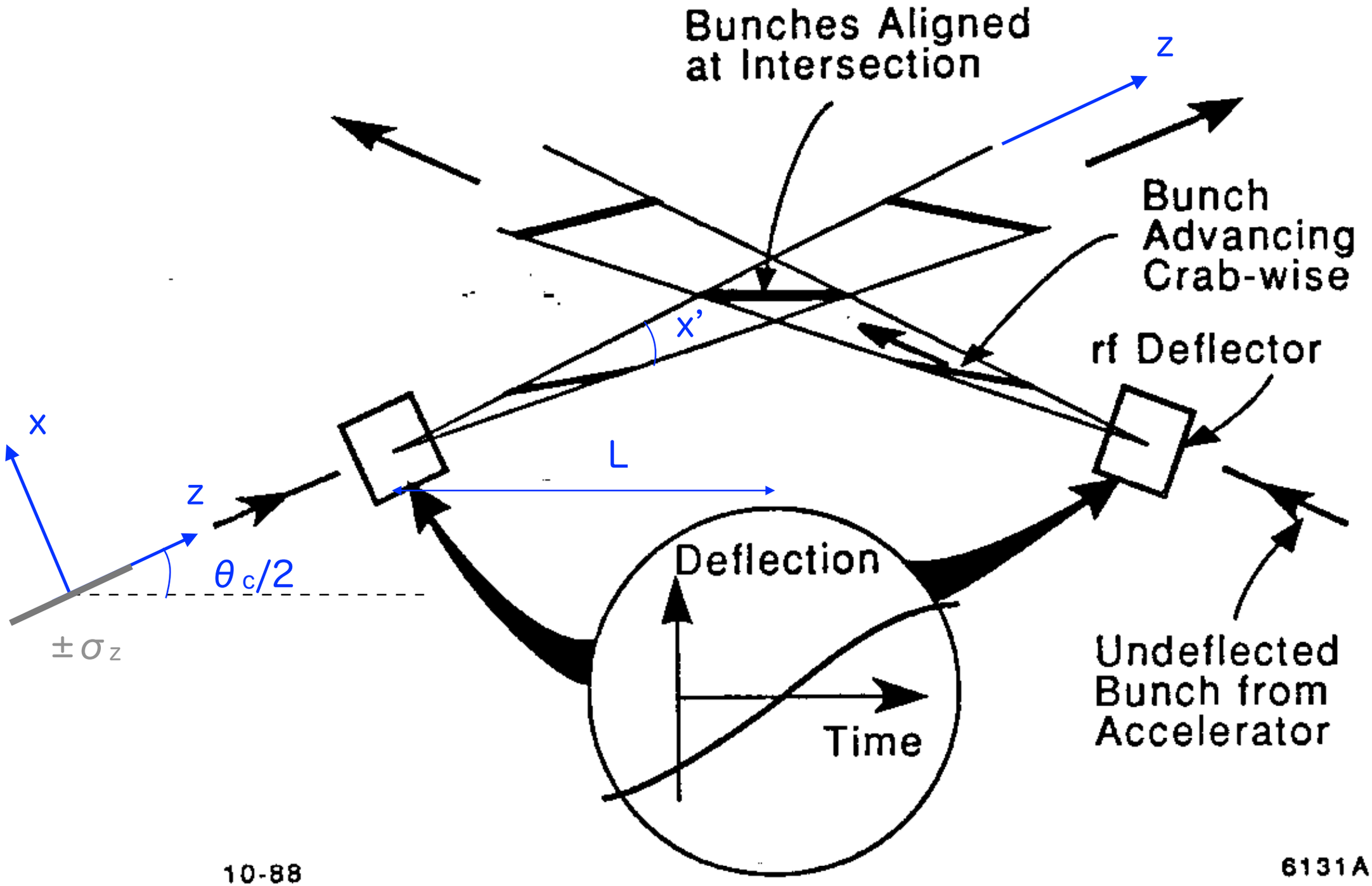

Fig. 2. Crab-wise crossing.

R.B. Palmer, “Energy scaling, crab crossing and the pair problem”, SLAC-PUB-4707, December 1988

Particles at the opposite side are deflected in the opposite direction

$$\pm x' L = \pm \sigma_z \frac{\theta_c}{2}$$

The deflection is given by the electromagnetic field in the RF cavity (magnetic field in the TM110 mode)

$$x' = \frac{\Delta P_x}{E},\ \Delta P_x = \Delta(V_{RF} \sin \omega t) \approx V_{RF} \omega \Delta t$$

$$V_{RF} = \frac{\theta_c E}{2L} \frac{\sigma_z}{\omega \Delta t} = \frac{\theta_c E}{2L} \frac{\lambda_{RF}}{2\pi} \frac{\sigma_z}{c\Delta t} \approx \frac{\theta_c E \lambda_{RF}}{4\pi L} \quad \because \sigma_z \approx c\Delta t$$

$$f = \frac{\omega}{2\pi} \ll \frac{1}{\Delta t} \approx 10^{12}\mathrm{Hz} \text{ for } \sigma_z = 300\mu m$$

E.g. for f=3.9GHz, L=13.4m, θ_c=14mrad and E(beam)=250GeV

V_{RF} = 1.6MV

Ref : Maximum amplitude at Ecm=1TeV = 2.64MV

C. Adolphsen et al., “Design of the ILC Crab Cavity System, EUROTeV-Report-2007-010

Crab cavity can create the horizontal offset with the timing error, i.e. the phase error

$$\pm x' L = \pm \sigma_z \frac{\theta_c}{2} = \pm c\Delta t \frac{\theta_c}{2} \because \sigma_z \approx c\Delta t$$

$$\therefore \Delta x = c\Delta t \frac{\theta_c}{2} \therefore \Delta t = \frac{2\Delta x}{c\theta_c}$$ the horizontal offset due to the timing error

Luminosity reduction factor due to the horizontal offset at IP

$$\eta = \exp\left(\frac{-(\Delta x)^2}{4\sigma_x^2}\right) \therefore \Delta x = 2\sigma_x \sqrt{(-\log \eta)}, \text{ and } \Delta x(\eta = 0.98) = 0.284\sigma_x$$

$\Delta t = 64$ fsec for $\sigma_x = 474\text{nm}, \theta_c = 14\text{mad}$ for the luminosity reduction by 2%

Simulation results by Cain242 :

$$\Delta t = 32 \text{ fsec}$$

Crab Cavities

ILC : 2 cavities at 13.4m from IP, 2~3m long, the phase jitter < 61fsec[TDR}

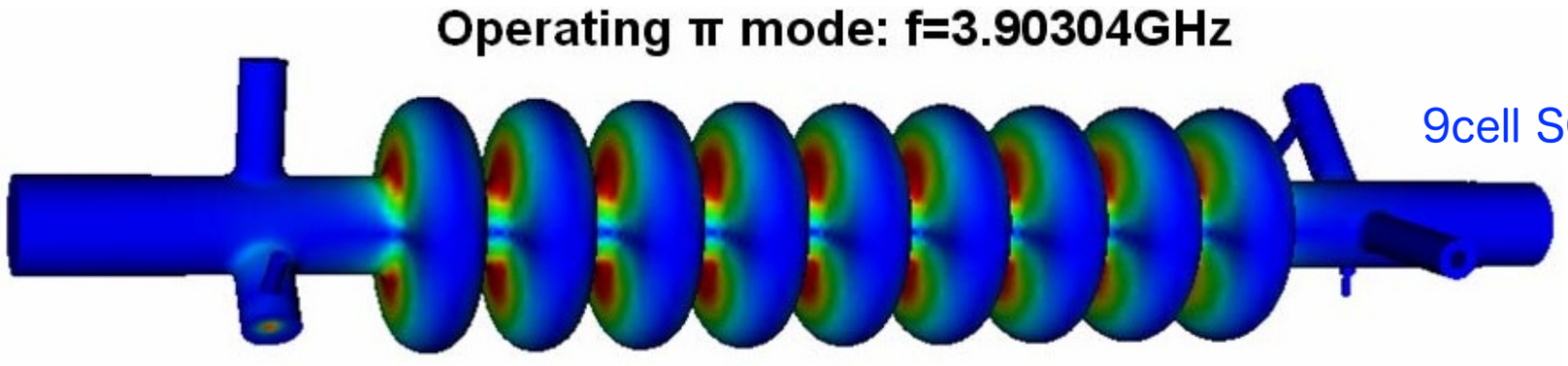

9cell SC cavities

Figure 10.18. Field distribution for the operating mode of the 3.9 GHz crab cavity

CLIC : ~3m long, the phase jitter < 0.02°(4.6fsec) and amplitude<2% at 12GHz

2% luminosity loss

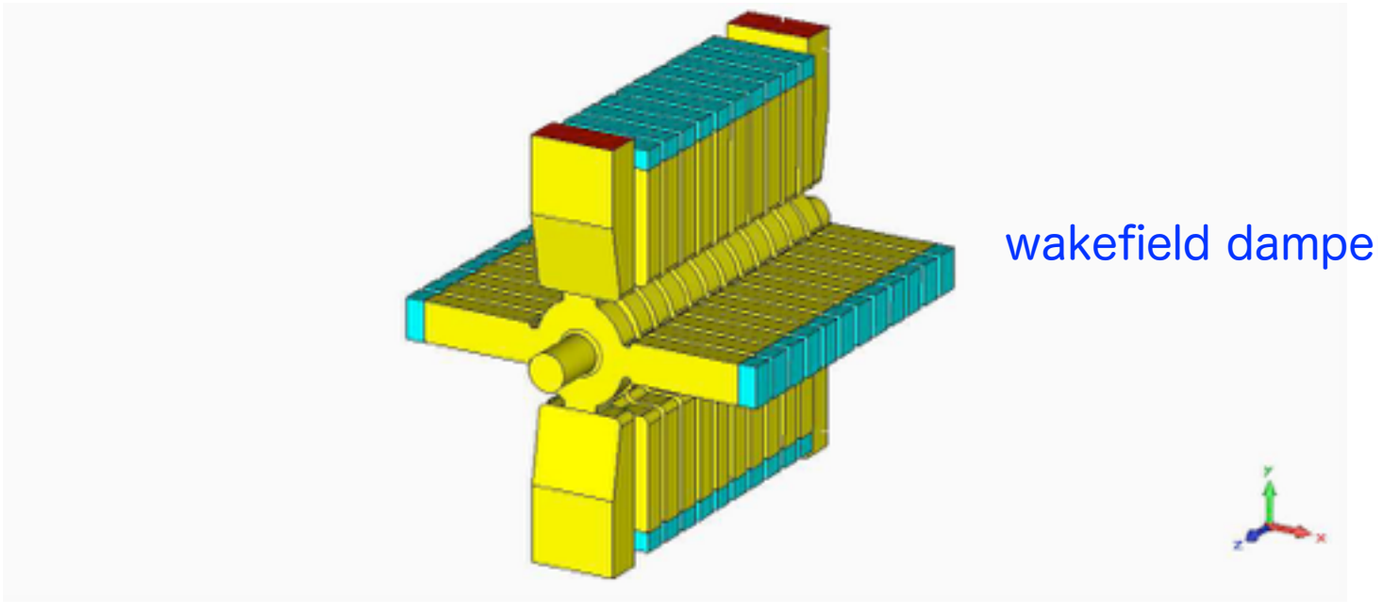

wakefield dampers

ILC TDR parameters

Table 3.1. Summary table of the 250–500 GeV baseline and luminosity and energy upgrade parameters. Also included is a possible 1st stage 250 GeV parameter set (half the original main linac length)

			Baseline 500 GeV Machine			1st Stage	L Upgrade	$E_{\rm CM}$ Upgrade	
Centre-of-mass energy	$E_{\rm CM}$	GeV	250	350	500	250	500	A 1000	B 1000
Collision rate	$f_{\rm rep}$	Hz	5	5	5	5	5	4	4
Electron linac rate	$f_{\rm linac}$	Hz	10	5	5	10	5	4	4
Number of bunches	$n_{\rm b}$		1312	1312	1312	1312	2625	2450	2450
Bunch population	N	$\times 10^{10}$	2.0	2.0	2.0	2.0	2.0	1.74	1.74
Bunch separation	$\Delta t_{\rm b}$	ns	554	554	554	554	366	366	366
Pulse current	$I_{\rm beam}$	mA	5.8	5.8	5.8	5.8	8.8	7.6	7.6
Main linac average gradient	$G_{\rm a}$	MV m^{-1}	14.7	21.4	31.5	31.5	31.5	38.2	39.2
Average total beam power	$P_{\rm beam}$	MW	5.9	7.3	10.5	5.9	21.0	27.2	27.2
Estimated AC power	$P_{\rm AC}$	MW	122	121	163	129	204	300	300
RMS bunch length	$\sigma_{\rm z}$	mm	0.3	0.3	0.3	0.3	0.3	0.250	0.225
Electron RMS energy spread	$\Delta p/p$	%	0.190	0.158	0.124	0.190	0.124	0.083	0.085
Positron RMS energy spread	$\Delta p/p$	%	0.152	0.100	0.070	0.152	0.070	0.043	0.047
Electron polarisation	P_-	%	80	80	80	80	80	80	80
Positron polarisation	P_+	%	30	30	30	30	30	20	20
Horizontal emittance	$\gamma\epsilon_{\rm x}$	μm	10	10	10	10	10	10	10
Vertical emittance	$\gamma\epsilon_{\rm y}$	nm	35	35	35	35	35	30	30
IP horizontal beta function	$\beta^*_{\rm x}$	mm	13.0	16.0	11.0	13.0	11.0	22.6	11.0
IP vertical beta function	$\beta^*_{\rm y}$	mm	0.41	0.34	0.48	0.41	0.48	0.25	0.23
IP RMS horizontal beam size	$\sigma^*_{\rm x}$	nm	729.0	683.5	474	729	474	481	335
IP RMS veritcal beam size	$\sigma^*_{\rm y}$	nm	7.7	5.9	5.9	7.7	5.9	2.8	2.7
Luminosity	L	$\times 10^{34}$ cm^{-2}s^{-1}	0.75	1.0	1.8	0.75	3.6	3.6	4.9
Fraction of luminosity in top 1%	$L_{0.01}/L$		87.1%	77.4%	58.3%	87.1%	58.3%	59.2%	44.5%
Average energy loss	$\delta_{\rm BS}$		0.97%	1.9%	4.5%	0.97%	4.5%	5.6%	10.5%
Number of pairs per bunch crossing	$N_{\rm pairs}$	$\times 10^3$	62.4	93.6	139.0	62.4	139.0	200.5	382.6
Total pair energy per bunch crossing	$E_{\rm pairs}$	TeV	46.5	115.0	344.1	46.5	344.1	1338.0	3441.0
Luminosity/bunch	L/bunch	x 10^{-3} nb^{-1}	1.14	1.52	2.74	1.14	5.49	5.49	7.47

minijet generation by Pythia, http://home.thep.lu.se/~torbjorn/pythia82php/Welcome.php

Table 9: Parameters for the CLIC energy stages. The power consumptions for the 1.5 and 3 TeV stages are from the CDR; depending on the details of the upgrade they can change at the percent level.

Parameter	**Symbol**	**Unit**	**Stage 1**	**Stage 2**	**Stage 3**
Centre-of-mass energy	$\sqrt{s}$	GeV	380	1500	3000
Repetition frequency	f_{rep}	Hz	50	50	50
Number of bunches per train	n_b		352	312	312
Bunch separation	Δt	ns	0.5	0.5	0.5
Pulse length	τ_{RF}	ns	244	244	244
Accelerating gradient	G	MV/m	72	72/100	72/100
Total luminosity	$\mathscr{L}$	$10^{34}\,\text{cm}^{-2}\text{s}^{-1}$	1.5	3.7	5.9
Luminosity above 99% of $\sqrt{s}$	$\mathscr{L}_{0.01}$	$10^{34}\,\text{cm}^{-2}\text{s}^{-1}$	0.9	1.4	2
Main tunnel length		km	11.4	29.0	50.1
Number of particles per bunch	N	10^9	5.2	3.7	3.7
Bunch length	σ_z	µm	70	44	44
IP beam size	σ_x/σ_y	nm	149/2.9	$\sim$ 60/1.5	$\sim$ 40/1
Normalised emittance (end of linac)	$\varepsilon_x/\varepsilon_y$	nm	920/20	660/20	660/20
Normalised emittance (at IP)	$\varepsilon_x/\varepsilon_y$	nm	950/30	—	—
Estimated power consumption	P_{wall}	MW	252	364	589

Table 2.1: CLIC main parameters for 500 GeV and 3 TeV

Description [units]	**500 GeV**	**3 TeV**
Total (peak 1%) luminosity	2.3 (1.4)$\times 10^{34}$	5.9 (2.0)$\times 10^{34}$
Total site length [km]	13.0	48.4
Loaded accel. gradient [MV/m]	80	100
Main Linac RF frequency [GHz]	12	
Beam power/beam [MW]	4.9	14
Bunch charge [10^9 e^+/e^-]	6.8	3.72
Bunch separation [ns]	0.5	
Bunch length [μm]	72	44
Beam pulse duration [ns]	177	156
Repetition rate [Hz]	50	
Hor./vert. norm. emitt. [$10^{-6}/10^{-9}$m]	2.4/25	0.66/20
Hor./vert. IP beam size [nm]	202/2.3	40/1
Beamstrahlung photons/electron	1.3	2.2
Hadronic events/crossing at IP	0.3	3.2
Coherent pairs at IP	200	6.8×10^8
Crossing angle at IP [mrad]	18.6	20

Table 3.26: Beam parameters of interest to the MDI region

Beam parameter	**Value**
Centre-of-mass energy	3 TeV
Total luminosity	5.9×10^{34} cm^{-2}s^{-1}
Luminosity L_{99} (within 1% of energy)	2×10^{34} cm^{-2}s^{-1}
Linac repetition rate	50 Hz
Number of bunches per train	312
Number of particles per bunch	3.72×10^9
Bunch separation	0.5 ns
Bunch-train length	156 ns
Beam power per beam	14 MW
Nominal horizontal IP β function	6.9 mm
Nominal vertical IP β function	0.068 mm
Horizontal IP beam size	45 nm
Vertical IP beam size	1 nm
Bunch length	44 μm

CLIC CDR parameters

Table A.4: Beam Delivery System, IP and background parameters

Parameter	**Symbol**	**Value**	**Unit**
Beam Delivery System + IP			
Total diagnostic section length	$l_{\rm coll}$	2x 0.37	km
Total collimation system length	$l_{\rm coll}$	2x 1.92	km
Total final focus system length	$l_{\rm FF}$	2x 0.46	km
Input transverse horizontal emittance	ε_x	660	nm rad
Input transverse vertical emittance	ε_y	20	nm rad
Nominal horizontal IP beta function	β_x^*	6.9	mm
Nominal vertical IP beta function	β_y^*	0.068	mm
Horizontal IP core beam size	σ_x^*	$\sim$45	nm
Vertical IP core beam size	σ_y^*	$\sim$0.9	nm
Bunch length	$\sigma_{s,\rm inj}$	44	μm
Initial r.m.s. energy spread	$\sigma^*_{\Delta E/E}$	0.34	%
Total energy spread		1	%
Crossing angle at IP	θ_C	20	mrad
Beamstrahlung energy loss	δ_B	28	%
No. of photons / electron	n_γ	2.1	
No. of coherent pairs / bunch crossing	$N_{\rm coh}$	68	10^7
No. of incoherent pairs / bunch crossing	$N_{\rm incoh}$	0.03	10^7
Hadronic events / crossing	$N_{\rm hadron}$	3.2	
Total luminosity	$L_{\rm pk}$	5.9	10^{34}cm^{-2}s^{-1}
Luminosity (in 1% of energy)	$L_{99\%}$	2.0	10^{34}cm^{-2}s^{-1}

BDS

Beam Delivery & MDI elements

1TeV CM, single IR, two detectors, push-pull

grid: 100m*1m

Diagnostics

Beam Switch Yard

polarimeter

Sacrificial collimators

Collimation: β, E

E-spectrometer

Final Focus

Tune-up & emergency Extraction

Tune-up dump

14mr IR

Muon wall

Main dump

Extraction with downstream diagnostics

IR Integration

- Very forward region
- Beam-CAL
- Lumi-Cal
- Vertex

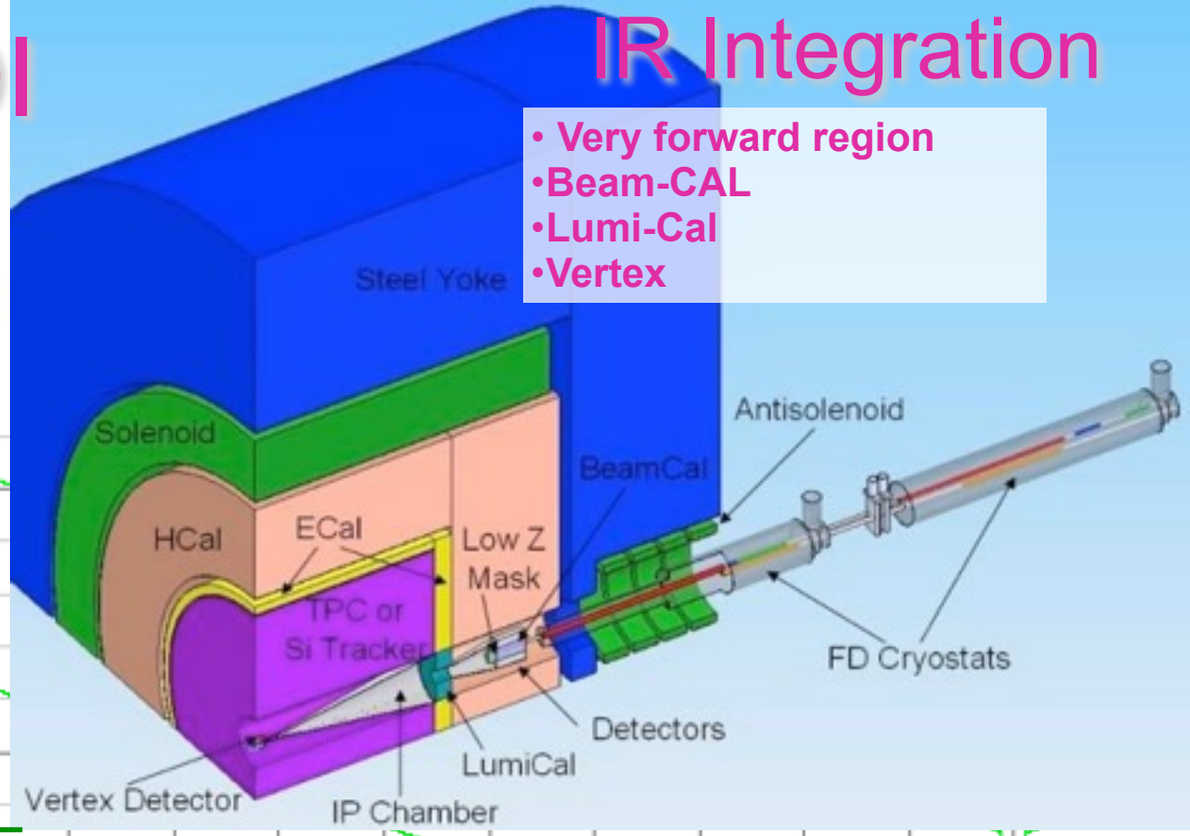

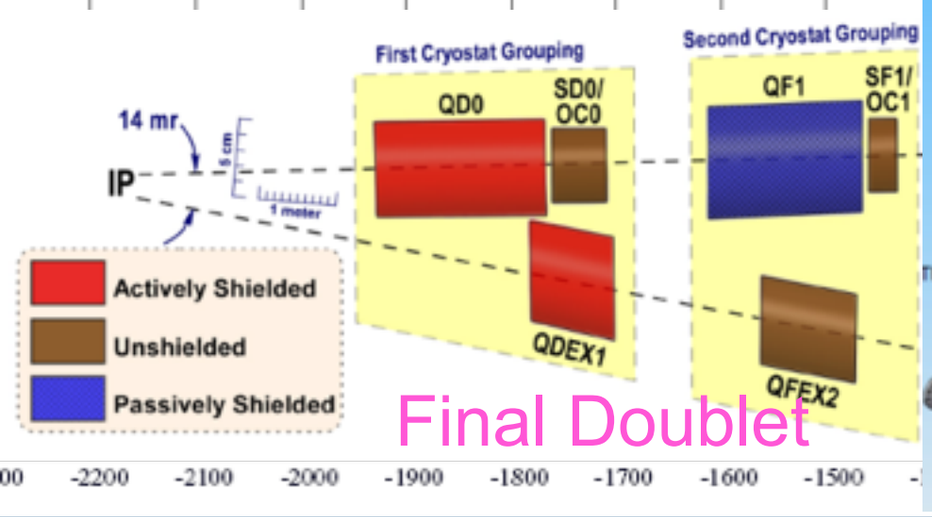

Final Doublet

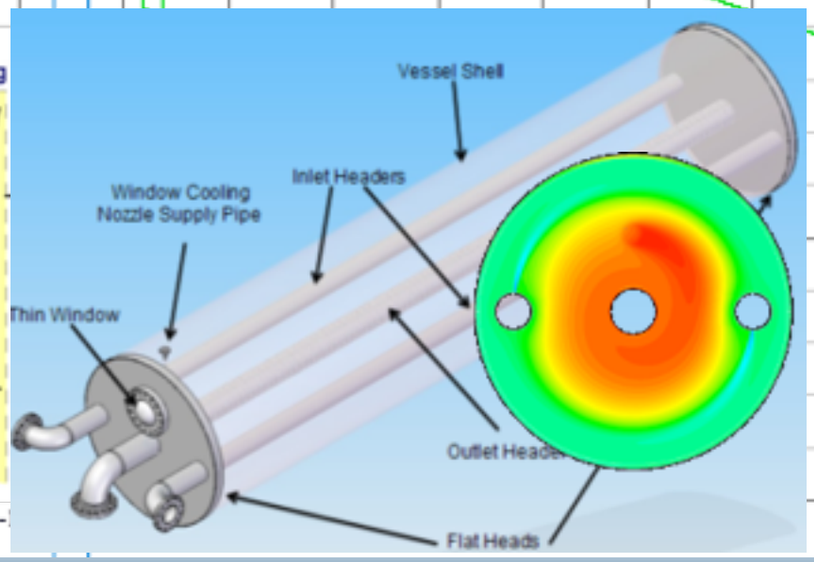

ILC BDS, E_{cm} =500GeV

to accommodate the upgrade to 1TeV center-of-mass energy

electron beam →

Diagnostics | Collimation | Matching | Final Focus | IR | EXT& Dump

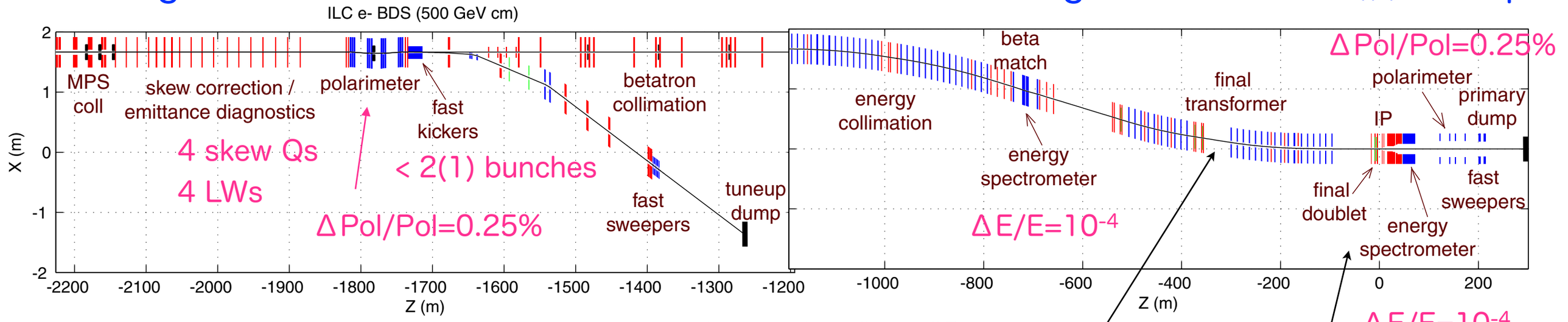

collimation depth = $9\sigma_x$ x $65\sigma_y$,
$\Delta\varepsilon_{x/y}/\varepsilon_{x/y}$=0.08%/4.4%

5m-long magnetized muon spoiler(1.5T)

σ_x=474nm
σ_y=5.9nm
Horizontal crossing angle =14mr

$\Delta\varepsilon_x$<1% at chicanes of polarimeter and energy spectrometer

$\Delta\varepsilon_x$<0.5(1)% in bends at E_{cm}=0.5 (1) TeV

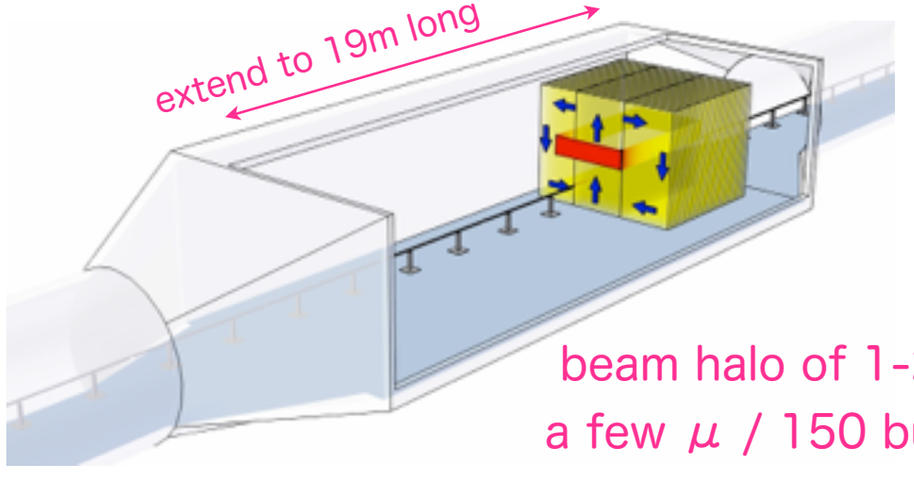

beam halo of 1-2 x 10^{-5} hit the collimators
a few μ / 150 bunches at IP

ILC-BDS/FF Optics

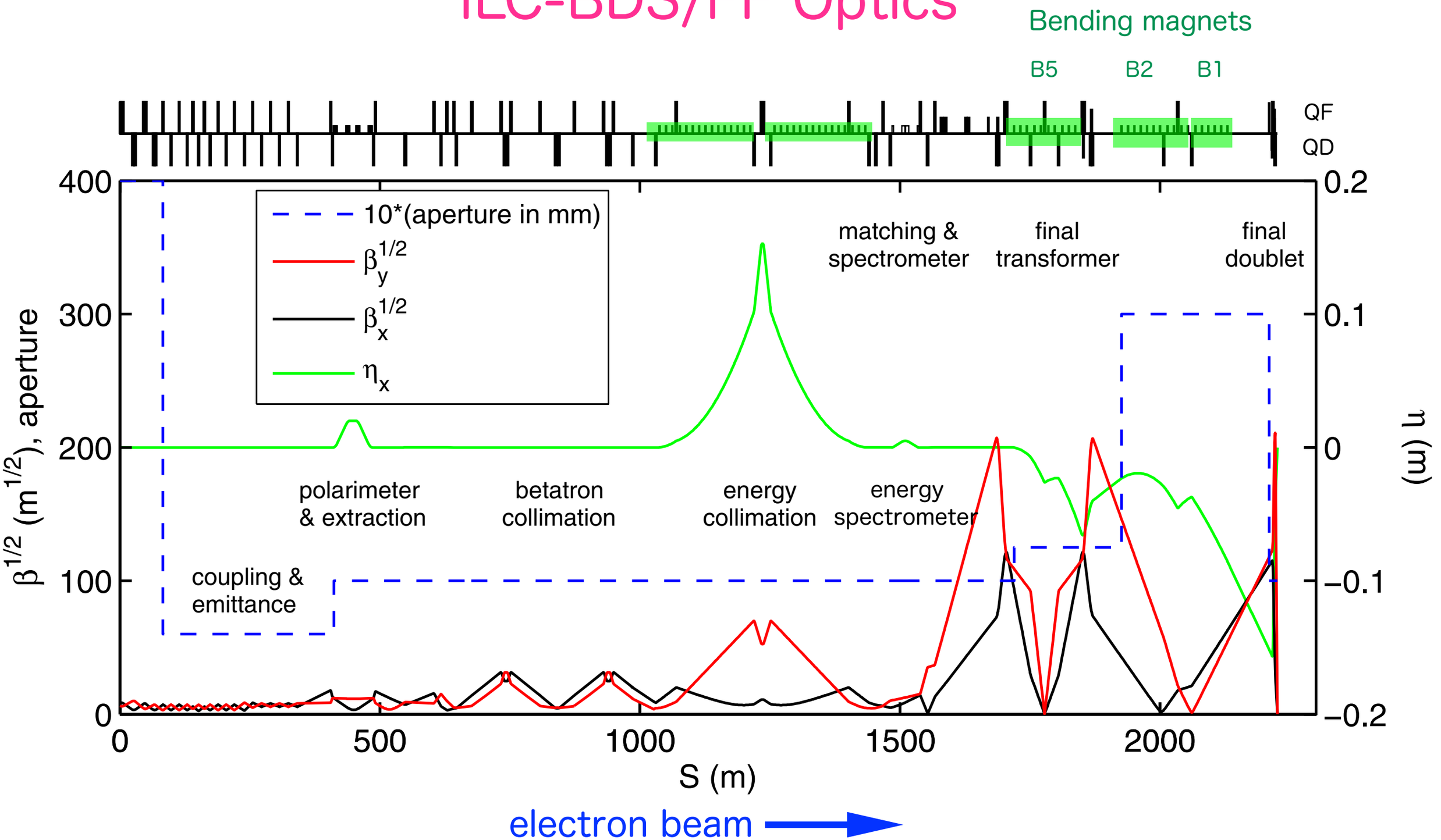

Figure 8.3. BDS optics, subsystems and vacuum chamber aperture; S is the distance measured from the entrance. (total length =2254 m)

ILC BDS, E_{cm} =500GeV

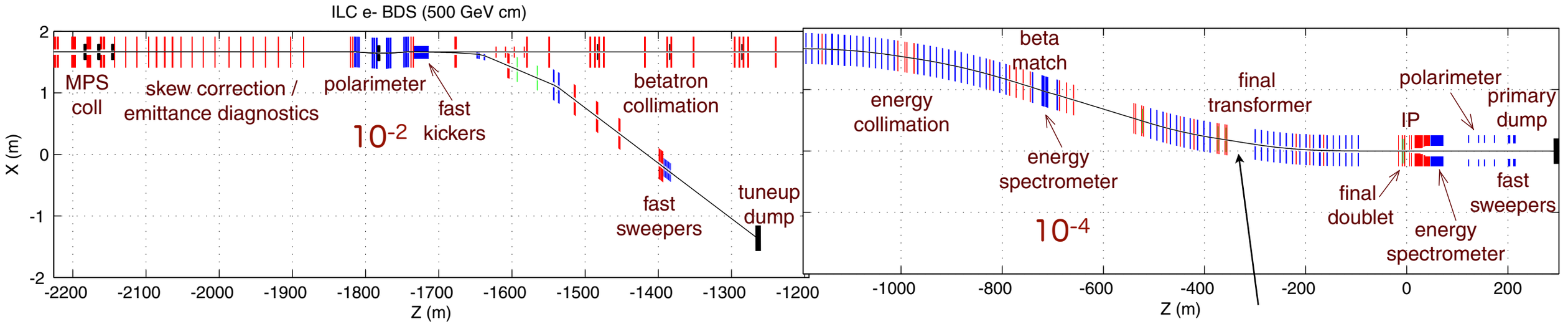

5m magnetized muon spoiler

CLIC BDS, E_{cm} =3TeV

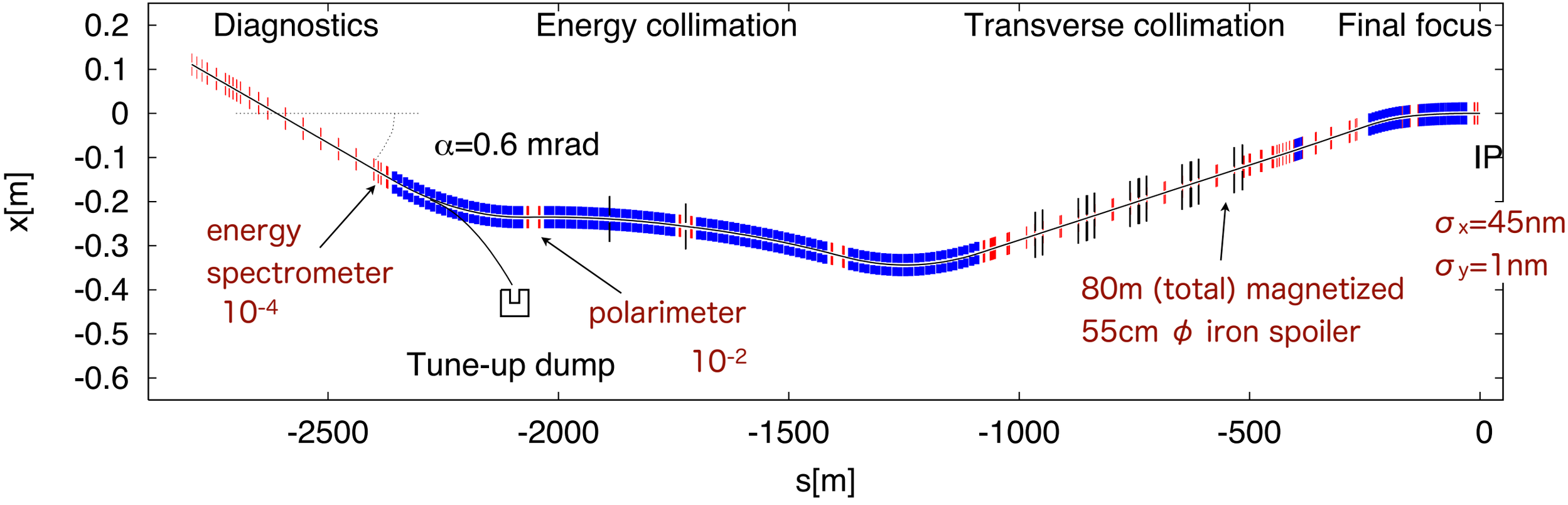

Both assume that beam halo of 10^{-5} hit the collimators -> 1 μ / bunch at IP

ILC : extraction line up to the downstream polarimeter

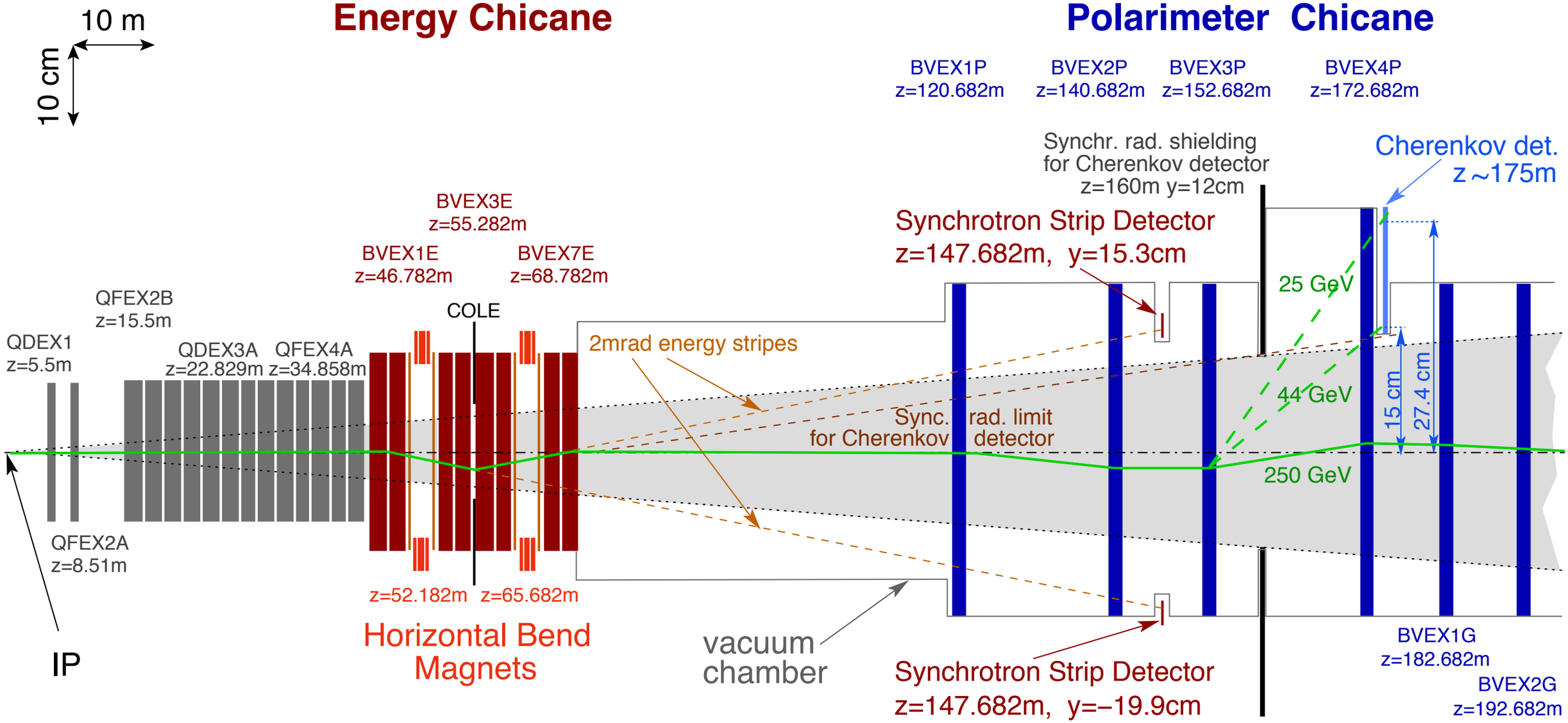

M.Beckmann, J.List, A.Vauth and B.Vormwald, Spin transport and polarimetry in the beam delivery system of the international linear collider, JINST 9 P07003, 2014

Quad name	Qty	L (m)	G (T/m)	R (mm)
QDEX1 (SC)	1	1.060	100.00	15
QFEX2A (SC)	1	1.200	23.08	26
QFEX2B,C,D	3	2.143	11.19	42
QDEX3A,B	2	2.106	11.93	42
QDEX3C	1	2.106	10.89	46
QDEX3D	1	2.106	9.63	52
QDEX3E	1	2.106	8.08	62
QFEX4A	1	1.945	7.11	71
QFEX4B,C,D,E	4	1.945	5.94	85

Parameters of the extraction quadrupoles at 250 GeV

Bend name	Qty	L (m)	B (T)	Half-gap (mm)	Diagnostics
BVEX1E,2E,…,8E	8	2.0	0.4170	85	Energy
BVEX1P,2P	2	2.0	0.4170	117	Polarimeter
BVEX3P	1	2.0	0.6254	117	
BVEX4P	1	2.0	0.6254	132	
BVEX1G,2G	2	2.0	0.4170	147	GAMCAL

Parameters of the chicane bends at 250 GeV

K. Moffeit, Workshop on polarization and energy measurements at ILC, 4/9-11, 2008, DESY, Zeuthen

ILC-BDS/EXT Optics

Beam with energy of greater than 30% and angles of > 0.5m rad to the dump. No net bending , i.e. the same dump for Beamstrahlung photons (< 0.75mr)

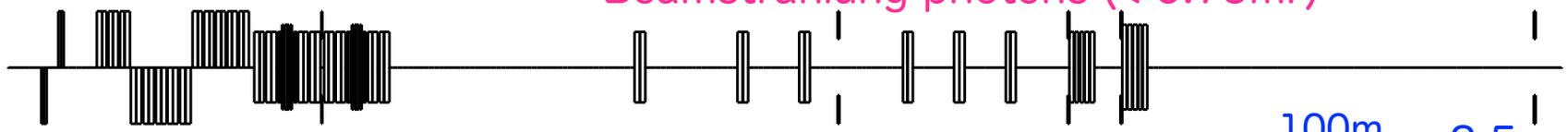

Extraction line for L*=4.5 m (Lext*=6.3 m).

100m

3.5m separation from incoming beam

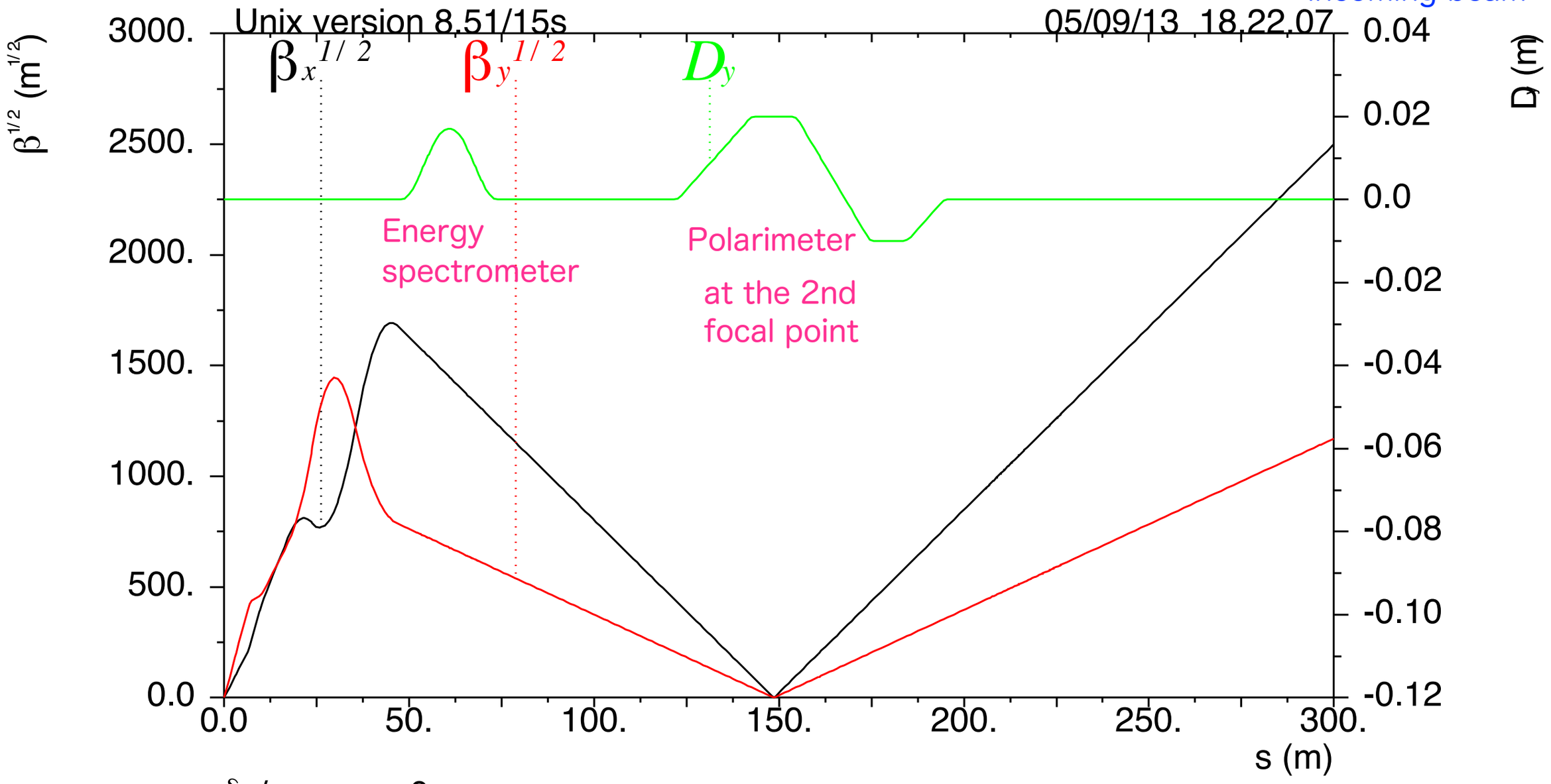

$\delta_E / p_0 c = 0.$

Table name = TWISS

electron beam →

6cm radius circle by 10 kickers in a 15cm radius dump window

Figure 7: Extraction line layout (top) and optics functions with the TDR parameters.

E.Marin, N.Nosochkov, Extraction Line Simulations with TDR Parameters, SLAC-PUB-15938, April 2014

Power Losses in the magnets and the collimators

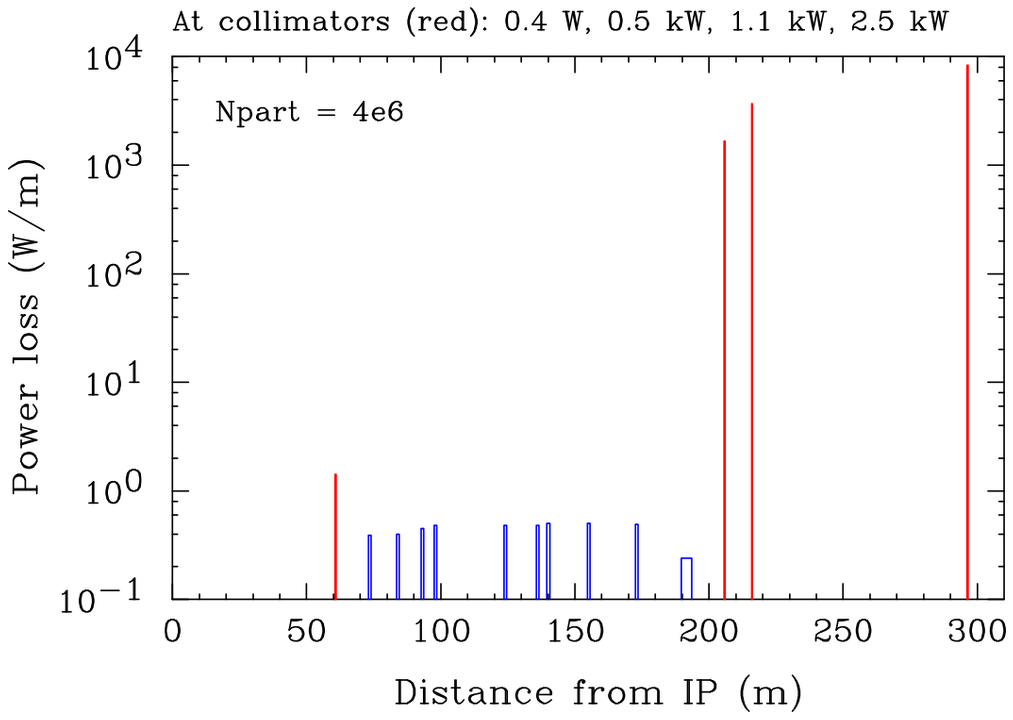

Figure 10: Power losses of the disrupted electron beam in the extraction line magnets and diagnostics (blue), and collimators (red) with the TDR parameters without detector solenoid.

Power losses are acceptable, but need a study of impact on the detectors (E-spec, Pol.)

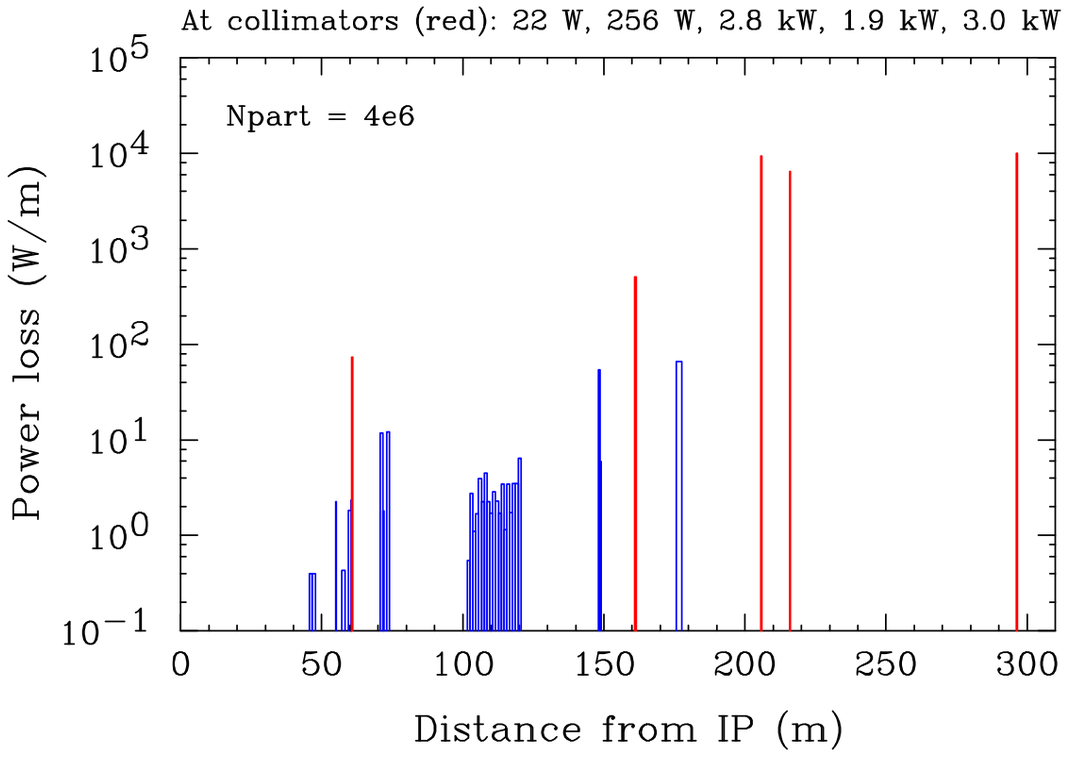

The total primary loss on the warm quadrupoles and bends is a few Watts,

Figure 13: Power losses of the disrupted electron beam in the extraction line magnets and diagnostics (blue), and collimators (red) with the TDR parameters and SiD detector solenoid.

E.Marin, N.Nosochkov, Extraction Line Simulations with TDR Parameters, SLAC-PUB-15938, April 2014

CLIC Post Collision Line

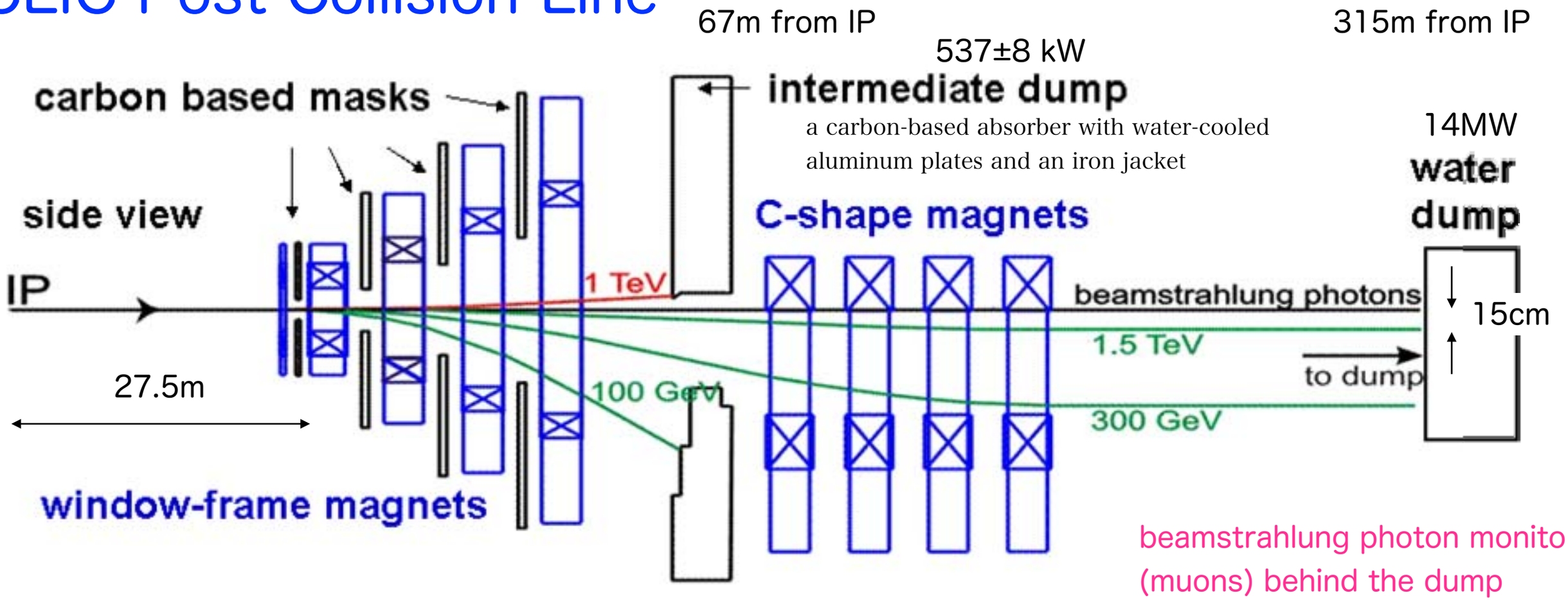

Table 3.31: List of magnets for the CLIC post-collision line.

Name	Quantity	Magnetic Length [m]	Full magnet aperture H/V [m]	Good field region H/V	Tuning Range [m]	Rel. Field Accuracy [%]	Higher Harmonics bn/b1
Mag1a Mag1b	2×2	2	0.222/0.577*	0.2/0.44	10	10^{-2}	<10%
Mag2	1×2	4	0.296/0.839*	0.27/0.702	10	10^{-2}	<10%
Mag3	1×2	4	0.37/1.157*	0.34/1.02	10	10^{-2}	<10%
Mag4	1×2	4	0.444/1.531*	0.41/1.394	10	10^{-2}	<10%
Mag C-type	4×2	4	0.45/0.75**	0.428/0.74	10	10^{-2}	<10%

Beam dump for 18MW/500GeV per beam

1.8 m-diameter cylindrical stainless-steel high-pressure (10 bar) water vessels with a 30 cm diameter, 11m($30X_0$) length, 1 mm-thick Ti (Ti 6Al-4V) window.

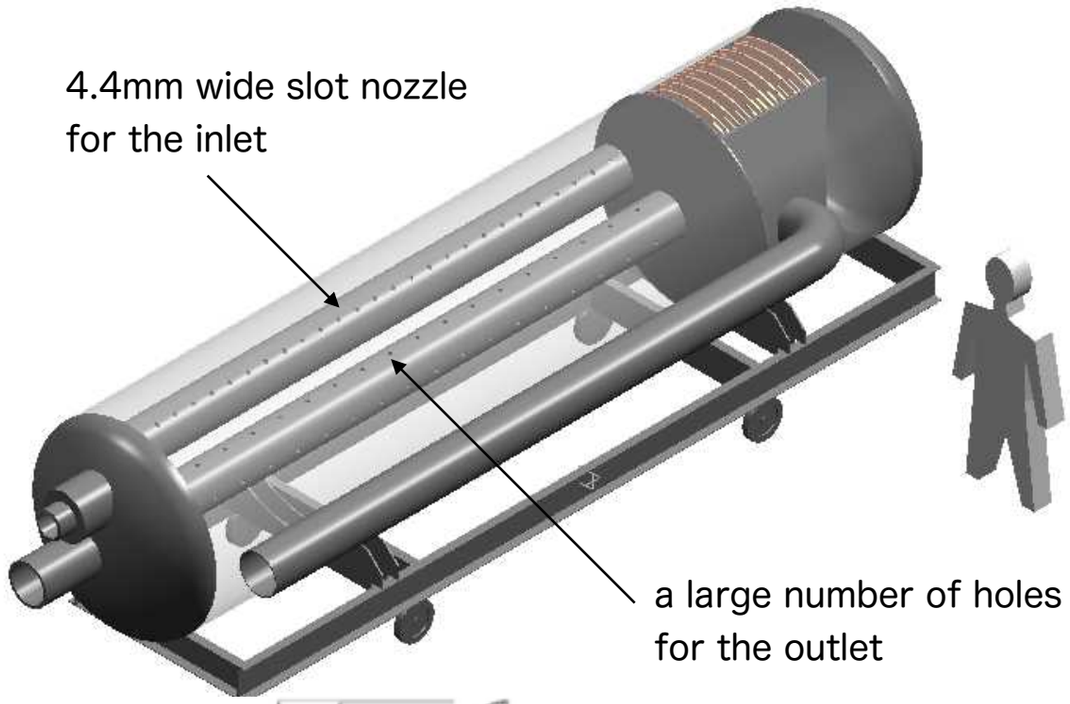

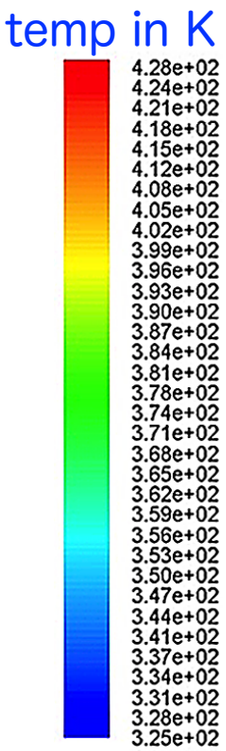

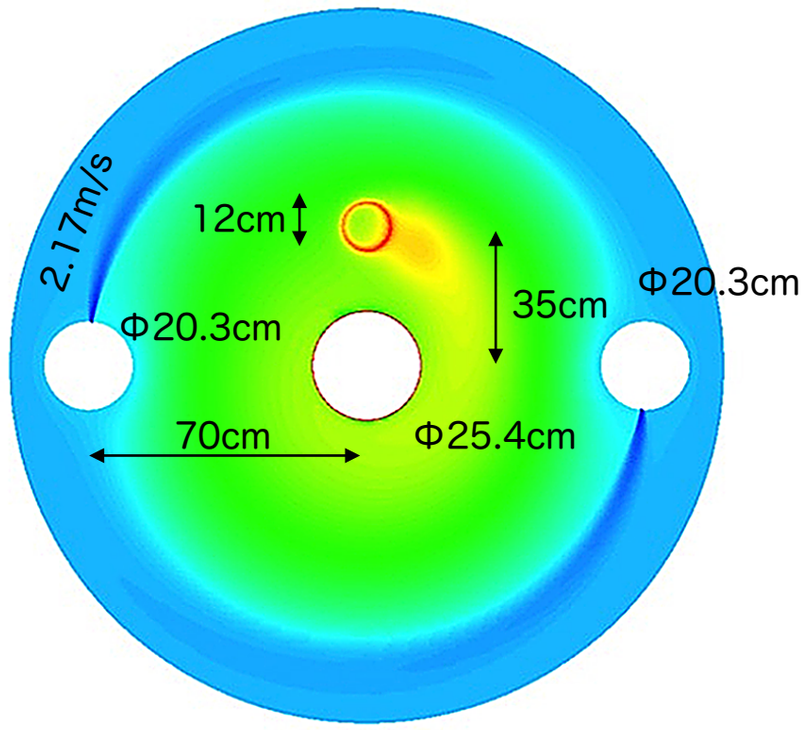

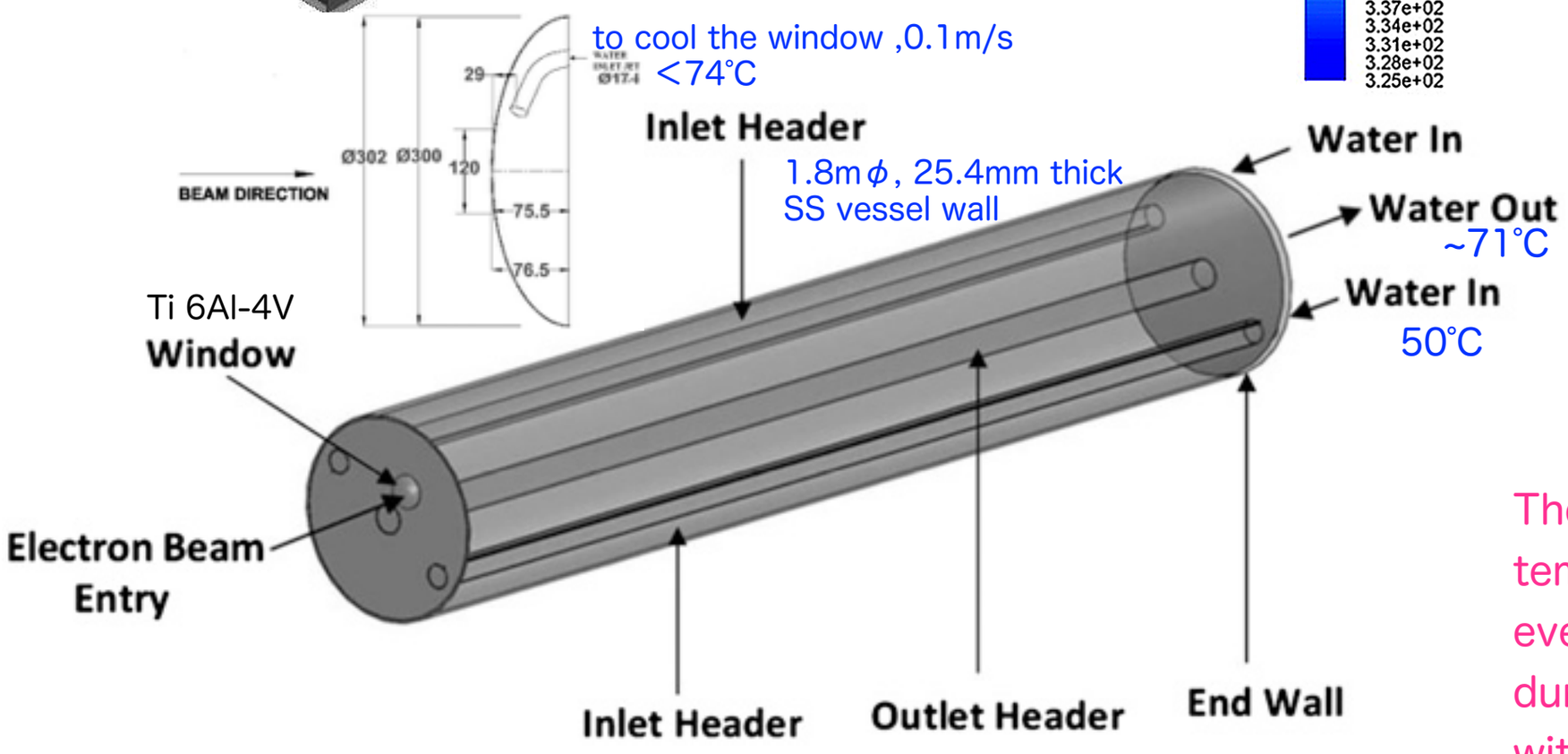

at z=2.9m ($8.1X_0$, shower max.)

Maximum temperature = 155℃
with the beam train passage
and ~1kHz sweep radius 6cm
(beam : σ_x=2.42mm, σ_y=0.27mm)

The pressurization raises the boiling temperature of the dump water; in the event of a failure of the sweeper, the dump can absorb up to 250 bunches without boiling the dump water

P. Satyamurthy et al., NIM A679 (2012) 67-81

Radioactive Cooling Water System

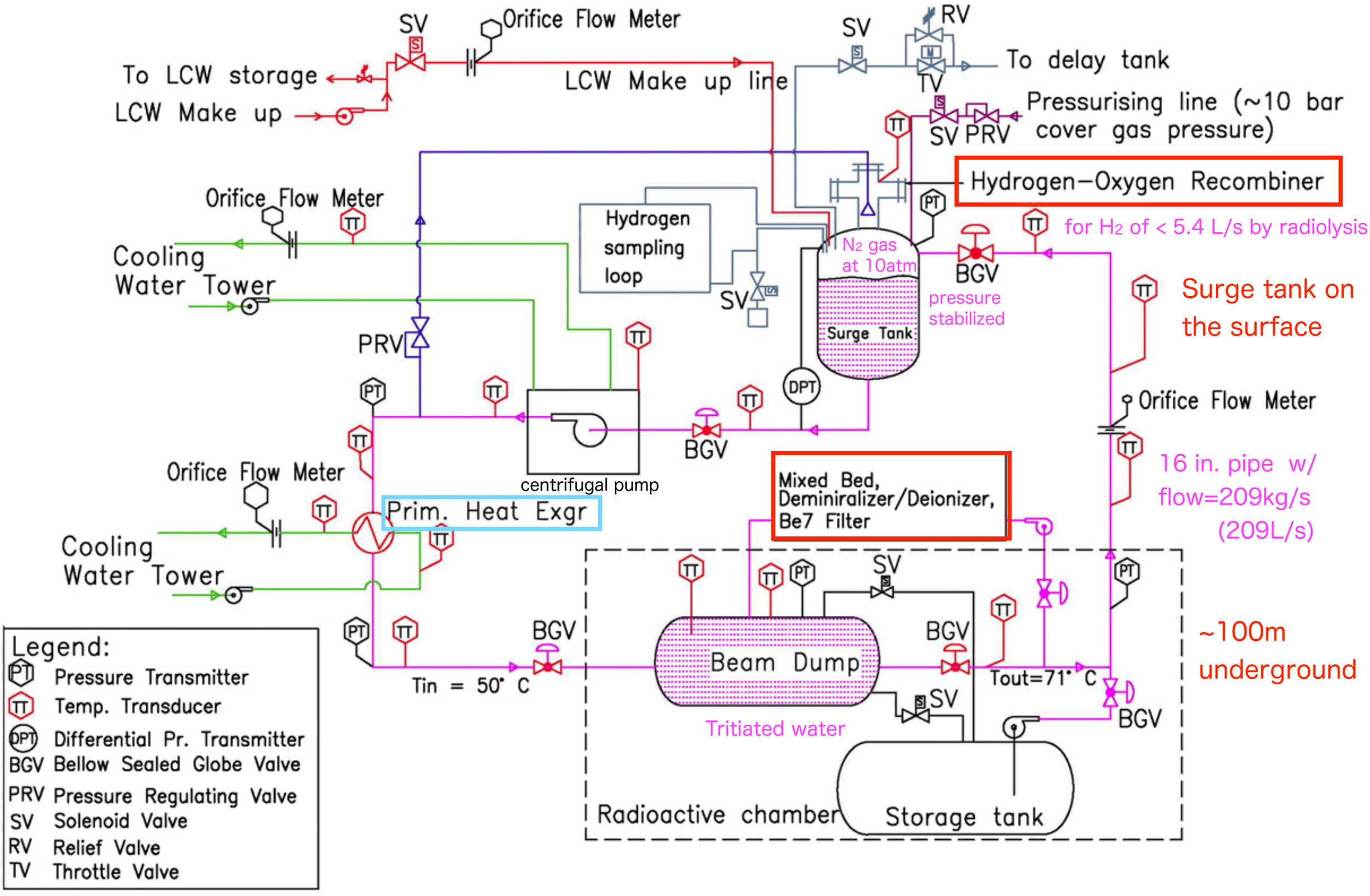

Fig. 28. Coolant circuit details.

P. Satyamurthy et al., NIM A679 (2012) 67-81

Radioactivities

Beam interactions with water, primarily photo-spallation on ^{16}O, result in production of ^{3}H, ^{7}Be, and other more short-lived radioactive isotopes; the latter decays to negligible levels in less than 3 h.

Table 2
Activities in the Beam Dump.

Isotope	Half life	Saturation activity, Bq
^{15}O	2.03 min	23×10^{15}
^{13}N	9.96 min	9×10^{14}
^{11}C	20.30 min	9×10^{14}

Most of the ^{7}Be is filtered out in the deionizer column and can be mechanically removed at the time of regeneration. Some ^{7}Be will deposit on all water-exposed surfaces. Tritium in the form of tritiated water will slowly build up to saturation levels.

Table 3
Activity after 3 h of cooling.

Isotope	Half life	Saturation activity, Bq	Radiation
^{7}Be	53.4 day	19×10^{13}	480 keV γ
^{3}H	12.35 years	26×10^{13}	<20 keV β

P. Satyamurthy et al., NIM A679 (2012) 67-81

Shielding and protection of site ground water

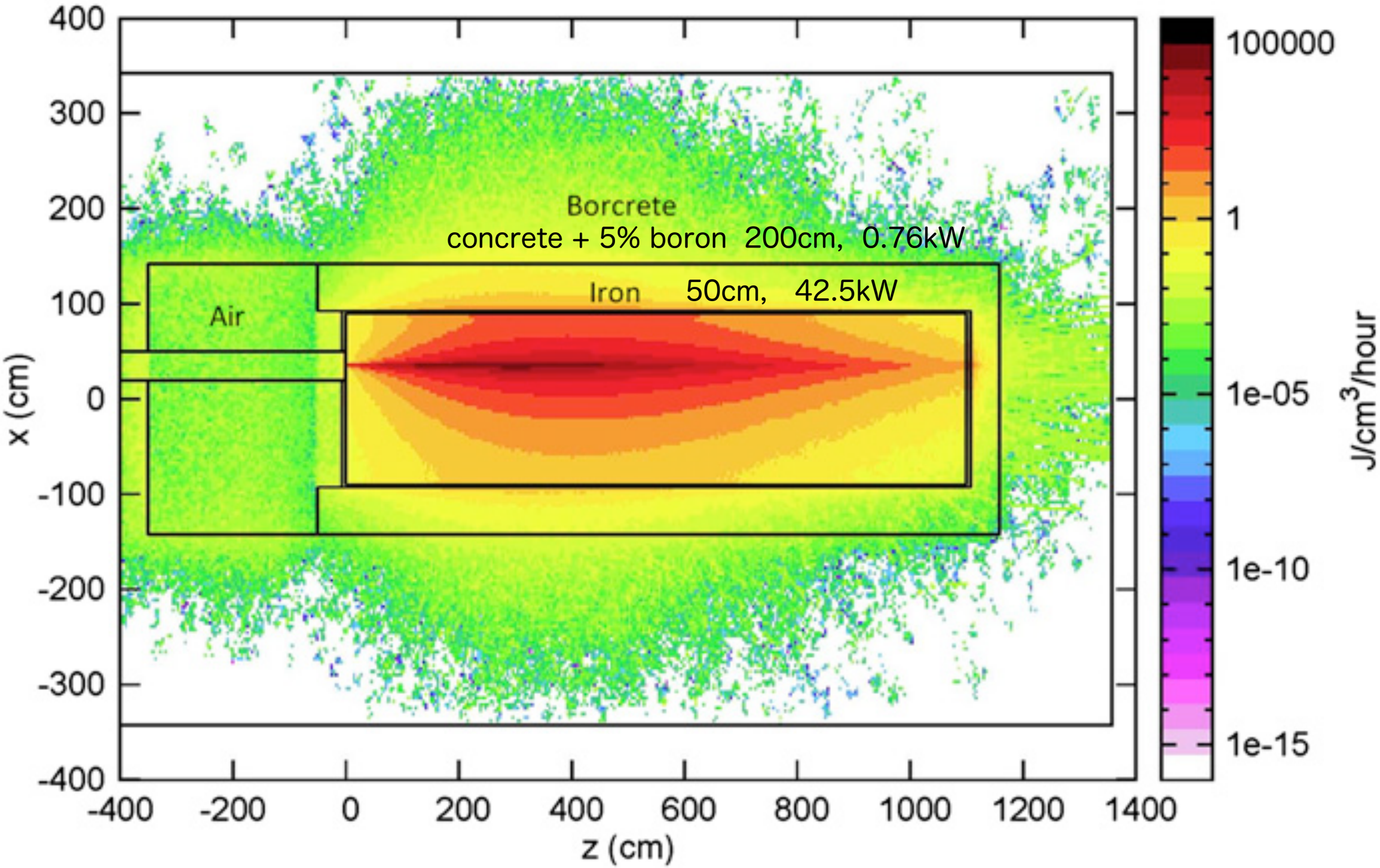

Power depositions in the entire dump region (average of y=-342.5 cm and +342.5 cm).

P. Satyamurthy et al., NIM A679 (2012) 67-81

Backgrounds

BDS

Backgrounds for experiments (1)

1. Synchrotron radiations

The intensity is almost same as the beam, i.e. ~10^{10} photons/bunch, where the photon energy continuously distributes up to MeV. It must be very serious problem if they enter into detectors. For an example, all readout channels are fulfilled with them in a gas drift chamber.

2. Bremsstrahlung photons from beam interaction with residual gas in the beam pipes

The rate is proportional to vacuum pressure in the beam pipes at the beam delivery system

3. Muons produced at the collimators

The rate depends on the collimation depths and the beam halo/tail intensity, where the collimation is absolutely needed to control the synchrotron radiations.

4. Backscattered photons and neutrons at downstream components, especially the beam dump

about 1 neutron/100MeV produced, e.g. 3 x 10^{17} neutrons /sec at the beam dump

Synchrotron Radiations

especially from the final doublet (QD0, QF1)

The synchrotron radiations spread along the envelop of the collimated beam profiles as shown. They should not hit the beam pipe for the exit hole with 38mm diameter inside of the detector.

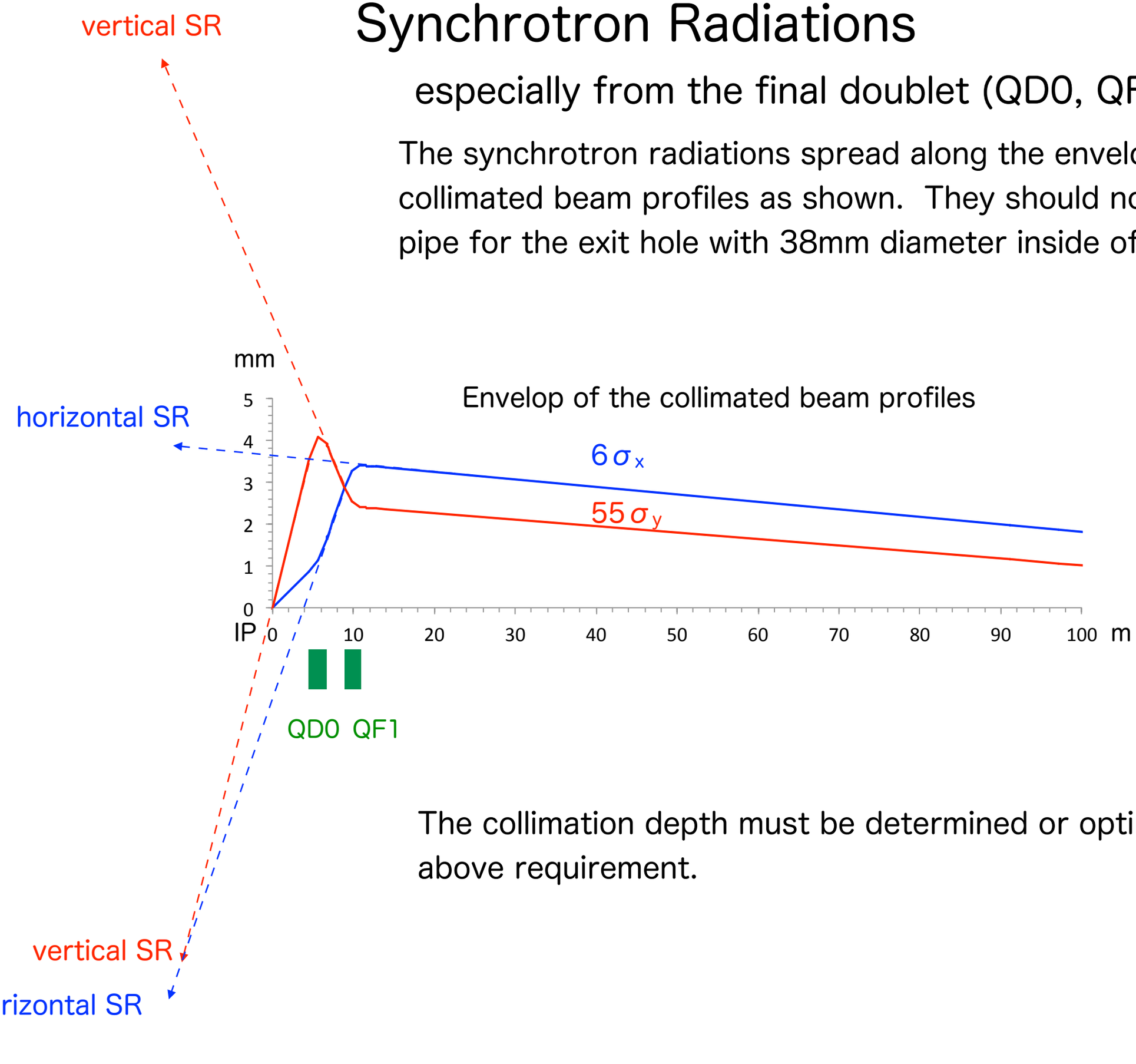

The collimation depth must be determined or optimized to fulfill the above requirement.

Bremsstrahlung in residual gas

$$dN = N_b \rho \cdot 4\alpha Z^2 r_e^2 F(x) \frac{dk}{k} ds$$

s = path length

for electrons

$$F(x) = (1 + x^2 - \frac{2}{3}x)\ln(183Z^{-1/3}) + \frac{x}{9}$$

for photons

$$F(y) = (y^2 - \frac{4}{3}y + \frac{4}{3})\ln(183Z^{-1/3}) + \frac{1-y}{9}$$

$x = \frac{E_e}{E_b}, \quad y = \frac{k}{E_b}, \quad x + y = 1 \qquad E_b = \text{beam energy}, \ E_e = \text{electron energy}, \ k = \text{photon energy}$

residual gas density: $\rho = \frac{N_A}{22.4 \times 10^3} \frac{P(\text{Pa})}{1.013 \times 10^5} \times 10^6 \quad \rho = \frac{N_A}{22.4 \times 10^3} \frac{P(\text{Torr})}{760} \times 10^6 \quad [\text{m}^{-3}]$

fine structure constant: $\alpha = 1/137$

classical electron radius: $r_e = 2.82 \times 10^{-15}\text{m}$

Avogadro constant: $N_A = 6.02 \times 10^{23}$

For residual gas, Z=14 of CO

beam intensity: $N_b = 2 \times 10^{10}$

Ref) J.C.Liu, W.R.Nelson and K.R.Kase, SLAC-PUB-6532, June 1994

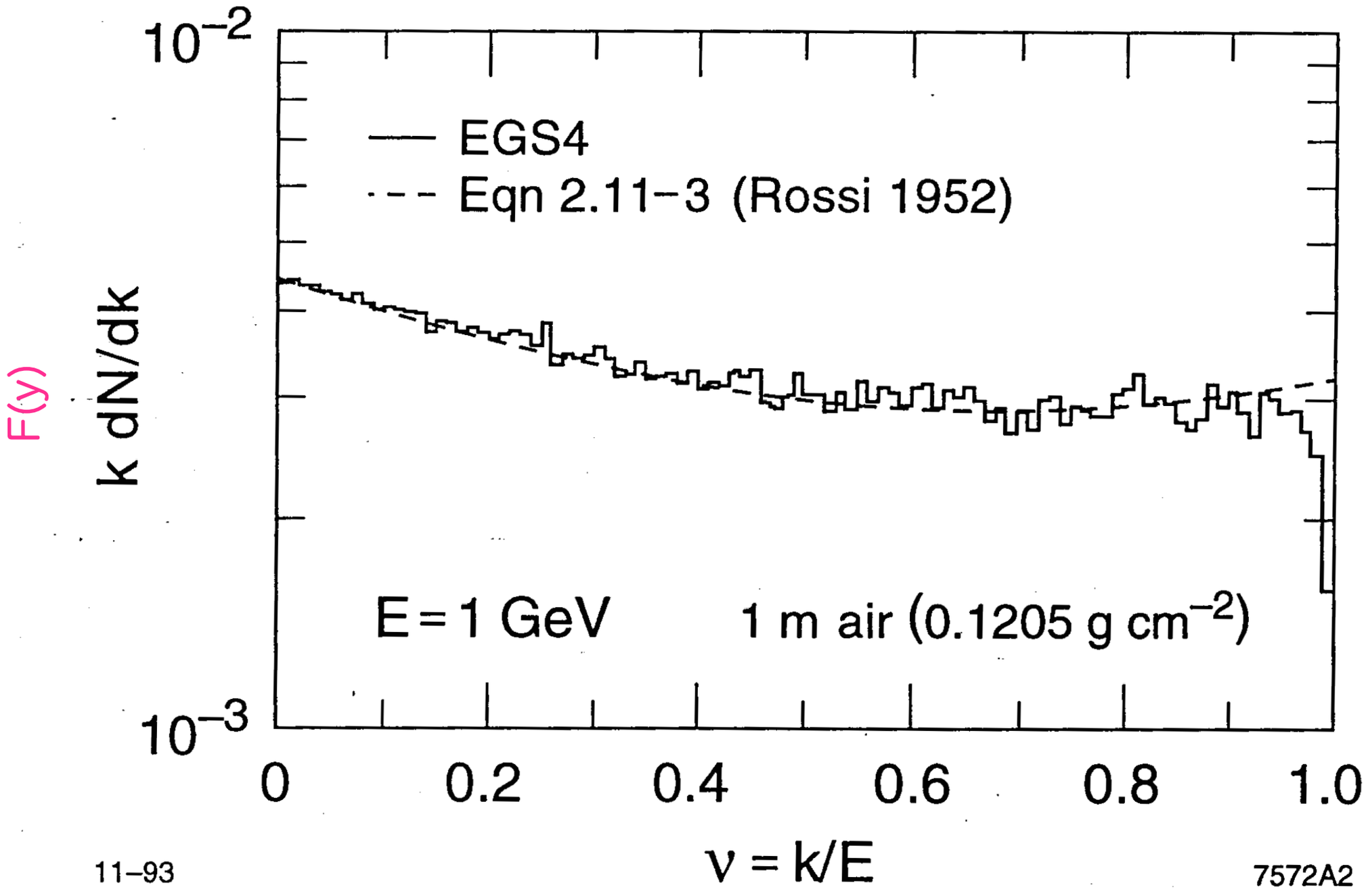

J.C.Liu, W.R.Nelson an K.R.Kase, SLAC-PUB-6532, June 1994

F(x) is factorized as a constant, F(x)=F(y)=4.5 .

$$dN = 2\times10^{10}\cdot1.21\times10^{-8}(1.61\times10^{-6})\cdot4.5\cdot\ln(k_{max}/k_{min})\cdot ds\cdot P \text{ in Pa(Torr)}$$

(1) E_e <150GeV, L_{BDS}=200m, ILC-Note-2007-016, L/Keller, T.Maruyama, and T.Markiewicz

N = 2.9 x10^7 ・P(Torr) / bunch = 2.2 x 10^5 ・P(P_a) /bunch

N = 0.29 / bunch at 10nTorr → 0.02 (0.04) by GEANT3 (TURTLE)

(2) IR within ± L* =4.5 m for Xray background in TPC ?

If k_{min} = 10keV and k_{max} = 0.26GeV ($m_e/k_{max} = R_{ex}/2L^*$, R_{ex}=1.75cm)

N = 1.5 x10^7 ・P(Torr) / bunch = 1.1 x 10^5 ・P(P_a) /bunch

N = 0.15 / bunch at 10nTorr

But, X-rays much go through the beam pipe, so they should be irrelevant .

(a) (b)

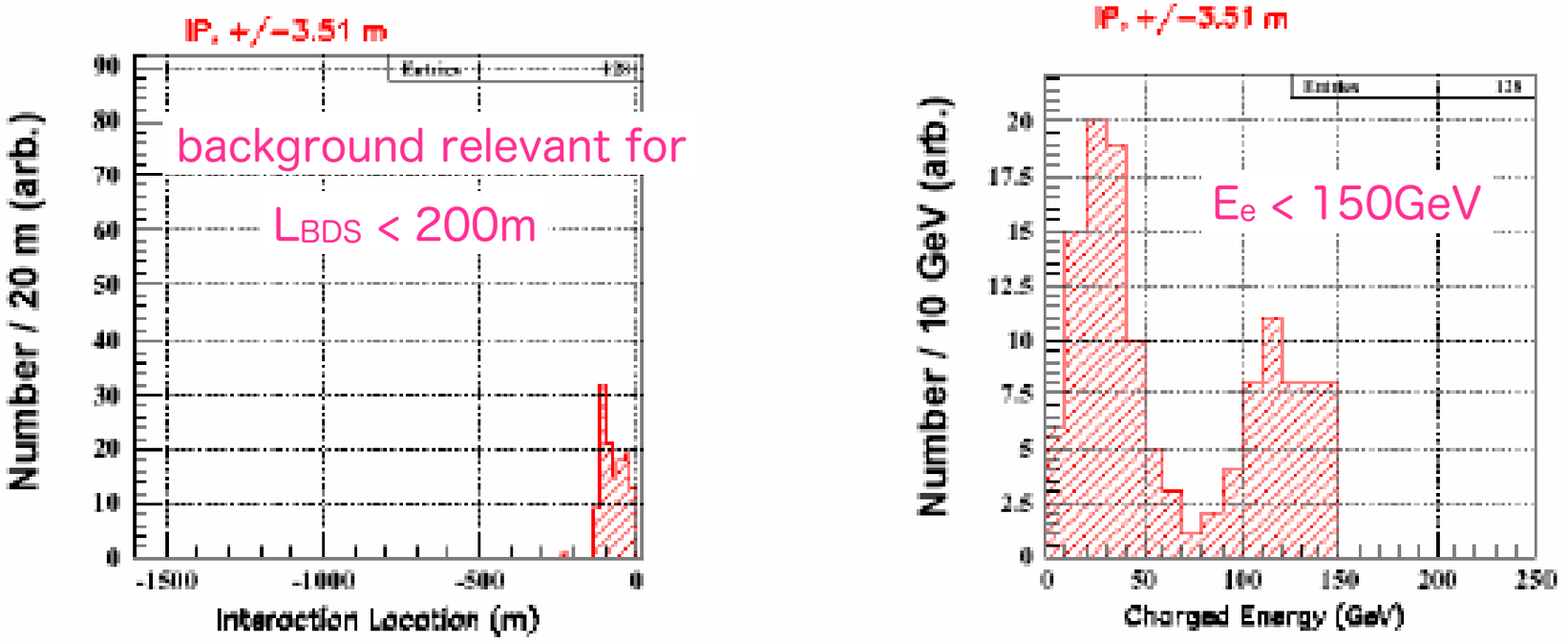

L/Keller, T.Maruyama, and T.Markiewicz
ILC-Note-2007-016

E_b = 250GeV

Figure 5. Points of origin (a) and energies (b) of bremsstrahlung interactions for those which hit within the drift section +/-3.51 m of the IP.

Summary of Hits/bunch and Hits/160 bunches (TPC) – both beams, 10 nTorr

Hits/bunch Hits/160 bunches (TPC)

Hit Location	GEANT3 Beam-gas brem (charged)	TURTLE Beam-gas brem (charged)		TURTLE Beam-gas brem (photons)		TURTLE Coulomb (charged)	
	Hits	Hits	<E>	Hits	<E>	Hits	<E>
FD Prot. Coll. |x| > 0.74 cm |y| > 0.45 cm	0.22 35	0.17 27	235 GeV	0.056 9.0	~50 GeV	0.009 1.4	250 GeV
Inside F.D. (QF1 to QD0)	0.014 2.2	0.006 1.0	~100 GeV	0	-	0	-
IP region (± 3.5 m) (R > 1 cm at Z = 3.5 m)	0.04 6.4	0.02 3.2	~100 GeV	0	-	0	-

Assuming ,
P_{BDS} = 10nTorr (10^{-6}Pa)

Table 1. Summary of GEANT3 and TURTLE simulations of BGB and coulomb single-scatters resulting in hits on apertures in the IP region for both beams and 10 nTorr. The upper (blue) entries are Hits/bunch; the lower (red) entries have been multiplied by 160.

Update on Conclusion 1

Track those 0.02-0.04 particles/BX in the SiD detector.

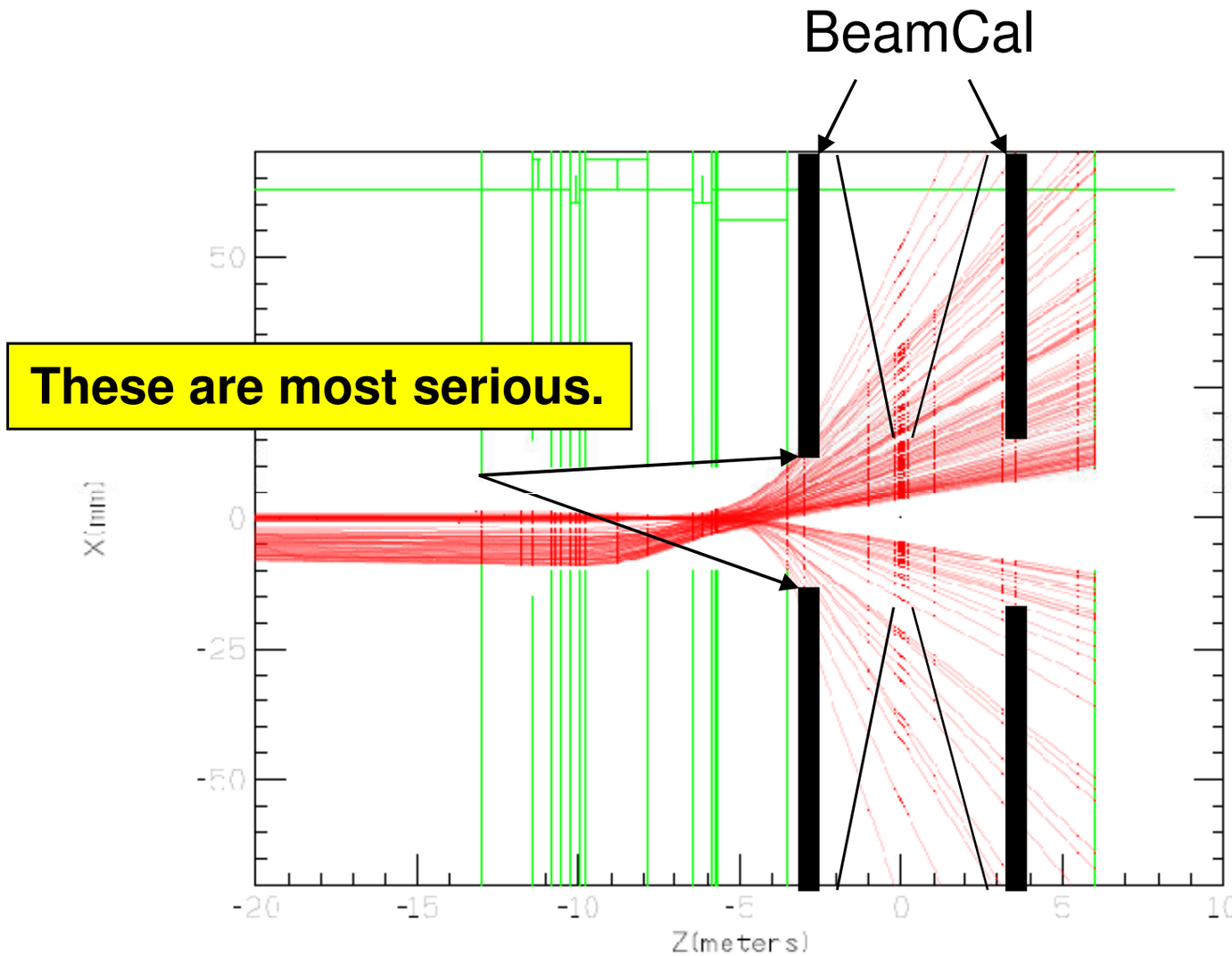

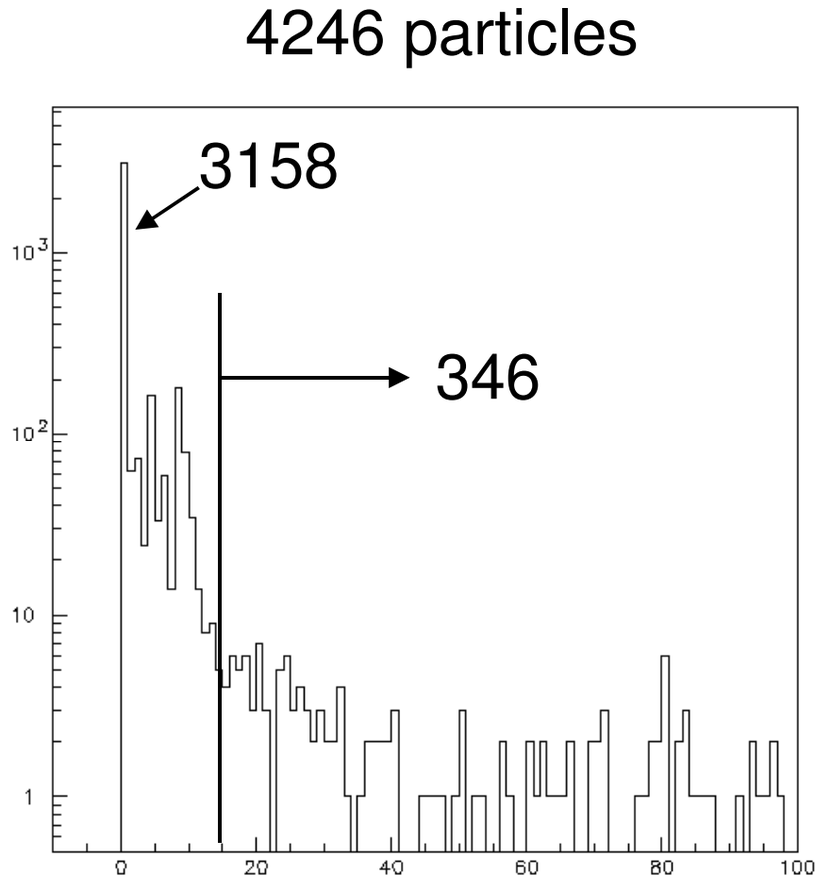

- NH = 0: 3158/4246 = 74%
- NH ≤ 15: 742/4246 = 17%
- NH > 15: 346/4246 = 8%

Only 10% of particles would generate significant number of hits.

→ 10 nTorr is acceptable.

Halo Collimation Systems

Betatron COLL SP2 & SP4

Energy COLL SPEX

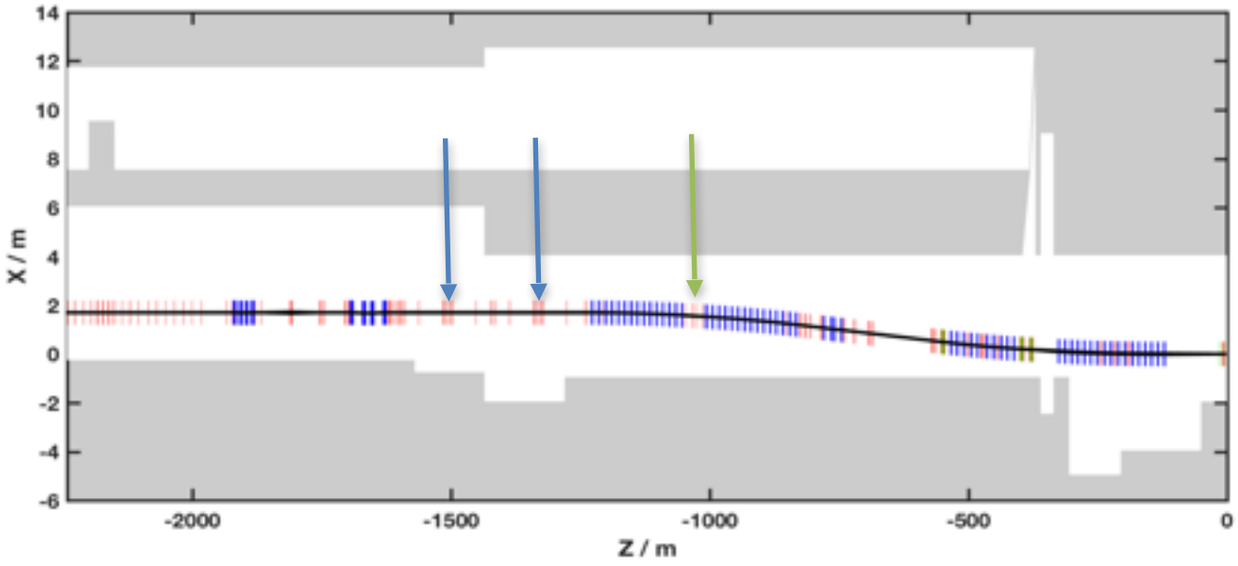

Betatron COLL SP2 & SP4 Energy COLL SPEX

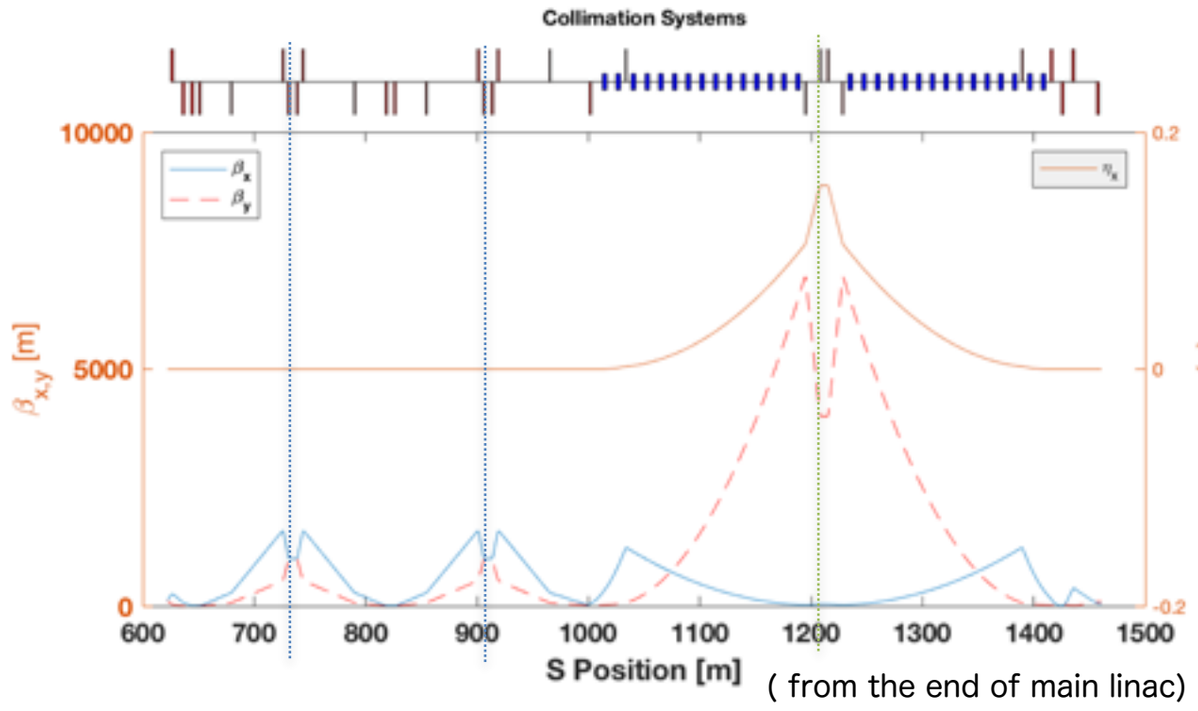

(from the end of main linac)

- Primary spoilers & absorbers source of muons in BDS
- Collimation apertures set to protect IR region from SR
  - Calculated from 6d particle tracking
  - Collimation types and settings recorded in BDS decks in ILC2015b

IR SR Fan in x-z plane

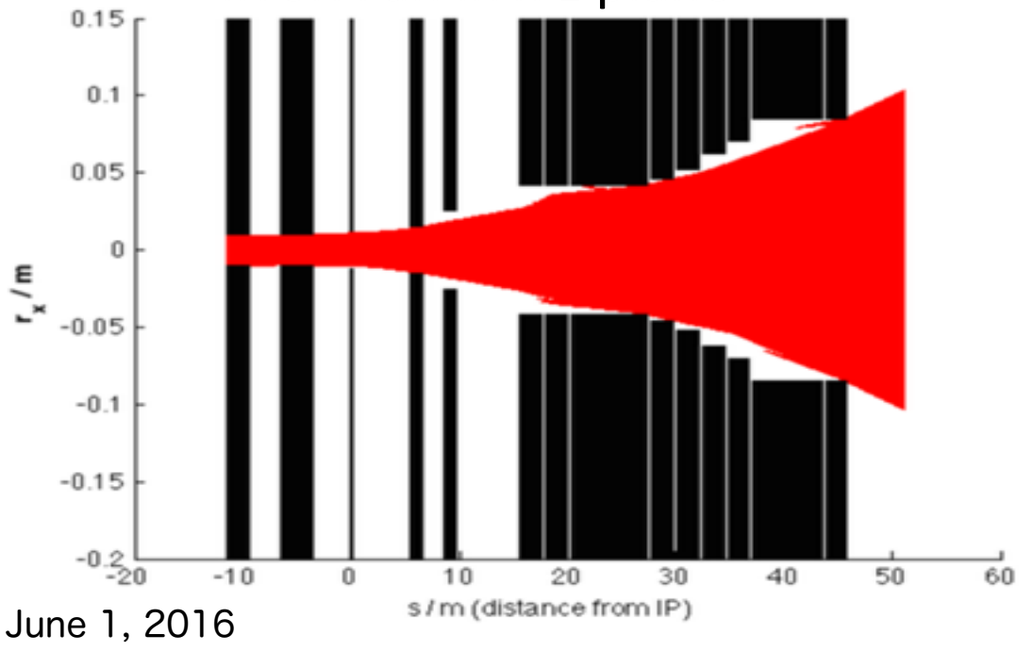

Table 1: ILC BDS adjustable jaw collimators

Device	Absorber (cm) material		Power (kW)	Full gap (mm) min, max
SPEX	3.6, Ti	1r.l.	0.01	1, 10
SP1–5	2.1, Ti	0.6 r.l.	0.01	1, 10
AB2–5	42.9, Cu	30 r.l.	1–20	0, 10
ABE	10.5, W	30 r.l.	0.1	0, 10
MSK1	10.5, W	30 r.l.	0.01	NA
MSK2	10.5, W	30 r.l.	0.01	NA

Collimator

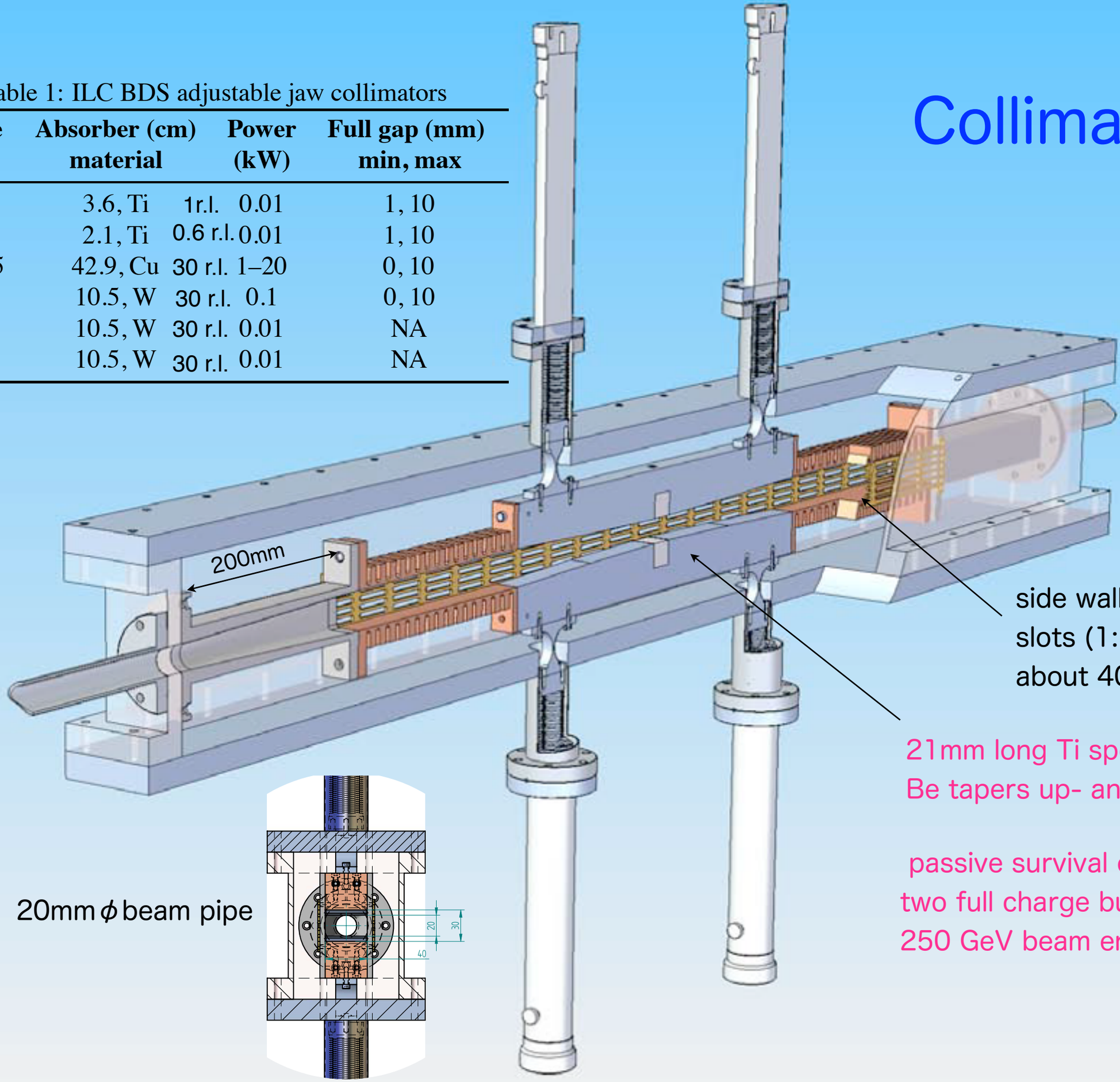

side walls with pumping slots (1:1 aspect ratio, about 40% transparency)

21mm long Ti spoiler block with Be tapers up- and downstream

passive survival of spoilers up to two full charge bunch impacts at 250 GeV beam energy

20mm ϕ beam pipe

Muons from the collimation section

The beam halo can be collimated by the collimators, where electromagnetic showers are generated in the absorbers. At the same time, muon pairs (μ^+, μ^-) are produced in the showers because the incident electron (positron) energy is large compared with the muon mass.

Roughly estimated production rate is

$$N_\mu = 3.9 \sim 2.3 \times 10^{-4} \left(\frac{E_{beam}(\mathrm{GeV})}{250} \right) \quad \text{for } E_{\mu^\pm} > 2 \sim 5\mathrm{GeV}$$

So the total number of muons are estimated to be produced for 0.1% beam halo as follows;

$$7.8 \sim 4.6 \times 10^3 / \text{bunch crossing}$$

Question : How many muons can be tolerable in the detector ?

Question : How do we suppress the muons if not tolerable ?

Muon walls

- Purpose:
  - **Personnel Protection: Limit dose rates in IR when beam sent to the tune-up beam dump**
  - **Physics: Reduce the muon background in the detectors**

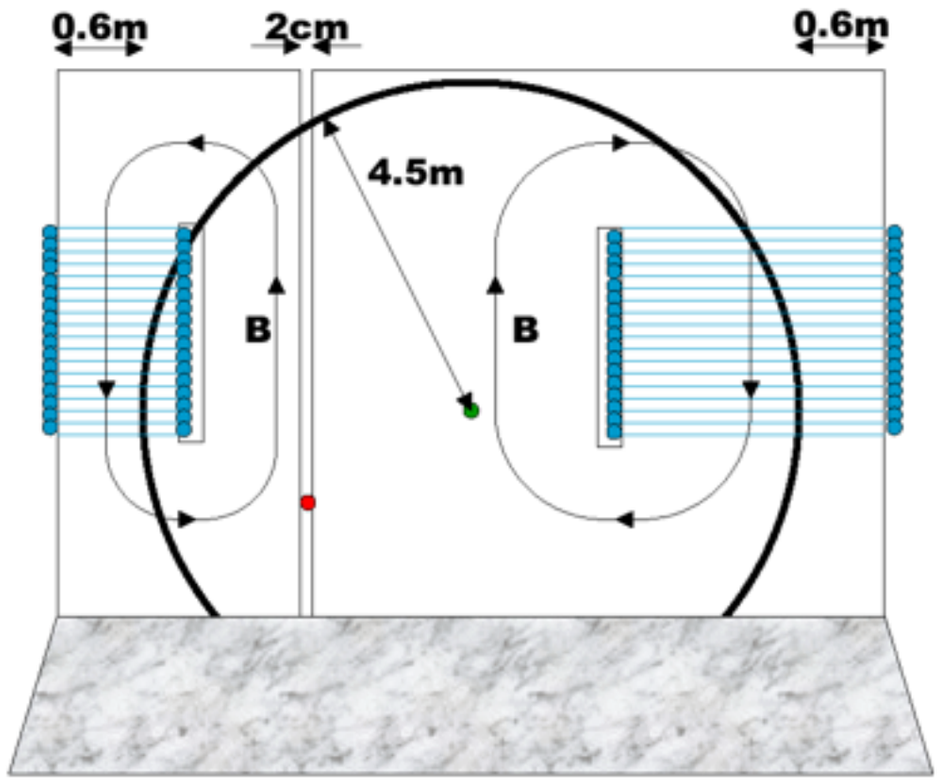

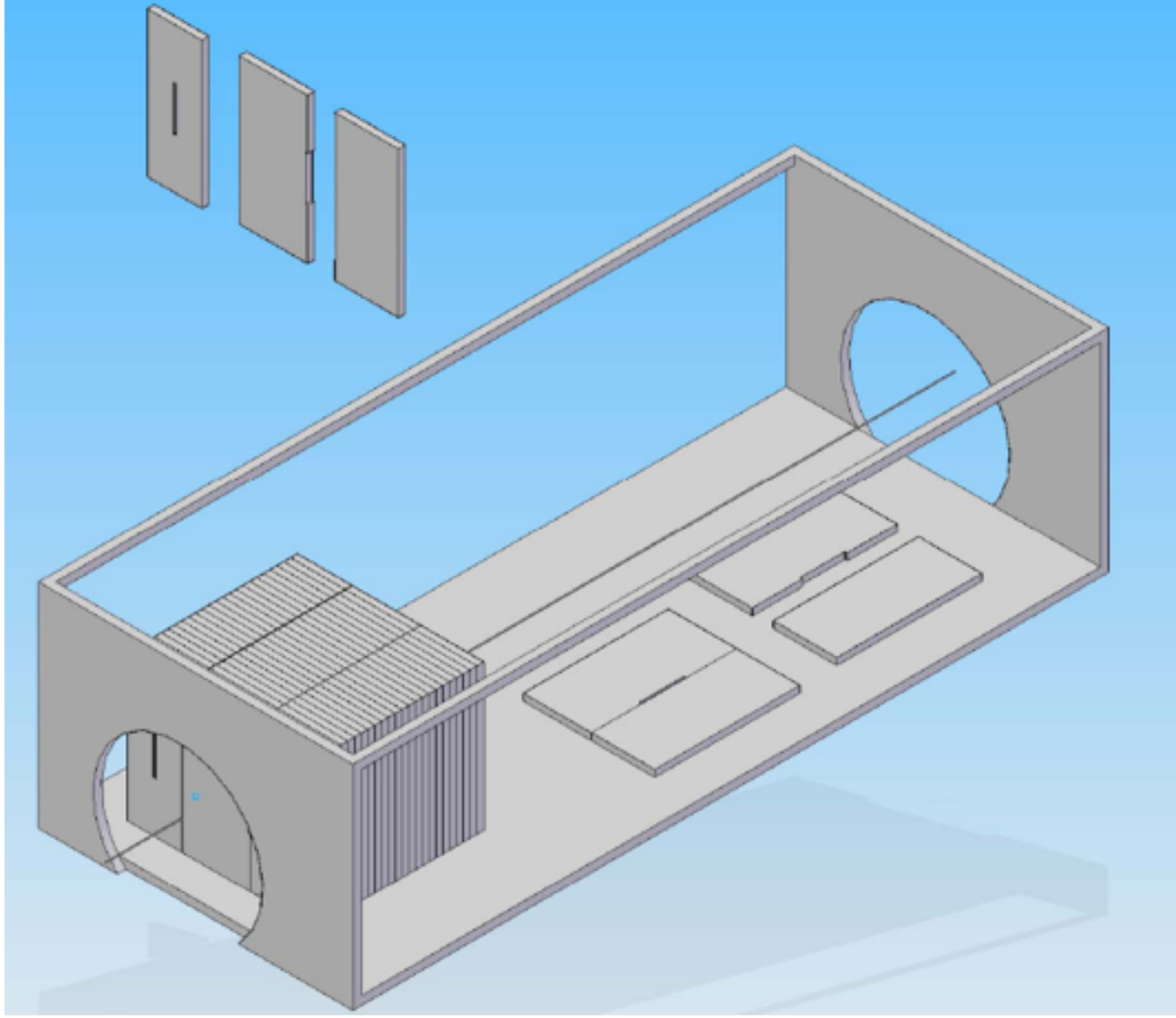

5m muon wall installed initially

If muon background measured too high, the 5m wall can be lengthened to 18m and additional 9m wall installed (Local toroids could be used also)

Muon Shielding – Toroid Spoilers

5 muon spoilers at z locations from IP:

- 800 m
- 973 m
- 1143 m
- 1231 m
- 1370 m

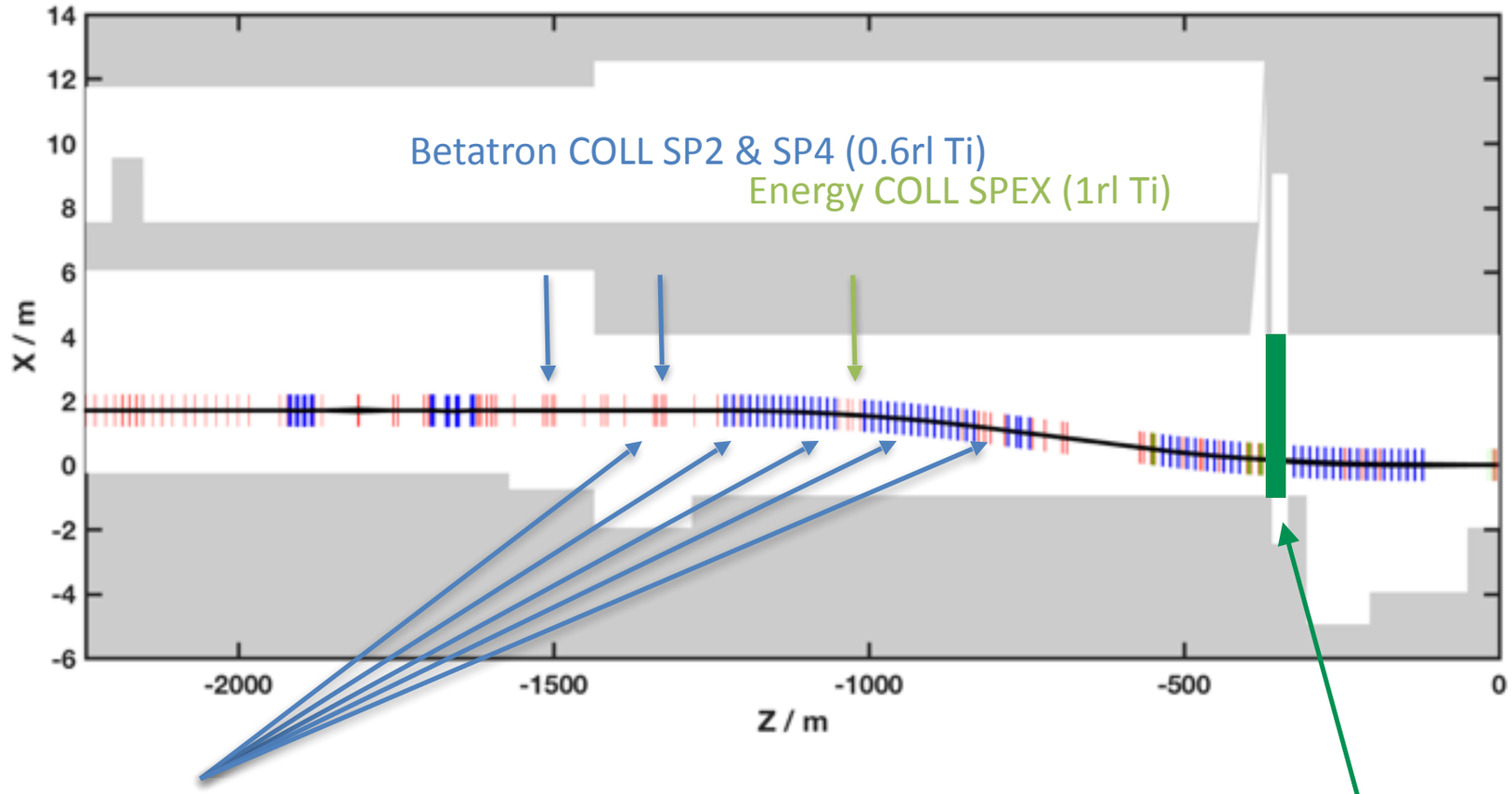

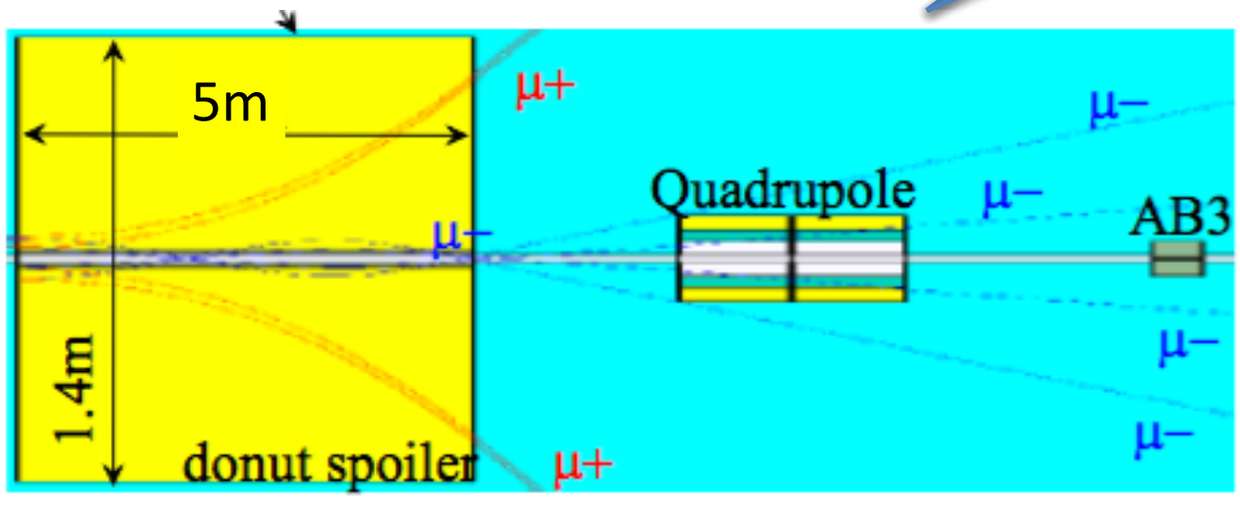

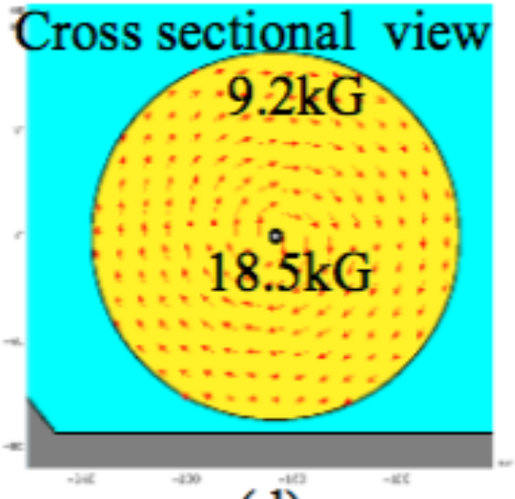

Muon Tracking

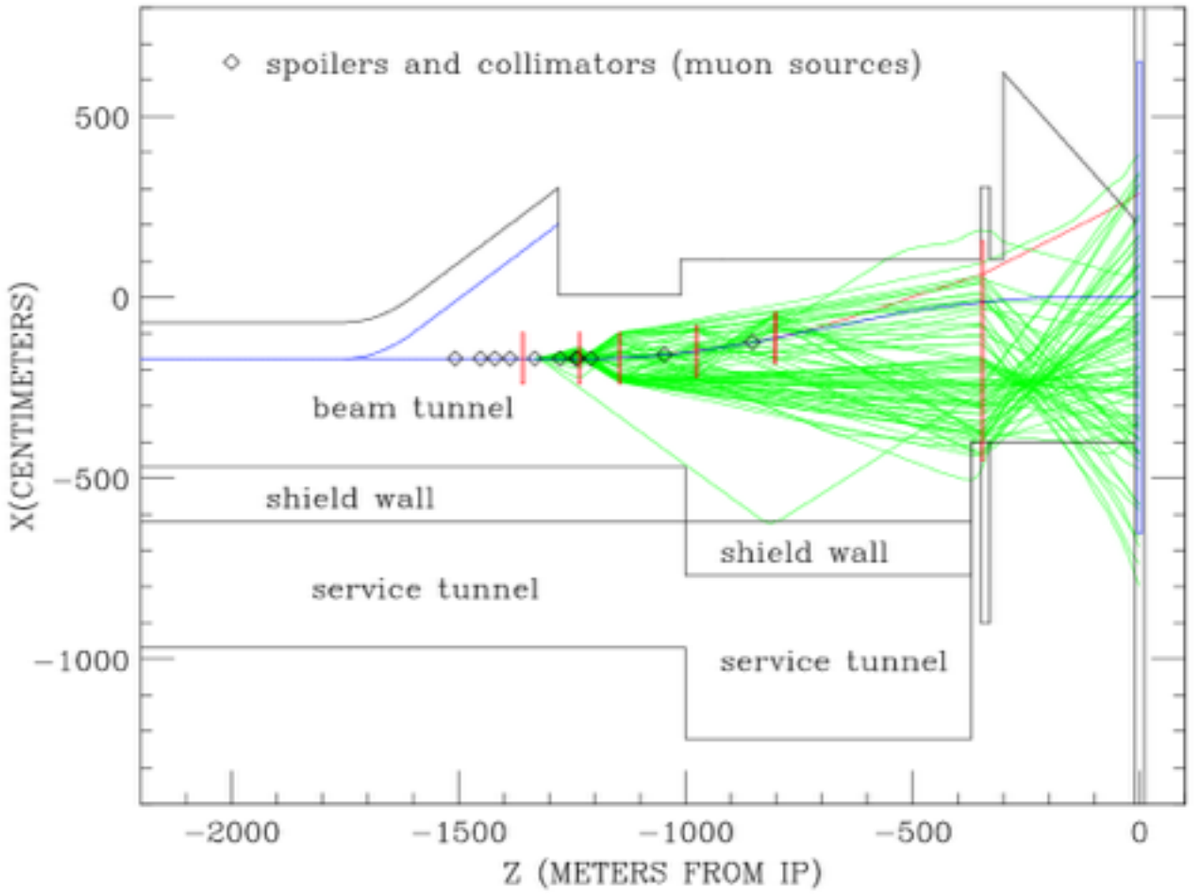

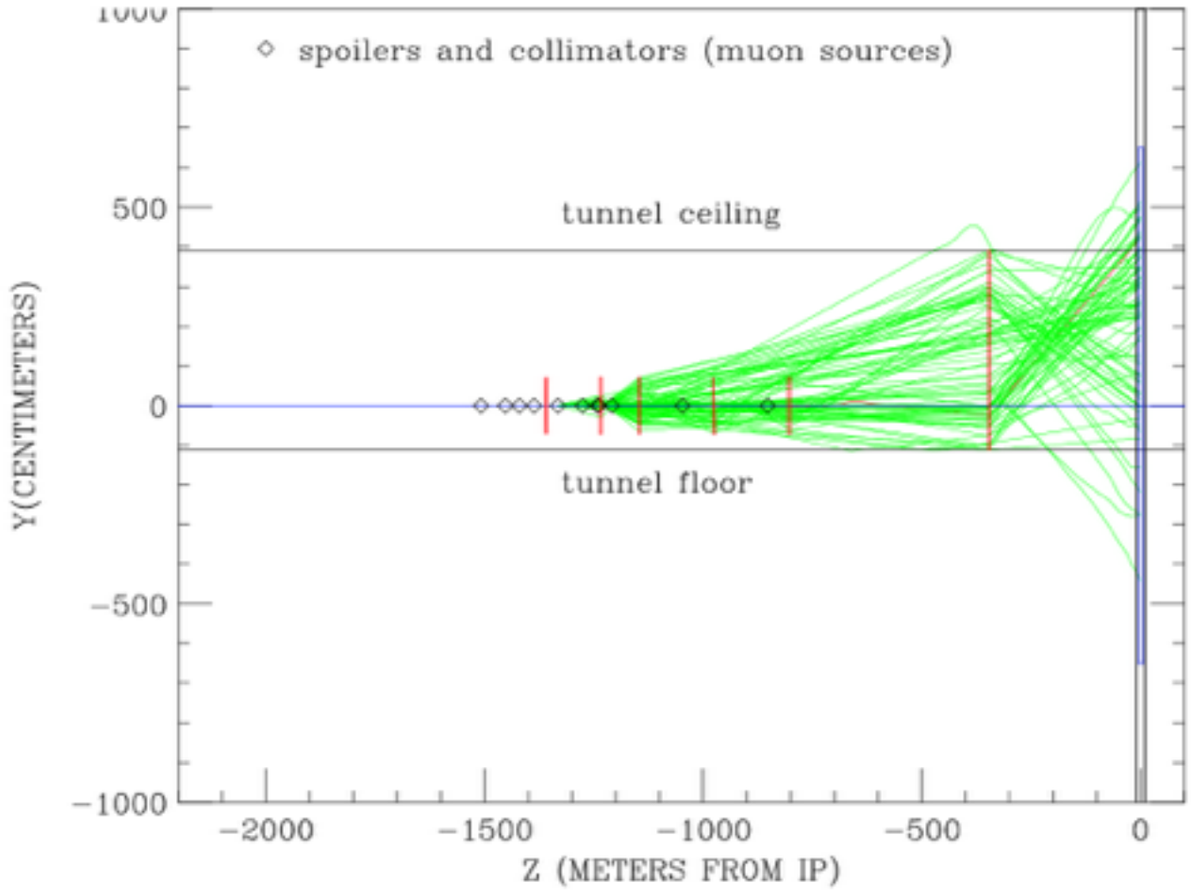

- Spoilers scatter one charge sign of muon preferentially.

Calculated Muon Rates at Detector

Tunnel Condition	R < 6.5 m (rate/bunch crossing)		R < 2.5 m (rate/bunch crossing)	
	GEANT4	*MUCARLO*	*GEANT4*	*MUCARLO*
No Spoilers	39.4	130	20.5	40
5 μ Spoilers	2.8	4.3	1.4	2.0
5 μ Spoilers + 5m Wall	--	0.6	--	0.1

- Total muon rates (from e- and e+ BDS sides) per bunch crossing
- Halo interception rate used = 0.1 % of main beam charge
- MUCARLO predicts more muons than GEANT4, mainly from d/s SPEX source. MUCARLO uses more generic magnet model, but uses much higher statistics and semi-analytic model for muon production.
  - 60k MUCARLO IP hitting mu tracks for 5 spoiler case compared with ~150 (from 500k generated) for GEANT4
  - Increased stats for GEANT4 model requires more work on process biasing and parallelization of muon tracking code

WIRED4 event display - 5 Spoilers

1 train's worth of muons ($\sim$ 2961 muons) **from the positron line only**:

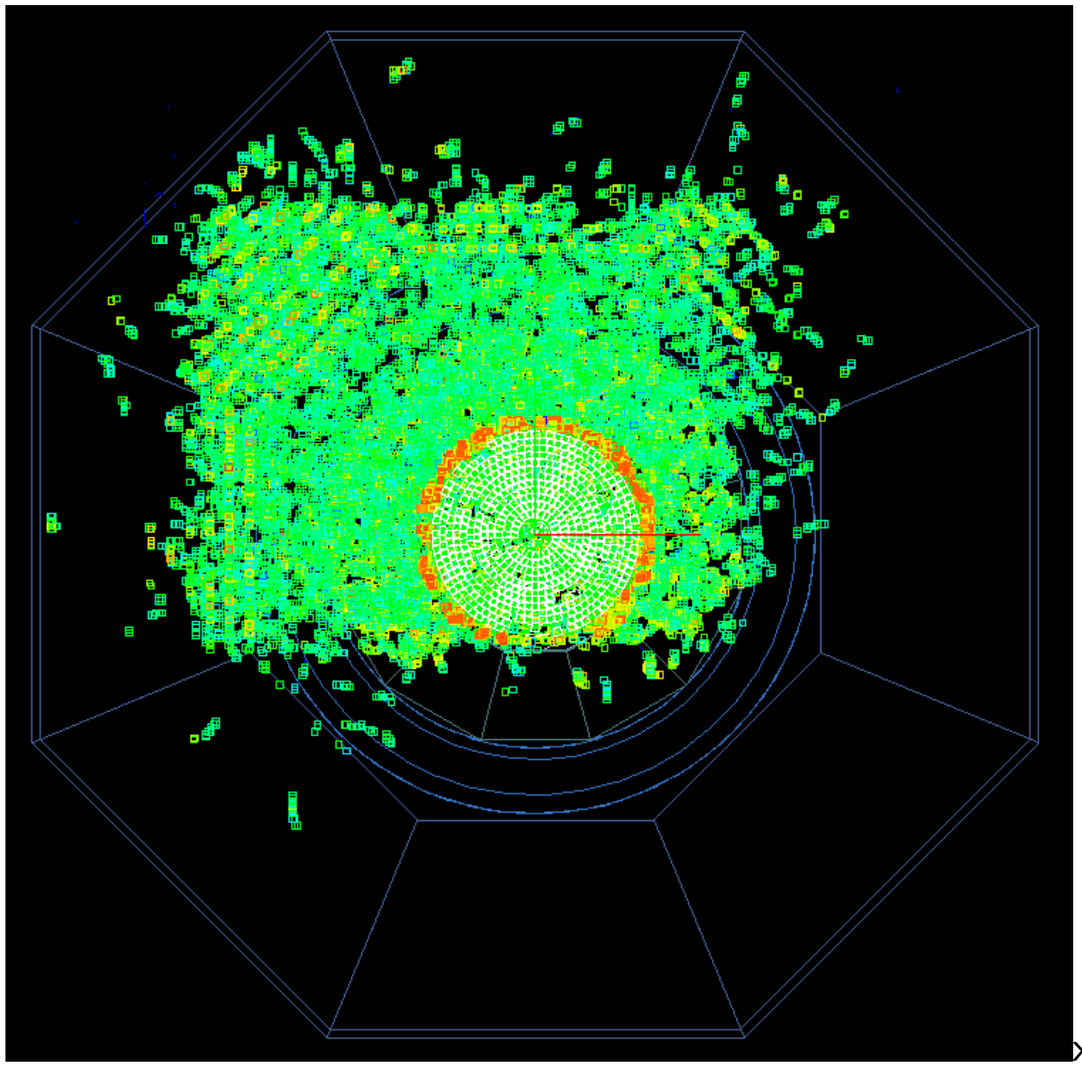

xy-view

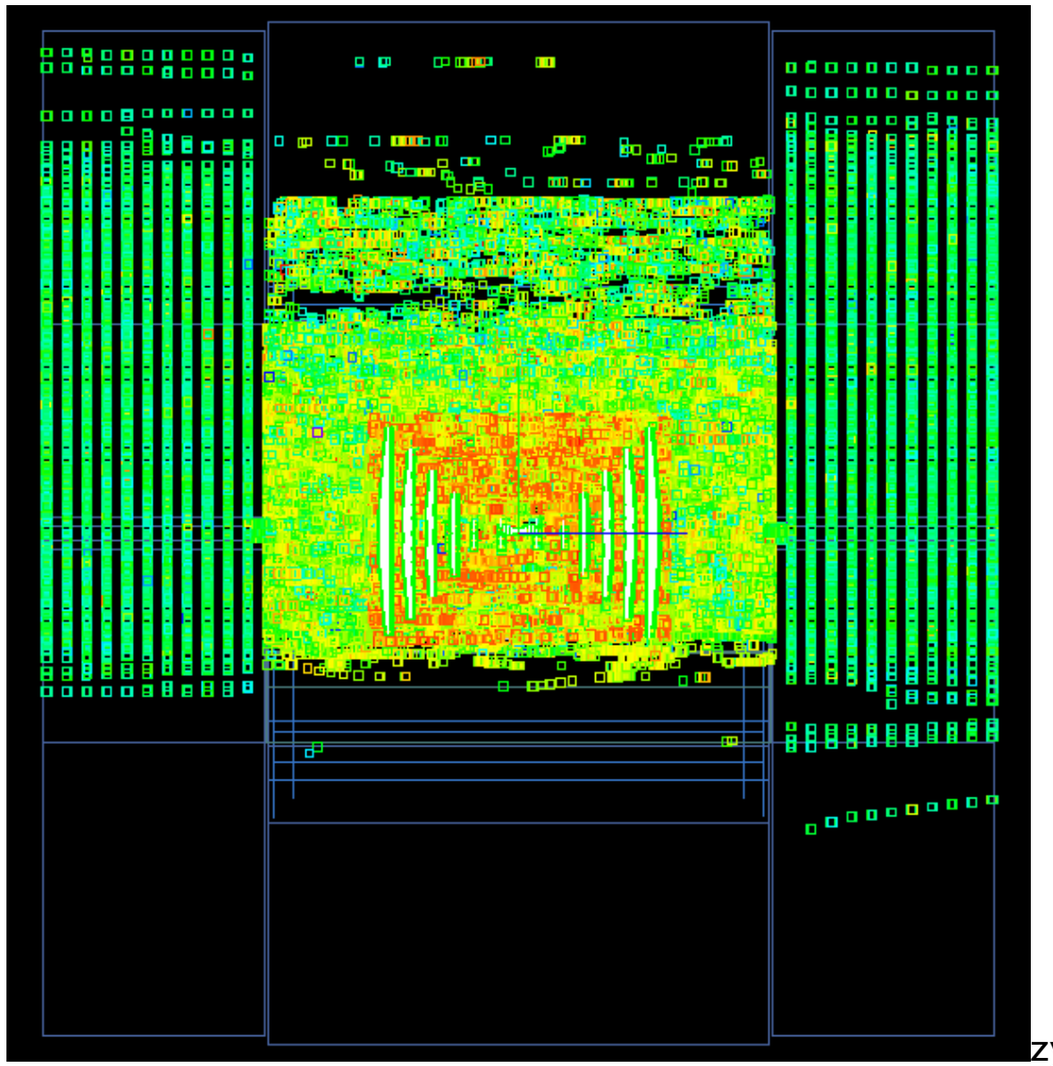

zy-view

Together with the muons from the e^- line, there will be $\sim$ **5600 muons per train in the '5 Spoilers' scenario**.

The spatial distribution is due to the tunnel shape and its shielding effects.

Muon Attenuator

E.A.Kushnirenko, LC92

(with 120m length at JLC study)

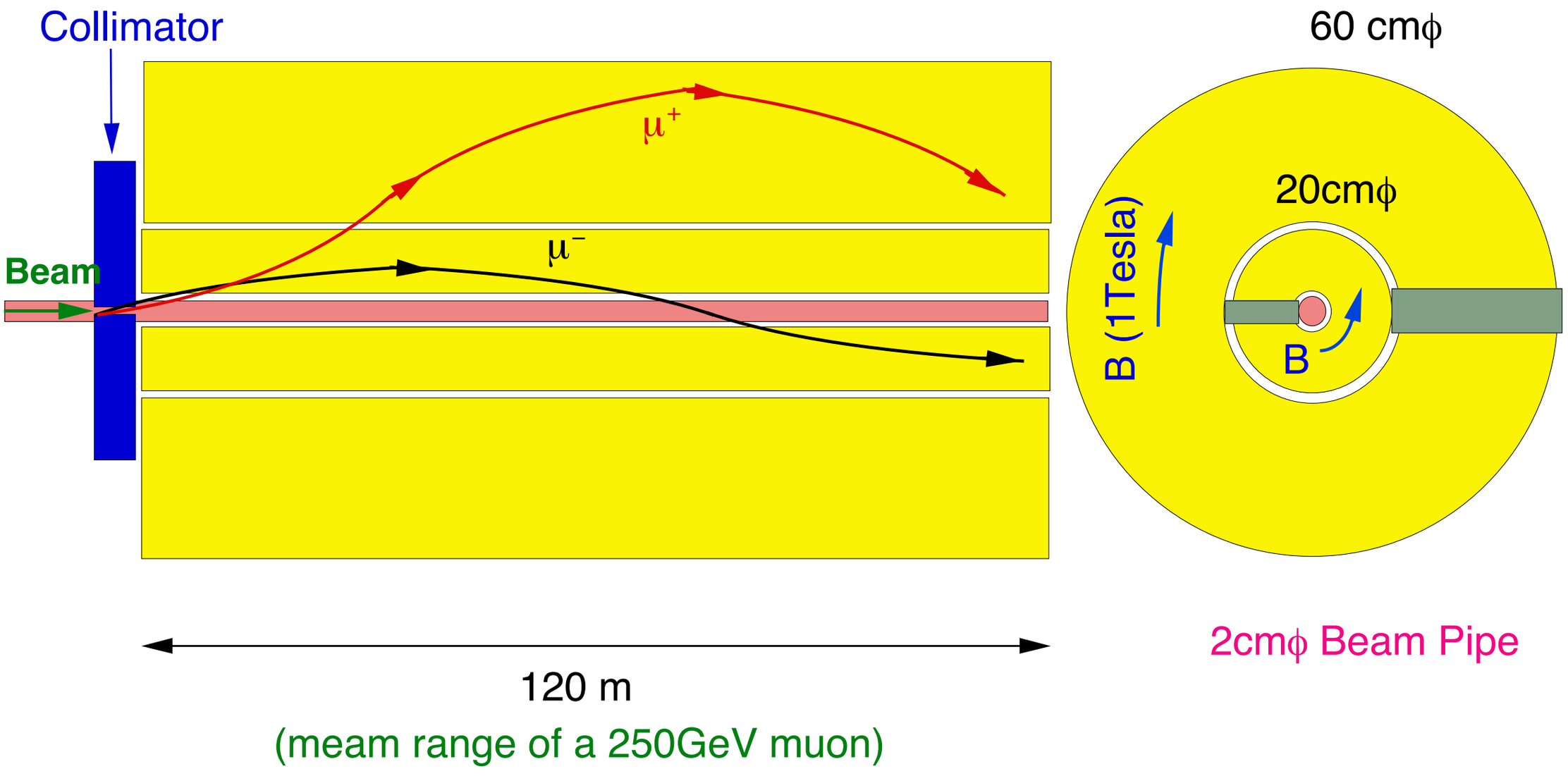

Suppression of muons = 10^{-3}~10^{-4} w.r.t. “no-shield case”

Luminosity degradation due to the collimators

ILC-TDR : collimation depth = $9\sigma_x$ x $65\sigma_y$, $\Delta\varepsilon_{x/y}/\varepsilon_{x/y}$=0.08%/4.4%

1. Collimation depth ($C_{dep,y}$), amplification(A_y) by wakefield and emittance growth

$$C_{dep,y} = \frac{\theta_y^{max}}{\sigma_y^{*\prime} \cdot (\text{safety factor})}$$

ILC-TDR

→ 34.6(y), 6.6(x)@Eb=100GeV

$$A_y = 0.0482\gamma^{-1}C_{dep,y}^{-1.5}\varepsilon_y^{-0.75}$$

→ 4.4 55(y), 15(x)@CLIC

$$\text{Emittance growth in y} = (0.4 \cdot \text{Jitter}_{train} \cdot A_y)^2$$

→ 0.12

Values in ILC-TDR (CLIC-CDR) ;

θ_y^{max} = 1 mrad, e.g. no syn.rad hit 20mmϕ beam pipe for ±10m around IP

(safety factor) = 1.5

Jitter_{train} = 0.2 (0.2), scaled by beam size with “FONT” feedback

note: emittance growth ∝ Jitter^2

Jitter_{bunch} = 0.1 (0.05), scaled by beam size

2. Bunch-to-bunch jitter effect on the luminosity

$$\sigma_{bunch} = \text{Jitter}_{bunch} \cdot \sqrt{1 + A_y^2}$$

→ 0.45

$$\mathcal{L}_{bunch} - \Delta\mathcal{L}_{bunch} = \exp\left(-\sigma_{bunch}^2/4\right)$$

→ 0.95 ~0.95

3. Energy jitter at the collimators

1% jitter → 2.2% emittance growth

ILC

TDR : Assume gamepsX,Y incoming already include emittance growth due to wakefields etc. and no effect of b-b jitter

	Nominal 200	Nominal 250	Nominal 350	Nominal 500	HL 500	Nominal 1000
Ecms [GeV]	200	250	350	500	500	1000
gamma	1.96E+05	2.45E+05	3.42E+05	4.89E+05	4.89E+05	9.78E+05
N e-	2.00E+10	2.00E+10	2.00E+10	2.00E+10	2.00E+10	1.74E+10
N e+	2.00E+10	2.00E+10	2.00E+10	2.00E+10	2.00E+10	1.74E+10
nb	1312	1312	1312	1312	2625	2450
Tsep [ns]	554.0	554.0	554.0	554.0	366.0	366.0
Iave in train [A] e-	0.0058	0.0058	0.0058	0.0058	0.0087	0.0076
f	5	5	5	5	5	4
Pb [W] e-	2.10E+06	2.63E+06	3.68E+06	5.25E+06	1.05E+07	1.37E+07
Electron polarization, %	80	80	80	80	80	80
Positron polarization, %	31	31	29	22	22	30
Electron E-spread, %	0.220	0.190	0.158	0.125	0.125	0.083
Positron E-spread, %	0.170	0.150	0.100	0.065	0.065	0.043
IP Parameters						
gamepsX incoming	1.00E-05	1.00E-05	1.00E-05	1.00E-05	1.00E-05	1.00E-05
gamepsY incoming	3.50E-08	3.50E-08	3.50E-08	3.50E-08	3.50E-08	3.00E-08
bx	1.60E-02	1.30E-02	1.60E-02	1.10E-02	1.10E-02	1.10E-02
by	3.40E-04	4.10E-04	3.40E-04	4.80E-04	4.80E-04	2.30E-04
sigx_geom	9.04E-07	7.29E-07	6.84E-07	4.74E-07	4.74E-07	3.35E-07
sigy_geom	7.8E-09	7.7E-09	5.9E-09	5.9E-09	5.9E-09	2.7E-09
sigx_effective	9.04E-07	7.29E-07	6.84E-07	4.74E-07	4.74E-07	3.35E-07
sigy_effective	7.8E-09	7.7E-09	5.9E-09	5.9E-09	5.9E-09	2.7E-09
sigxp	5.65E-05	5.61E-05	4.27E-05	4.31E-05	4.31E-05	3.05E-05
sigyp	2.29E-05	1.87E-05	1.73E-05	1.22E-05	1.22E-05	1.15E-05
gamepsX effective	1.00E-05	1.00E-05	1.00E-05	1.00E-05	1.00E-05	1.00E-05
gamepsY effective	3.50E-08	3.50E-08	3.50E-08	3.50E-08	3.50E-08	3.00E-08
L* [m]	3.50	3.50	3.50	3.50	3.50	3.50
Max divergence X	4.00E-04	4.00E-04	4.00E-04	4.00E-04	4.00E-04	4.00E-04
Max divergence Y	1.00E-03	1.00E-03	1.00E-03	1.00E-03	1.00E-03	1.00E-03
Collim safety factor	1.5	1.5	1.5	1.5	1.5	1.5
Coll depth X	6.6	6.6	6.2	6.2	6.2	8.7
Coll depth Y	34.6	42.5	38.5	54.6	54.6	57.7
BDS Inc. t-t jitter, sigma	0.2	0.2	0.2	0.2	0.2	0.2
BDS Inc. b-b jitter, sigma	0.1	0.1	0.1	0.1	0.1	0.1
Coll wake kick power xi, K~1/r^xi/ga	1.5	1.5	1.5	1.5	1.5	1.5
Coll wake Ay	4.4	3.1	3.3	1.8	1.8	1.5
Coll wake Y-emit growth	**0.124**	**0.060**	**0.068**	**0.020**	**0.020**	**0.015**
Increased b-b jitter, sigma	0.451	0.322	0.341	0.203	0.203	0.183
Lum reduct due to b-b jitter	**0.950**	**0.974**	**0.971**	**0.990**	**0.990**	**0.992**
sigz	3.00E-04	3.00E-04	3.00E-04	3.00E-04	3.00E-04	3.00E-04
Dx e+	0.2	0.3	0.2	0.3	0.3	0.3
Dy e+	24.6	24.8	24.6	24.9	24.9	33.9
Theta0	6.39E-04	6.33E-04	4.83E-04	4.86E-04	4.86E-04	3.00E-04
xp_max_out	4.89E-04	4.84E-04	3.70E-04	3.71E-04	3.71E-04	2.30E-04
yp_max_out	1.09E-04	1.07E-04	8.21E-05	8.18E-05	8.18E-05	3.90E-05
Uave e+	0.013	0.021	0.031	0.063	0.063	0.156
Umax e+						
delta_B	0.0055	0.0100	0.0151	0.0389	0.0389	0.0910

Split FD at E_{cm}=200 and 250GeV

CLIC

15 (x)

55 (y)

Collimation depth

emittance growth

Lum loss 5%

Lum degradation

P_Beamstrahlung [W]	1.15E+04	2.62E+04	5.55E+04	2.04E+05	4.09E+05	1.24E+06
ngamma e+	0.94	1.15	1.22	1.71	1.71	2.00
Hdx	1.1	1.1	1.1	1.2	1.2	1.1
Hdy	4.5	5.4	4.5	6.1	6.1	3.3
Hd	1.7	1.8	1.7	2.0	2.0	1.6
Geo Lum (cm-2 s-1)	2.96E+33	3.74E+33	5.18E+33	7.51E+33	1.50E+34	2.65E+34
Lum. dil.	***0.950***	***0.974***	***0.971***	***0.990***	***0.990***	***0.992***
Lum. (cm-2 s-1)	**5.02E+33**	**6.85E+33**	**8.79E+33**	**1.47E+34**	**2.95E+34**	**4.13E+34**
Lum/bc	*7.66E+29*	*1.04E+30*	*1.34E+30*	*2.25E+30*	*2.25E+30*	*4.21E+30*
Coherent pairs/bc	5.36E-167	4.31E-105	1.15E-67	1.00E-28	1.00E-28	9.82E-07
Inc. pairs/bc (LL)	1.39E+04	2.00E+04	2.80E+04	5.12E+04	5.12E+04	1.13E+05
Inc. pairs/bc (BW)	1.63E+03	2.23E+03	2.05E+03	3.55E+03	3.55E+03	3.69E+03
Inc. pairs/bc (BH)	1.22E+05	1.81E+05	2.23E+05	4.33E+05	4.33E+05	7.80E+05
Inc. Pairs/bc (tot)	1.38E+05	2.04E+05	2.53E+05	4.88E+05	4.88E+05	8.97E+05
Caliculations by CAIN						
Lum. (cm-2 s-1)	5.08E+33	7.11E+33	8.90E+33	1.55E+34	3.10.E+34	3.54E+34
Lum. (cm-2 s-1) w/ waist shift	5.71E+33	7.85E+33	1.00E+34	1.68E+34	3.37.E+34	4.19E+34
Lum top 1% : L(0.01)/L	0.914	0.841	0.790	0.613	0.613	0.476
Lum top 1% w/ waist shift	0.911	0.840	0.784	0.612	0.612	0.463
Lum 1nm offsetY : L(1nm)/L	0.969	0.959	0.949	0.927	0.927	0.854
Lum 1nm offsetY w/ waist shift	0.959	0.952	0.937	0.916	0.916	0.828
energy loss	0.034	0.046	0.044	0.072	0.072	0.084
energy loss w/ waist shift	0.034	0.045	0.044	0.072	0.072	0.083
Inc. Pairs/bc (tot)	2.54E+04	4.17E+04	5.50E+04	1.23E+05	1.23.E+05	2.13E+05
Inc. Pairs/bc (tot) w/ waist shift	2.84E+04	4.45E+04	6.11E+04	1.30E+05	1.30.E+05	2.44E+05
Caliculations by GP						
Lum -ratio : analytic/GP	0.85	0.86	0.84	0.87	0.87	0.92
Date of run	25.Sep.12	25.Sep.12	25.Sep.12	25.Sep.12	25.Sep.12	25.Sep.12
Lum GP-beam-beam (cm-2 s-1)	5.89E+33	7.96E+33	1.04E+34	1.70E+34	3.40E+34	4.47E+34
Lum top 1% : L(0.01)/L	0.922	0.846	0.790	0.615	0.615	0.460
Lum(Ecms) /Lum (500GeV)	0.35	0.47	0.61	1.00	2.00	2.63
Ecms/500	0.4	0.5	0.7	1	1	2
relative to the scaled Lum	0.87	0.94	0.88	1.00	2.00	1.31
Inc. pairs/bc (LL)	18,811	25,793	34,409	111,658	223,316	101,258
Inc. pairs/bc (BW)	1,481	2,270	2,256	4,242	8,485	4,648
Inc. pairs/bc (BH)	20,974	35,687	49,000	111,658	223,316	218,083
Inc. Pairs/bc (tot)	41,266	63,751	85,666	227,558	455,117	323,989
energy loss	0.0060	0.0113	0.0165	0.0422	0.0422	0.0896
	Nominal 200	**Nominal 250**	**Nominal 350**	**Nominal 500**	**HL 500**	**Nominal 1000**

Backgrounds

IR

International Large Detector (ILD)

Detector solenoid : 3.5T

ILD is on purpose a large detector. At large radii particles within a jet are more separated, thus making it easier to measure them precisely. Having a large inner radius of the calorimeter does open the possibility to use a technology like the TPC as a central tracker. Last but not the least a large detector adapts more easily to higher energies of the collider than originally designed for.

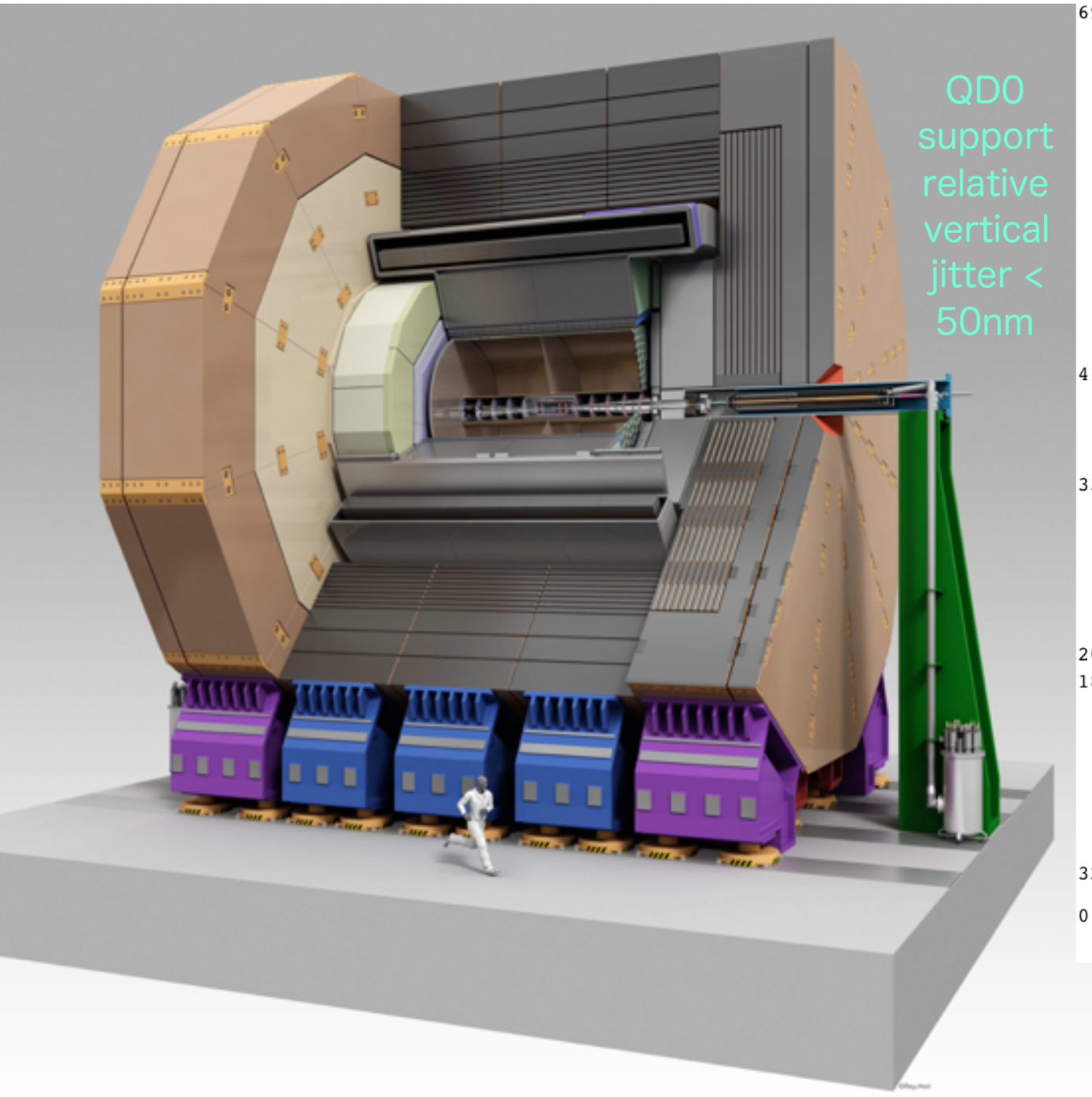

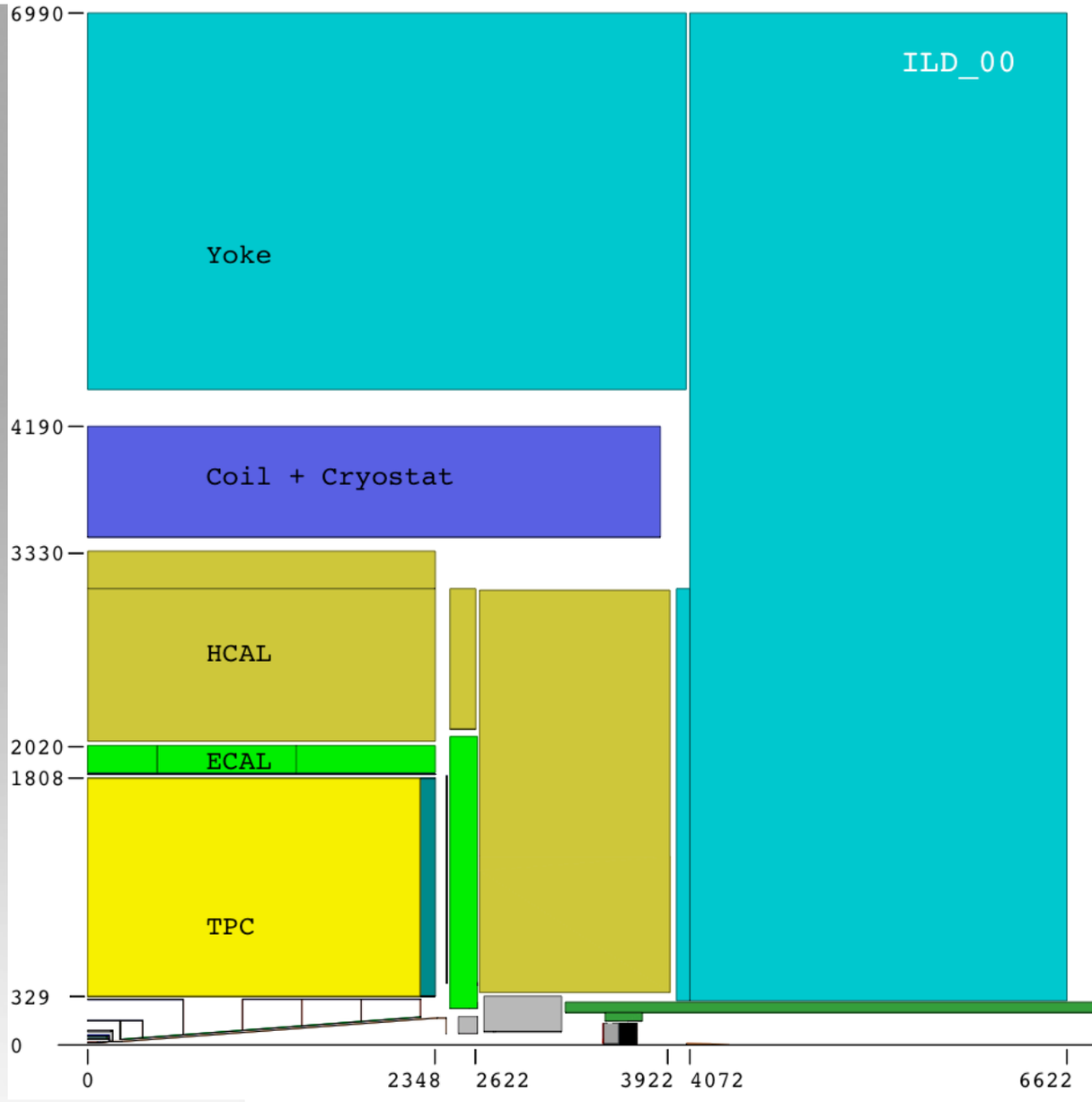

Forward Calorimeter System for MDI

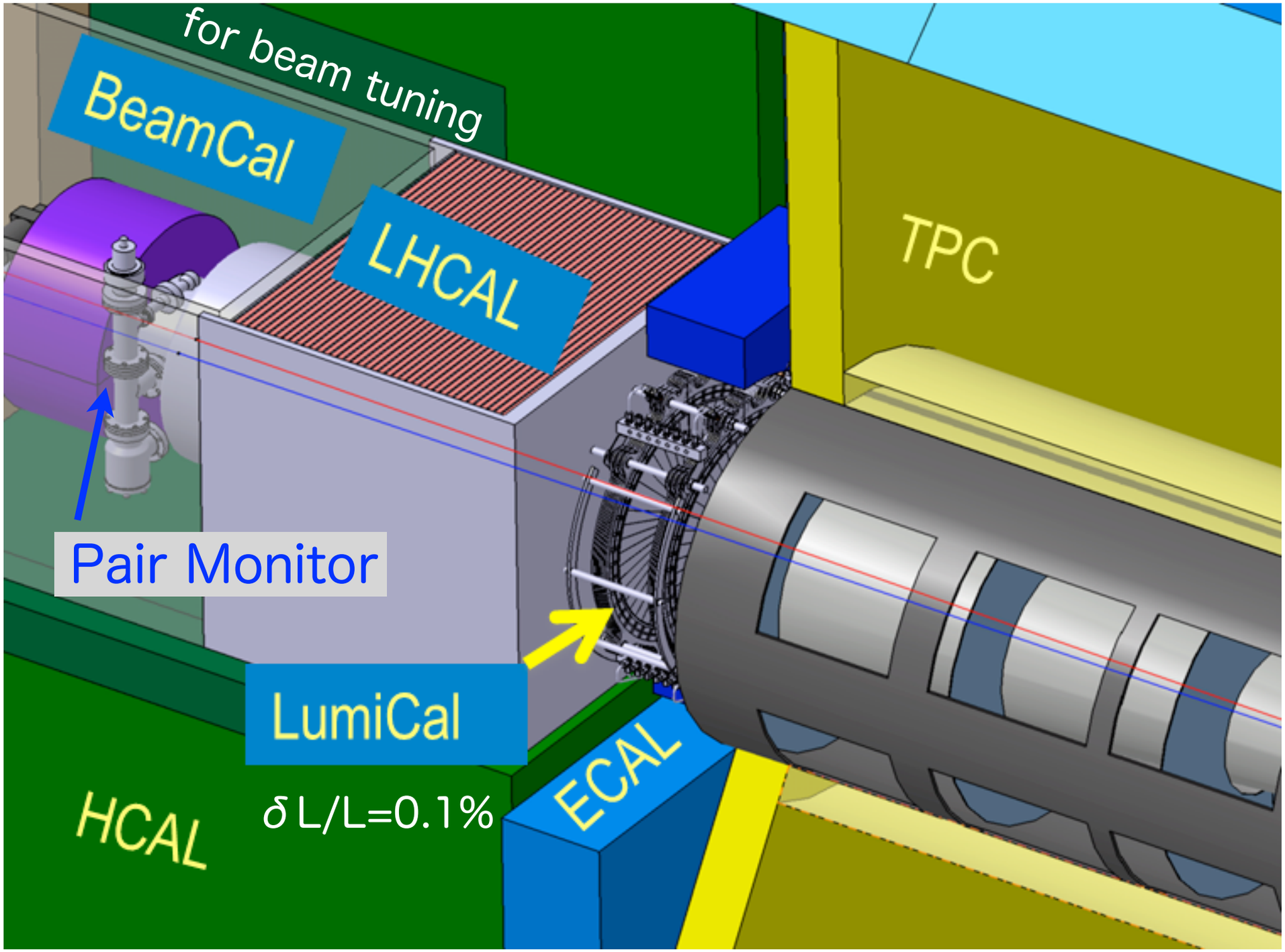

Silicon Detector (SID)

a powerful silicon pixel vertex detector, silicon tracking, silicon-tungsten electromagnetic calorimetry and highly segmented hadronic calorimetry.

Detector solenoid : 5T

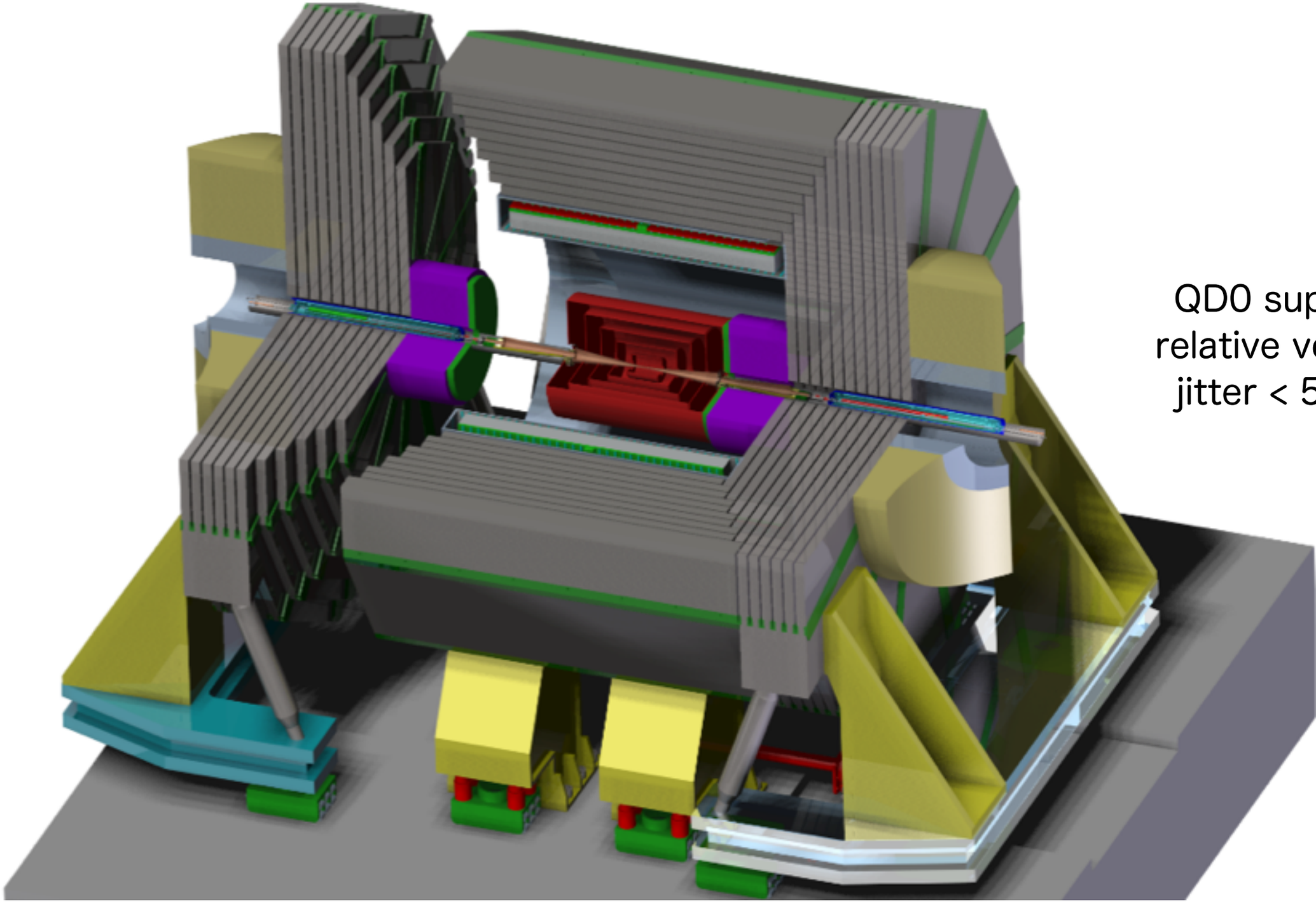

QD0 support relative vertical jitter < 50nm

SiD

A compact, cost-constrained detector

designed to make precision measurements and be sensitive to a wide range of new phenomena

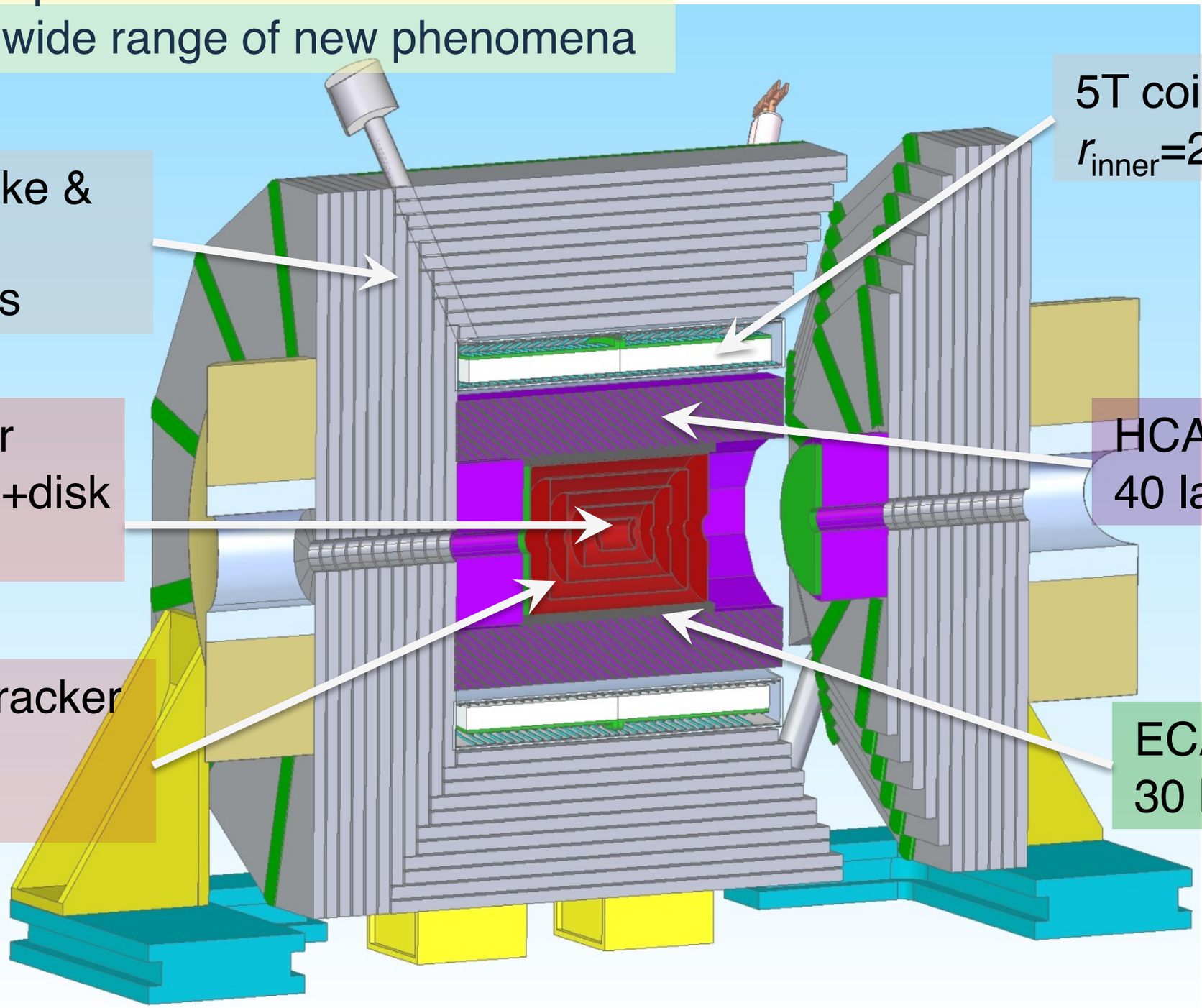

Post-CDR CLIC detector model

- Two detector models, CLIC_ILD and CLIC_SiD, were used in the CDR and for physics studies

- A new optimised model, **CLICdet**, has been developed for the next round of benchmark studies

- Implemented in simulation/ reconstruction software in DD4Hep (Detector Description for HEP)

- Public note under collaboration review at the moment

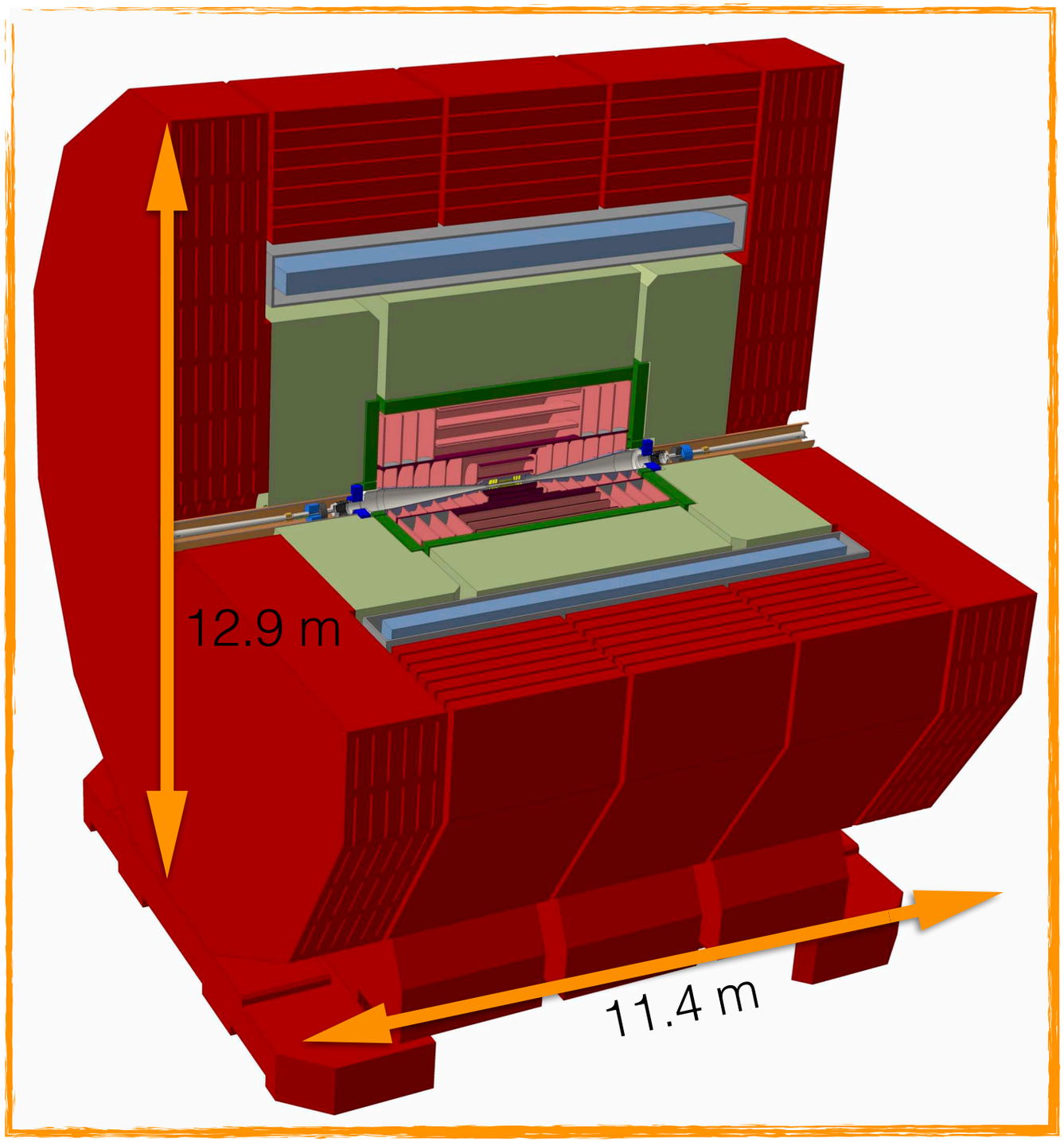

A single detector at CLIC

- Single detector
- All silicon tracker
- 4 Tesla magnet
- Return yoke:
  - Smaller outer radius due to less stringent requirements on stray fields
- Last quadrupole magnet (QD0) now outside of the detector at L* = 6 m allowed by the thinner yoke endcaps
  - Provides significantly better forward HCAL coverage

Concept	CLICdet	CLIC_ILD	CLIC_SiD
Vertex inner radius [mm]	31	31	27
Tracker technology	Silicon	TPC/Silicon	Silicon
Tracker half length [m]	2.2	2.3	1.5
Tracker outer radius [m]	1.5	1.8	1.3
ECAL barrel r_{min} [m]	1.5	1.8	1.3
ECAL barrel Δr [mm]	202	172	139
ECAL endcap z_{min} [m]	2.31	2.45	1.66
ECAL endcap Δz [mm]	202	172	139
HCAL absorber barrel / endcap	Fe / Fe	W / Fe	W / Fe
HCAL λ_I	7.5	7.5	7.5
HCAL barrel r_{min} [m]	1.74	2.06	1.45
HCAL barrel Δr [mm]	1590	1238	1177
HCAL endcap z_{min} [m]	2.45	2.65	1.80
HCAL endcap Δz [mm]	1590	1590	1595
Solenoid field [T]	4	4	5
Solenoid bore radius [m]	3.5	3.4	2.7
Solenoid length [m]	8.3	8.3	6.5
Overall height [m]	12.9	14.0	14.0
Overall length [m]	11.4	12.8	12.8
Overall weight [t]	8100	10800	12500

Backgrounds for experiments (2)

1. Incoherent low energy electron-positron pairs

They are produced by electromagnetic beam-beam interactions during collisions with beamstrahlung process. They are deflected into detectors by the strong magnetic field of oncoming beam. The rate is proportional to the luminosity, but the deflection depends on the beam parameters so that they are also used to estimate the beam parameters as online information to the accelerator operation.

2. Mini-jets

They are produced by “hadronic” interactions during collisions actually between real photons which have hadronic components consisting of vector mesons ρ, ω, ϕ etc. in the vector meson dominance model. The rate is proportional to the luminosity and becomes larger at the higher center-of-mass energy. The mini-jets may overlap with interesting physics events. So, an identification of interacting bunch is important to resolve such overlaps.

Beam-beam Interaction

Beam-beam Interactions

electron beam

positron beam with
a cylindrical shape

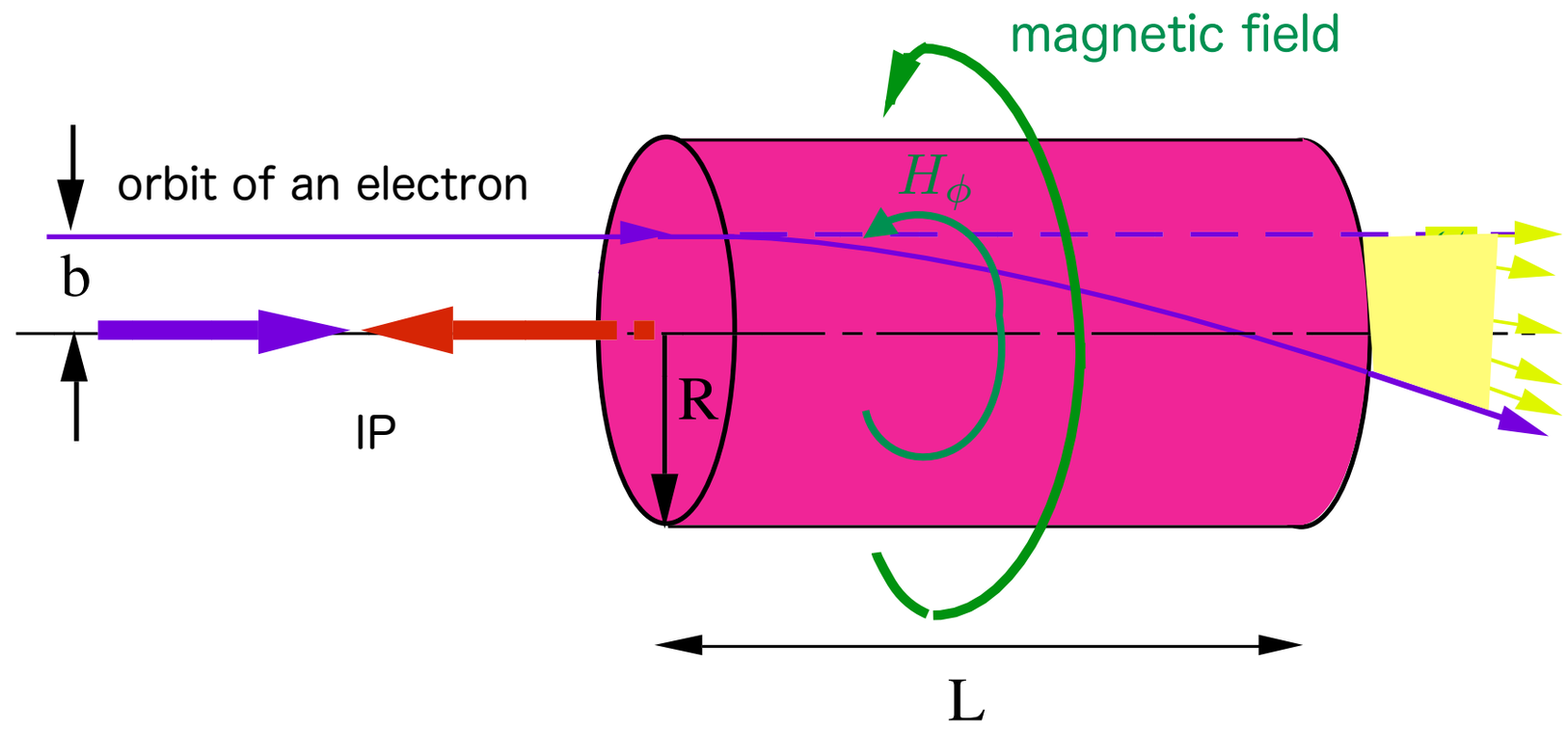

synchrotron
radiations

"beamstrahlung"

$\hbar\omega_c = E_c$

Estimation of the magnetic field produced by oncoming beam

$$\oint H_\phi d\ell = I \quad \therefore \; 2\pi b H_\phi = I = \frac{Ne(b^2/R^2)}{\Delta t}, \; \Delta t = \frac{L}{2c}$$

$$H_\phi = \frac{c}{\pi}\frac{Ne}{L}\frac{b}{R^2} \; [A/m] \rightarrow \times \frac{4\pi}{10^7} \; [T]$$

$$H_\phi \sim 2 \times 10^6 \; T \text{ for } N = 10^{10}, \; L = 100\mu m, \; b \sim R = 1nm$$

Estimation of the deflection by the magnetic field

the Lorentz force is given by $F_r = -ev \times H_\phi$ in the radial direction

the impact Δp in Δt is given by $\Delta p = F_r \times \Delta t = -evH_\phi \cdot L/(2c)$

∴ the deflection angle Δr' can be estimated by

$$\Delta r' = \frac{\Delta p}{p} = -\frac{evH_\phi L/(2c)}{mc^2\gamma\beta c} = -2\frac{Nr_e}{\gamma}\frac{b}{R^2} \sim -0.11 \text{ radian}$$

,where $r_e = \frac{\alpha}{mc^2} = 2.8 \times 10^{-15} m$:classical electron radius, $\alpha = \frac{e^2}{4\pi\varepsilon_0\hbar c}$

For actual flat beam at linear colliders

$$\Delta x' = -\frac{2Nr_e}{\gamma}\frac{1}{\sigma_x+\sigma_y}\frac{x}{\sigma_x} \equiv D_x\frac{x}{\sigma_z} \qquad \Delta y' = -\frac{2Nr_e}{\gamma}\frac{1}{\sigma_x+\sigma_y}\frac{y}{\sigma_y} \equiv D_y\frac{y}{\sigma_z}$$

$$\therefore \Delta x' \sim \Delta y' \sim \Delta r'/100 \text{ for the aspect ratio of } R \equiv \sigma_x/\sigma_y = 100$$

Ref : K.Yokoya and P.Chen, Lecture at US CERN School on Particle Accelerators, Nov. 7-14, 1990, Hilton Head Island So. Carolina USA. Lecture Notes in Physics 400. Frontiers of Particle Beams: Intensity Limitations, Springer Verlag, pp. 415-445

The disruption parameter D is defined as the ratio of the r.m.s. bunch length σ_z to the focal length, i.e. $D = \sigma_z/(\text{focal length})$, and $R \equiv \sigma_x/\sigma_y = D_y/D_x$

$$D_{x(y)} \equiv \frac{2Nr_e}{\gamma} \frac{\sigma_z}{\sigma_{x(y)}(\sigma_x + \sigma_y)}$$

ILC at $\sqrt{s} = 500\text{GeV}$:

$$N = 2 \times 10^{10}, \sigma_x = 474\text{nm}, \sigma_y = 5.9\text{nm}, \sigma_z = 300\mu\text{m} \text{ and } \gamma = 4.89 \times 10^5$$

$$\therefore D_x = 0.31, \ D_y = 24.9$$

The approximate number of oscillation is given by $\frac{3^{1/4}}{2\pi}\sqrt{D_{x(y)}} \sim 0.2\sqrt{D_{x(y)}}$

Luminosity is inversely proportional to area of focussed beam $\pi R^2, \ \pi\sigma_x\sigma_y$

The magnetic field is inversely proportional to circumference of focussed beam

$2\pi R, \ \pi(\sigma_x + \sigma_y)$

Estimation of electromagnetic fields generated in the moving system

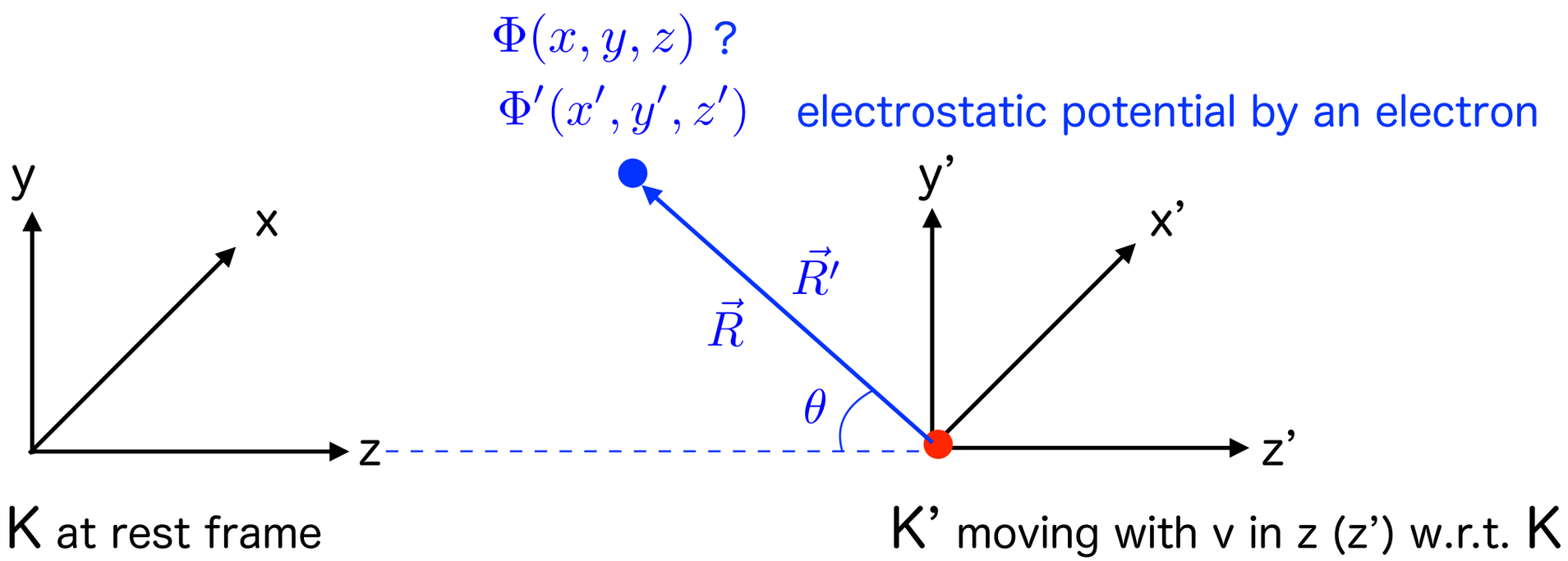

K and K' are the same position at t=0, i.e. the origin of K' = (0, 0, vt) in K coordinates.

Coulomb potential : $\Phi' = \dfrac{e}{R'}$ and $\Phi = \gamma\Phi',\ \gamma = \dfrac{1}{\sqrt{1 - v^2/c^2}}$

$x' = x,\ y' = y,\ z' = \gamma(z - vt)$

$R'^2 = x'^2 + y'^2 + z'^2 = \gamma^2 R^2 \left\{1 - (v^2/c^2)\sin^2\theta\right\}$ where $\vec{R} = (x, y, z - vt),\ \sin^2\theta \equiv \dfrac{x^2 + y^2}{R^2}$

$$\therefore \Phi = \frac{e}{R\sqrt{1 - (v^2/c^2)\sin^2\theta}} \to \gamma\frac{e}{R_\perp} \text{ as } v \to c$$

$$\because R^2 = x'^2 + y'^2 + z'^2/\gamma^2 \to x'^2 + y'^2 \equiv R'_\perp = R_\perp \text{ as } v \to c$$

The electric field in the K' frame $$\vec{E}' = -\nabla\Phi' = \frac{e\vec{R}}{\gamma R^3 \left\{1 - (v^2/c^2)\sin^2\theta\right\}^{1/2}}$$

The electromagnetic fields in the K frame are calculated by the Lorentz transformation from $\vec{E}'$ for $\vec{H}' = 0$

$$\therefore E_z = E'_z,\ E_\perp = \gamma E'_\perp,\ H_z = 0,\ H_\perp = \gamma(\vec{v}/c) \times \vec{E}'$$

$$\therefore E_\perp = \gamma \frac{e}{R^2}\frac{R_\perp}{R} \text{ for } \sin^2\theta = 1 \qquad E_z < \frac{e}{R^2} \ll E_\perp \text{ for } \sin^2\theta = 0$$

Therefore only the transverse fields are effectively applied, becoming 2 dimensional Coulomb potential problem.

The size and time of Lorentz contraction are given by,

$$1 - (v^2/c^2)\sin^2\theta \to 0,\ \Delta\theta = \frac{1}{\gamma} \text{ for } \theta \sim 1/2\pi + \Delta\theta$$

$$\sin^2\theta = \frac{R_\perp^2}{R_\perp^2 + (v\Delta t)^2}, \Delta t = \frac{R_\perp}{\gamma v} \text{ for } \theta \sim 1/2\pi + \Delta\theta$$

Forces from on- and co-coming beams are calculated by,

$$\frac{\vec{F}}{e} = \vec{E} \pm \frac{\vec{v}}{c} \times \vec{H} = \left(1 \mp \frac{v^2}{c^2}\right)\vec{E} \pm \frac{\vec{v}}{c^2}(\vec{v}\cdot\vec{E}) \sim 0\ (2\vec{E}) \text{ for the same (opposite) direction}$$

Two major effects in the beam-beam interactions

(1) Luminosity enhancement due to the focussing force from on-coming beam, i.e. Pinch effect

First the luminosity reduction by the horizontal crossing and the recover by the crab crossing

$$L \equiv L_0 \times \eta = \frac{N^2}{4\pi\sigma_x\sigma_y} \times \eta(\phi_c, \sigma_x/\sigma_z), \text{ where } \phi_c = \text{crossing angle}$$

$$\eta \approx \frac{4}{\pi}\frac{1}{\phi_c}\left(\frac{\sigma_x}{\sigma_z}\right) \text{ for } 1 \gg \phi_c > \frac{\sigma_x}{\sigma_z}$$ assuming rigid elliptical beams

$$\therefore \eta \approx 0.14 \text{ with } \sigma_x/\sigma_z = 0.0016, \phi_c = 14\text{mrad at ILC, which is fully recovered by the Crab crossing}$$

It is good agreement with the CAIN results : η = 0.15 and the full recovery is confirmed.

The luminosity enhancement : $H_D = L/L_0$

Assuming the disruption is not large, the analytic formulas are approximately given by,

$H_{DX(DY)} = $ ones by the Pinch effects in the horizontal (vertical) directions

$$H_{DX(DY)} = 1 + D_{x(y)}^{1/4}\frac{D_{x(y)}^3}{D_{x(y)}^3+1}\left\{\ln\left(\sqrt{D_{x(y)}}+1\right) + 2\ln(0.8/A_{x(y)})\right\}$$

$$H_D \approx \sqrt{H_{DX}}H_{DY}^{(1+2R^3)/6R^3}, \text{ where } R = \sigma_x/\sigma_y \ , A_{x(y)} = \sigma_z/\beta^*_{x(y)}$$

$$H_{DX} = 1.2, H_{DY} = 6.1 \text{ and } H_D \approx 2.0 \text{ at } \sqrt{s} = 500\text{GeV, ILC}$$

(2) Kink instability and deflection with collisions with an off-set

the vertical center-of-mass beam position v.s. time

Figure 3: Evolution of the kink instability. The beams collide with initial vertical offset Δ_y=0.2σ_y. The time range, -0.5< t < 2.25 (t in units of σ_z), is shown with time mesh 0.25. In each plot the vertical center-of-mass y/σ_y is shown as a function of the longitudinal position s/σ_z. Flat beam with D_y=20.

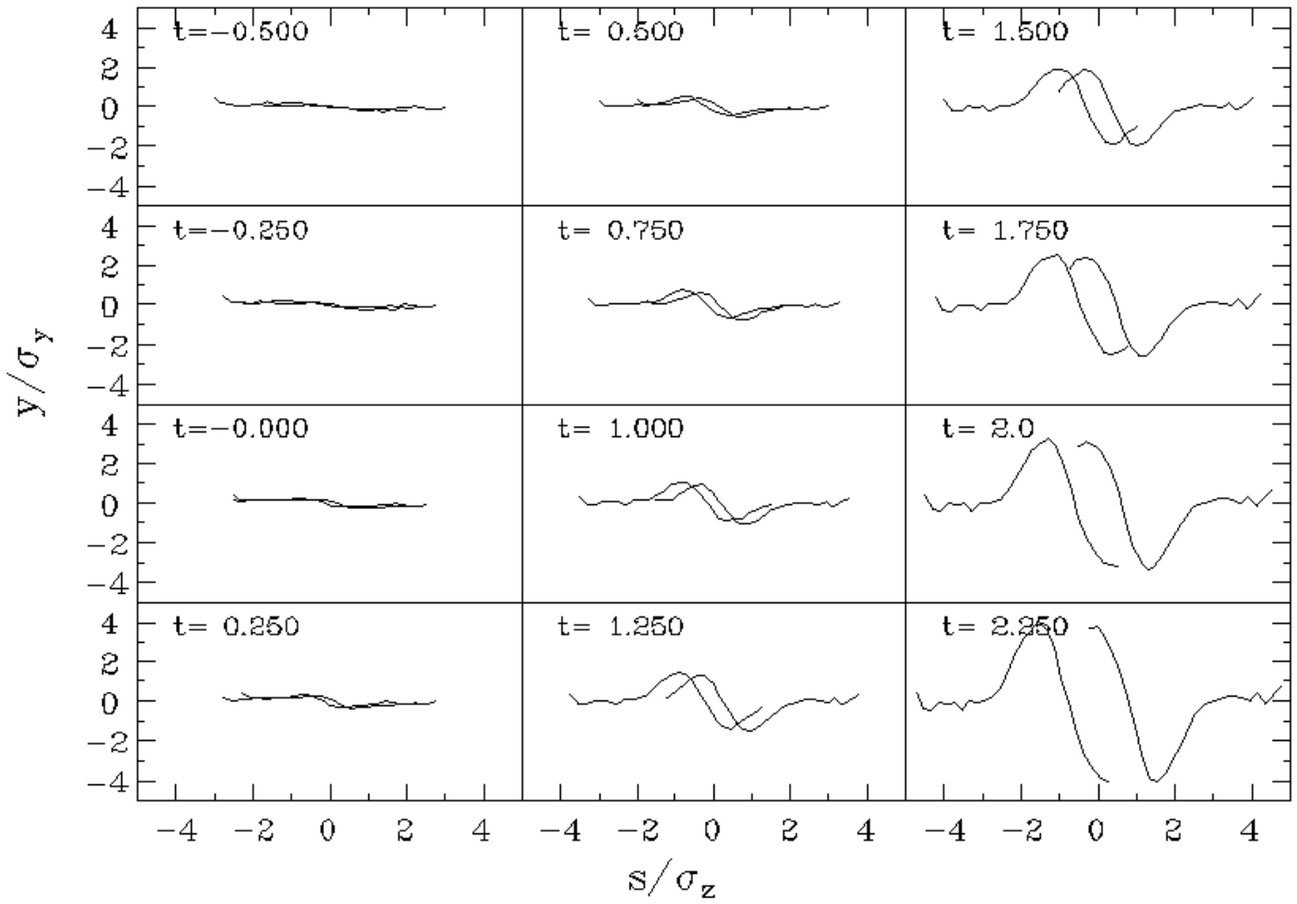

The instability suppress the luminosity enhancement. So, the initial vertical offset must be zeroed by a fast feedback (e.g. FONT) .

Actually the beam beam interactions must be estimated by simulations of CAIN and Guineapig.

CAIN : the version of 2.42 can be downloaded from https://ilc.kek.jp/~yokoya/CAIN/Cain242
the author is Kaoru Yokoya (KEK)

GuineaPig : the homepage is http://www-project.slac.stanford.edu/lc/bdir/programs/guinea_pig/gp_index.html , the author is Daniel Schulte (CERN)

Disruption of the beam

Particles in a bunch are deflected by the electromagnetic fields of the on-coming beam, whose the deflection angles depend on their locations in the bunch and from the on-coming beam with any offsets. These angles are called as disruption angle.
The angle is characterized by a parameter of

$$\theta_0 \equiv \frac{2Nr_e}{\gamma(\sigma_x+\sigma_y)} = \frac{D_x\sigma_x}{\sigma_z} = \frac{D_y\sigma_y}{\sigma_z} = 4.86\times10^{-4} \qquad \theta_0 \to \frac{2Nr_e}{\gamma\sigma_x} \ \text{ at } \frac{\sigma_x}{\sigma_y} \gg 1$$

The disruption angles depend on the initial particle positions, (x_0, y_0)

For flat beam with a small D_y

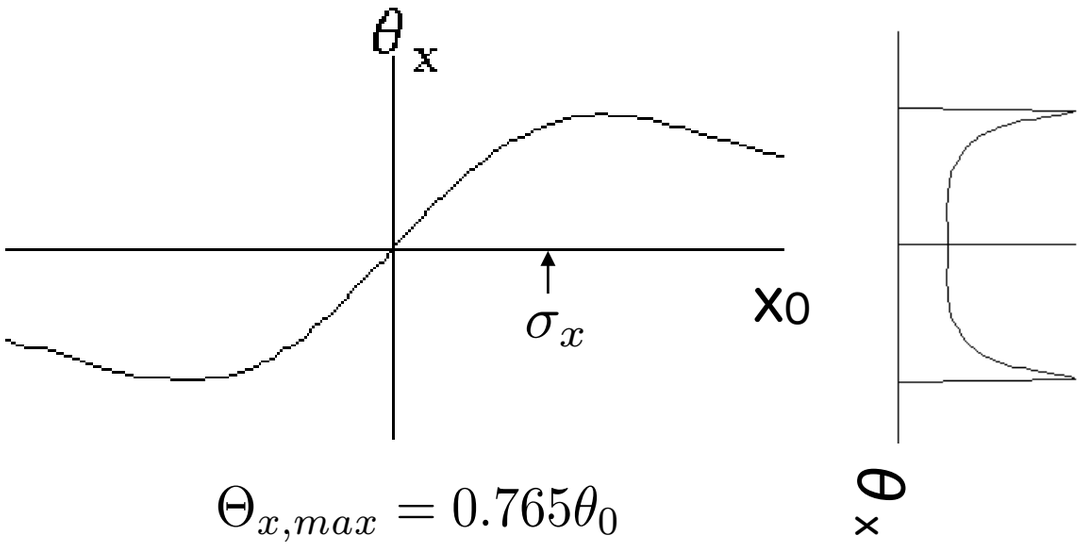

$$\Theta_{x,max} = 0.765\theta_0$$

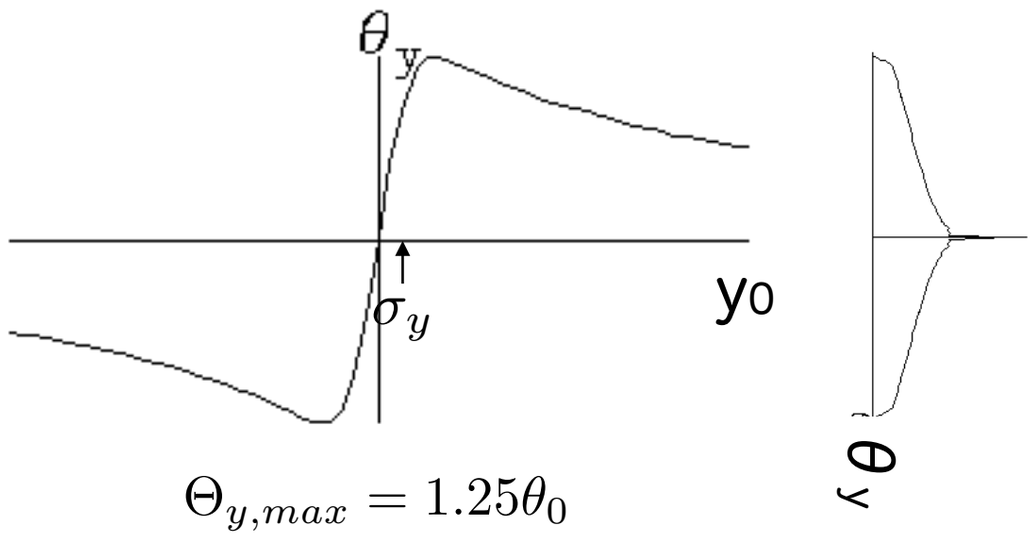

$$\Theta_{y,max} = 1.25\theta_0$$

The maximum angles give an information for the minimum radius of beam pipe for extracted beam.

For low energy particles (with the same charge as the on-coming beam)

$$\theta_{x(y),max} \sim \theta_0 \left[\log(4\sqrt{3}D_x/\varepsilon)/(\sqrt{3}\varepsilon D_x)\right]^{1/2} \text{ for } D_{x(y)}/\varepsilon > 1, E = E_{beam}\varepsilon$$

Center-of-Mass Deflection as a function of offset Δ_y

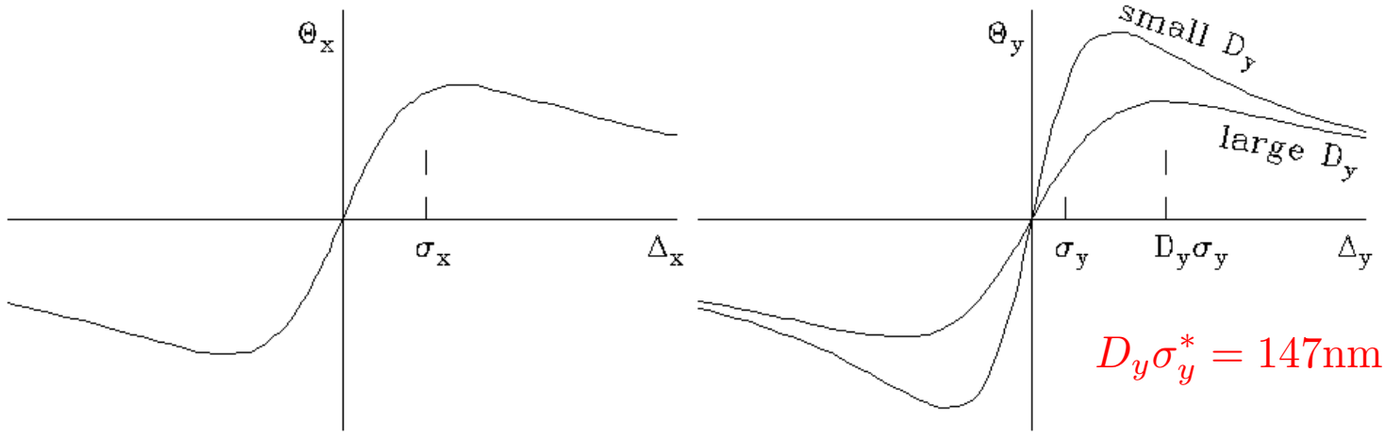

$D_y\sigma_y^* = 147\text{nm}$

Figure 7: Center-of-mass deflection as a function of the displacement.

In general, we define the form factor F for the vertical deflection by

$$\Theta_y = \tfrac{1}{2}\theta_0 F(\Delta_y/\sigma_y).$$

The form factor can be parametrized from simulated results.

$$F = \delta[C_1 + C_2\delta^2 + \frac{1}{\pi^2}\delta^4]^{-1/4} \qquad (\delta < 3) \qquad\qquad \delta \equiv \frac{\Delta_y}{\sigma_y}$$

$$C_1 = (1 + A_y^2)[1 + \frac{0.5}{0.6 + (\sqrt{D_y} - 2.5)^2}]^2 = 1.6$$

$$C_2 = [\frac{1.2D_y^2}{D_y + 10}]^2 = 445$$

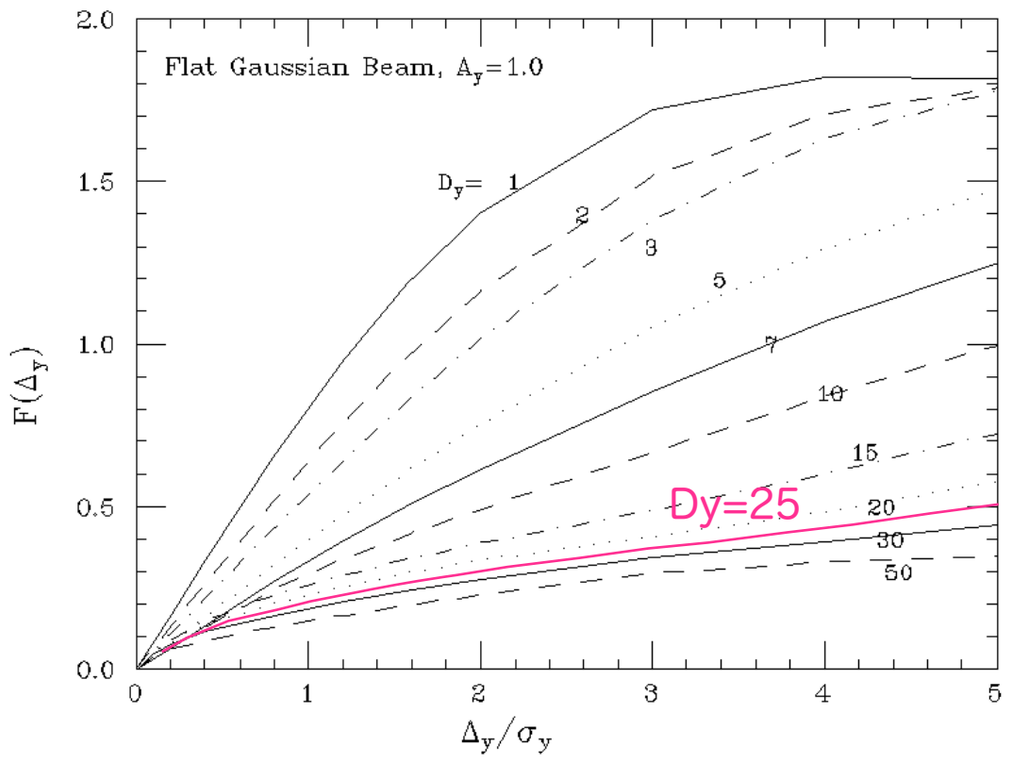

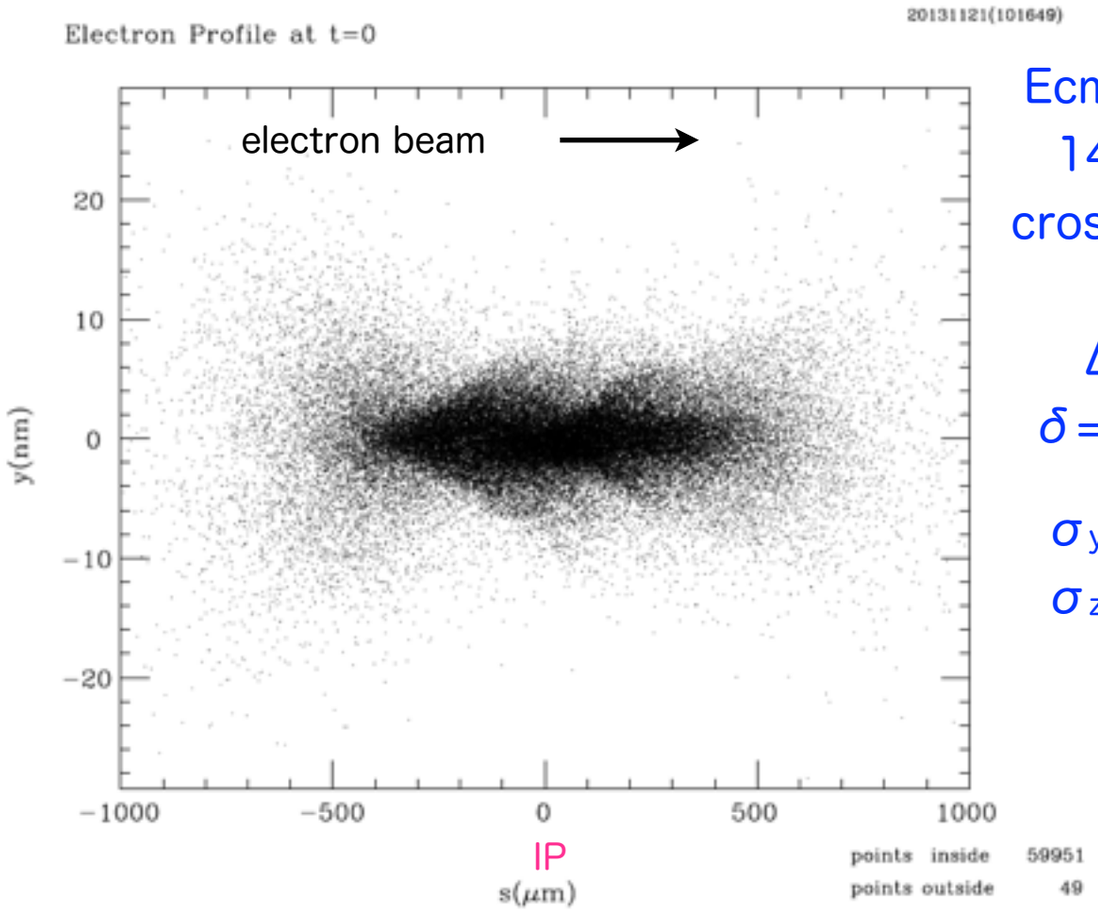

Ecm=500GeV
14mr, crab crossing, waist scan
Δy=0nm
$\delta = \Delta y / \sigma_y$=0

σ_y= 5.9nm
σ_z=300μm

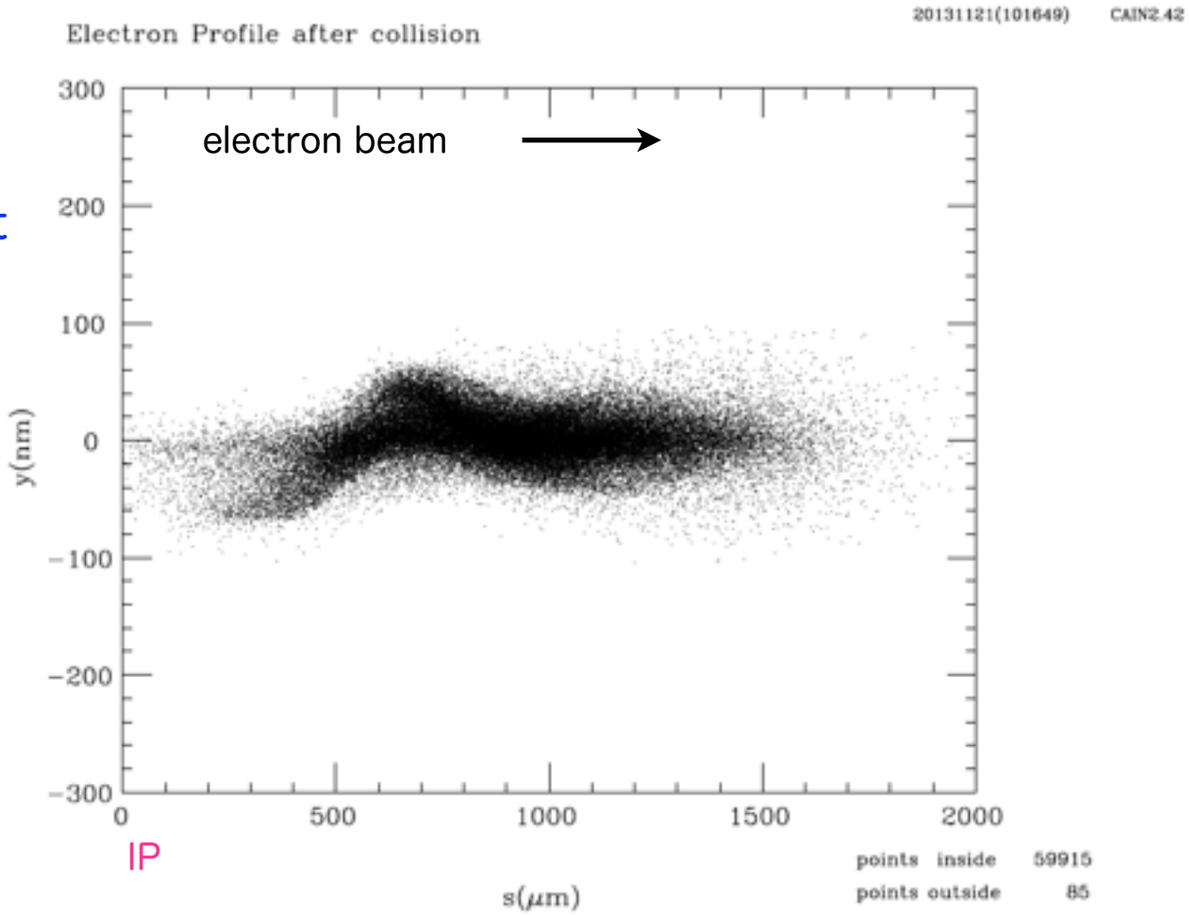

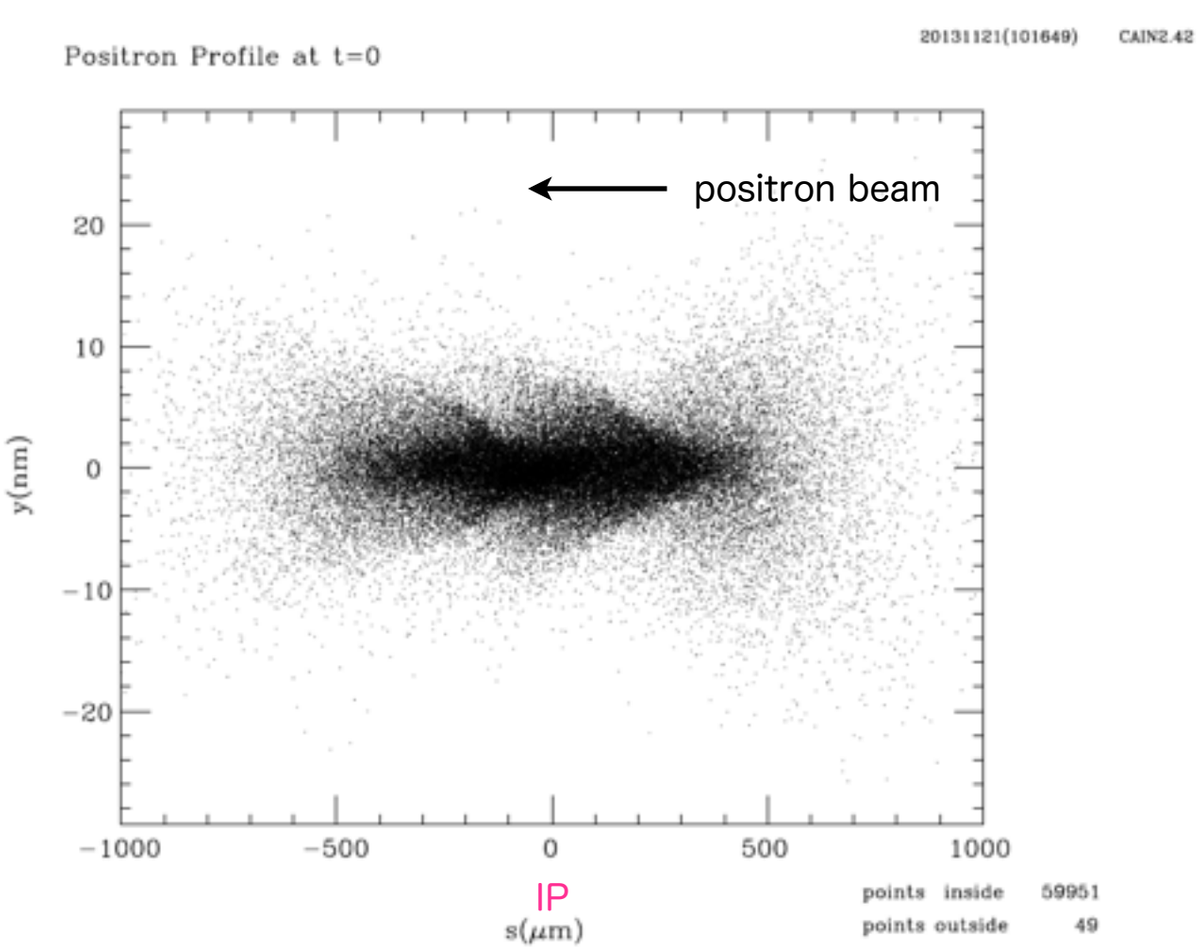

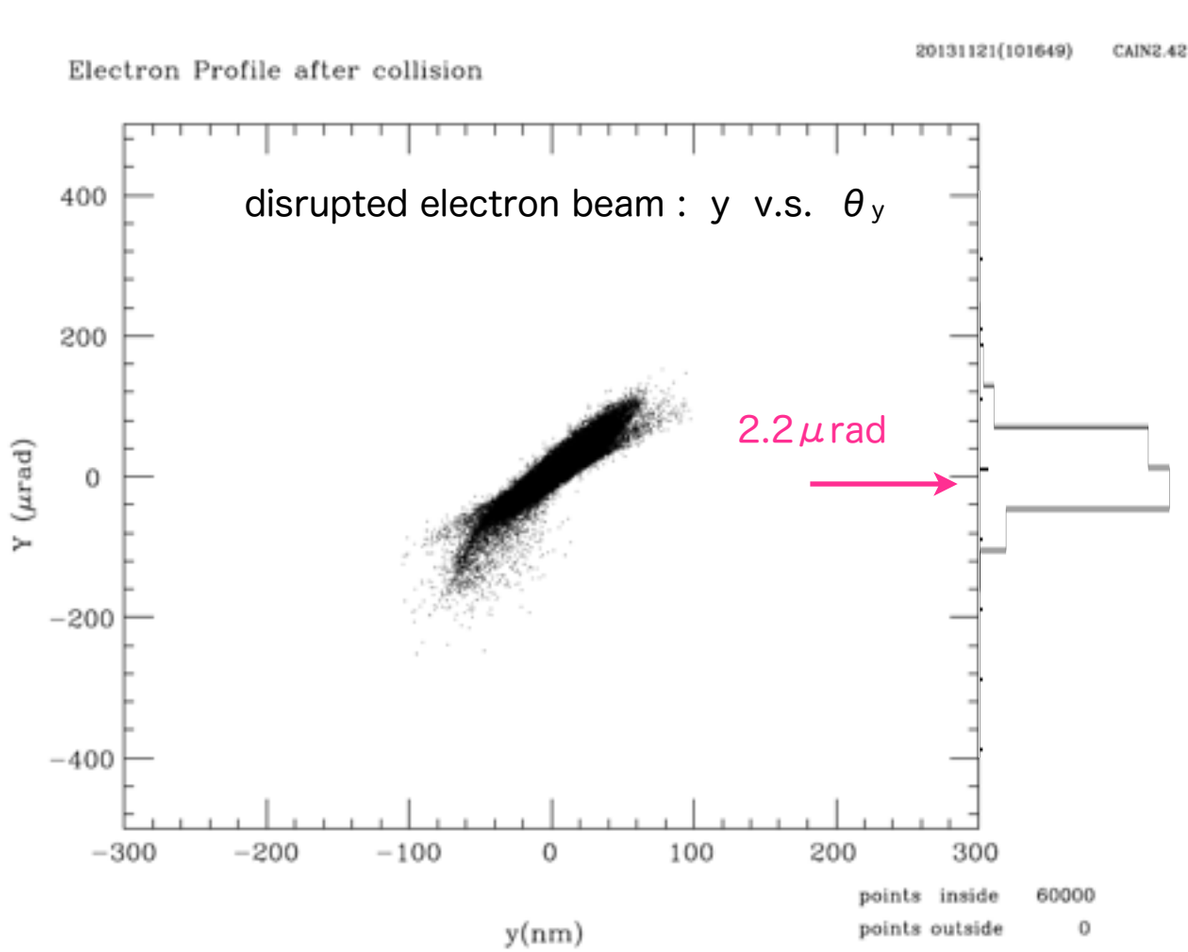

Ecm=500GeV
14mr, crab crossing, waist scan
Δy=10nm
$\delta = \Delta y / \sigma_y$=1.7

σ_y= 5.9nm
σ_z=300μm

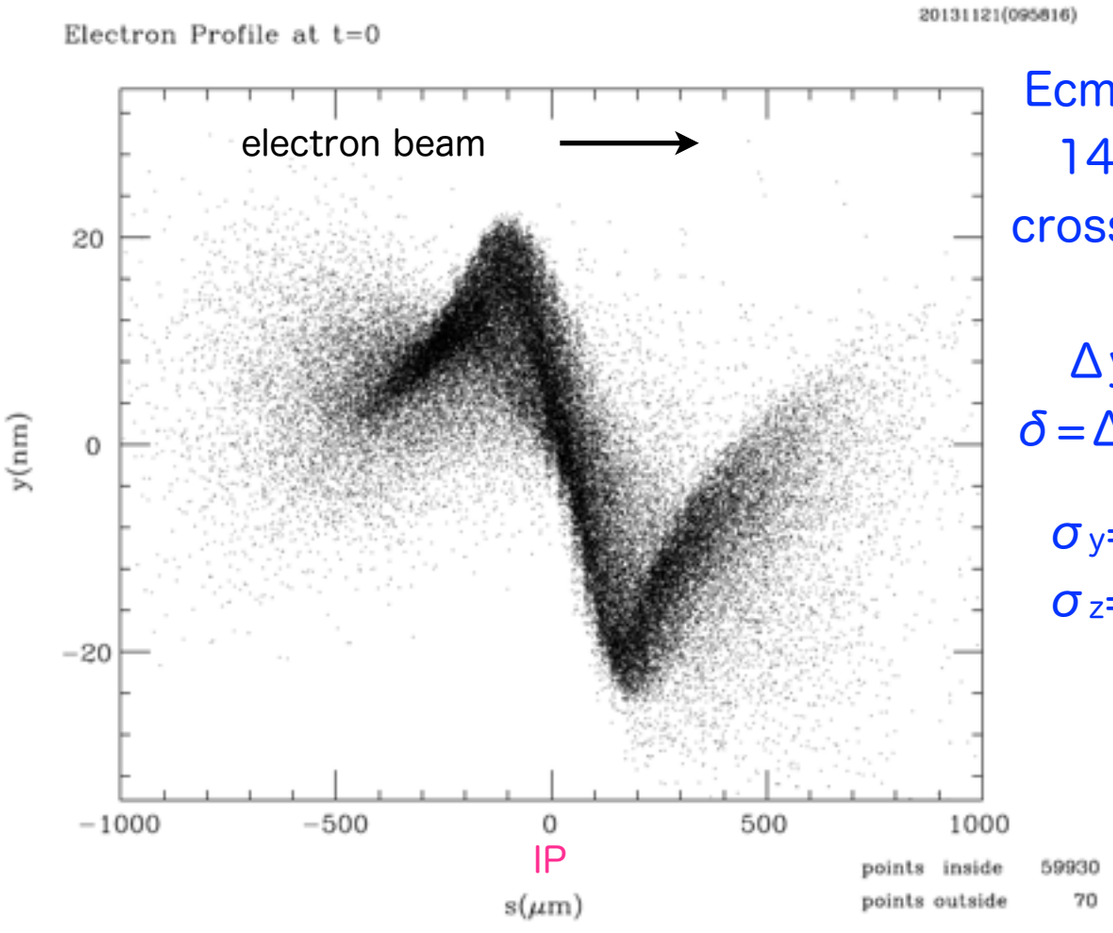

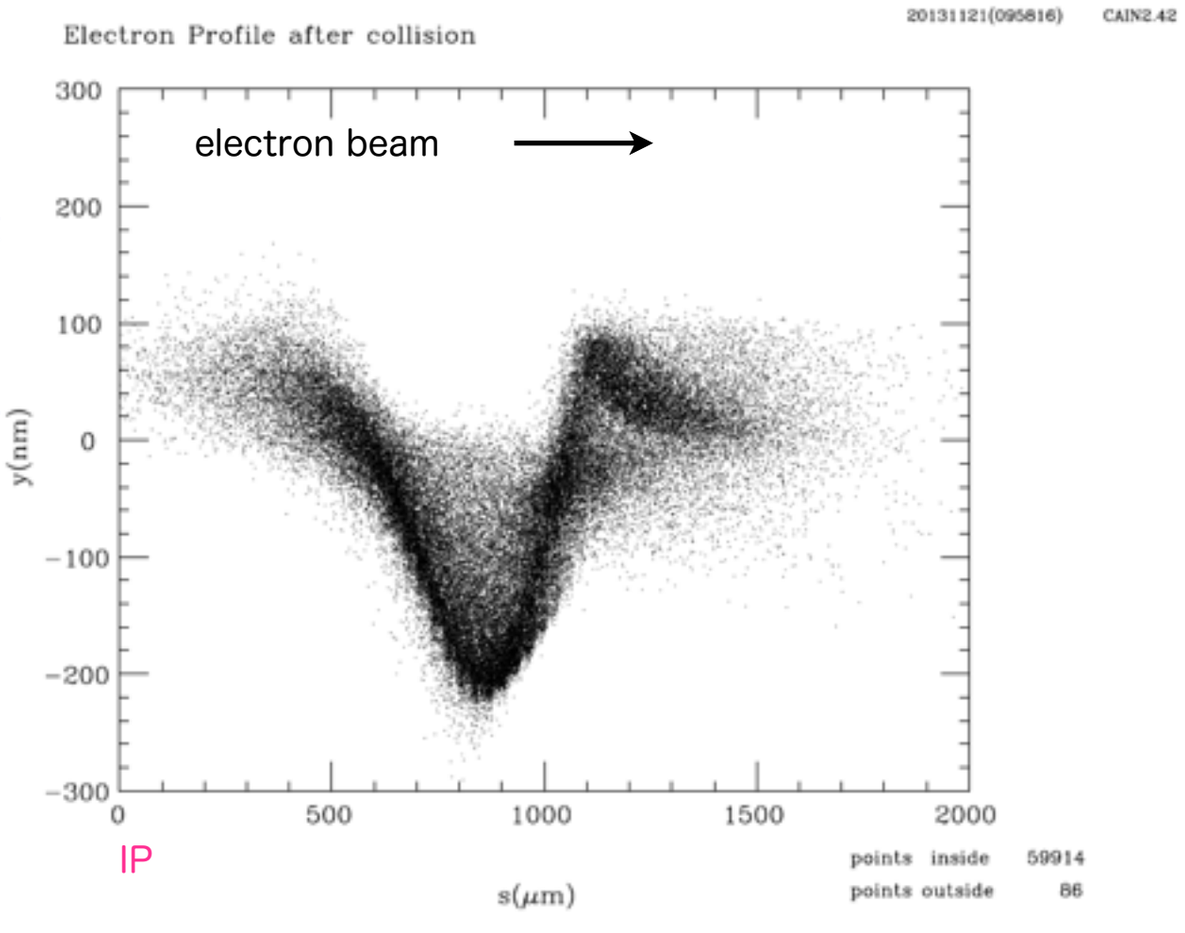

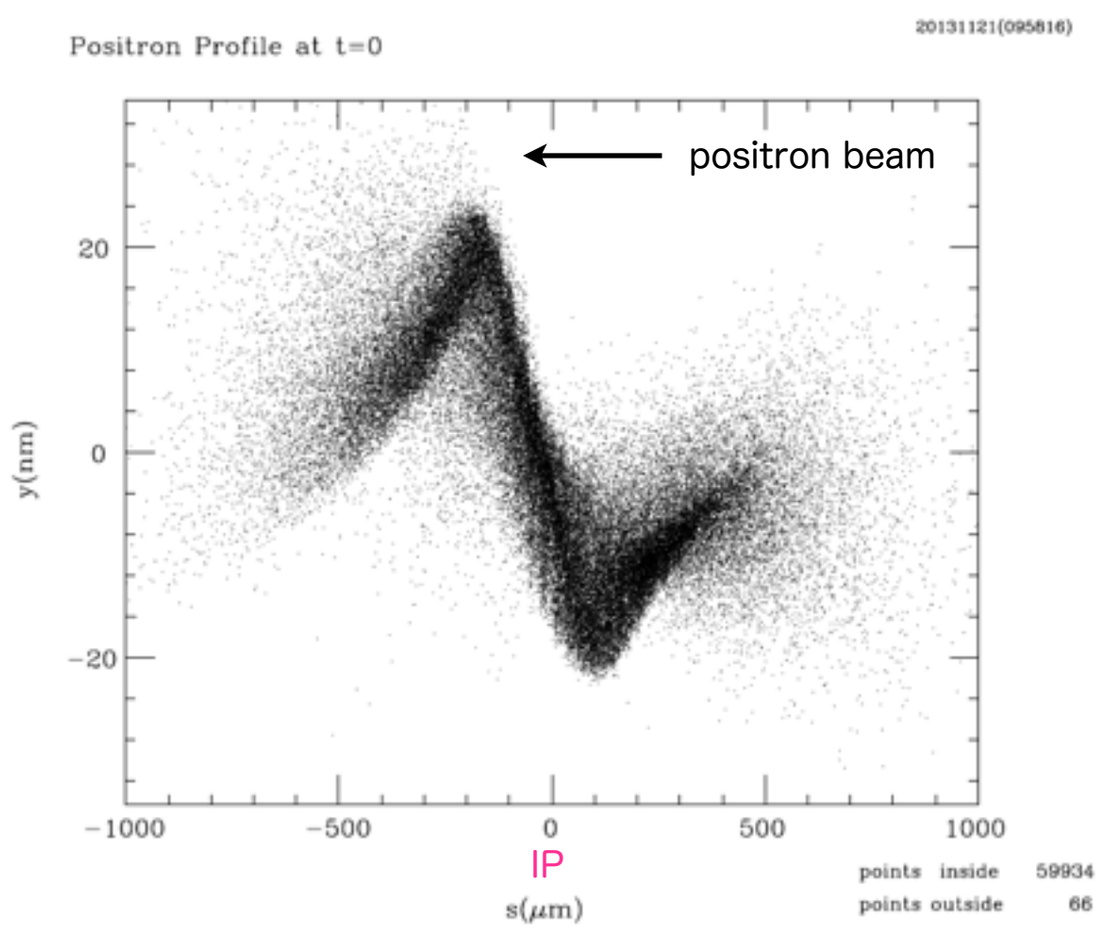

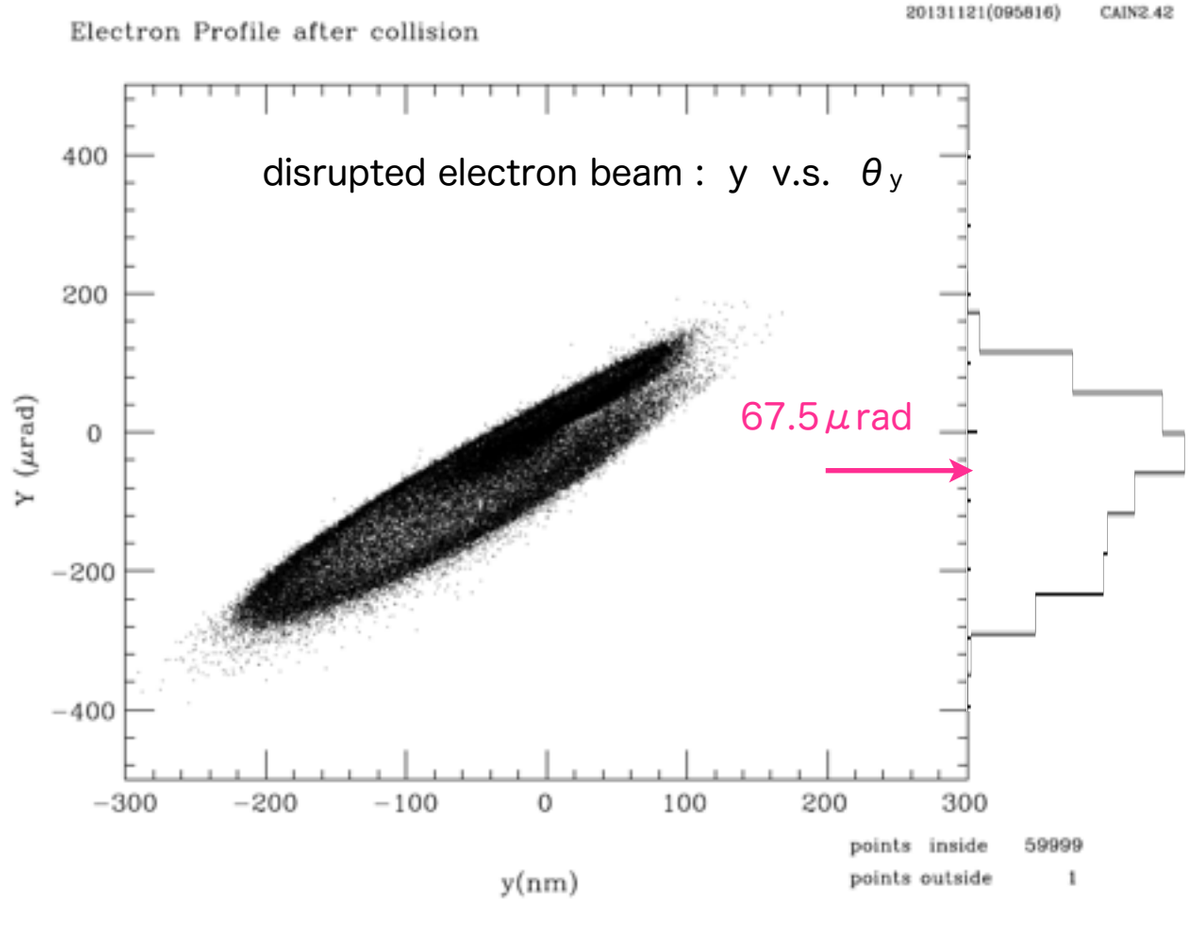

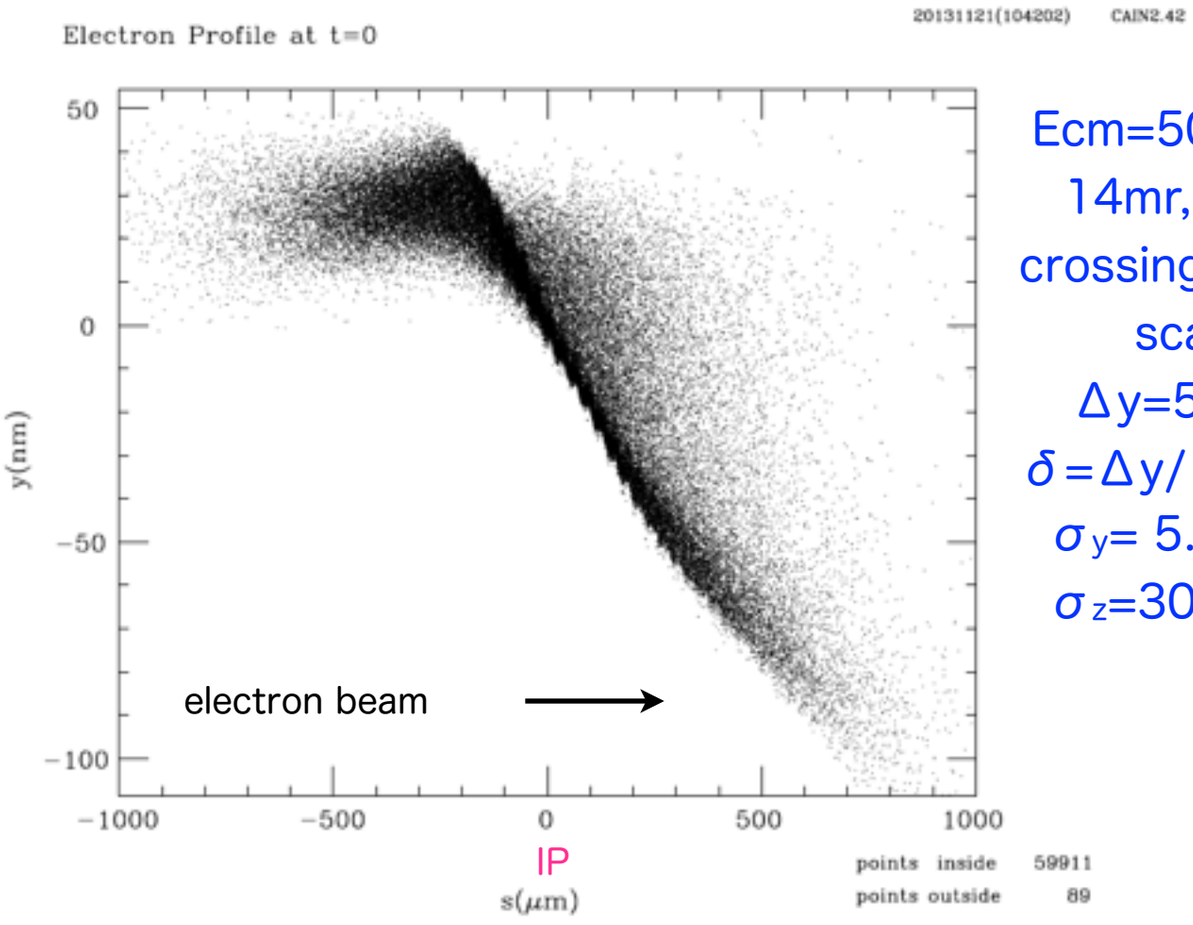

Ecm=500GeV
14mr, crab crossing, waist scan
Δy=50nm
$\delta = \Delta y / \sigma_y$=8.5
σ_y= 5.9nm
σ_z=300μm

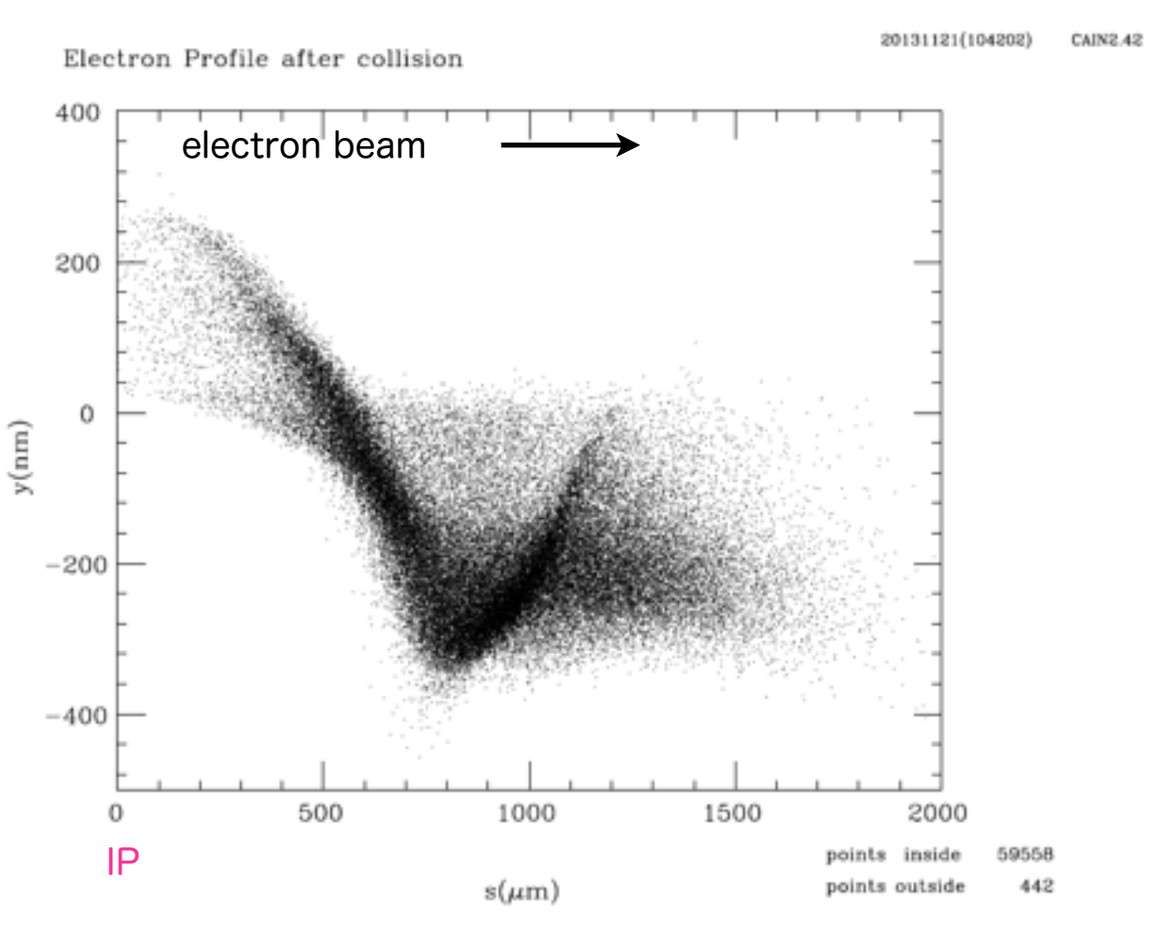

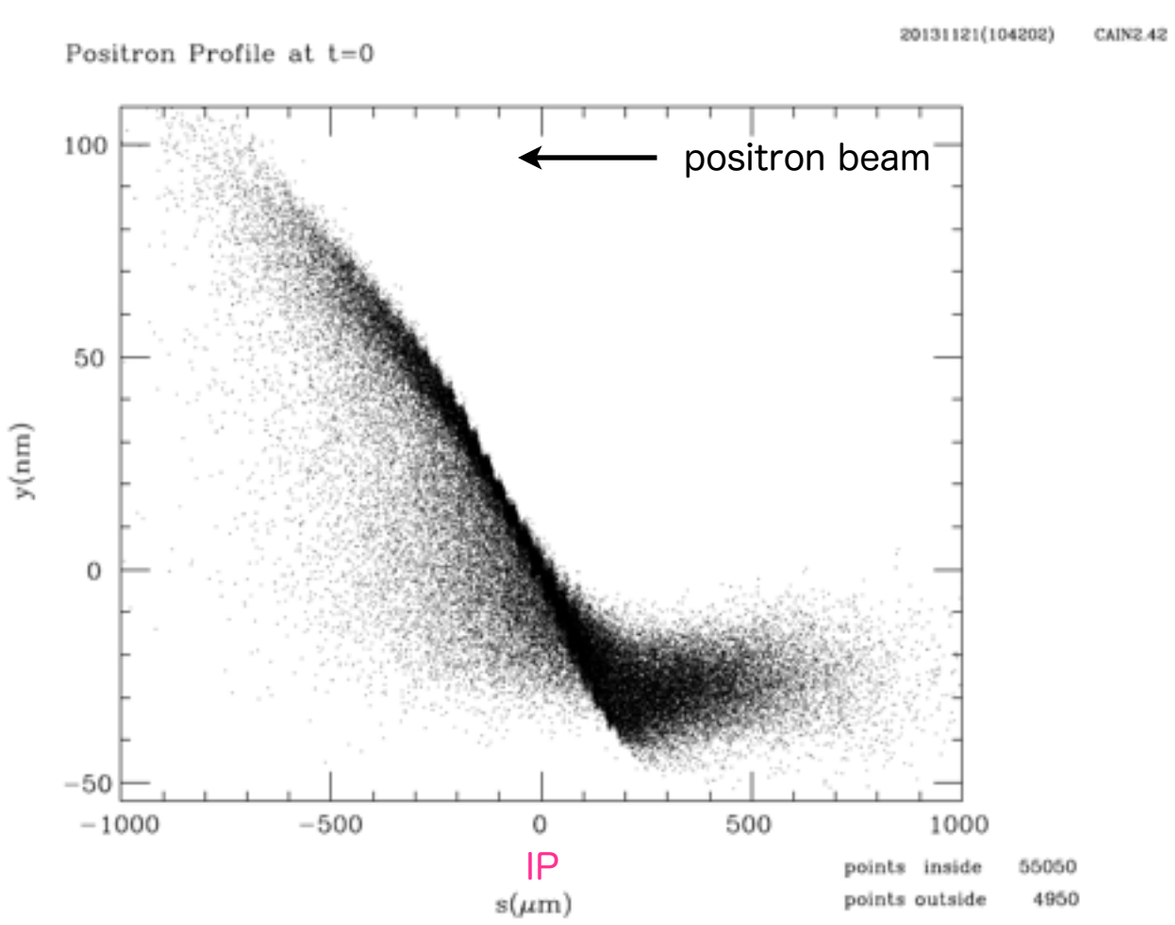

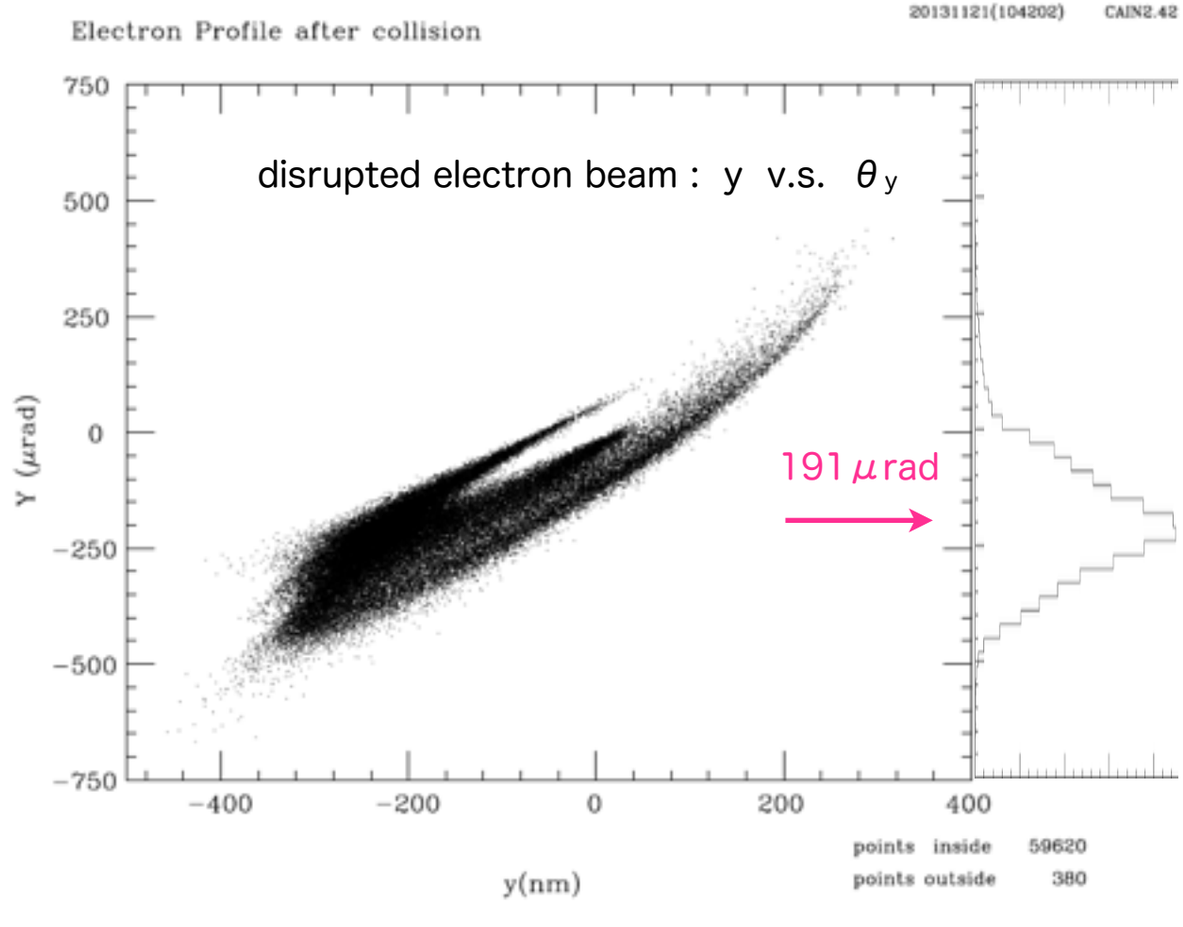

animation of collisions with $2\sigma^*_y$ offset, calculated by CAIN and made by K.Kubo

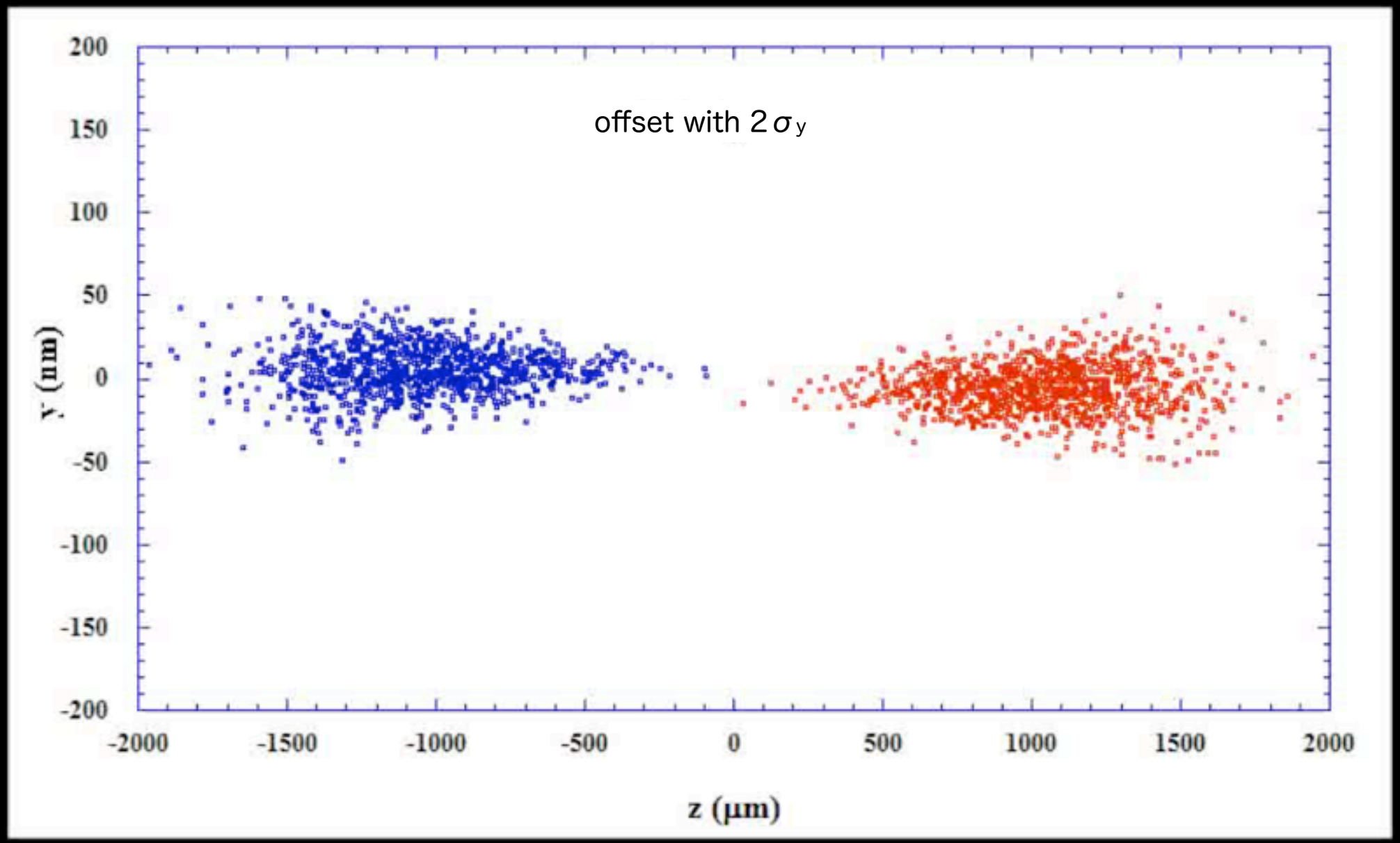

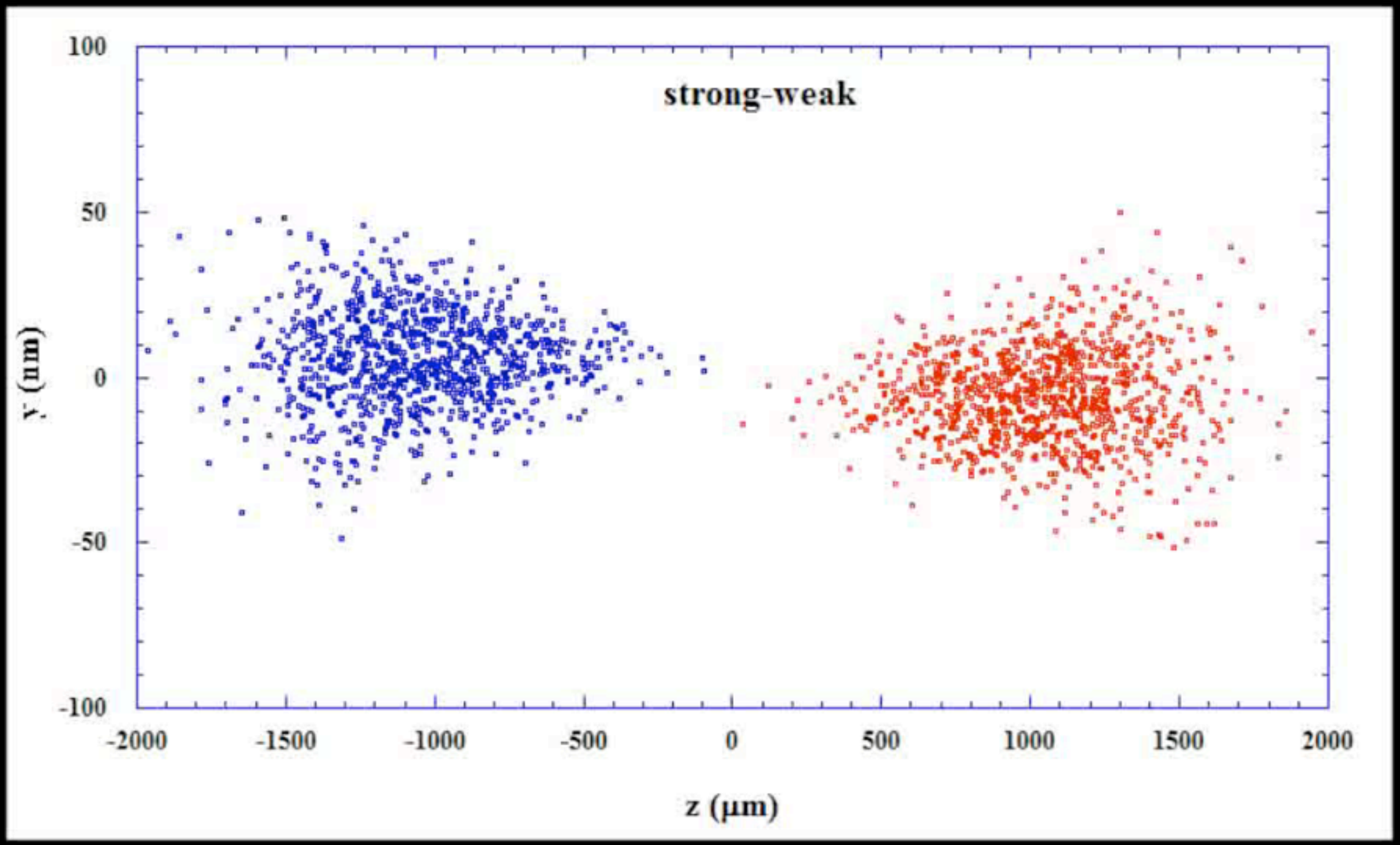
strong-weak
100
50
0
-50
-100
-2000
-1500
-1000
-500
0
500
1000
1500
2000
z (μm)

ILC TDR at E_{cm}=500,250GeV and 1TeV

14mr crab crossing with the waist scan (by $\pm 0.6\sigma_z$)

calculated by CAIN V2.42

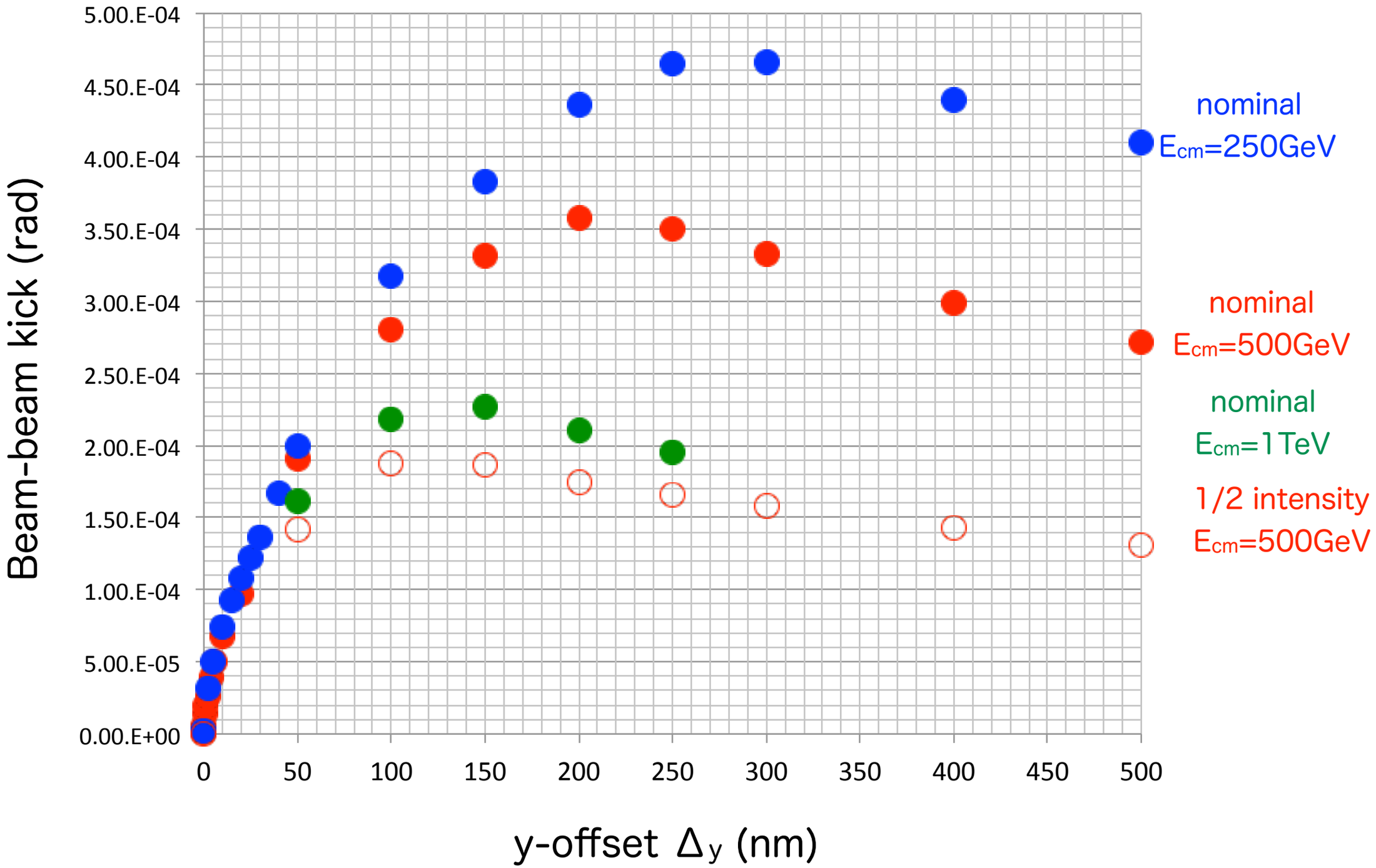

ILC TDR at E_{cm}=500GeV

14mr crab crossing with the waist scan

calculated by CAIN V2.42

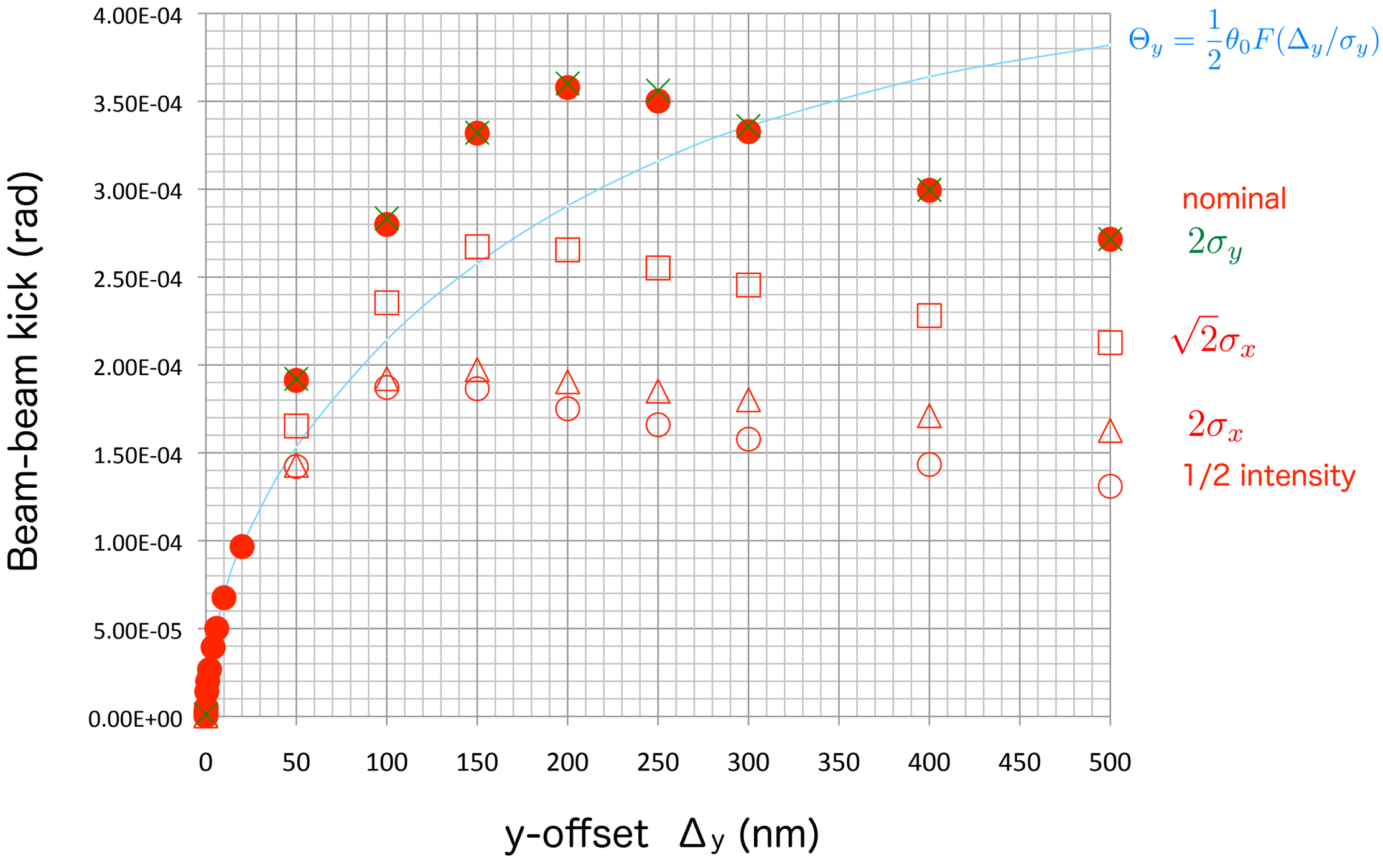

ILC TDR at E_{cm}=500GeV

14mr crab crossing with the waist scan

calculated by CAIN V2.42

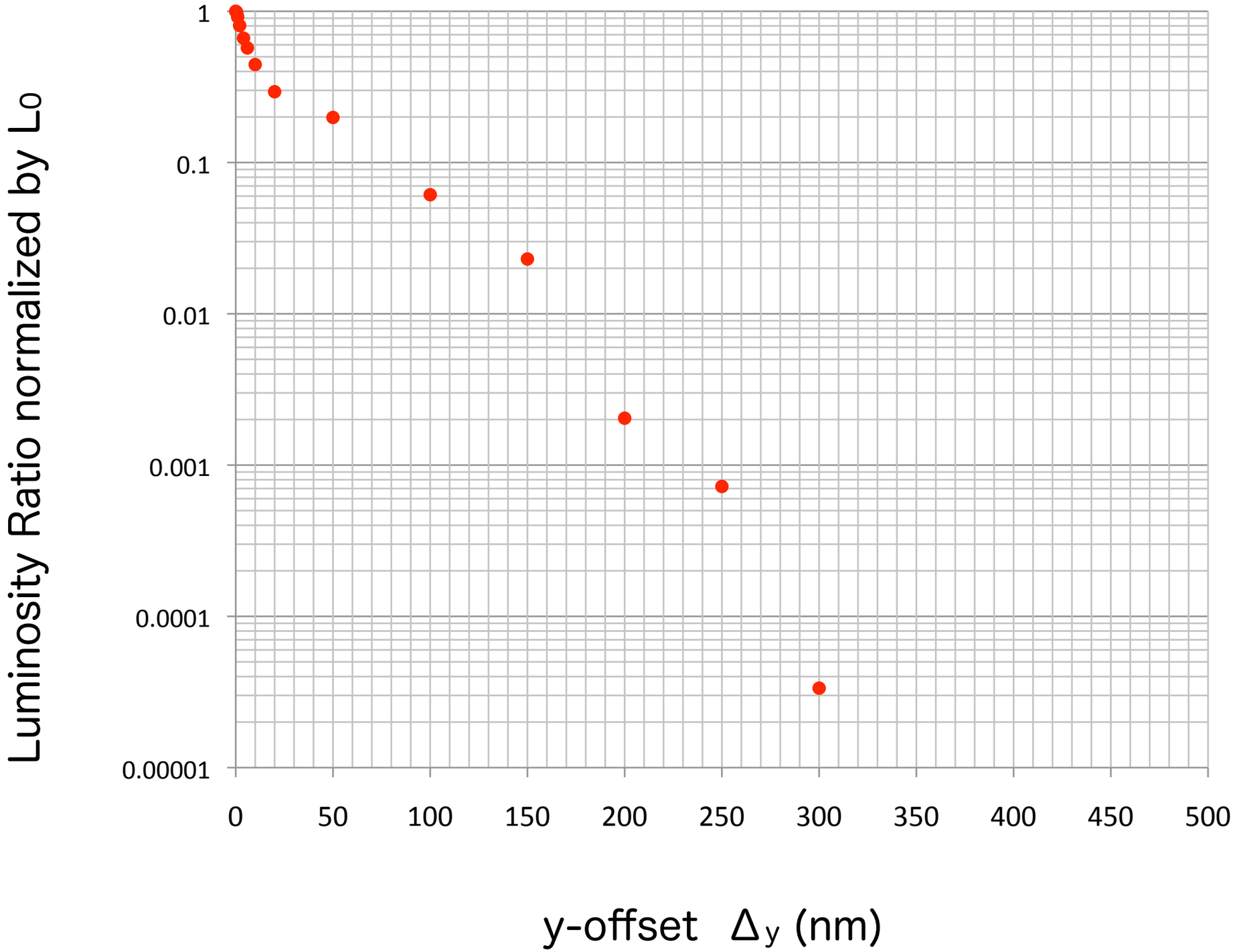

ILC TDR at E_{cm}=500GeV nominal

calculated by CAIN V2.42

14mr crab crossing with the waist scan

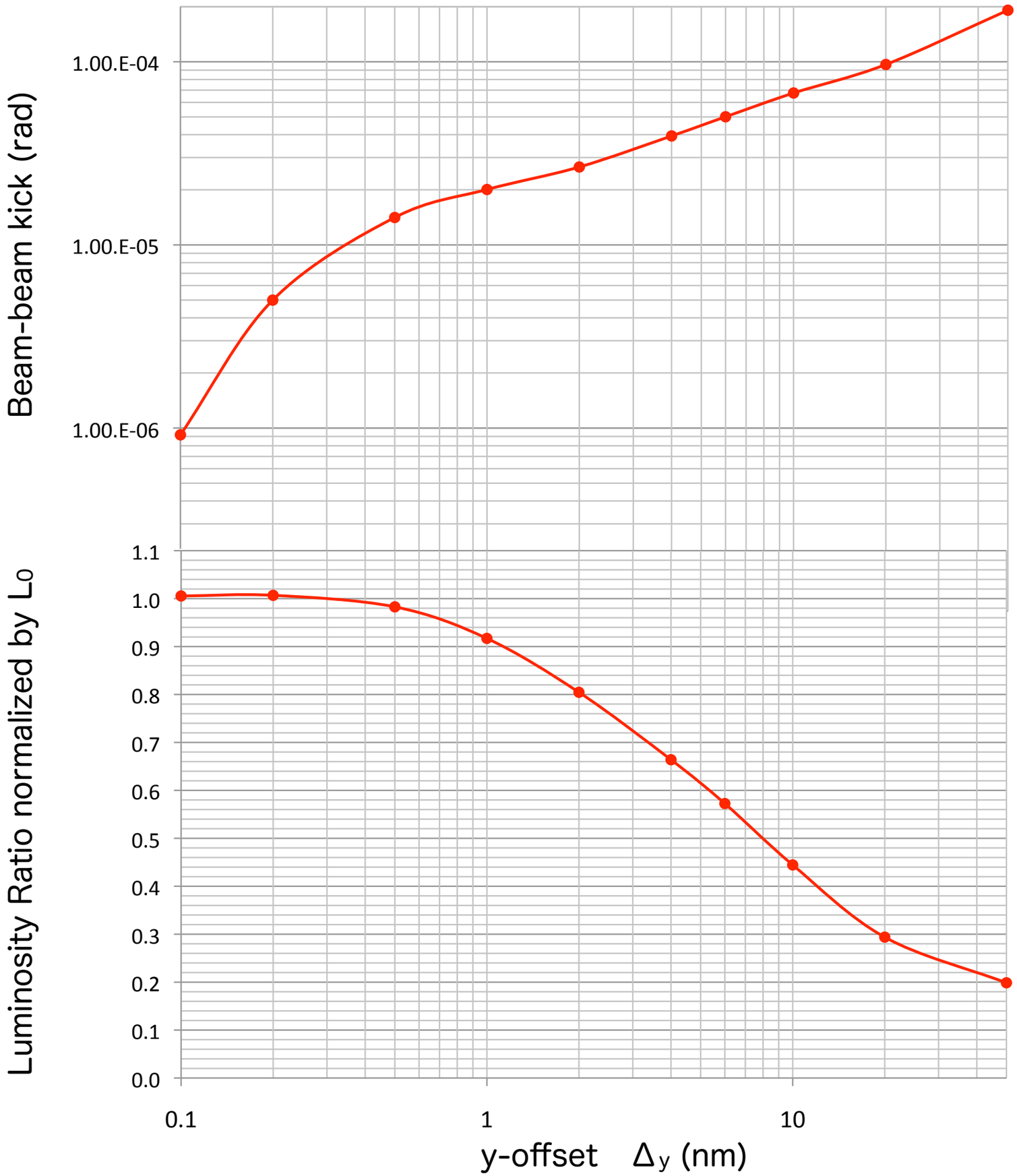

Intra-Pulse IP Feedback

G.White, ALCPG11, RDR parameters

- Use ILC IP FFB, tuned for ‘noisy’ conditions (like those simulated for TESLA)
- Assume BDS-entrance FFB has perfectly flattened beam train (flat trajectory into Final Doublet).
- No systematic or random intra-pulse distortions.
- Calculate Luminosity from measured bunches, with mean of last 50 weighted to account for the rest of the beam train (1320 bunches).

● ILC TDR E_{cm}=500GeV

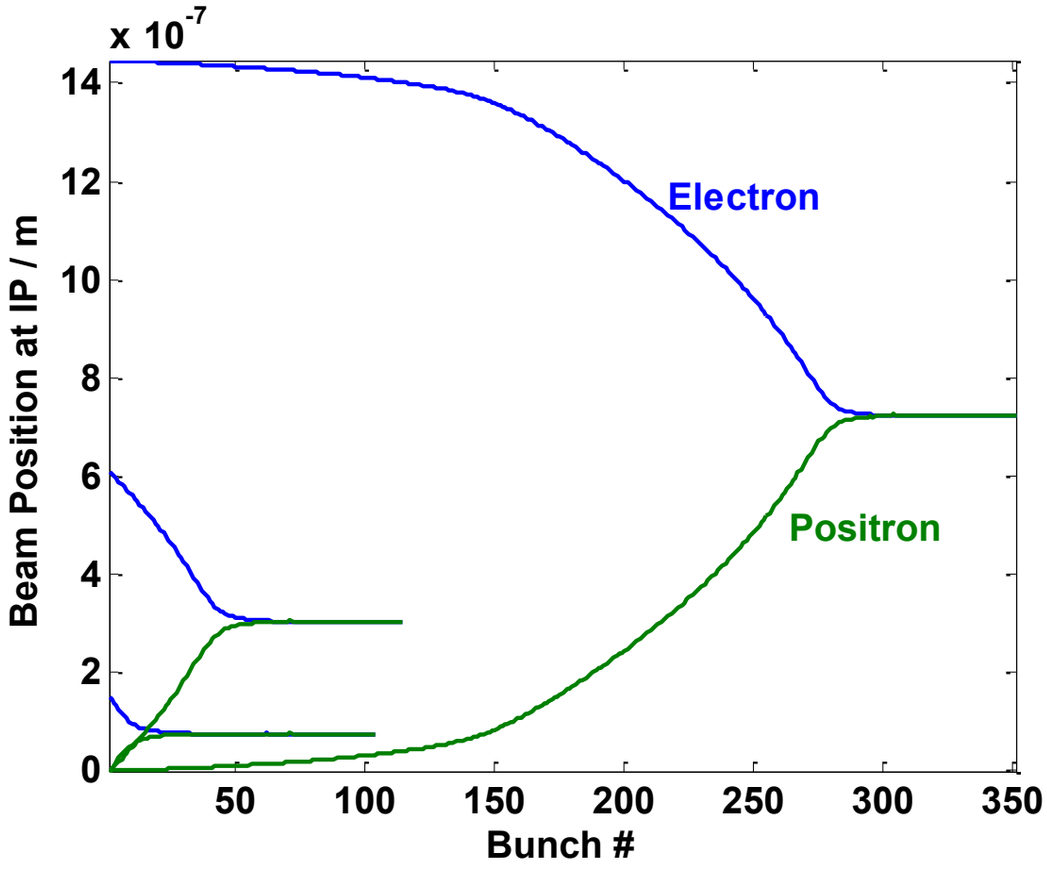

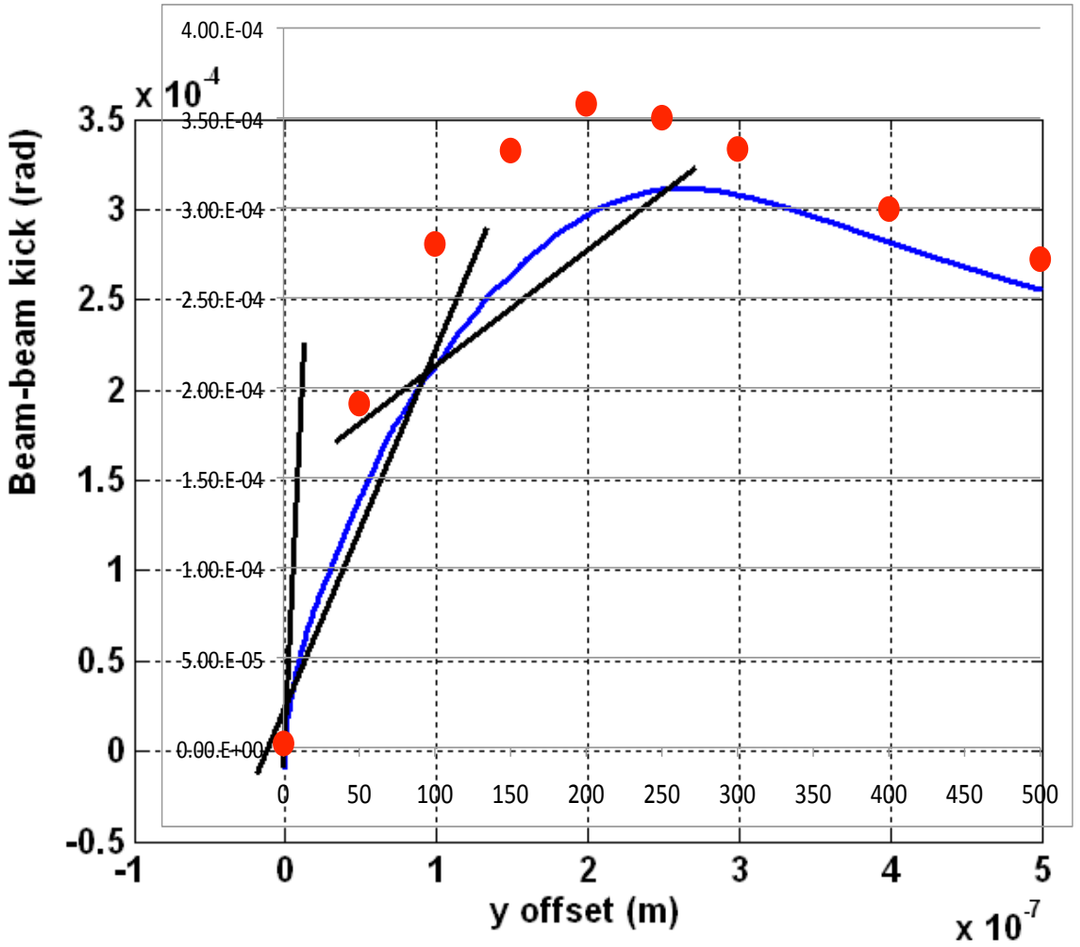

Luminosity Loss vs. QD0 Jitter

G.White, ALCPG11, RDR parameters

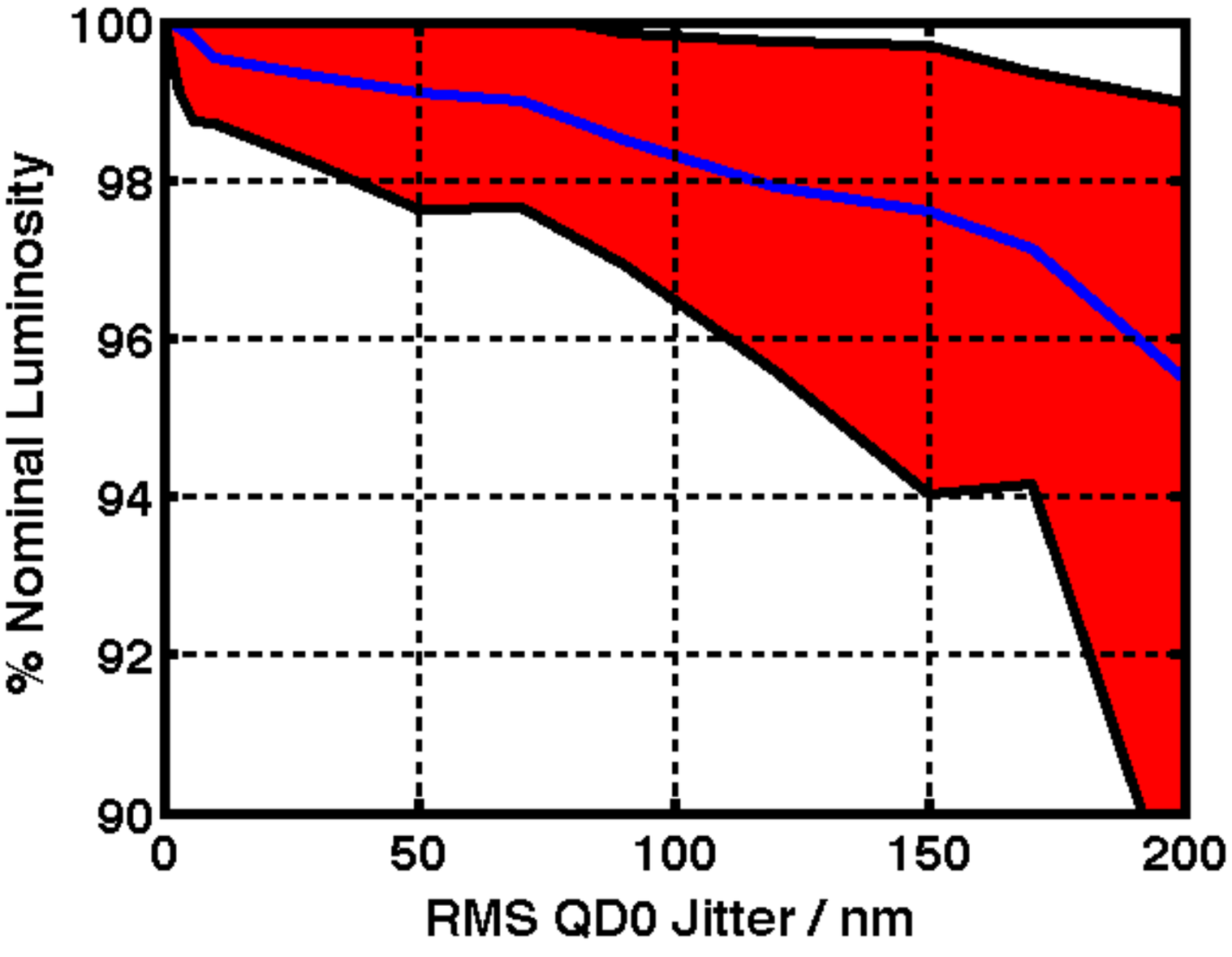

- Data shown gives % nominal luminosity for different levels of uncorrelated QD0 jitter.
  - 100 pulses simulated per jitter cases with FFB
  - Mean, 10% & 90% CL results shown for each jitter point from 100 pulse simulations
- **Tolerance to keep luminosity loss <1% is <50nm RMS QD0 jitter.**

Quantum Beamstrahlung

(1) magnetic field produced by the beam

H = about 2,800 Tesla at ILC (√s=500GeV)

bending radius ρ=p/(eH)=p[250GeV]/(0.3 H[Tesla])=0.3m

radiation coherent length $l_R = \rho/\gamma$ =0.6μm bending angle $\theta = l_R/\rho$, $\therefore$ $\theta = 1/\gamma$

(2) critical energy and the dimensionless Lorentz invariant parameter Υ

$$\Upsilon \equiv \frac{2}{3}\frac{\hbar\omega_c}{E} = \frac{2}{3}\frac{\hbar}{E}\frac{3}{2}\frac{c\gamma^3}{\rho} = \frac{\hbar}{m_e c}\frac{\gamma^2}{\rho} = \lambda\!\!\!^{-}_e \frac{\gamma^2}{\rho} = \gamma\frac{H}{H_c}, \text{ where } H_c \equiv \frac{m_e^2 c^3}{e\hbar}$$

for Gaussian beam $\Upsilon_{av} \approx \frac{5}{6}\frac{N r_e^2 \gamma}{\alpha\sigma_z(\sigma_x+\sigma_y)}$ as the average during the collision

Υ_{av} = 0.063 at ILC

(3) number of emitted photons per electron

$$n_\gamma \approx 1.08\alpha r_e N \frac{2}{\sigma_x+\sigma_y}\frac{1}{(1+\Upsilon^{2/3})^{1/2}} \approx 2.59\left[\frac{\alpha\sigma_z\Upsilon_{av}}{\lambda\!\!\!^{-}_e\gamma}\right]\frac{1}{(1+\Upsilon^{2/3})^{1/2}} \longrightarrow 1.7$$

$$\left[\frac{\alpha\sigma_z\Upsilon_{av}}{\lambda\!\!\!^{-}_e\gamma}\right] = 0.7 \text{ at ILC}$$

(4) The energy spectrum of the beamstrahlung photons

$$n_\gamma(y) = \frac{1}{\pi}\Gamma\left(\frac{2}{3}\right)\left[\frac{\alpha\sigma_z}{\lambda\!\!\!^{-}_e\gamma}\right](3\Upsilon)^{2/3}y^{-2/3} \equiv Ay^{-2/3}$$

A=1.63 at ILC

(5) the relative energy loss

$$\delta_E = \left\langle -\frac{\Delta E}{E}\right\rangle \approx 0.209\frac{r_e^3 N^2\gamma}{\sigma_z}\left(\frac{2}{\sigma_x+\sigma_y}\right)^2\frac{1}{[1+(1.5\Upsilon)^{2/3}]^2} \approx 1.20\left[\frac{\alpha\sigma_z\Upsilon_{av}}{\lambda\!\!\!^{-}_e\gamma}\right]\Upsilon_{av}\frac{1}{[1+(1.5\Upsilon)^{2/3}]^2} \longrightarrow 0.04$$

e^+e^- Pairs

P.Chen and V.Telnov,Phys. Rev. Lett. 62 (1989)1213

Low energy electron-positron pair creation

(1) Coherent process

The beamstrahlung photons interact with the magnetic field produced by the on-coming beam, then create e^+e^- pairs which is called the coherent process.

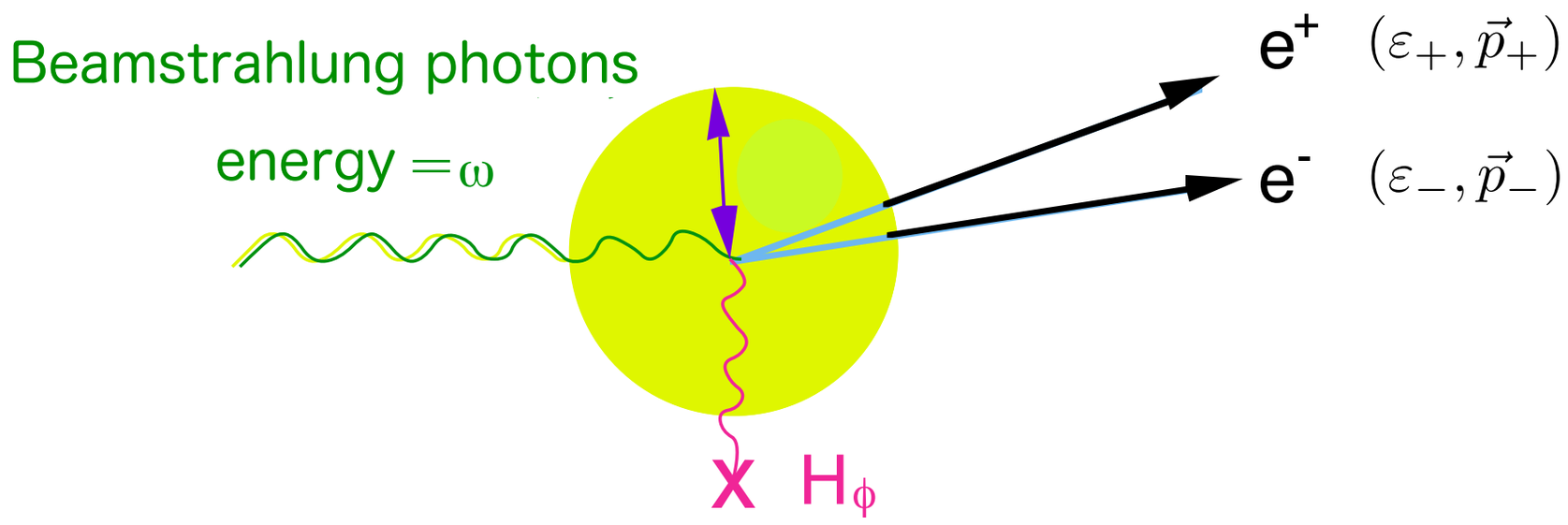

Electric field at the rest frame of e^+e^- pairs $E = \dfrac{\omega}{2m_e} H_\phi$

for the Lorentz boost of the photon energy ω divided by the invariant mass ($W = 2m_e$)

At the pair creation, a virtual electron acquires the electron mass when it is accelerated in the Compton wavelength, i.e. $eE\lambda\!\!\!^{-}_e = m_e,\ \lambda\!\!\!^{-}_e = 3.86 \times 10^{-13}\mathrm{m}$

$$\therefore W^2 = 2m_e \cdot 2eE\lambda\!\!\!^{-}_e = 2e\omega H_\phi \lambda\!\!\!^{-}_e$$

The invariant mass W of the final state in the laboratory frame is given by,

$$W^2 = (\varepsilon_+ + \varepsilon_-)^2 - (\vec{p}_+ - \vec{p}_-)^2 \approx \frac{m_e^2\omega^2}{\varepsilon_+\varepsilon_-} \qquad \text{,where } \varepsilon_{+(-)} = \sqrt{m_e^2 + |\vec{p}_{+(-)}|^2}$$

$$\because W^2 = 2m_e^2 + 2\varepsilon_+\varepsilon_- - 2p_+p_-\cos\theta \text{ , where } \theta \approx \frac{2m_e}{\omega} \therefore \cos\theta \approx 1 - \theta^2/2$$

$$\varepsilon_+\varepsilon_- \approx p_+\left(1 + \frac{m_e^2}{2p_+^2}\right)p_-\left(1 + \frac{m_e^2}{2p_-^2}\right) \approx p_+p_-\left(1 + \frac{m_e^2}{2p_+^2} + \frac{m_e^2}{2p_-^2}\right)$$

$$\therefore W^2 \approx m_e^2\frac{\omega^2(p_+ + p_-)^2 + 4p_+^2p_-^2}{p_+p_-\omega^2} \approx \frac{m_e^2\omega^2}{\varepsilon_+\varepsilon_-} \text{ for } 4p_+^2p_-^2 \ll \omega^2(p_+ + p_-)^2$$

$$\because \omega = \varepsilon_+ + \varepsilon_-,\ p_{+(-)} \sim \varepsilon_{+(-)}$$

for $\varepsilon_+ \ll \varepsilon_- \sim \omega$ to calculate the threshold energy

$$\varepsilon_+ > \frac{m_e^2}{2eH_\phi\lambda\!\!\!^{-}_e} = \frac{m_e}{2}\frac{H_c}{H_\phi},\ \text{where } H_c \equiv \frac{m_e^2c^3}{e\hbar} = 4.4\times10^9\text{Tesla for the Schwinger critical field}$$

$$\varepsilon_+ > \frac{E_{beam}}{2\Upsilon},\ \text{,where } \Upsilon \equiv \gamma\frac{H_\phi}{H_c},\ \gamma = \frac{E_{beam}}{m_e}$$ as the naive or intuitive estimation

Υ_{av} = 0.06 at ILC

Total number of pairs per primary electron

$$n_b = \left[\frac{\alpha\sigma_z\Upsilon}{\lambda\!\!\!^{-}_e\gamma}\right]^2 \frac{7}{128}\exp(-16/3\Upsilon) \text{ for } \Upsilon < 1$$ $\therefore n_b$ =0 at ILC

(2) Incoherent process

P. Chen, T. Tauchi, and D. V. Schroeder, proceedings of Snowmass 1990, ed. E. L. Berger, World Scientific, Singapore, 1992

T.Tauchi,K.Yokoya and P.Chen, Particle Accelerators 41 (1993) 29

T.Tauchi and K.Yokoya, Phys. Rev. E51 (1993) 6119

The pairs are created by individual scatterings.

the total cross section and pairs

based on the equivalent photon approximation

(Luminosity =2.74 x 10^{-3} nb^{-1}/bunch at ILC)

(a) BW (Breit-Wheeler) process

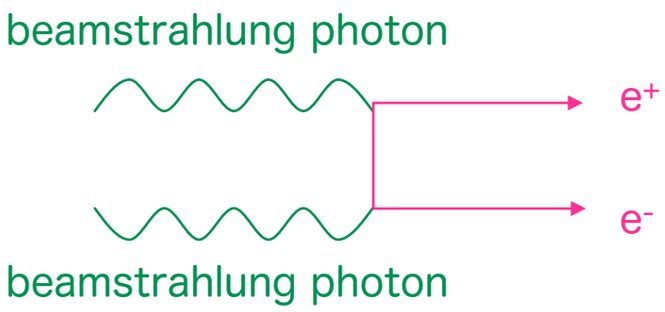

$$\sigma_{BW} = \frac{3}{16}\left(\ln 4 + \frac{3}{2}\right)\pi r_e^2 \gamma^{-2/3}(L - \ln 4)A^2$$

$$L \equiv \ln 4\gamma^2$$

3,470 (7.5)/bunch

values in () with θ >0.1, Pt >20MeV

(a) BH (Bethe-Heitler) process

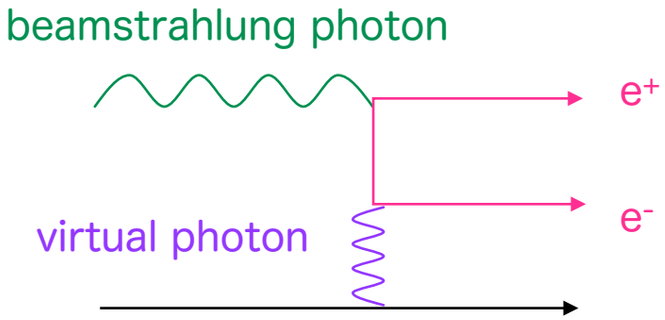

$$\sigma_{BH} = \frac{28}{3}\alpha r_e^2 (L - \frac{235}{42})A$$

445,000 (16)/bunch

(a) LL (Landau-Lifshits) process

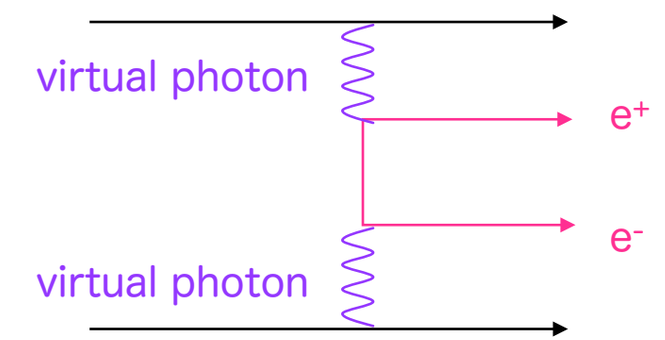

$$\sigma_{LL} = \frac{\alpha^2 r_e^2}{\pi}\left(\frac{28}{27}L^3 - 6.59L^2 - 11.8L + 104\right)$$

51,200 (4.3)/bunch

Equivalent photon approximation to regard virtual photons as real ones in scattering

$$\sigma = g \int dc \int dy_1 \int dy_2 \; n_\gamma(y_1) n_\gamma(y_2) \sigma_{\gamma\gamma \to e^+e^-}(y_1, y_2)$$

y_1, y_2 are the photon energies scaled each by the beam energy, and

$n_\gamma(y)$ is the energy distribution of the virtual photons during collisions.

$$\sigma_{\gamma\gamma \to e^+e^-}(y_1, y_2) \sim \frac{\pi r_e^2}{\gamma^2 y_1 y_2} \frac{1}{1 - c^2}$$

this approximation shows the upper limit by a factor of 2 for the analytic calculations

the fractional energy of positron (or electron) with the scattered angle θ, c=cosθ,

$$x = \frac{2 y_1 y_2}{y_1(1 - c) + y_2(1 + c)}$$

, where c should be replaced with βc in the exact formulas.

The spectrum of the virtual photons are given by,

$$dn_\gamma = \frac{\alpha}{\pi} \frac{dy}{y} \int_{y_{\perp min}}^{y_{\perp max}} \frac{y_\perp^2 \, dy_\perp^2}{(y_\perp^2 + y^2/\gamma^2)^2} = \frac{\alpha}{\pi} \frac{dy}{y} \log\left(\frac{y_{\perp max}^2 + y^2/\gamma^2}{y_{\perp min}^2 + y^2/\gamma^2} \right) \approx \frac{\alpha}{\pi} \frac{dy}{y} \log\left(\frac{y_{\perp max}^2}{y^2/\gamma^2} \right)$$

$$y_{\perp max} = 1/\gamma \text{ for } k_{\perp max} = m_e \text{ and } y_{\perp min} = y/\gamma^2 \qquad \therefore n_\gamma(y) = \frac{2\alpha}{\pi} \frac{1}{y} \log\left(\frac{1}{y} \right)$$

V.B. Berestetskii, E.M.Lifshitz and L.P.Pitaevskii, Quantum Electrodynamics, Pergamon Press

Estimation of the minimum transverse energy of the virtual photons

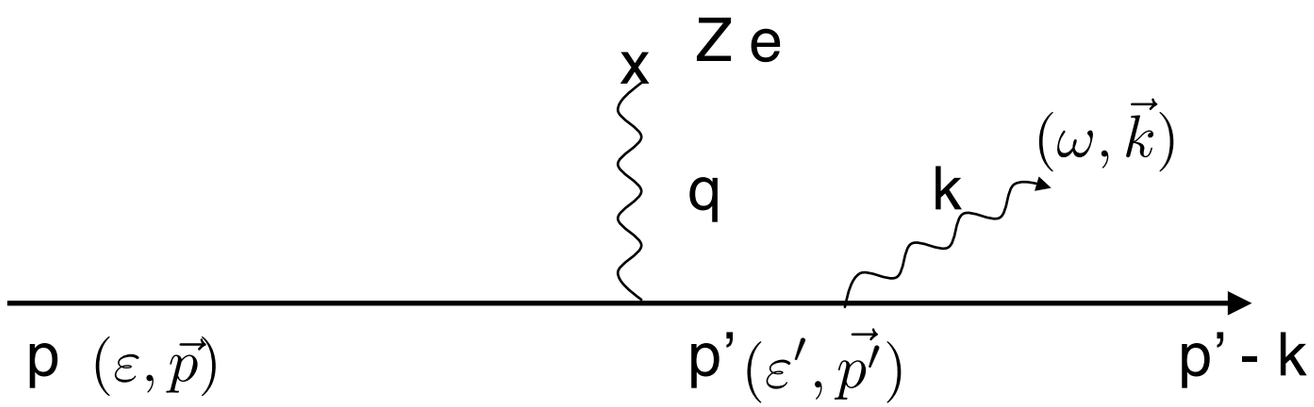

bremsstrahlung process

$\delta q = (p' - k - p) - (p' - p) = \delta p' - k,\ \delta p' = \omega \dfrac{\partial p'}{\partial \varepsilon'} = \omega/\beta$ due to a soft photon emission

$\dfrac{\delta q}{|\vec{q}|} \ll 1$ and $\omega \ll \varepsilon$ for soft photon emission

(1) in the non-relativistic case, i.e. $\beta \sim 0$

$$\delta q \approx \delta p' \therefore \frac{\delta p'}{|\vec{q}|} = \frac{\omega}{|\vec{q}|\beta} = \omega \frac{b}{\beta} = \omega\tau \ll 1,\ b \equiv \frac{1}{|\vec{q}|}, \tau \equiv \frac{b}{\beta c}$$

b = impact parameter

τ = characteristic time

(2) in the relativistic case, i.e. $\beta \sim 1$

$$\delta q = \omega/\beta - k = \omega(1/\beta - 1) \approx \omega/(2\gamma^2) \to \omega/\gamma^2$$

the minimum transverse momentum

for a virtual photon is regarded as a soft photon with the transverse momentum

Two important effects in the incoherent process

(1) Geometric Reduction

The transverse momentum ($k_\perp$) of the virtual photons are equivalent to the impact parameter (b) by conversion of $b = \hbar c/k_\perp,\ \hbar c = 197\mathrm{MeV}\cdot\mathrm{fm}$

If the impact parameter exceeds the beam size, the pair creation is suppressed. The vertical beam size (σ_y) is the relevant one for the flat beam at linear colliders. so, the cut-off $k_\perp$ is approximately estimated to be $k_{\perp cut-off} = \hbar c/(2\sigma_z)$

$$\therefore n_\gamma \to \frac{\alpha}{\pi}\frac{1}{y}\log\left(\frac{1/\gamma^2}{k^2_{\perp cut-off}/E^2 + y^2/\gamma^2}\right) = \frac{\alpha}{\pi}\frac{1}{y}\log\left(\frac{1}{\left(\frac{\lambda\!\!\!^{-}_e}{2\sigma_y}\right)^2 + y^2}\right)$$

$$\sigma(e^+e^- \to e^+e^-e^+e^-) \approx \sigma_{LL}\frac{\log(\sigma_y/\lambda\!\!\!^{-}_e)}{2\log\gamma} \approx 0.37\sigma_{LL} \text{ at ILC}$$

ref : V.N.Baier et al., Phys. Lett. 229B (1989) 135

For the experimental verification : A.E.Blinov et al., Phys.Lett. 113B (1982) 423

(2) Effect of the strong external field

The incoherent pair creation processes are suppressed if the electron is radiated in the strong electromagnetic field produced by the on-coming beam, the former processes can be regards as the virtual photon radiation in free space while the latter is one in the strong field.

Comparing the two radiation coherent (photon formation) lengths,

$$l_R = \rho/\gamma \text{ and } l_{RH} = (\rho/\gamma)(\omega_c/\omega)^{1/3} \text{ for } \omega \ll \omega_c, \text{ respectively,}$$

$l_R > l_{RH}$ to take place the incoherent pair creations

$$\therefore \theta > \theta_H \text{ for } l_R = \rho\theta,\ l_{RH} = \rho\theta_H$$

i.e. longer the coherent length for photons with larger the transverse momentum

$$\therefore k_\perp > \omega\theta_H = \frac{\omega}{\gamma}\left(\frac{\omega_c}{\omega}\right)^{1/3}, \text{and } y_\perp > \frac{y}{\gamma}\left(\frac{\Upsilon}{y}\right)^{1/3}$$

So the strong external field suppresses the virtual photons with small transverse transverse momenta similar to the geometric reduction.

The low energy pair particles are deflected by the on-coming beams.

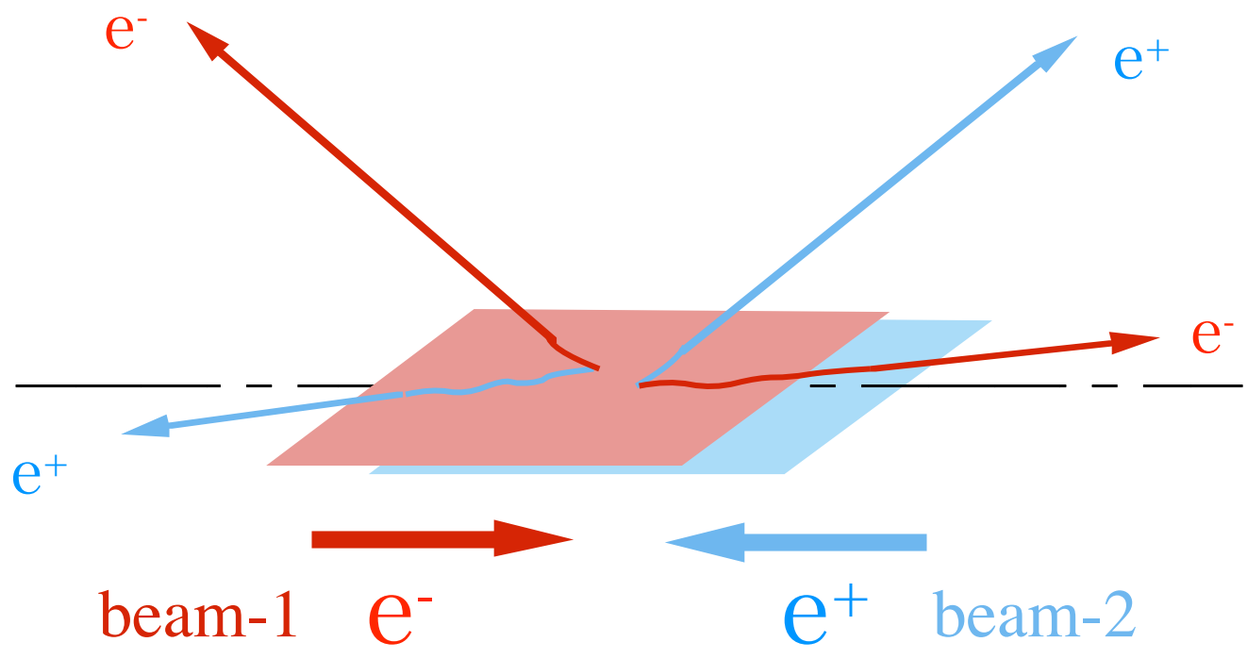

simulations of the ILC (head-on collisions) at √s =500GeV by CAIN v2.42

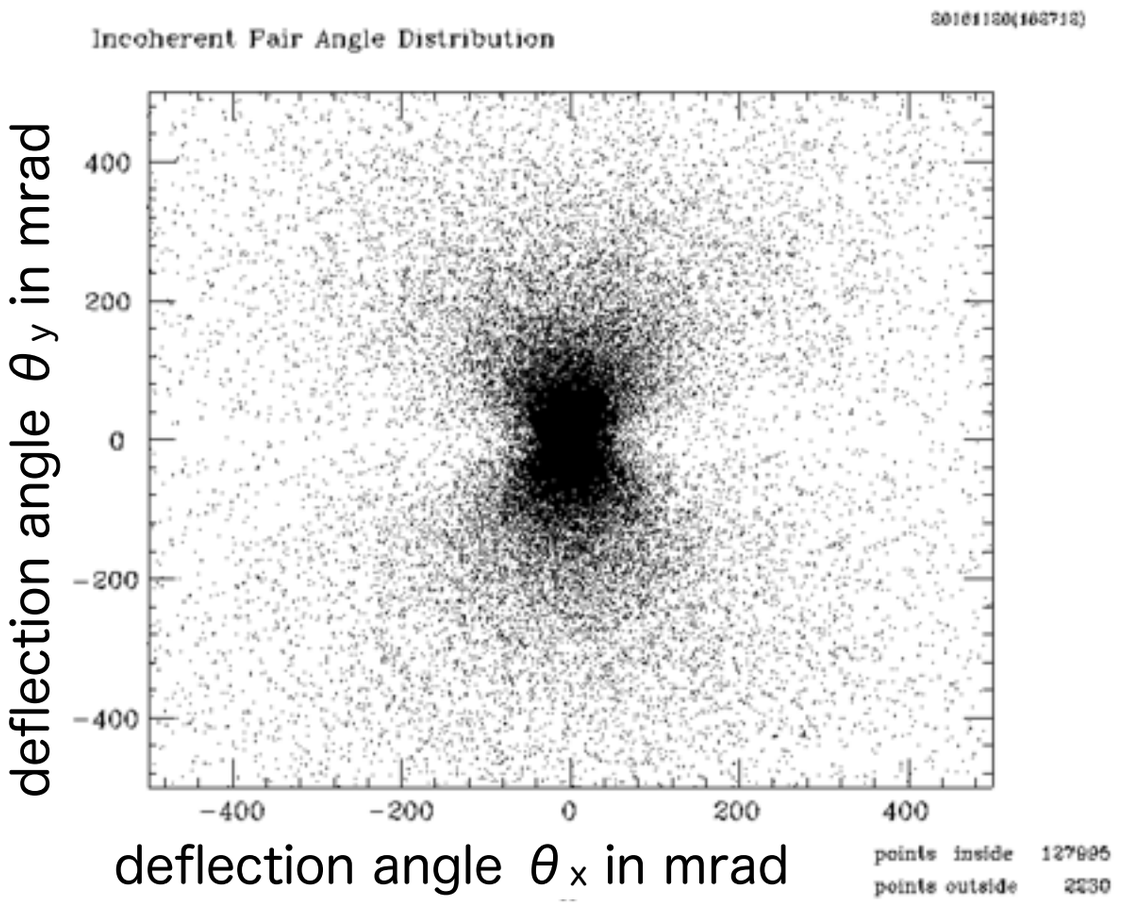

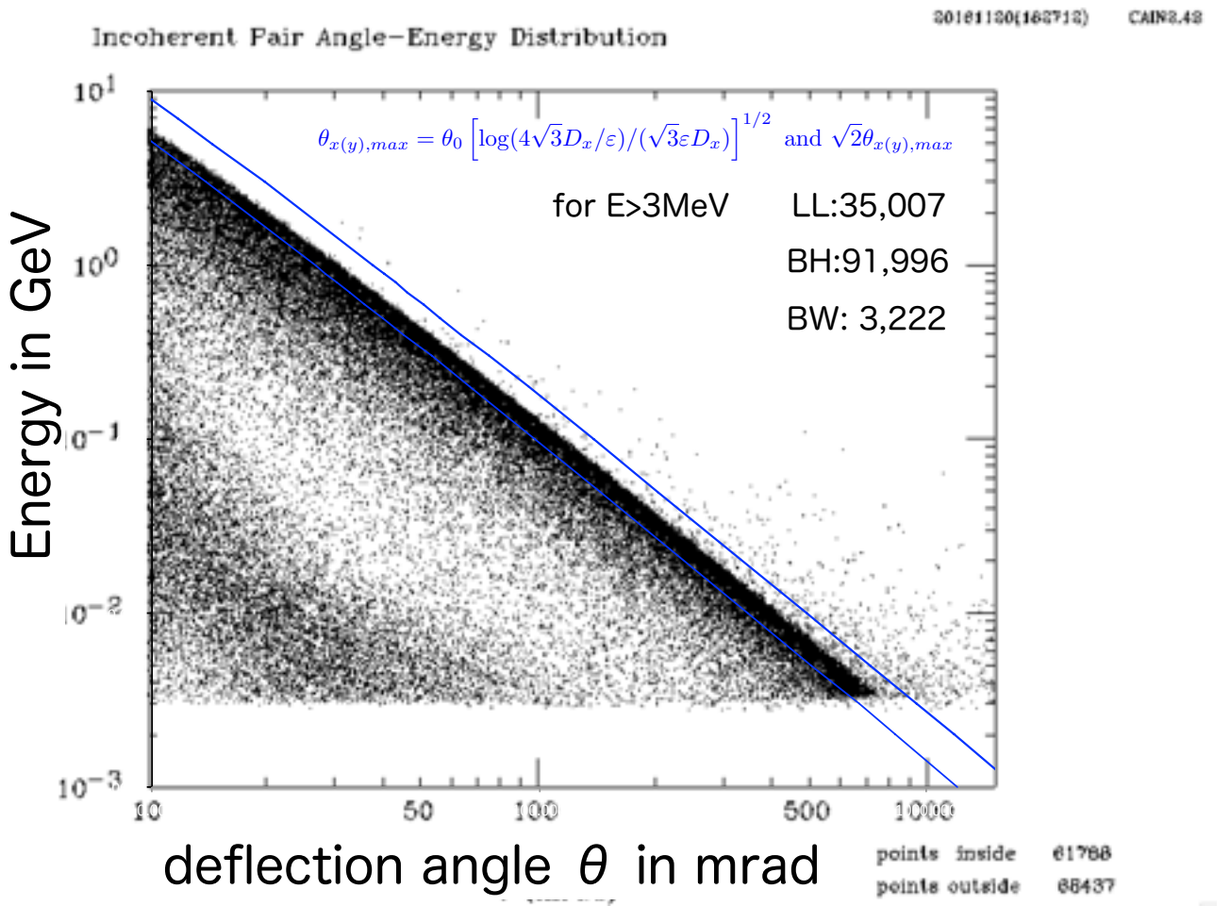

Helical movements of charged particles in the magnetic field

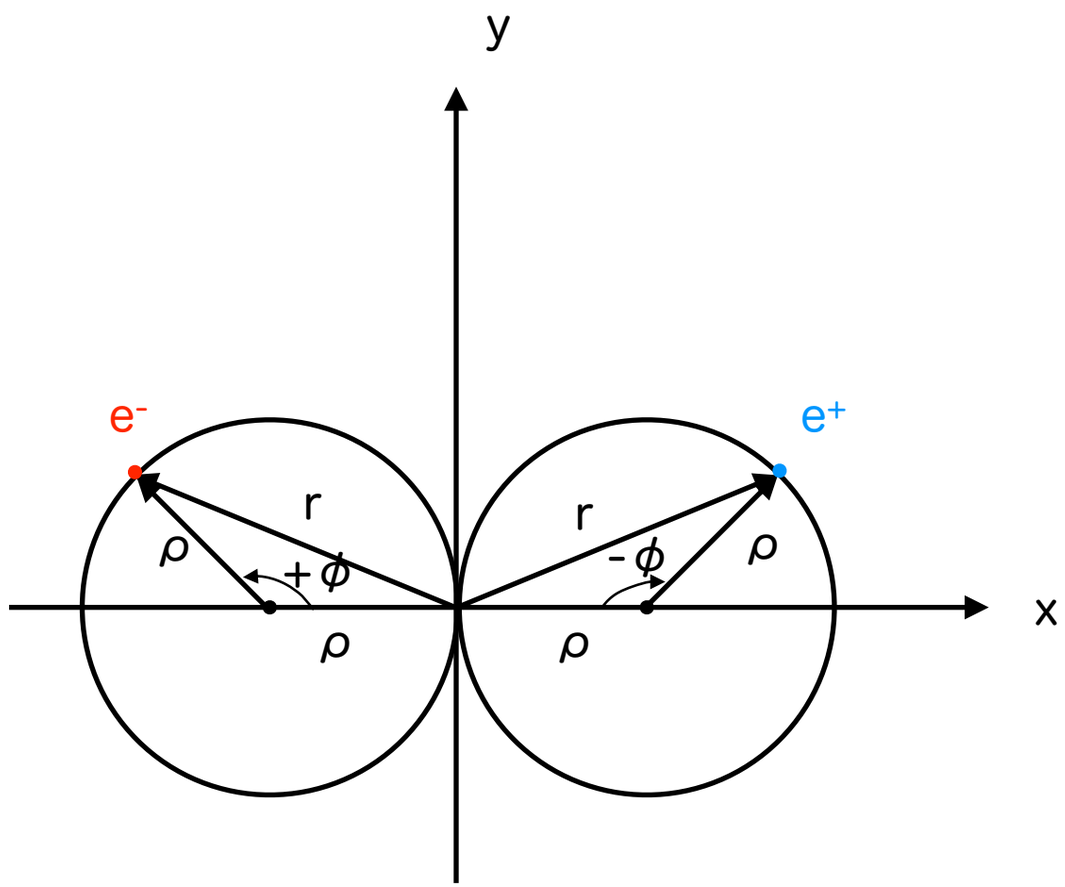

$\vec{B} \parallel z$

$\vec{P}_0 \parallel y$

$\vec{P}_0 : \;\; P_x = P\cos\phi_0 \sin\theta_0, \;\; P_y = P\sin\phi_0 \sin\theta_0, \;\; P_z = P\cos\theta_0$

$$r = 2\rho \sin\left(\frac{\phi}{2}\right), \;\; \rho = \frac{\sqrt{P_x^2 + P_y^2}}{0.3B}, \;\; \phi = \frac{0.3Bz}{P_z}$$

$$x = r\cos\left(\theta_0 \mp \frac{\phi}{2}\right), y = r\sin\left(\theta_0 \mp \frac{\phi}{2}\right), \;\; \text{where - for positrons and + for electrons}$$

head-on collisions

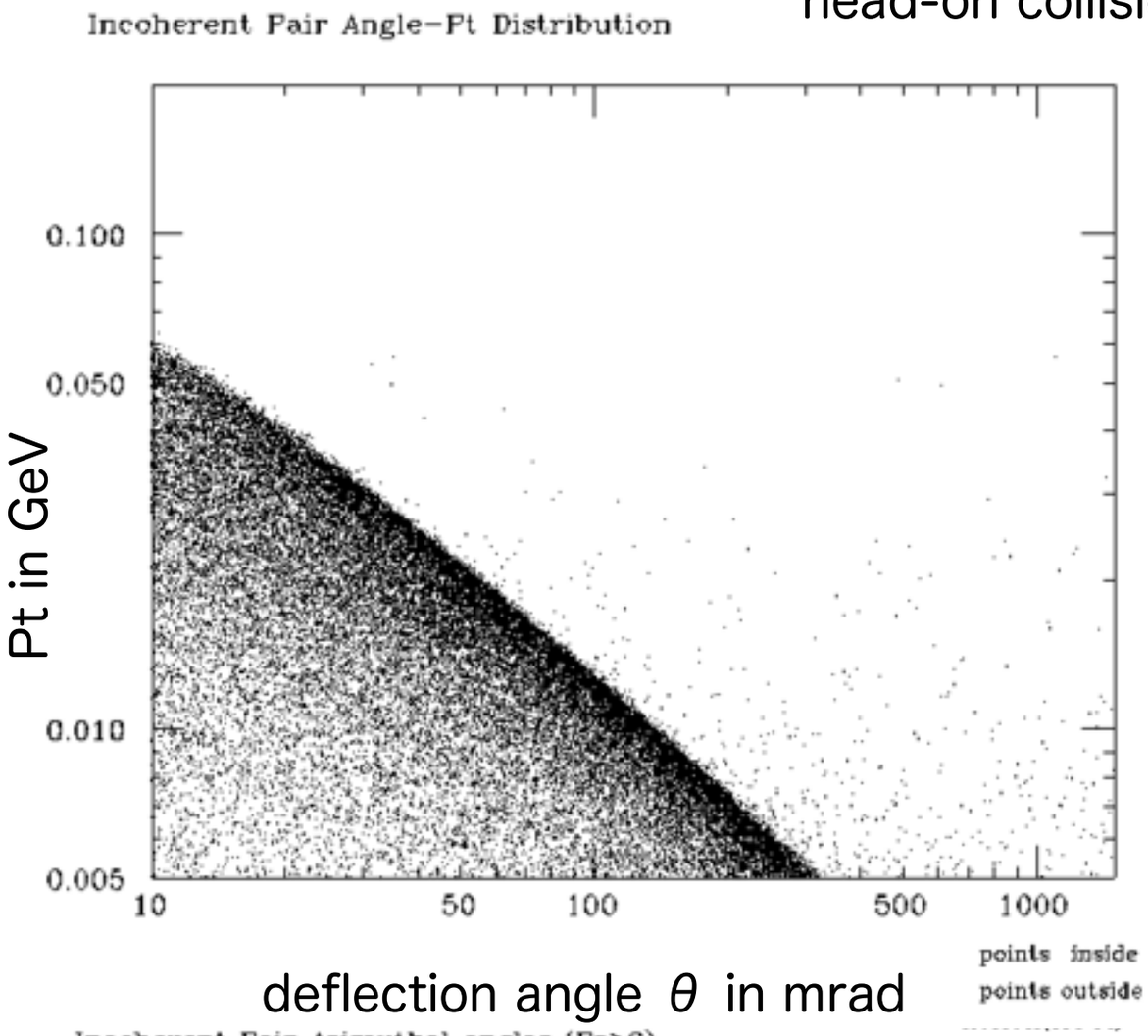

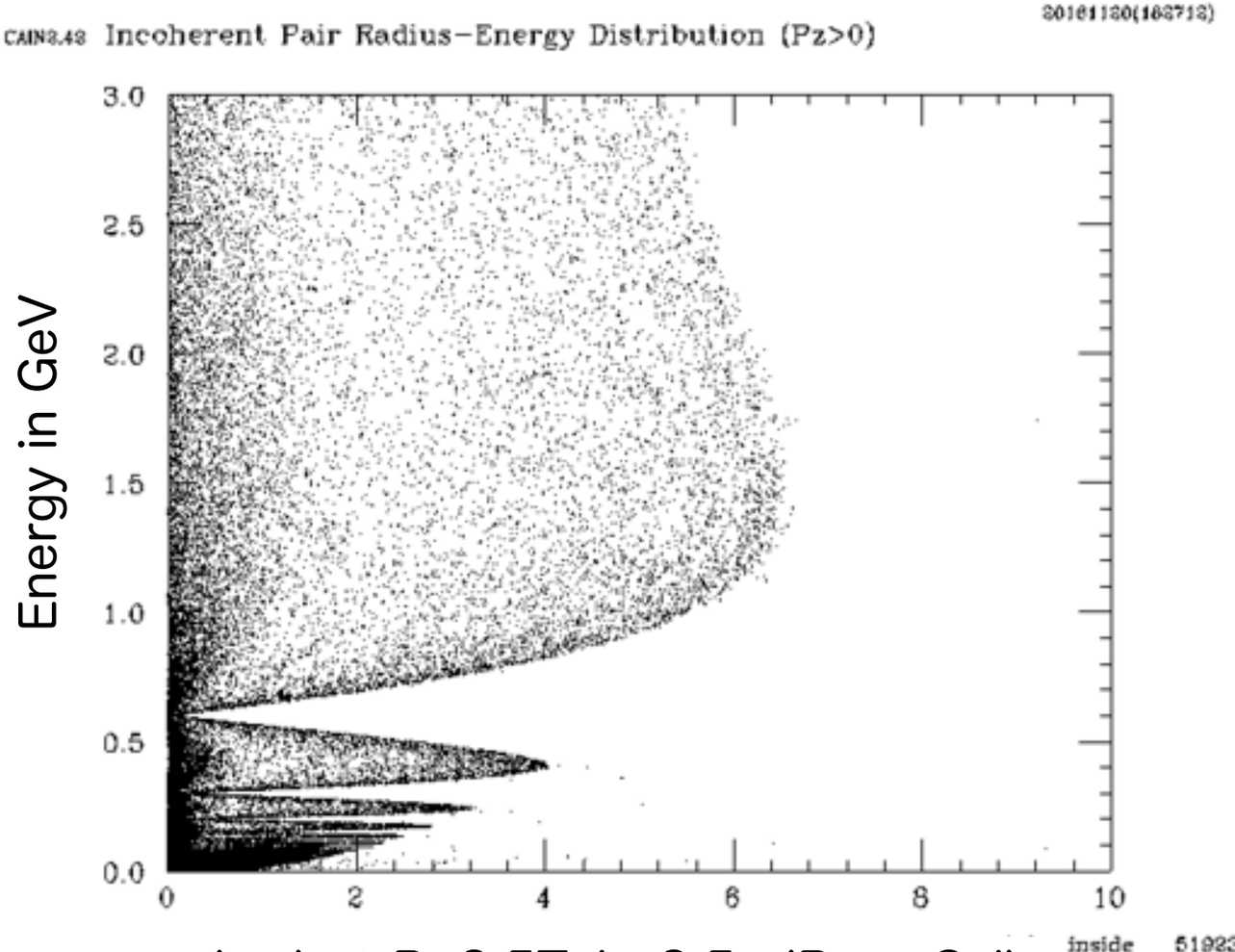

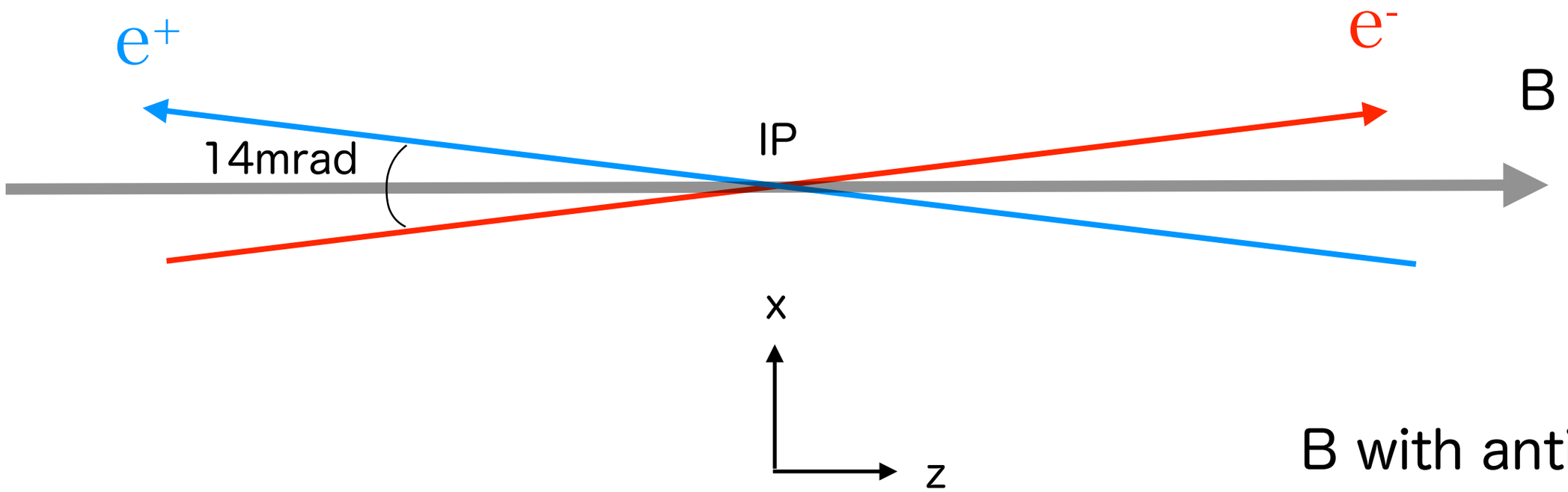

B with anti-DID

(Detector Integrated Dipole)

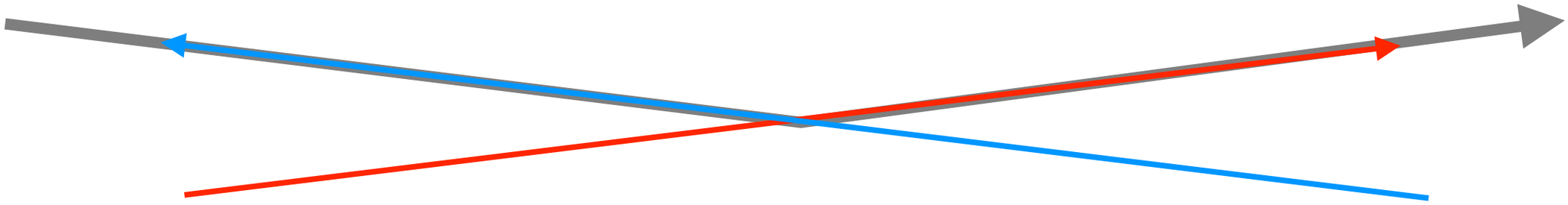

good for the scattered low energy particles

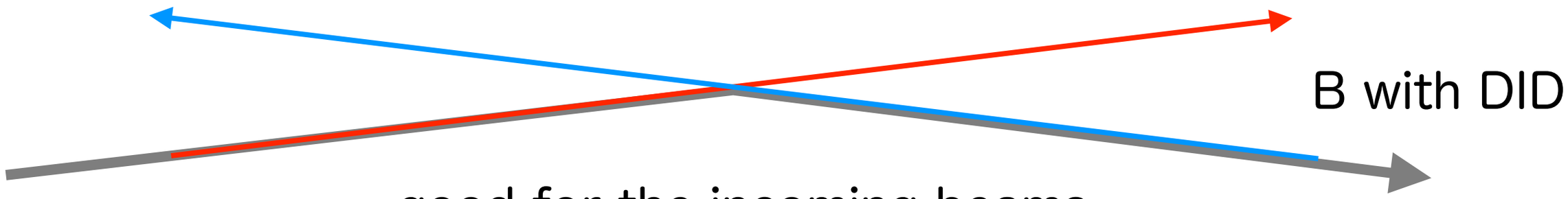

good for the incoming beams

no synchrotron radiation, no spin precession …

head-on collisions (anti-DID)

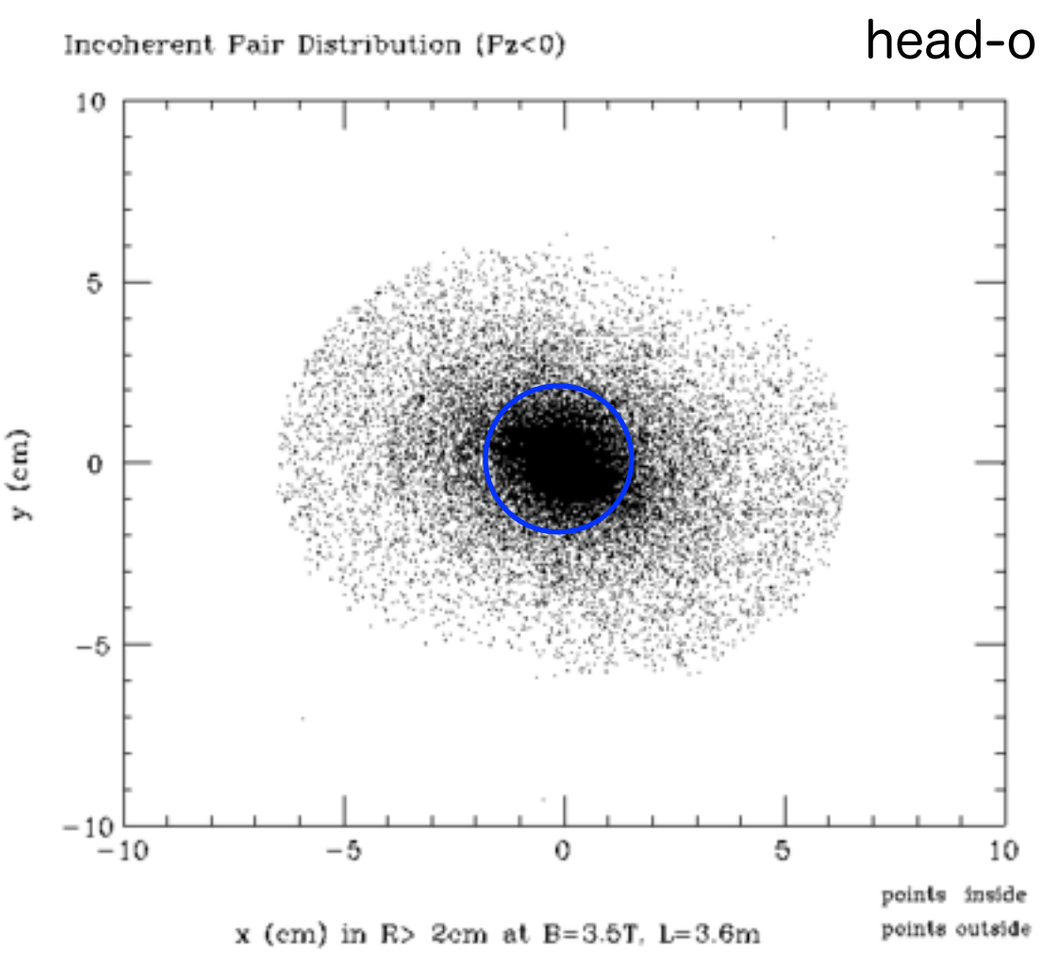

beam pipe

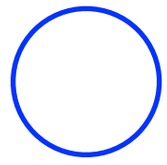

in/out
4cmϕ

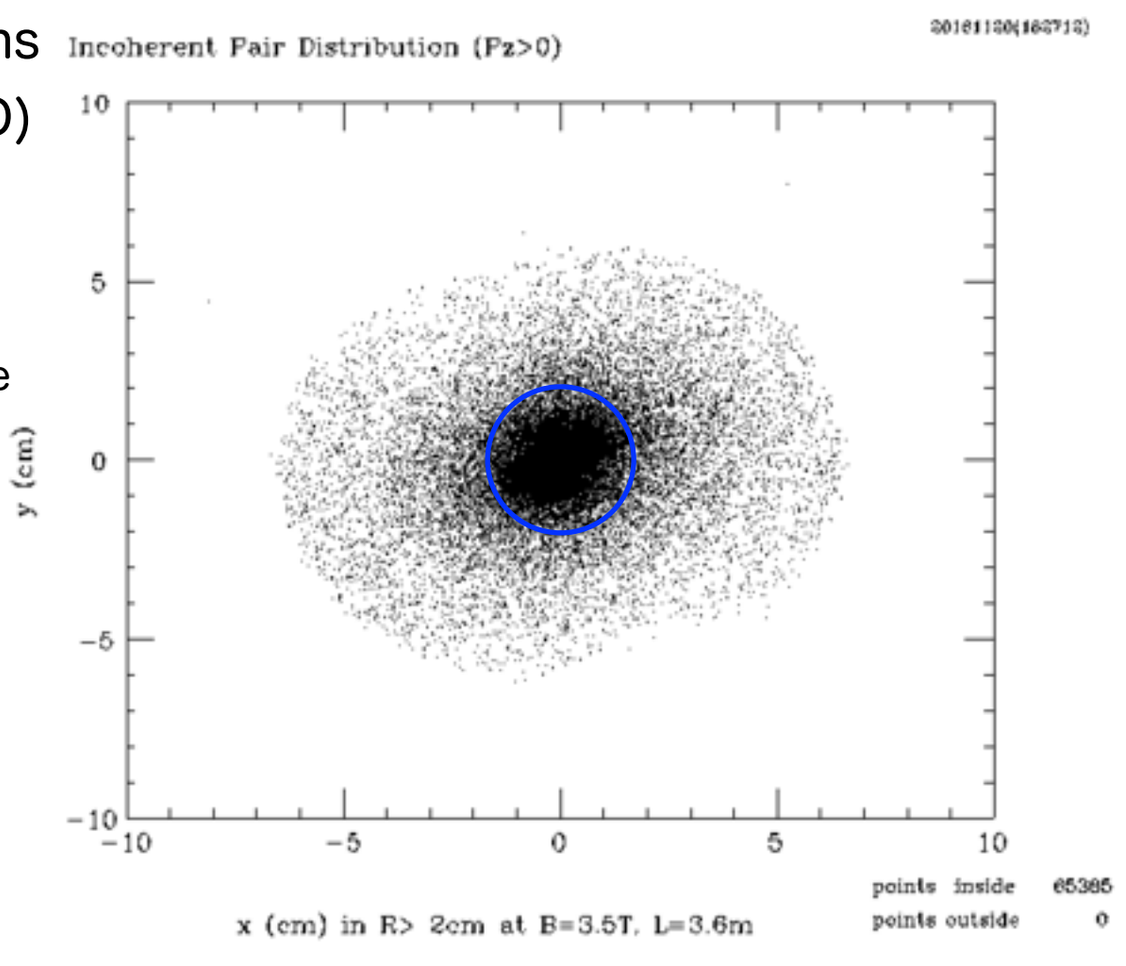

14mrad collisions

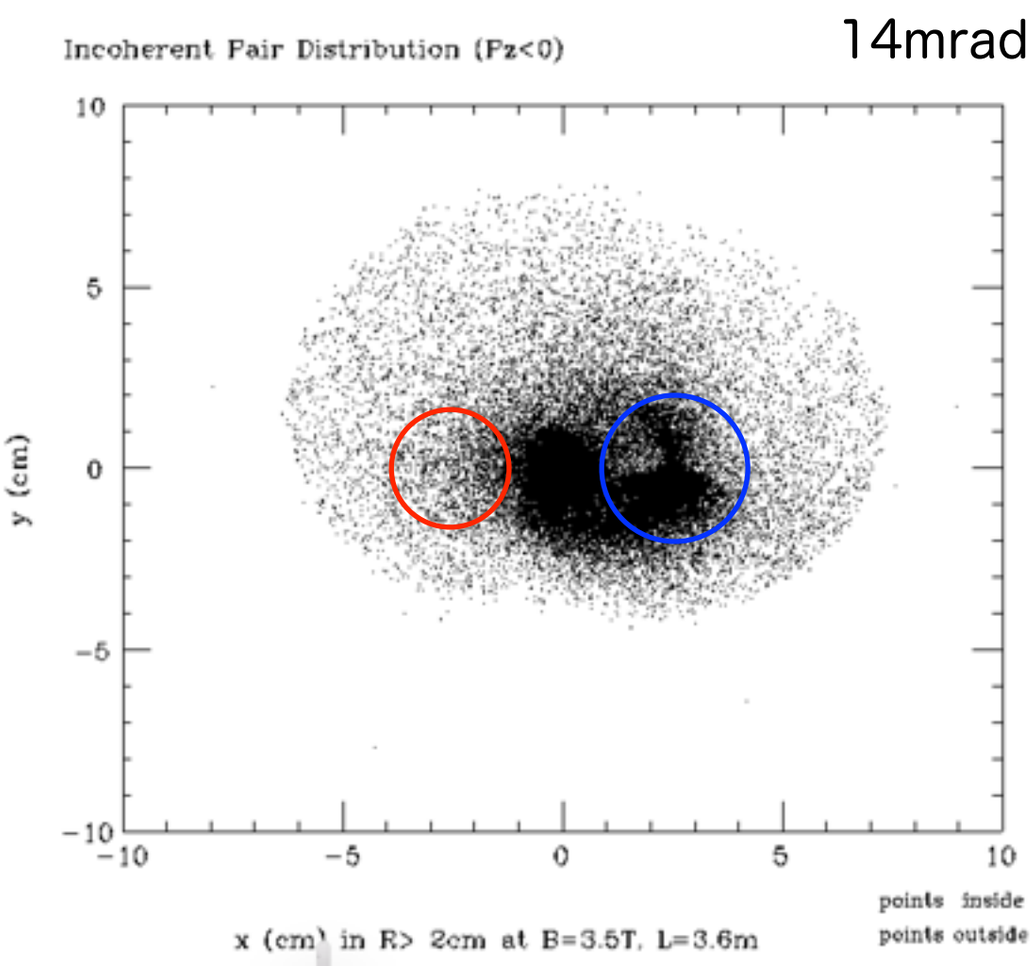

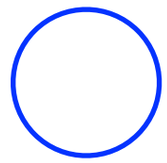

out
4cmϕ

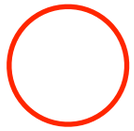

in
3.2cmϕ

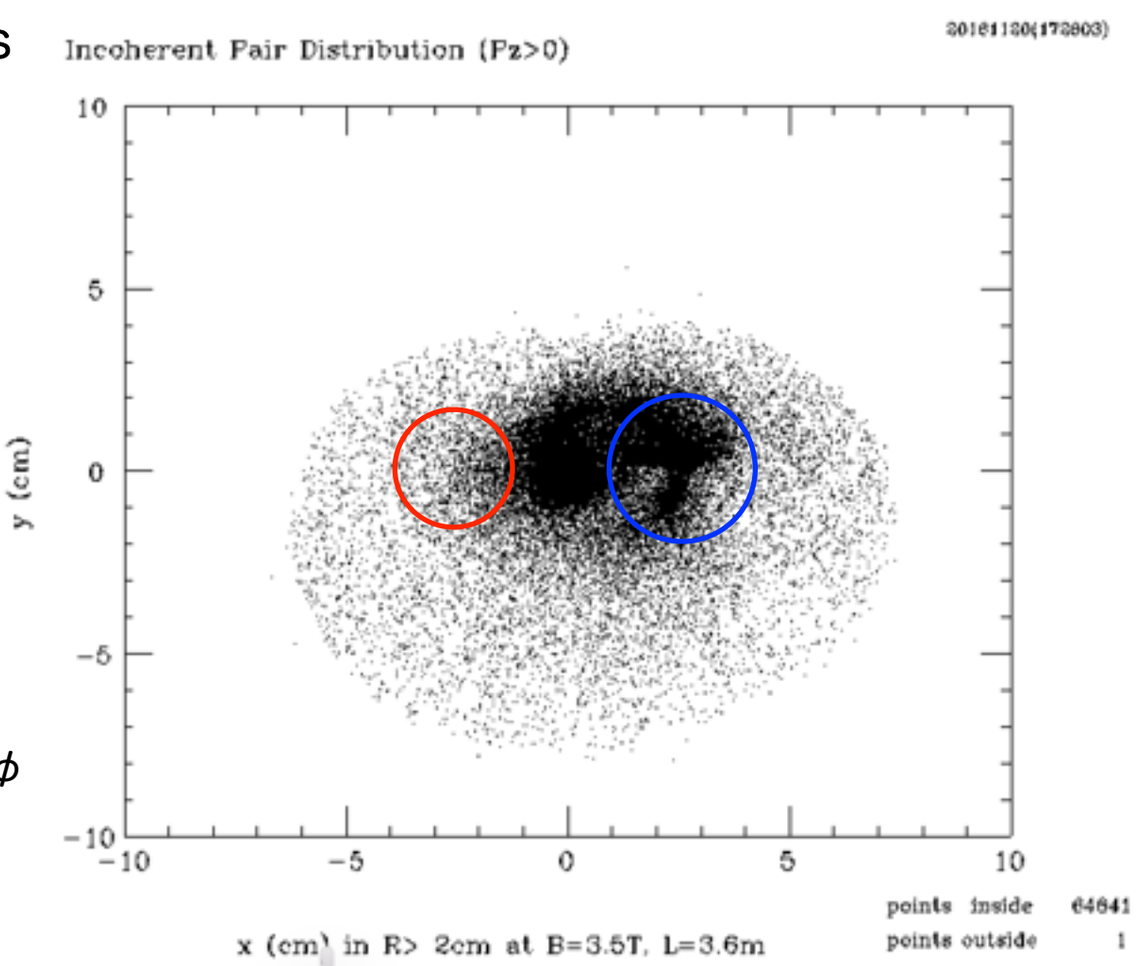

Minimum Veto Angle

Primary requirement from SUSY

$e^+e^- \rightarrow \tilde{\tau}^+_{L(R)}\tilde{\tau}^-_{L(R)}$

M.Nojiri, K.Fujii and T.Tsukamoto, Phys. Rev. D54(1996)6756.

$$\sqrt{s} = 500\mathrm{GeV}$$

$$m_{\tilde{\tau}} = 150\mathrm{GeV},\ m_{\tilde{\chi}^0_1} = 100\mathrm{GeV}$$

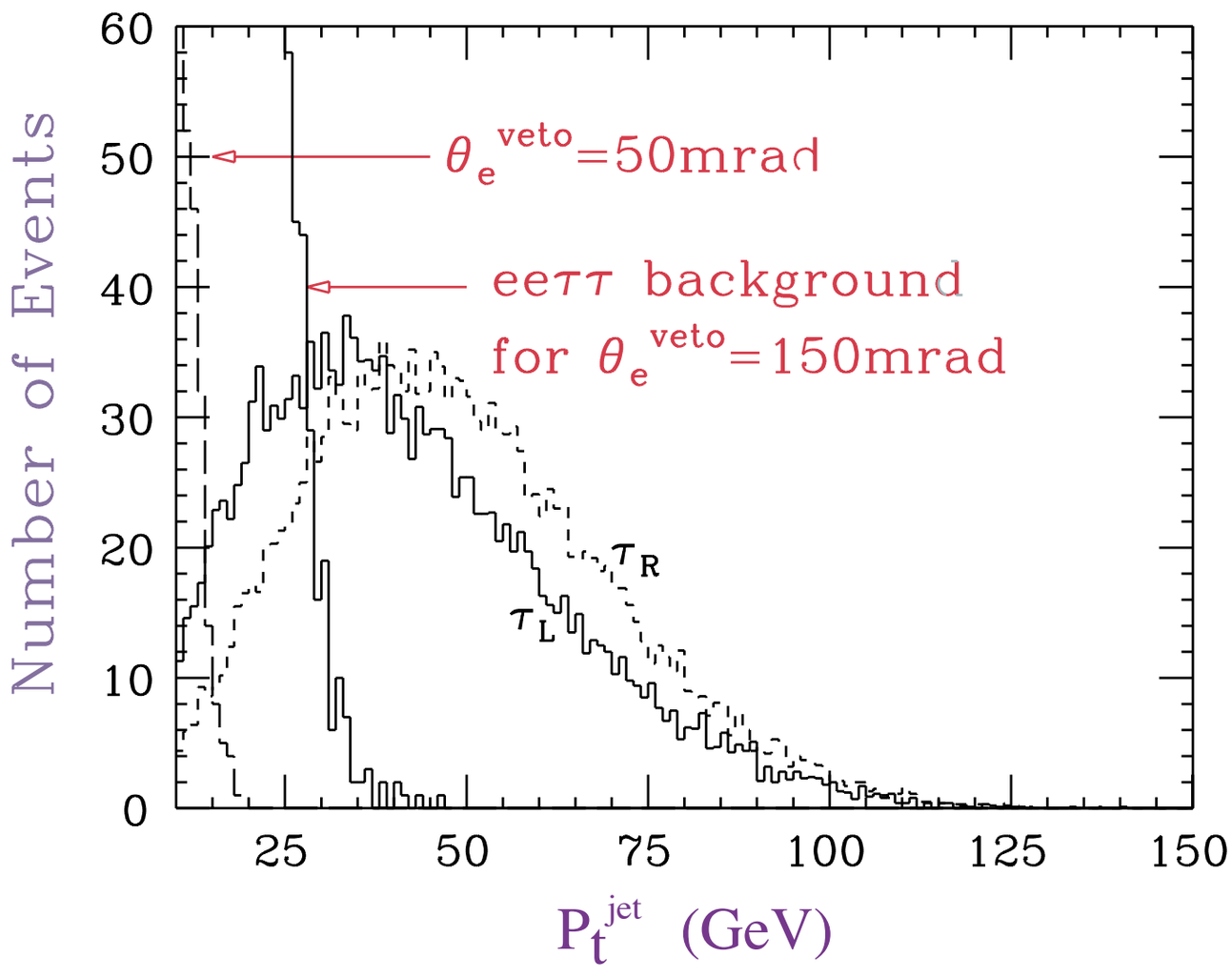

→ Δm=50GeV

θ veto =50mrad

mSUGRA
WMAP data

$\Omega_{CDM}\, h^2$ =0.094 - 0.129
(2 σ)

more stringent

Δm=5GeV

θ_{veto} =5mrad

P. Bambade et al. hep-ph/0406010

Electron tagging efficiency by BeamCal

studies with the RDR nominal parameter

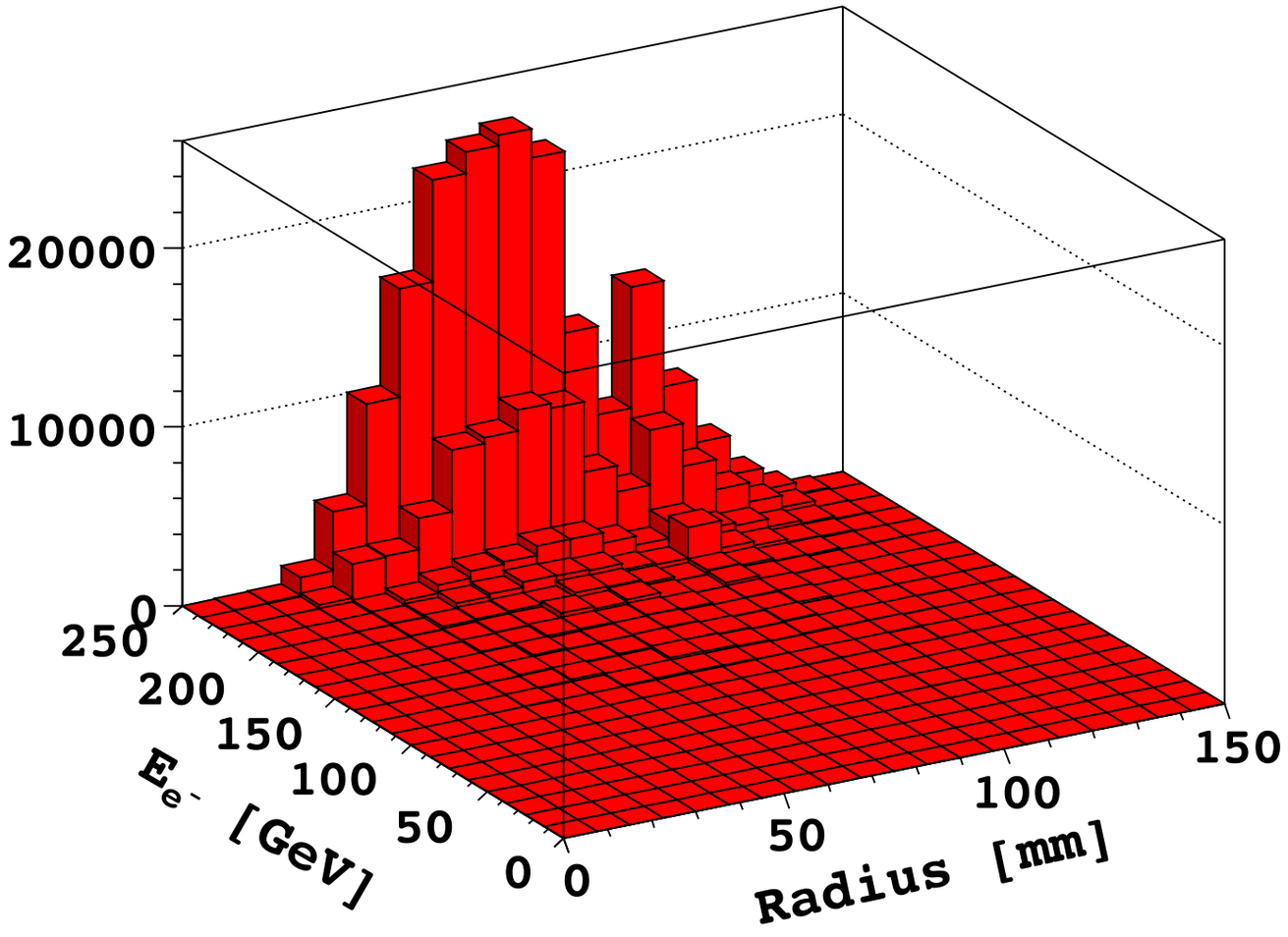

for head-on collision

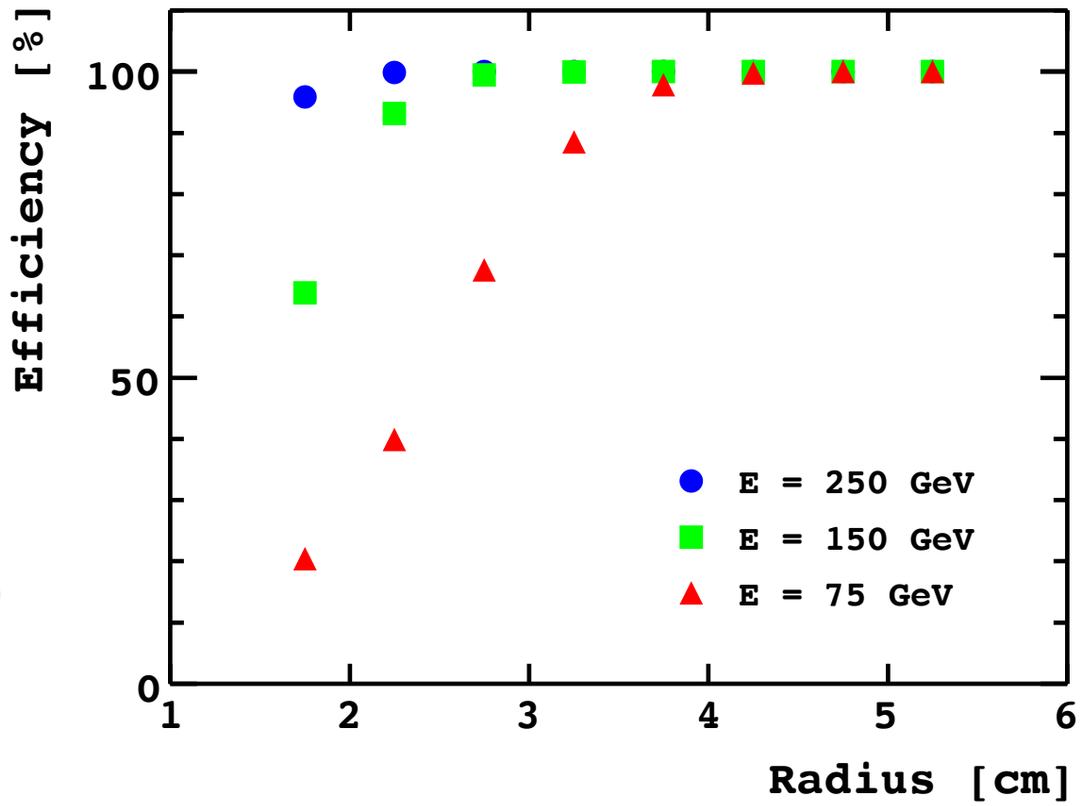

Figure 2: *Left: Electron energy and spatial distribution of the 2-photon background events passed all selection cuts except the BeamCal veto. Right: The efficiency to veto an electron of energy 75, 150, 250 GeV as a function of the radius in the BeamCal.*

The BeamCal is located 370 cm from the interaction point. The inner radius is 1.5 cm for 0 mrad crossing angle and 2 cm for 20 mrad. The outer radius is 16.5 cm.

P.Bambade, V.Drugakov and W. Lohmann, The impact of BeamCal performance at different ILC beam parameters and closing angles on stay searches, LAL 06-145, October 2006

Pair background & BeamCal (2005, RDR nominal)

head-on

~ 14mrad with antiDID

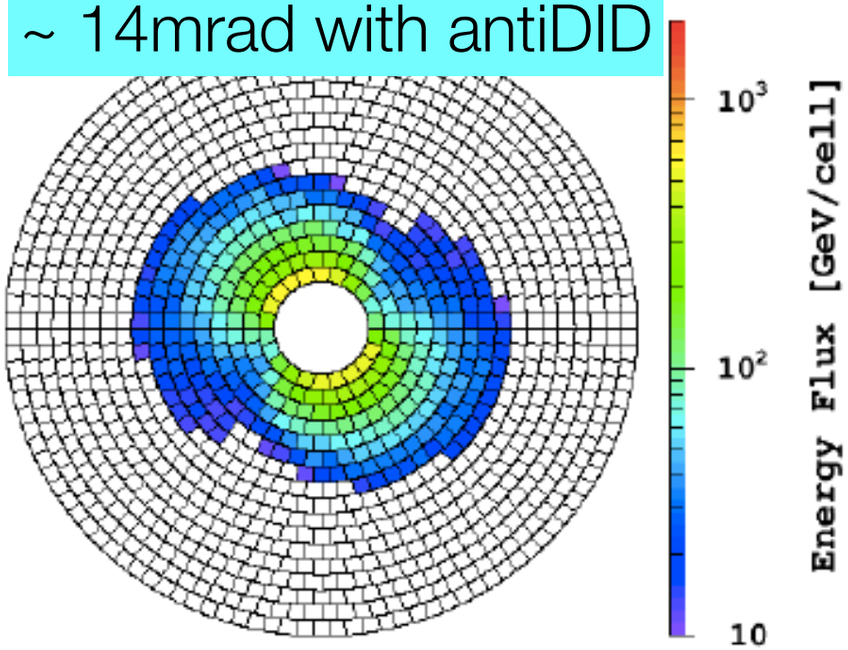

X-angle

~ without antiDID

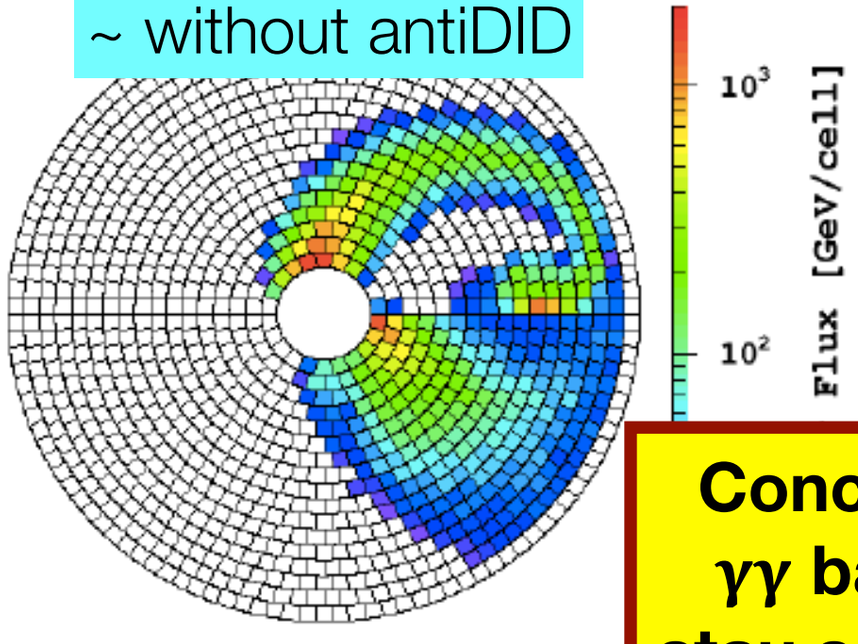

Conclusion in 2005: γγ background for stau search increases by factor ~ 8.5

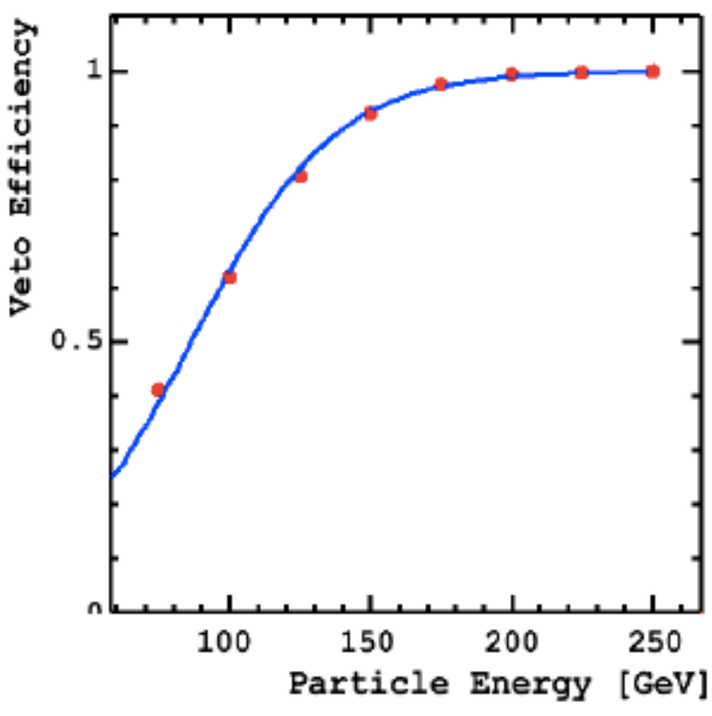

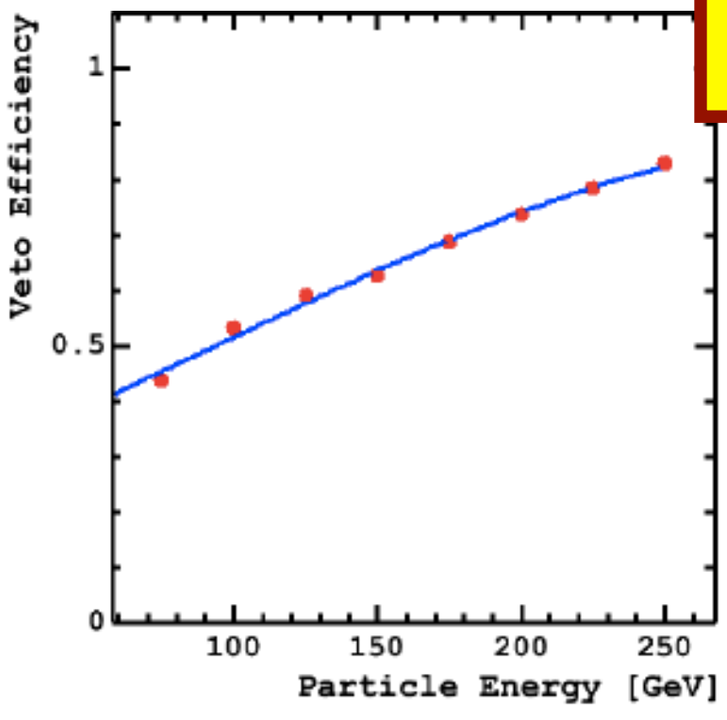

due to two holes of 32 and 40mm diameter in BeamCal for the incoming and out-going beams, respectively.

… and with ILD 2009

[Bechtle et al Phys.Rev. D82 (2010) 055016, Berggren 1308.1461]

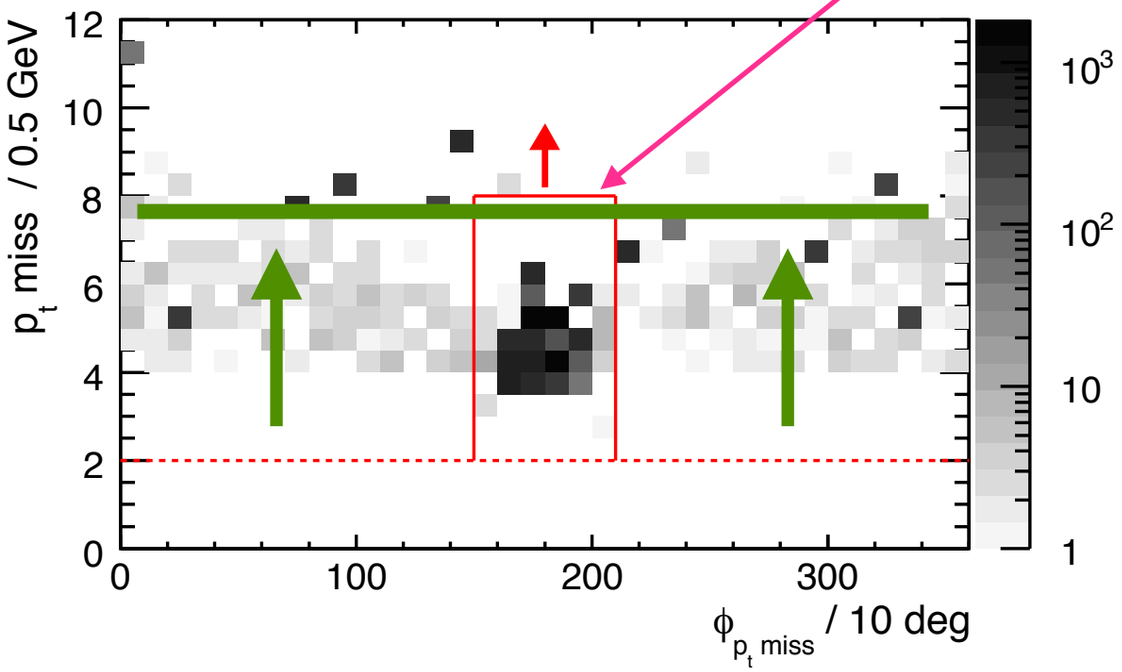

- with parametrised BeamCal response from full sim with pair background (14mrad, antiDID)
- gamma-gamma bkg: fake missing pt if beam electron goes down the incoming beam pipe - **or not visible above pair background!**

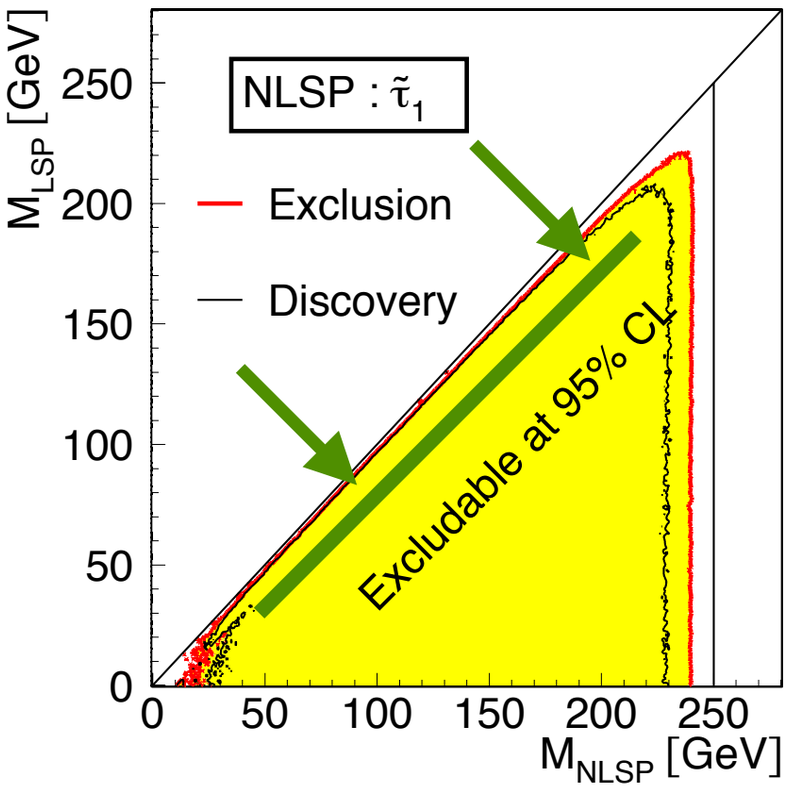

- "grey band" similar to what SiD calls "plug region"
- more background => grey band turns black => can't use this kinematic region
- loose low-delta-M region (at diagonal) **=> loose complementarity with LHC**

WIMP Dark Matter

so called Single Photon Events

- model-independent dark matter searches using mono-photon signature
- complementary to LHC, direct detection, indirect detection [arxiv:1604.02230]
- backgrounds:
  - $\nu\nu$ +(n)γ: reduced by 1/100 with P=(+80%,-30%)
  - rad. Bhabhas: crucially depends on hermeticity

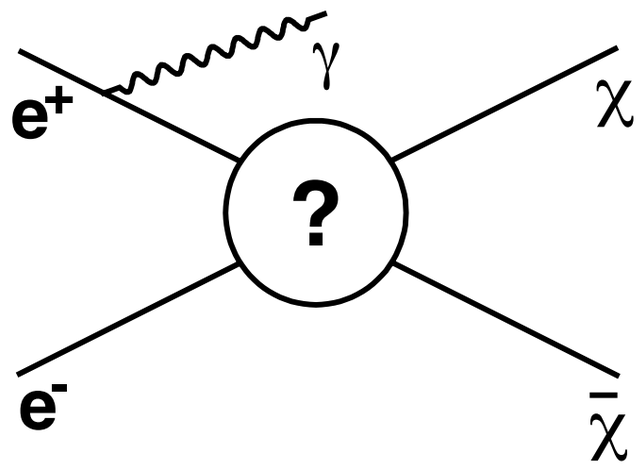

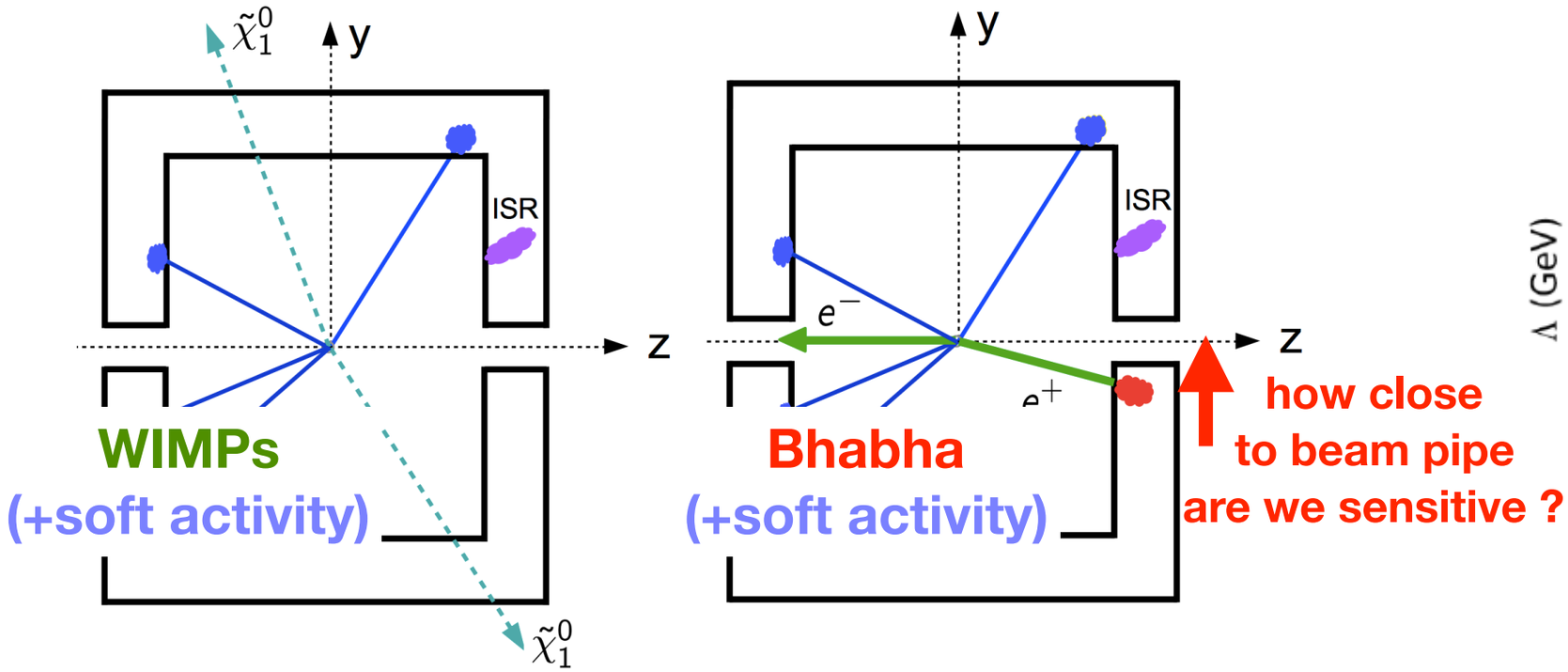

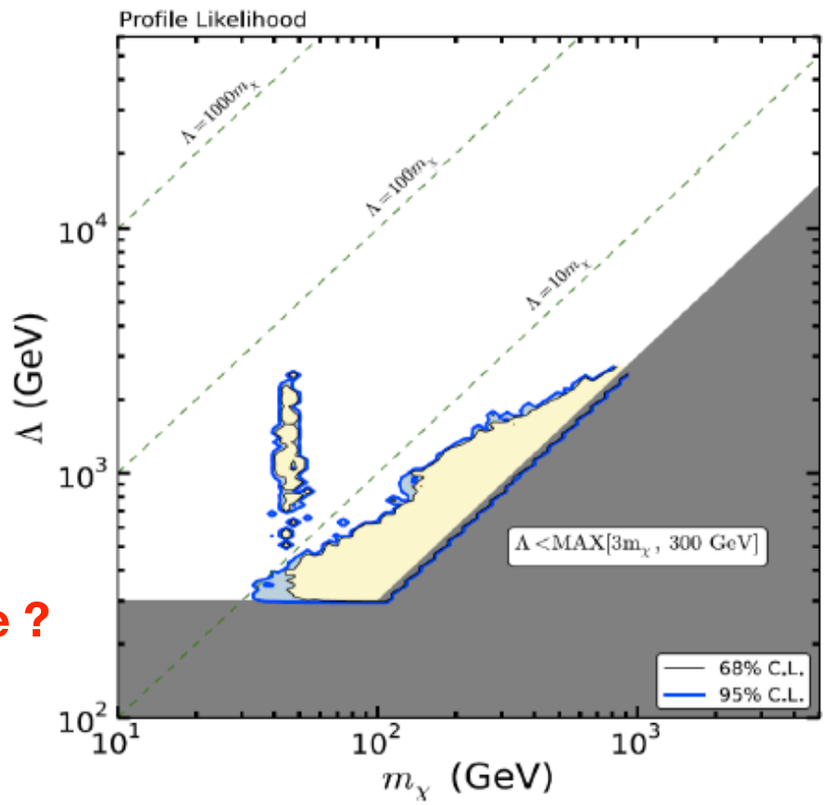

Near-degenerate New Particles (e.g. Higgsinos)

- "blind spot" of LHC
  => ILC direct discovery potential
- ILC precision spectroscopy allows determination of gaugino masses even if in multi-TeV regime
- visible part of event:
  - very few, very soft tracks

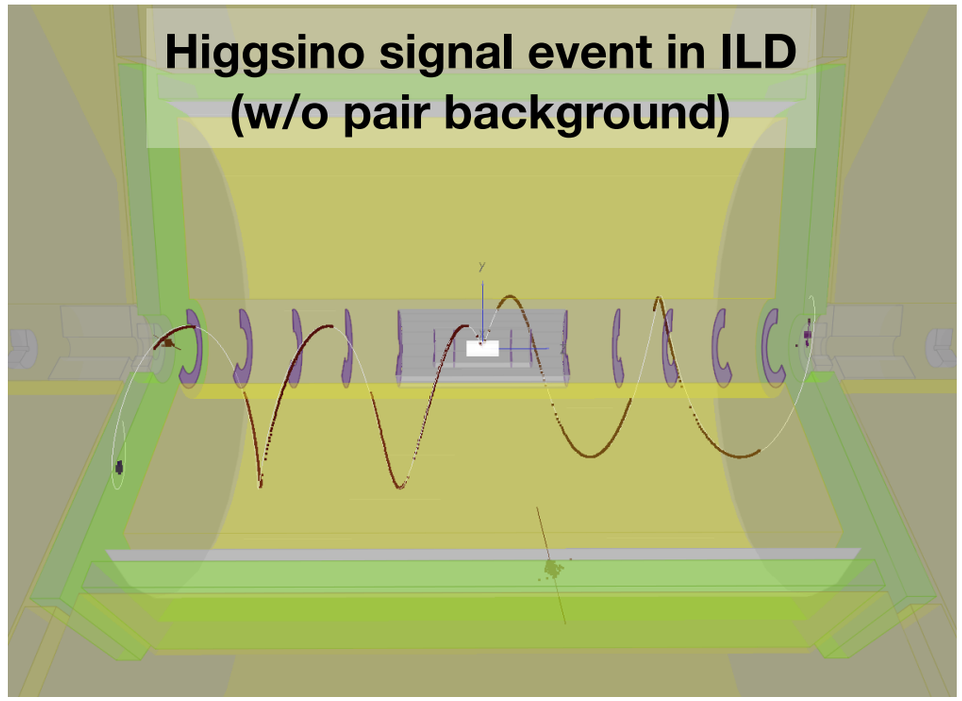

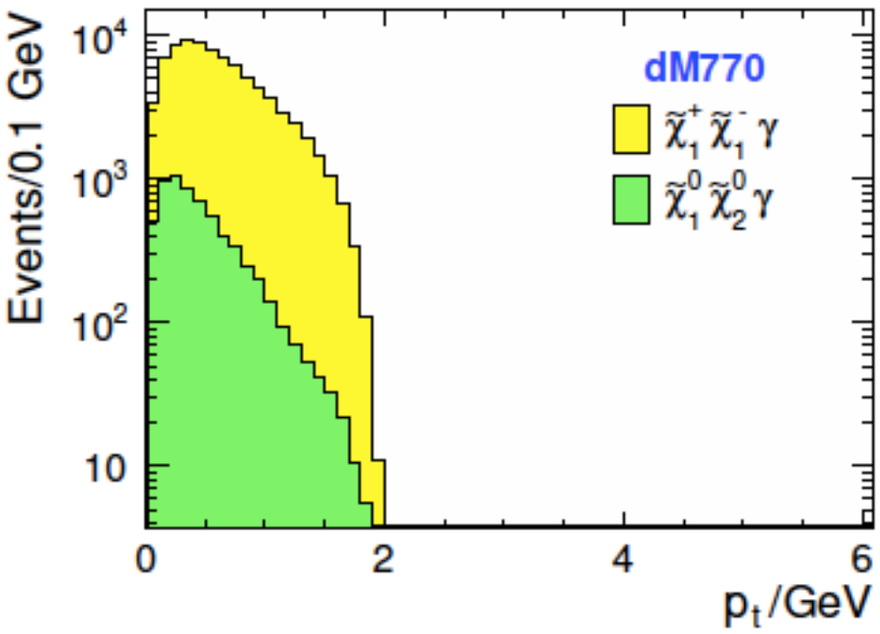

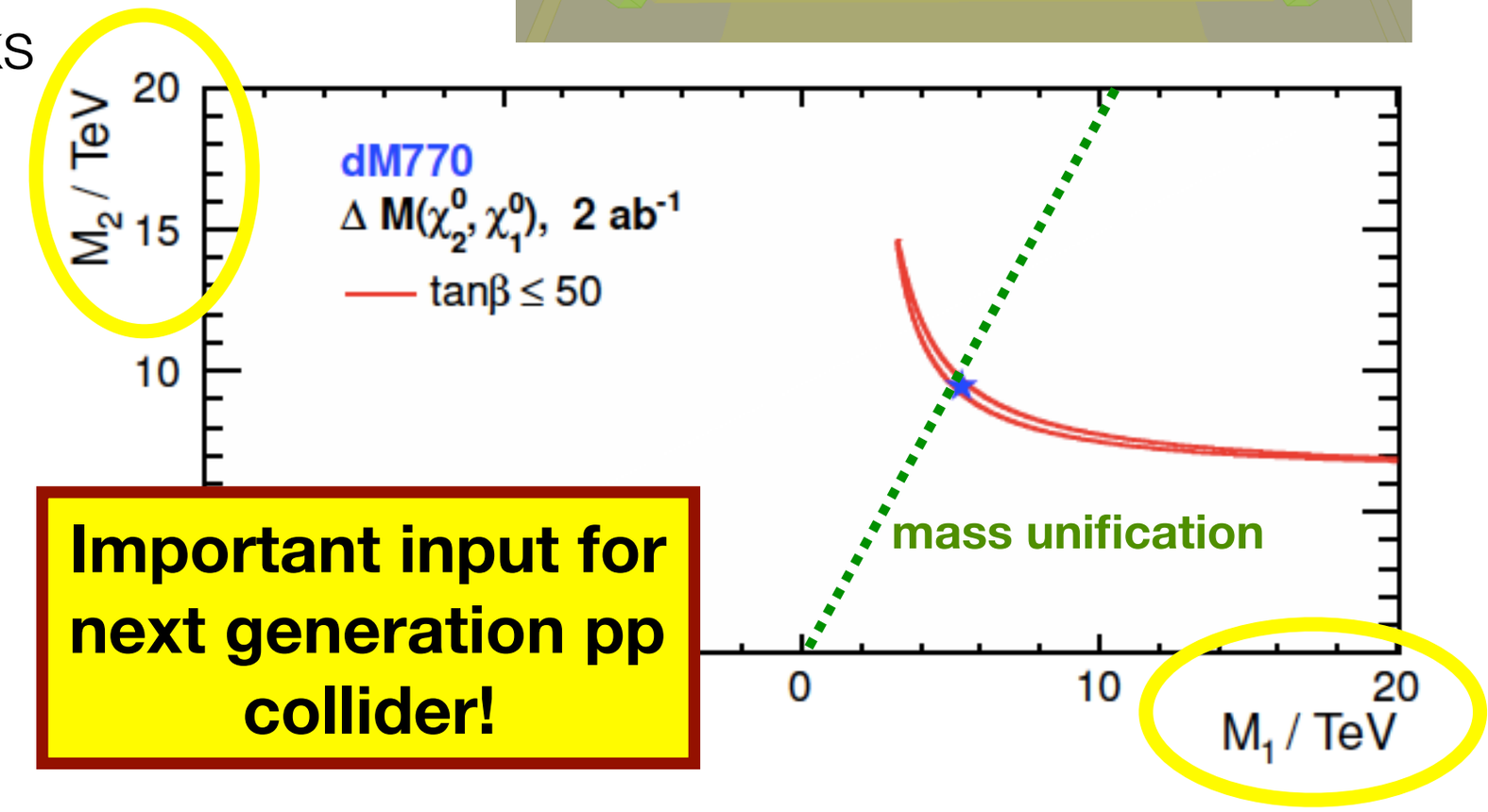

Important input for next generation pp collider!

MiniJets

Mini-jets

M.Drees, R.M.Godbole, PRL67(1991)1189

High P_t jets in $\gamma\gamma$ collisions at e^+e^- colliders

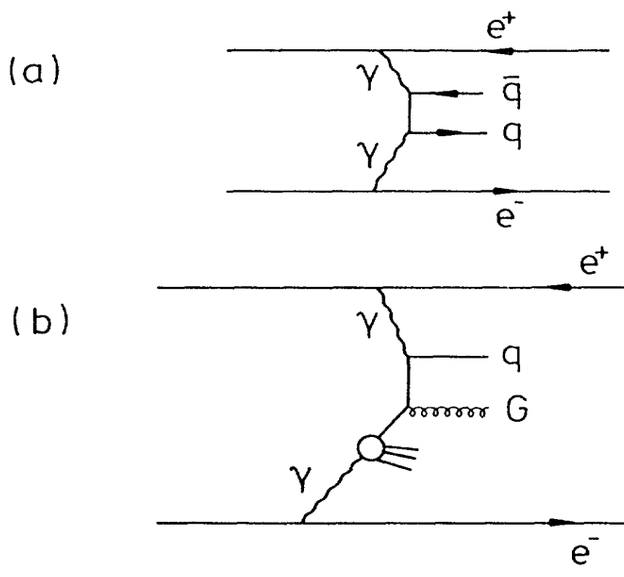

direct process

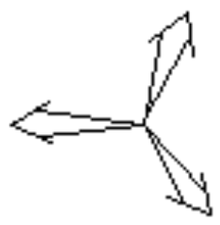

once-resolved process

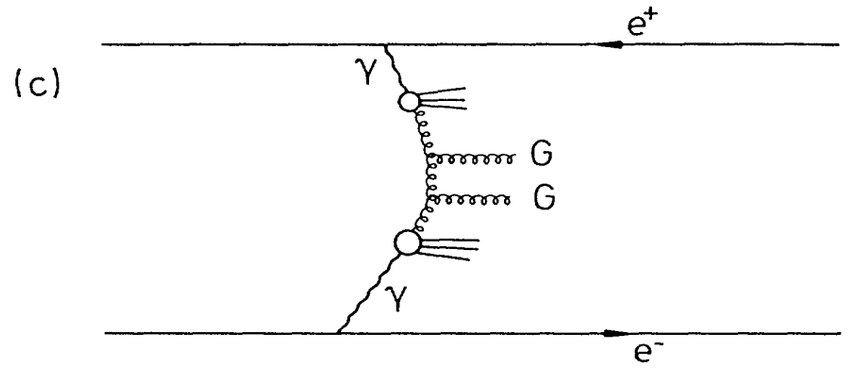

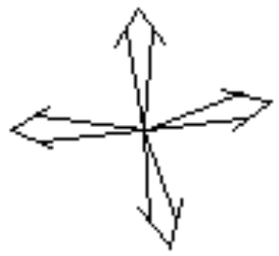

twice-resolved process

for the once-resolved process

$$d\sigma = f_{\gamma/e}(x_1)q^{\gamma}(x_2, Q^2)f_{\gamma/e}(x_3)q^{\gamma}(x_4, Q^2)d\hat{\sigma}$$

, where the parton densities in a photon, i.e. the hadronic components are $q^{\gamma} = (u^{\gamma}, d^{\gamma}, G^{\gamma})$

and the photon flux of an electron $f_{\gamma/e}(x_i)$ for the sum of bremmstrahlung and beamstrahlung

Problematic issue : violation of unitarity condition

“Realistic” model with Eikonal approximation

P.Chen, T.L.Barklow, M.E.Peskin, PRD49(1994)3209

Total hadronic cross section of photon photon interaction based on the VMD

$$\sigma(\gamma\gamma \to \text{hadrons}) = \sigma_0\{1 + (6.30 \times 10^{-3})[\ln(s)]^{2.1} + (1.96)s^{-0.37}\}$$

$$\sigma_0 = 200\mu\text{b}$$

VMD (Vector Meson Dominance) model : $\gamma = \rho + \omega + \phi + \cdots$

Jet yield is calculated by

$$\mathcal{Y}(p_*) = \int_0^1 dz_1 F(z_1) \int_0^1 dz_2 F(z_2) \int_{-1}^1 d\cos\theta \frac{d\sigma}{d\cos\theta}(gg \to gg)\theta(p_\perp - p_*)$$

parton distribution of the photon

$F(z) = f_g(z) + \frac{4}{9}\sum_i [f_{qi}(z) + f_{\overline{q}i}(z)]$ using the parametrization of Drees and Grassie (DG)

all of the parton cross sections are approximated by the gluon-gluon cross section:

$$\frac{d\sigma}{d\cos\theta}(gg \to gg) = \frac{9}{16}\frac{\pi\alpha_s^2}{\hat{s}}\left[\frac{(2+\cos^2\theta)^3}{\sin^4\theta}\right]$$

Jet yields in photon photon collisions

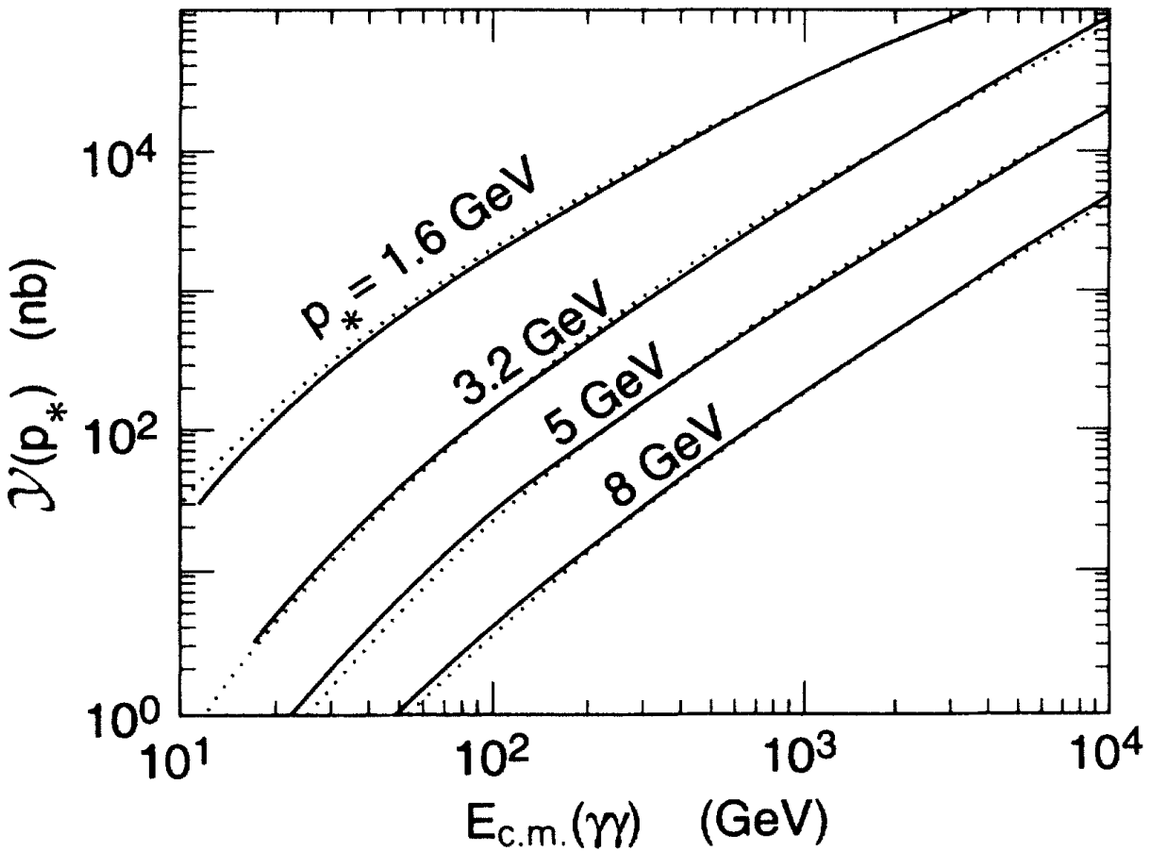

minimum bias events + mini-jets, double counting ?

mini-jets cross sections exceed the total cross section ?

The rise of total cross section can be described by scattering with a disk, i.e. the soft "gray" hadronic interactions become "black" by the effect of gluon-gluon scattering saturating the total cross section.
"eikonalization" to produce multiple scatterings

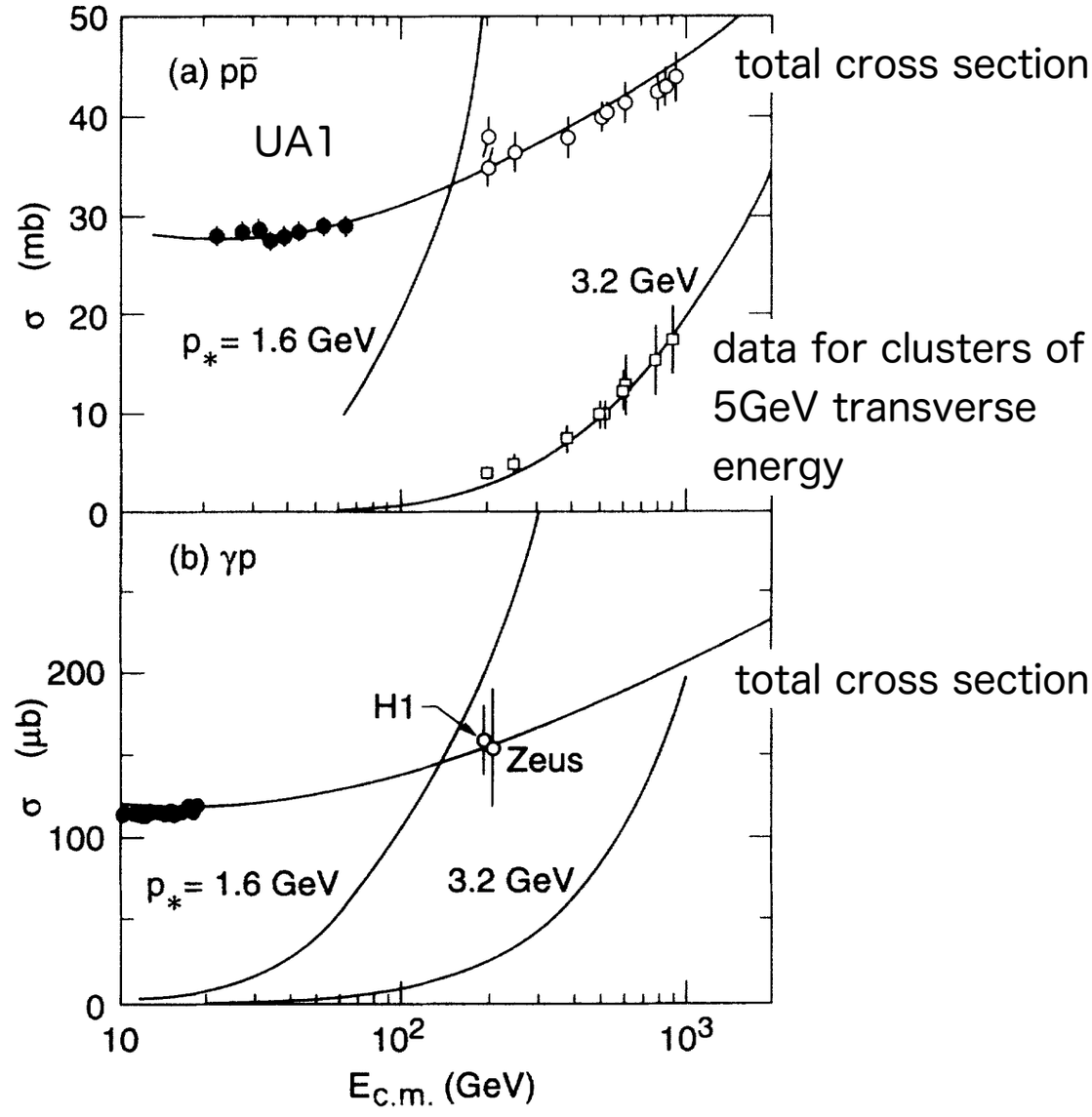

FIG. 3. (a) Comparison of the jet yield in $p\bar{p}$ collisions to the observed total cross section. The data are taken from Ref. [42]. The upper set of data points represents measurements of the inelastic $p\bar{p}$ cross section; these measurements are well fit by the formula of Ref. [28]. The lower set of data points represents the UA1 measurements of the jet cross section as described in the text. The two curves show the energy dependence of $\frac{1}{2}\mathcal{Y}(p_*)$ for $p\bar{p}$ collisions, for $p_* = 1.6$ and 3.2 GeV. (b) Comparison of the jet yield in γp collisions to the observed total cross section. The data is taken from Refs. [41,9,10]. The smooth curve through these points is proportional to (3.1). The two rising curves show the energy dependence of $\frac{1}{2}\mathcal{Y}(p_*)$ for γp collisions, for $p_* = 1.6$ and 3.2 GeV.

Reference Model (RM)

Approximation : The jet yield $\mathcal{Y}(p_*)$ should be a valid estimate of the total number of jets produced even when the jet yield substantially overestimated the total hadronic cross section.

So, the number of pairs of jets per event is expected to follow a Poisson distribution with the mean number of jets per event is

$$< n_{jet} >= \mathcal{Y}(p_*)/\sigma$$

The cross section for events with jets of $p_\perp > p_*$

$$\sigma(p_*) = \sigma\{1 - \exp[-\mathcal{Y}(p_*)/2\sigma]\}$$

the soft interactions by minimum bias events (ISAJET) for $p_\perp < p_*$

Time structure of e+ e- reactions in a linear collider, where the dots represent the bunch crossings

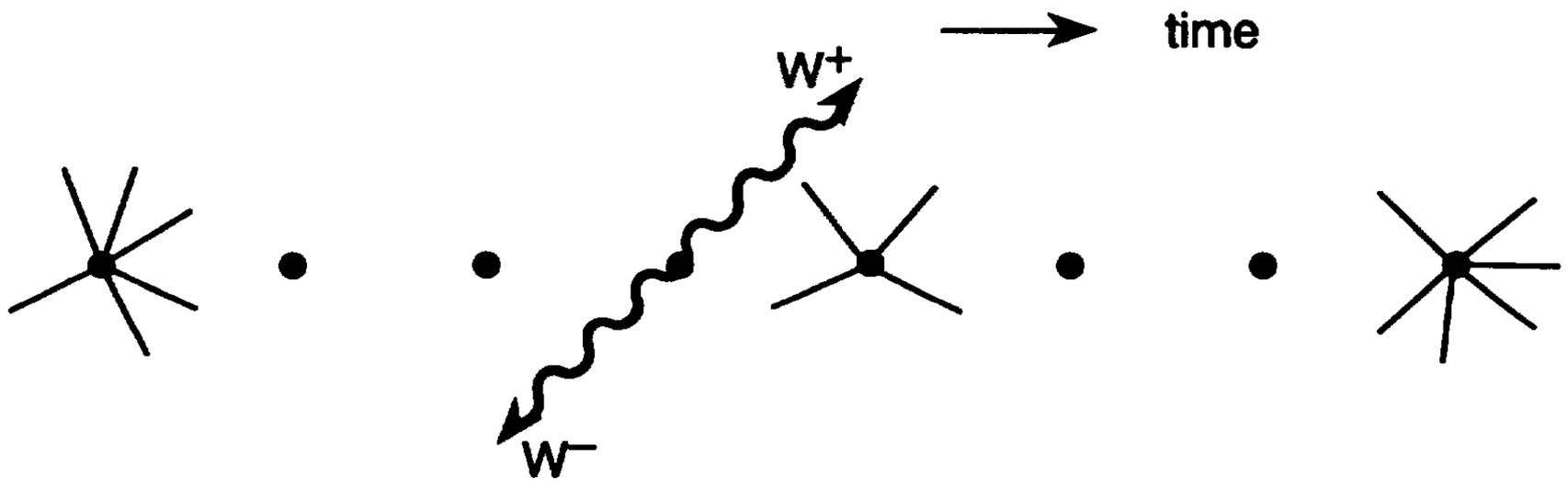

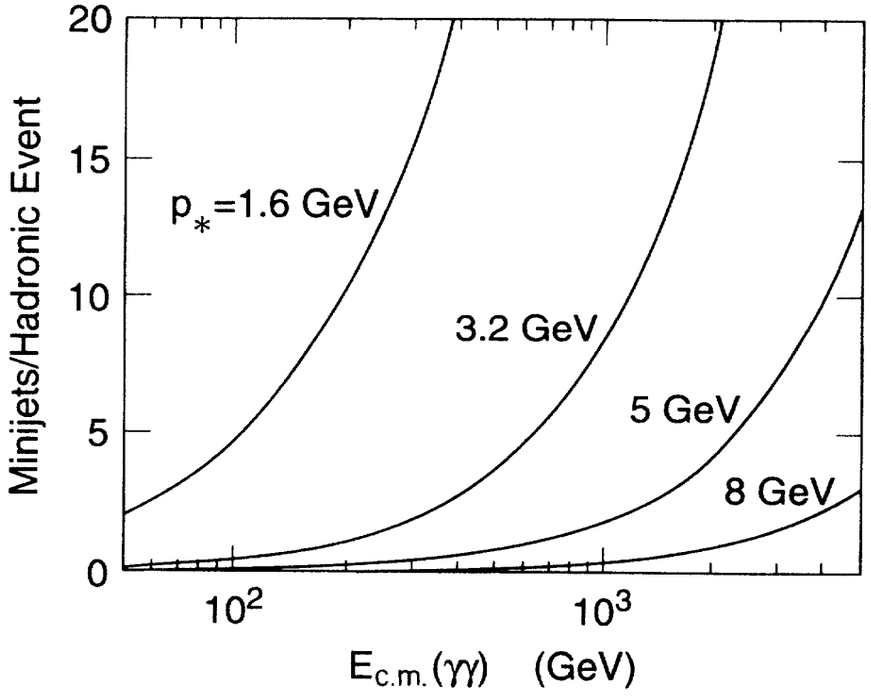

FIG. 5. Number of jets with transverse momentum greater than p_* per hadronic $\gamma\gamma$ event, for $p_*=1.6$, 3.2, 5, and 8 GeV, according to the model of Eq. (3.10). The ordinate is the $\gamma\gamma$ center-of-mass energy.

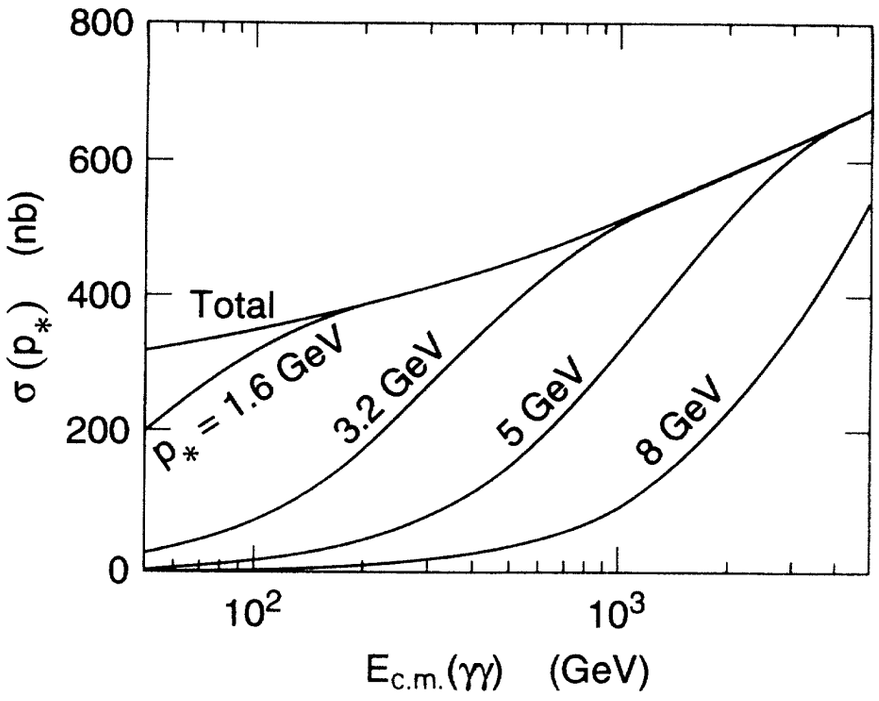

FIG. 6. Cross sections for hadron production in $\gamma\gamma$ collisions accompanied by jets of transverse momentum greater than p_*, for $p_*=1.6$, 3.2, 5, and 8 GeV, according to the model of Eq. (3.11). The ordinate is the $\gamma\gamma$ center-of-mass energy.

$$< n_{jet} >= \mathcal{Y}(p_*)/\sigma \quad \text{Eq. (3.10)}$$

$$\sigma(p_*) = \sigma\{1 - \exp[-\mathcal{Y}(p_*)/2\sigma]\} \quad \text{Eq. (3.11)}$$

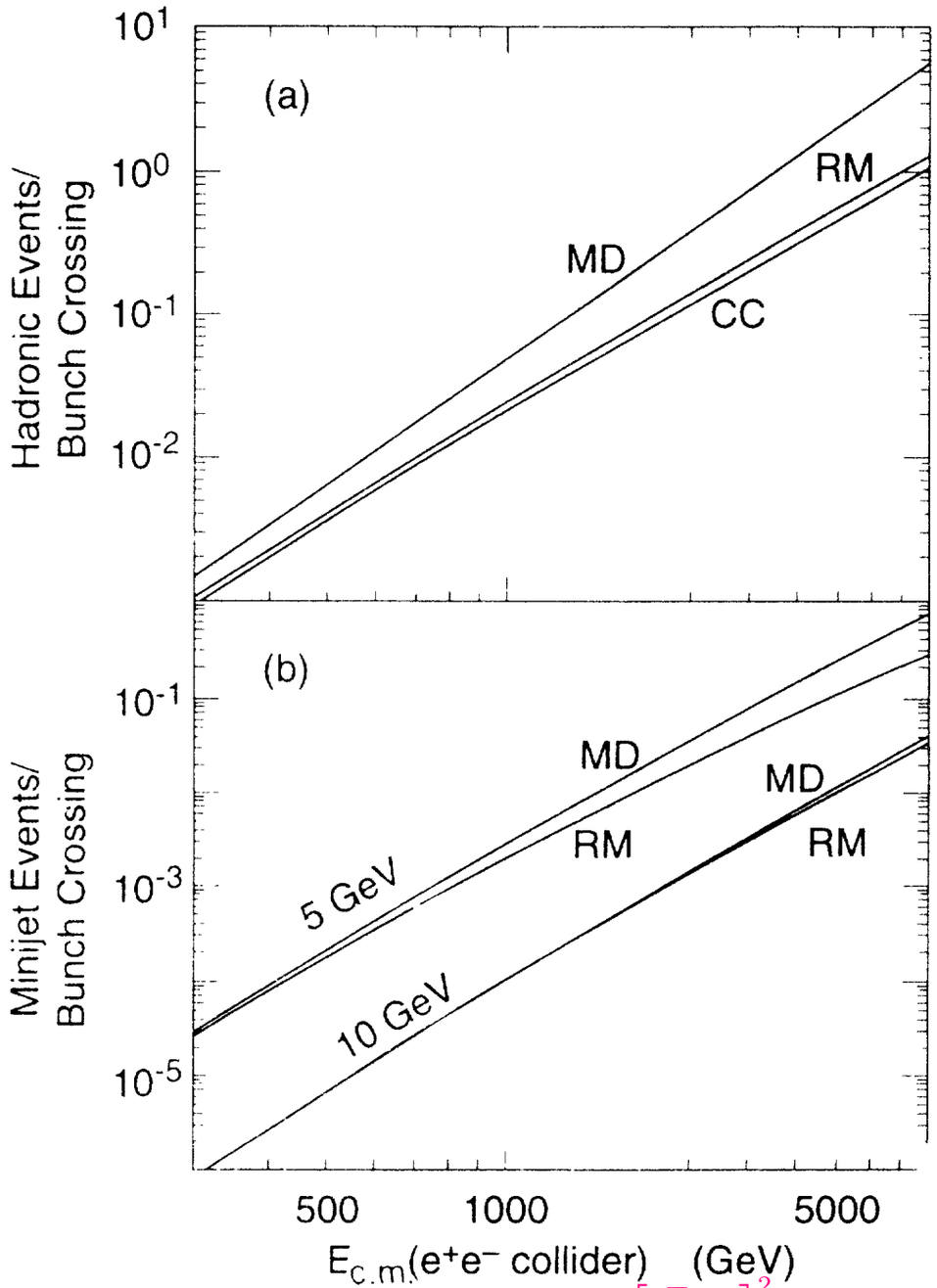

$\mathcal{L}_1 = \mathcal{L}/(f_{rep} n_b) = 10^{-3} \left[\frac{E_{cm}}{1\mathrm{TeV}}\right]^2 \mathrm{nb}^{-1}$

FIG. 7. Comparison of the predictions of three models of the $\gamma\gamma$ total cross section for the rate of hadronic background events in e^+e^- colliders. Beamstrahlung is ignored, and the luminosity per bunch crossing is taken to have the canonical dependence (4.2): (a) predictions of the RM, MD, and CC models (described in the text) for the total rate of $\gamma\gamma$ events; (b) predictions of the RM and MD models for the rate of events with observable minijets of transverse energy 5 and 10 GeV.

$p_* = 3.2$ and $8\mathrm{GeV}$

CC = Constant Cross section model

$$\sigma(\gamma\gamma \to \mathrm{hadrons}) = 300\mathrm{nb}$$

MD = Minijet Dominance model

$$\sigma(\gamma\gamma \to \mathrm{hadrons}) = 300\mathrm{nb} + \frac{1}{2}\mathcal{Y}(p_*)$$

RM = Reference Model

$$< n_{jet} >= \mathcal{Y}(p_*)/\sigma$$

$$\sigma(\gamma\gamma \to \mathrm{hadrons}) = \sigma_0\{1 + (6.30 \times 10^{-3})[\ln(s)]^{2.1} + (1.96)s^{-0.37}\}$$

$$\sigma_0 = 200\mu\mathrm{b}$$

$$\sigma(p_*) = \sigma\{1 - \exp[-\mathcal{Y}(p_*)/2\sigma]\}$$

for events with jets of $p_\perp > p_*$

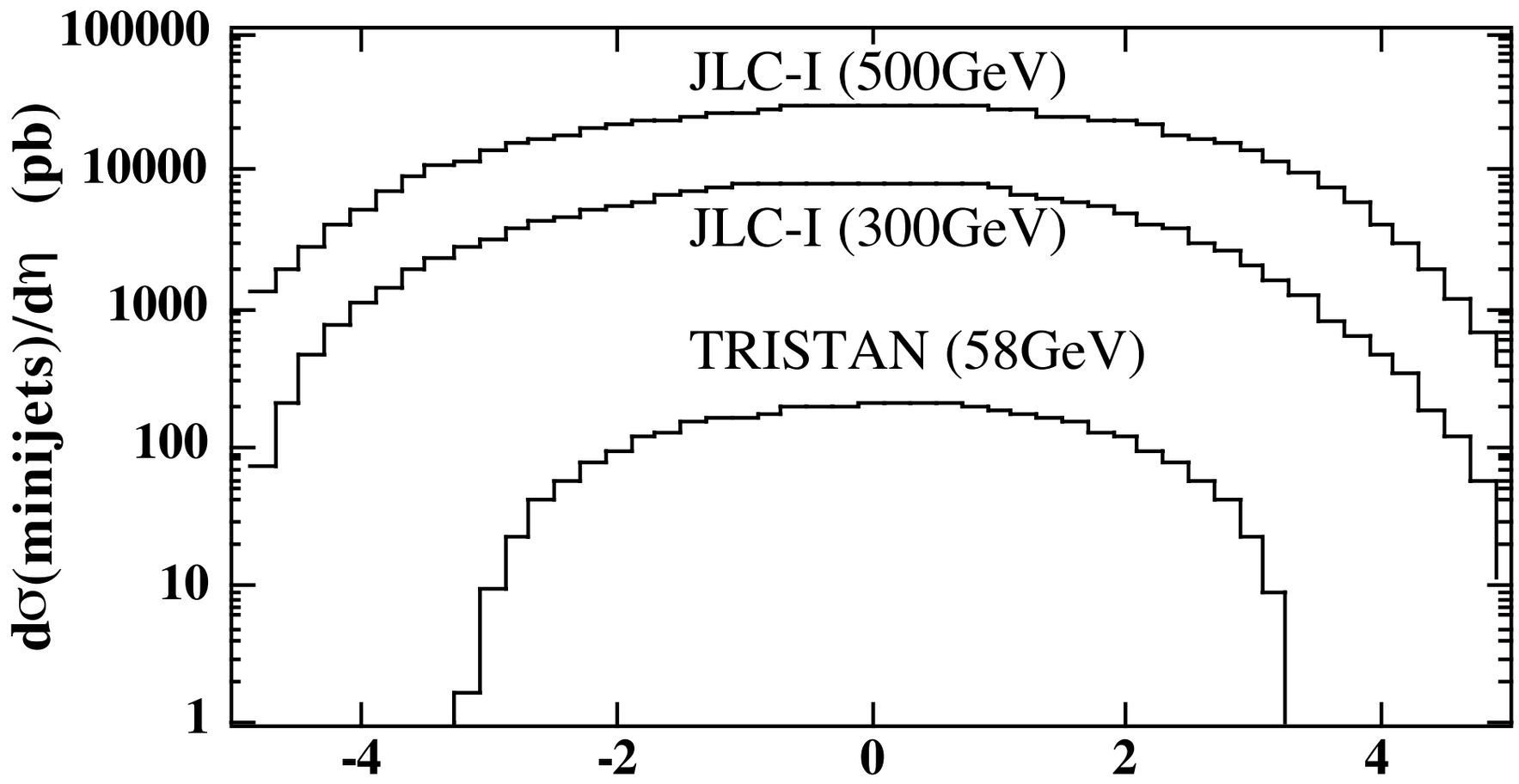

: Angular distribution

Event rate : < 0.2 mini-jets / bunch crossing at Ecm=500GeV

(JLC-1, Pt>2.4GeV, LAC1)

$$\eta \equiv -\ln\left[\tan\left(\frac{\theta}{2}\right)\right],\ \eta = 0,\ 0.88,\ 2.44 \text{ at } \theta = 90^o,\ 45^o,\ 10^o$$

TABLE I. Parameters and hadronic backgrounds for 0.5-TeV linear colliders.

Linear colliders	CLIC	DLC	JLC	NLC	TESLA	VLEPP
$\mathcal{L}$ (10^{33}cm^{-2}sec^{-1})	2.7	2.4	6.8	6.0	2.6	12
$f_{\rm rep}$ (Hz)	1700	50	150	180	10	300
n_b	4	172	90	90	800	1
$\mathcal{L}_1$ (10^{-3} nb^{-1})	0.40	0.27	0.50	0.37	0.33	40
N (10^{10})	0.6	2.1	0.7	0.65	5.15	20
σ_x/σ_y (nm)	90/8	400/32	260/3	300/3	640/100	2000/4
σ_z (μm)	170	500	80	100	1000	750
β_x^*/β_y^* (mm)	2.2/0.16	16/1	10/0.1	10/0.1	10/5	100/0.1
D_x/D_y	1.3/15	0.70/8.8	0.09/8.2	0.08/8.2	1.25/8.0	0.43/—
A_x/A_y	0.08/1.06	0.03/0.5	0.008/0.8	0.01/1.0	0.1/0.2	0.008/—
$\bar{\sigma}_x/\bar{\sigma}_y$ (nm)	40/5.5	246/19	259/2.0	300/2.2	304/50	1587/4
H_D	3.3	2.8	1.5	1.4	4.2	1.3
$\bar{\mathcal{L}}$ (10^{33} cm^{-2}sec^{-1})	8.80	6.67	10.1	8.22	11.1	15.1
$\bar{\mathcal{L}}_1$ (10^{-3} nb^{-1})	1.30	0.76	0.74	0.51	1.39	50.2
Υ_0	0.16	0.043	0.15	0.095	0.031	0.059
Υ	0.35	0.071	0.15	0.096	0.065	0.074
δ_B	0.36	0.08	0.05	0.03	0.14	0.14
n_γ	4.6	3.1	1.0	0.84	5.8	5.1
e^+e^- mode						
$N_{\rm had}$	1.37	0.32	0.07	0.04	1.57	45.3
$N_{\rm jet}$ (10^{-2})	5.80	0.44	0.22	0.10	1.62	56.2
$N_{\rm jet10}$ (10^{-4})	16.4	1.16	0.69	0.31	3.90	139
$\gamma\gamma$ mode						
$N_{\rm had}$	0.15	0.10	0.19	0.14	0.13	15.2
$N_{\rm jet5}$ (10^{-2})	6.90	4.72	8.61	6.43	5.68	685
$N_{\rm jet10}$ (10^{-4})	32.4	22.3	40.7	30.4	26.9	3240

TABLE II. Parameters and hadronic backgrounds for 1.0-TeV linear colliders.

Linear colliders	DLC	JLC	NLC	TESLA
$\mathcal{L}$ (10^{33} cm^{-2}sec^{-1})	2.5	8.8	12.8	10.6
f_{rep} (Hz)	50	150	90	10
n_b	50	20	90	800
$\mathcal{L}_1$ (10^{-3} nb^{-1})	0.99	2.17	1.58	1.31
N (10^{10})	2.8	1.8	1.3	5.8
σ_x/σ_y (nm)	223/28.3	372/3.2	425/2	404/50.5
σ_z (μm)	500	113	100	1100
β_x^*/β_y^* (mm)	5/0.8	24.6/0.12	40/0.1	8/2.5
D_x/D_y	1.40/11.0	0.08/9.7	0.04/8.5	1.95/15.6
A_x/A_y	0.1/0.625	0.005/0.9	0.0025/1.0	0.14/0.44
$\bar{\sigma}_x/\bar{\sigma}_y$ (nm)	100/17.1	372/2.2	425/1.5	172/27.0
H_D	3.7	1.5	1.4	4.4
$\bar{\mathcal{L}}$ (10^{33} cm^{-2}sec^{-1})	9.2	12.8	17.5	46.6
$\bar{\mathcal{L}}_1$ (10^{-3} nb^{-1})	3.70	3.10	2.18	5.86
Υ_0	0.20	0.38	0.27	0.10
Υ	0.42	0.38	0.27	0.24
δ_B	0.53	0.14	0.07	0.50
n_γ	8.1	1.7	1.1	10.4
e^+e^- mode				
N_{had}	15.3	0.83	0.34	40.1
N_{jet5}	1.53	0.09	0.03	2.65
N_{jet10} (10^{-2})	5.53	0.37	0.12	8.54
$\gamma\gamma$ mode				
N_{had}	0.42	0.93	0.68	0.56
N_{jet5}	0.31	0.68	0.50	0.41
N_{jet10} (10^{-2})	2.50	5.61	4.10	3.40

Total cross section of $\gamma\gamma$ interactions

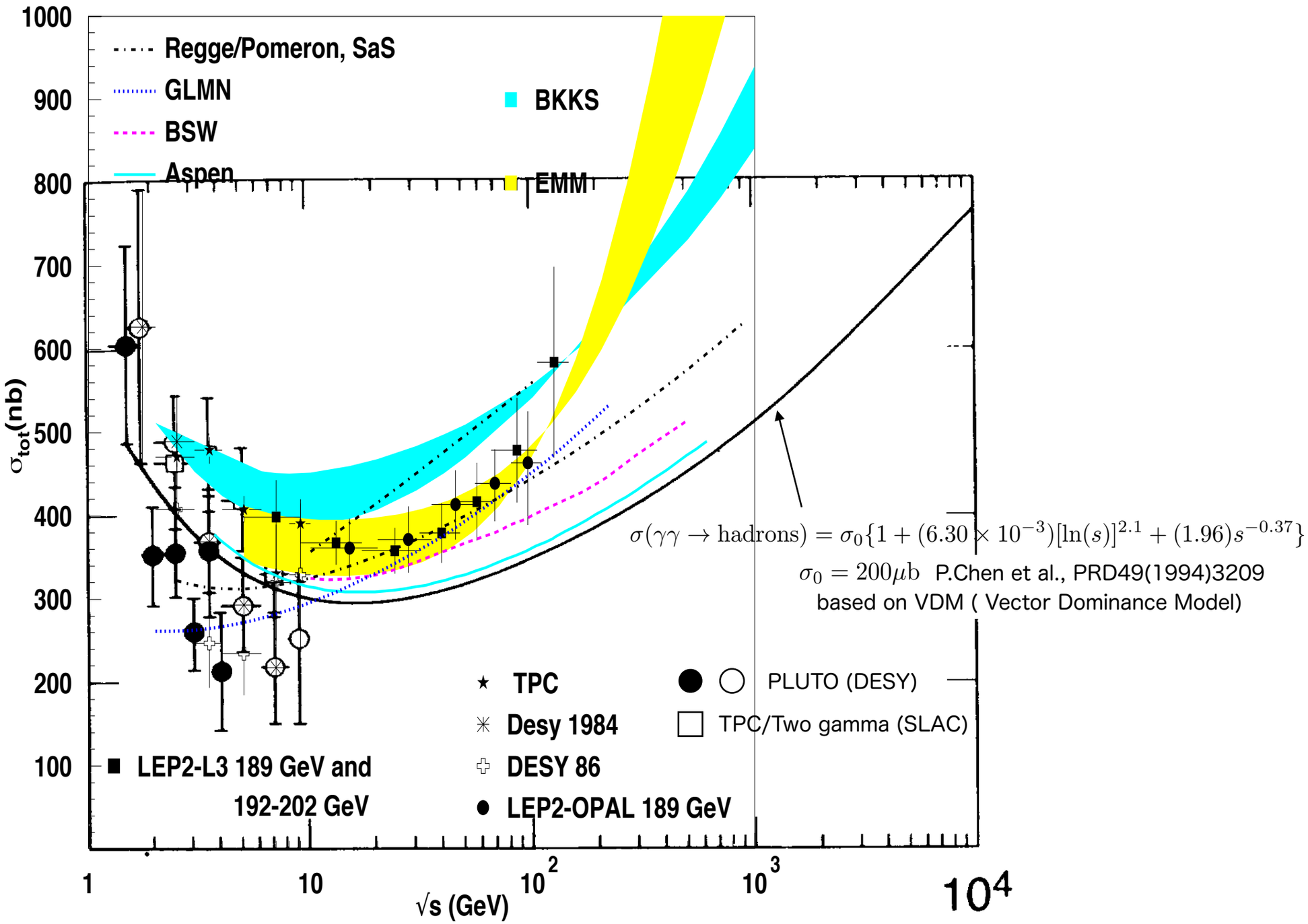

Ref : R.M. Godbole and G. Pancheri, Hadronic cross-sections in $\gamma\gamma$ processes and the next linear collider, Eur. Phys. J. C 19 (2001) 129

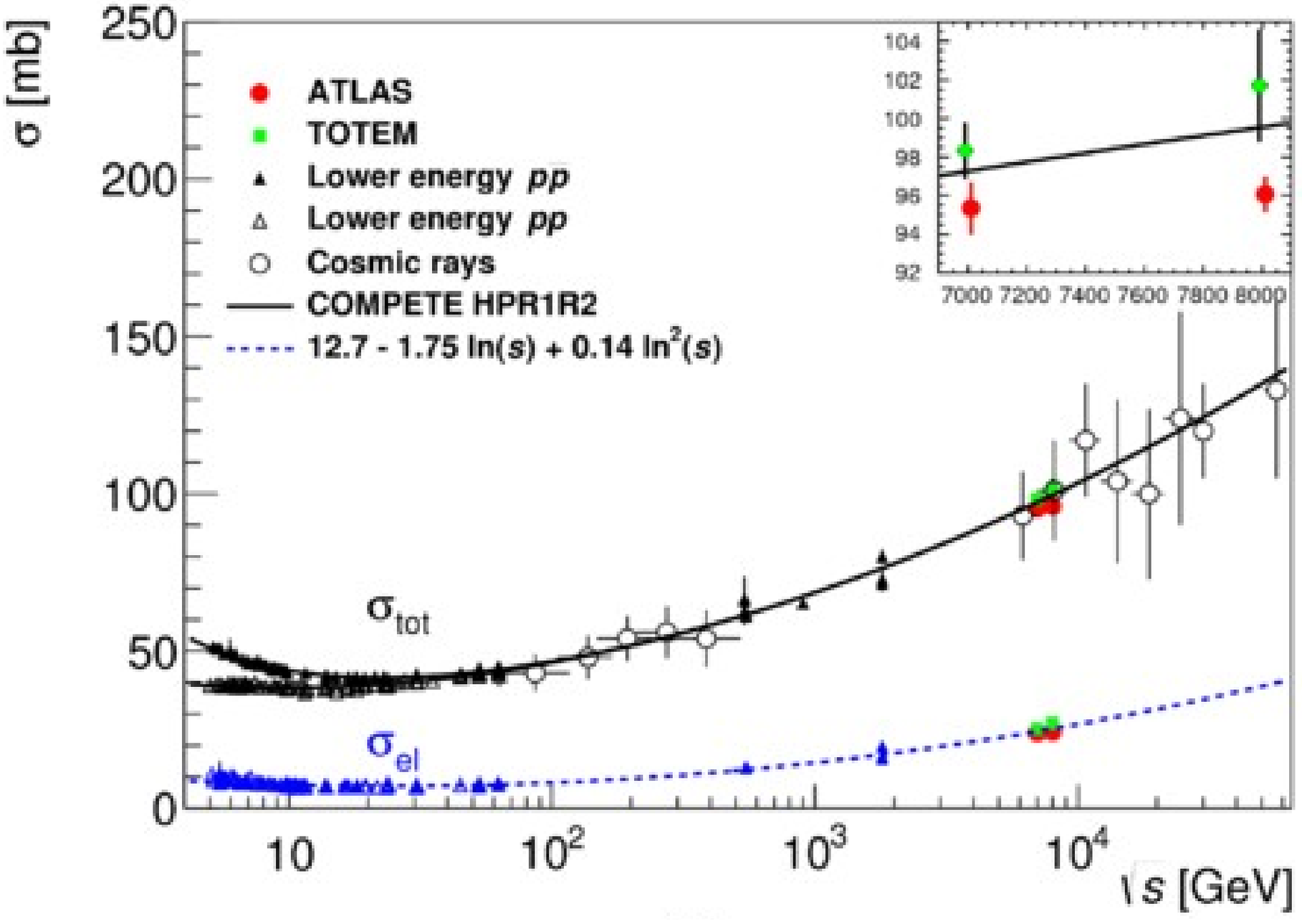
σ [mb]
250
200
150
100
50
0
ATLAS
TOTEM
Lower energy pp
Lower energy pp
Cosmic rays
COMPETE HPR1R2
12.7 - 1.75 ln(s) + 0.14 ln²(s)
σtot
σel
10
10²
10³
10⁴
√s [GeV]
104
102
100
98
96
94
92
7000 7200 7400 7600 7800 8000

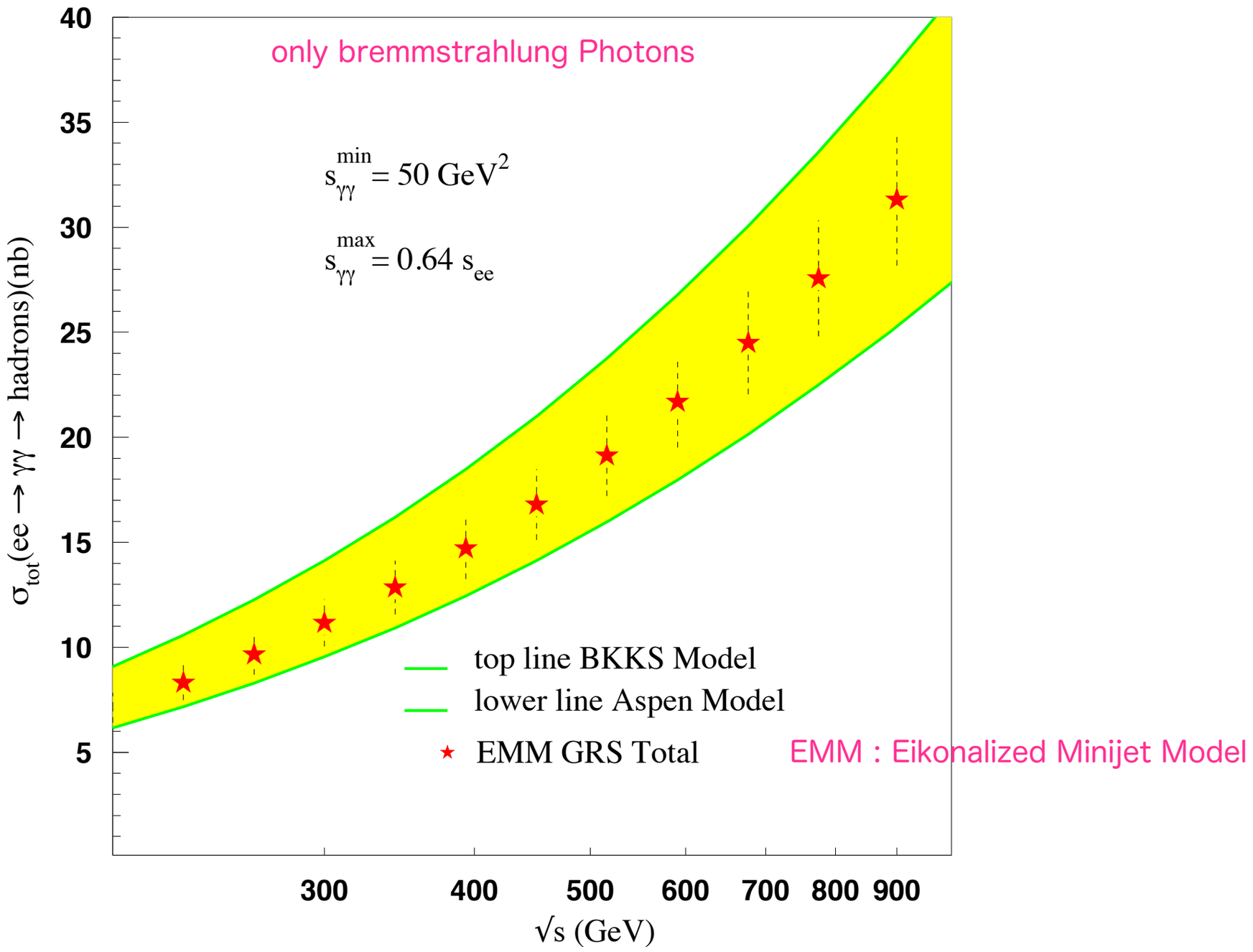

Figure 5: Cross-sections for hadron production due to $\gamma\gamma$ interactions in e^+e^- reactions.

Ref: Rohini M. Godbole, Albert De Roeck, Agnes Grau and Giulia Pancheri, JHEP06(2003)061

ILC TDR parameters

Table 3.1. Summary table of the 250–500 GeV baseline and luminosity and energy upgrade parameters. Also included is a possible 1st stage 250 GeV parameter set (half the original main linac length)

			Baseline 500 GeV Machine			1st Stage	L Upgrade	$E_{\rm CM}$ Upgrade	
Centre-of-mass energy	$E_{\rm CM}$	GeV	250	350	500	250	500	A 1000	B 1000
Collision rate	$f_{\rm rep}$	Hz	5	5	5	5	5	4	4
Electron linac rate	$f_{\rm linac}$	Hz	10	5	5	10	5	4	4
Number of bunches	$n_{\rm b}$		1312	1312	1312	1312	2625	2450	2450
Bunch population	N	$\times 10^{10}$	2.0	2.0	2.0	2.0	2.0	1.74	1.74
Bunch separation	$\Delta t_{\rm b}$	ns	554	554	554	554	366	366	366
Pulse current	$I_{\rm beam}$	mA	5.8	5.8	5.8	5.8	8.8	7.6	7.6
Main linac average gradient	$G_{\rm a}$	MV m^{-1}	14.7	21.4	31.5	31.5	31.5	38.2	39.2
Average total beam power	$P_{\rm beam}$	MW	5.9	7.3	10.5	5.9	21.0	27.2	27.2
Estimated AC power	$P_{\rm AC}$	MW	122	121	163	129	204	300	300
RMS bunch length	$\sigma_{\rm z}$	mm	0.3	0.3	0.3	0.3	0.3	0.250	0.225
Electron RMS energy spread	$\Delta p/p$	%	0.190	0.158	0.124	0.190	0.124	0.083	0.085
Positron RMS energy spread	$\Delta p/p$	%	0.152	0.100	0.070	0.152	0.070	0.043	0.047
Electron polarisation	P_-	%	80	80	80	80	80	80	80
Positron polarisation	P_+	%	30	30	30	30	30	20	20
Horizontal emittance	$\gamma\epsilon_{\rm x}$	μm	10	10	10	10	10	10	10
Vertical emittance	$\gamma\epsilon_{\rm y}$	nm	35	35	35	35	35	30	30
IP horizontal beta function	$\beta^*_{\rm x}$	mm	13.0	16.0	11.0	13.0	11.0	22.6	11.0
IP vertical beta function	$\beta^*_{\rm y}$	mm	0.41	0.34	0.48	0.41	0.48	0.25	0.23
IP RMS horizontal beam size	$\sigma^*_{\rm x}$	nm	729.0	683.5	474	729	474	481	335
IP RMS veritcal beam size	$\sigma^*_{\rm y}$	nm	7.7	5.9	5.9	7.7	5.9	2.8	2.7
Luminosity	L	$\times 10^{34}$ cm^{-2}s^{-1}	0.75	1.0	1.8	0.75	3.6	3.6	4.9
Fraction of luminosity in top 1%	$L_{0.01}/L$		87.1%	77.4%	58.3%	87.1%	58.3%	59.2%	44.5%
Average energy loss	$\delta_{\rm BS}$		0.97%	1.9%	4.5%	0.97%	4.5%	5.6%	10.5%
Number of pairs per bunch crossing	$N_{\rm pairs}$	$\times 10^3$	62.4	93.6	139.0	62.4	139.0	200.5	382.6
Total pair energy per bunch crossing	$E_{\rm pairs}$	TeV	46.5	115.0	344.1	46.5	344.1	1338.0	3441.0
Luminosity/bunch	L/bunch	x 10^{-3} nb^{-1}	1.14	1.52	2.74	1.14	5.49	5.49	7.47

minijet generation by Pythia, http://home.thep.lu.se/~torbjorn/pythia82php/Welcome.php

L,E,P

Measurements

L,E,P Measurement Goals

Luminosity, Luminosity Spectrum

• Total cross sections:	absolute δL/L to ~0.1%
• Z-pole calibration scan for Giga-Z:	relative δL/L to ~0.02%
• threshold scans (ex. top mass):	relative δL/L to 1%
	+L(E) spectrum: core width to <0.1% and tail population to <1%

Energy

• Top mass:	200 ppm (35 MeV)
• Higgs mass:	200 ppm (25 MeV for 120 GeV Higgs)
• W mass:	50 ppm (4 MeV) ??
• 'Giga'-Z A_{LR}:	200 ppm (20 MeV) (comparable to ~0.25% polarimetry)
	50 ppm (5 MeV) (for sub-0.1% polarimetry with e^+ pol) ??

Polarization

• Standard Model asymmetries:	< 0.5%
• 'Giga'-Z A_{LR}:	< 0.25% (<0.1% with e^+ pol)

Polarization

Two polarimeter systems at the upstream and downstream, i.e. UP and DP, respectively at ILC.

(1) Cross calibration of the polarimeters in absence of collisions at IP

Key issues : the spin transportation, .i.e. the reversibility and imperfection of magnets, alignment etc. , in the BDS

Polarization differences between UP and DP estimated by the simulation

Different beam angular divergence : $\Delta\mathcal{P}_z/\mathcal{P}_z = 8 \times 10^{-5}$

10% variation of the emittance : $\Delta\mathcal{P}_z/\mathcal{P}_z = 3 \times 10^{-5}$

Synchrotron radiations : negligibly small, $\Delta\mathcal{P}_z/\mathcal{P}_z = 5 \times 10^{-5}$ by the orbit changes

Spin flip : $\Delta\mathcal{P}_z/\mathcal{P}_z < 10^{-6}$

However, any net bend angle produces the spin precession as

$$\theta_{spin} = \left(1 + \gamma\frac{g-2}{g}\right)\theta_{bend} \approx \gamma\frac{g-2}{g}\theta_{bend} = \frac{E(\mathrm{GeV})}{0.44065}\theta_{bend}$$

so, θ_{bend}=50μrad produces θ_{spin}=28.3mrad, cosθ_{spin}=0.9996 for the 250GeV beam. There are two error sources at the spin rotators in front of the main linac and the alignment error between UP and DP. Since the both are the same contributions,

$$\Delta\mathcal{P}_z/\mathcal{P}_z(UP-DP) < 1 - \cos\left(\sqrt{2}\theta_{spin}\right) = 0.8 \times 10^{-3}$$ “envisaged precision”

M.Beckmann, J.List, A.Vauth and B.Vormwald, Spin transport and polarimetry in the beam delivery system of the international linear collider, JINST 9 P07003, 2014

The change of a particle spin vector $\vec{S}$ with time under the influence of electromagnetic fields is described by the Thomas-Bargmann-Michel-Telegdi (T-BMT) equation [18, 19]. Since neither the beam delivery system nor the extraction line contains components with sizable electric fields, the full T-BMT equation simplifies to

$$\frac{d}{dt}\vec{S} = \vec{\Omega}_B\left(\vec{B},\vec{r},\vec{p},t\right) \times \vec{S} = -\frac{q}{m\gamma}\left((1+a\gamma)\,\vec{B} - \frac{a\,\vec{p}\cdot\vec{B}}{(\gamma+1)\,m^2c^2}\,\vec{p}\right) \times \vec{S}. \tag{3.1}$$

Here, $\vec{B}\,(\vec{r},t)$ denotes the magnetic field, γ the relativistic Lorentz factor, c the vacuum speed of light and $a \equiv (g-2)/2$ the anomaly of the gyro-magnetic moment, with $a \approx 0.001159652$ for electrons.

The expression for $\vec{\Omega}_B$ in equation (3.1) can be decomposed in two parts for the field components, $\vec{B}_\parallel$ parallel to $\vec{p}$ and $\vec{B}_\perp$ perpendicular to it:

$$\vec{\Omega}_B\left(\vec{B},\vec{r},\vec{p},t\right) = -\frac{q}{m\gamma}\left((1+a\gamma)\,\vec{B}_\perp \;+\; (1+a)\,\vec{B}_\parallel\right) \tag{3.2}$$

In presence of only perpendicular magnetic fields, the momentum $\vec{p}$ and the spin $\vec{S}$ behave very similarly:

$$\frac{d}{dt}\vec{p} = -\frac{q}{m\gamma}\left(\qquad\quad \vec{B}_\perp\right) \times \vec{p} \tag{3.3}$$

$$\frac{d}{dt}\vec{S} = -\frac{q}{m\gamma}\left((1+a\gamma)\,\vec{B}_\perp\right) \times \vec{S} \tag{3.4}$$

Thus, the spin vector precesses in a perpendicular magnetic field about $\vec{B}$ by the angle

$$\xi_{\text{spin}} = (1+a\gamma)\;\xi_{\text{orbit}}, \tag{3.5}$$

where ξ_{orbit} is the deflection angle of the particle [20, 21]. For an electron beam with an energy of 250 GeV, the amplification factor is $(1+a\gamma) \approx 568$; for an energy of 500 GeV, it rises to ≈ 1136.

Depolarization during collisions

For very flat beam , i.e. $\sigma_x \gg \sigma_y,\ D_y \gg D_x$ and $D_x \ll 1$

$$\theta_{x(y),rms} = \frac{1}{2}\frac{\sigma_{x(y)}}{\sigma_z}\frac{D_{x(y)}}{\left[1+\left(D_{x(y)}/2\right)^5\right]^{1/6}} = \frac{\theta_0}{2}\frac{1}{\left[1+\left(D_{x(y)}/2\right)^5\right]^{1/6}}$$

$$\theta_{x(y),rms} = 2.43(0.227)\times 10^{-4}$$

The final depolarization due to the spin precession is given by,

$$\langle \Delta P \rangle = \frac{1}{2}(a\gamma)^2\left[\theta_{x,rms}^2 + \theta_{y,rms}^2\right] = 9.95\times 10^{-3}$$

The final depolarization due to the spin flip is given by,

$$\langle \Delta P \rangle \approx 2n_\gamma U_f(\xi_0)/U_0(\xi_0) \rightarrow \frac{7}{27}n_\gamma \xi_0^2 \text{ for } \xi_0 \ll 1 \text{ and } \xi = \frac{3}{2}\Upsilon$$

$$\langle \Delta P \rangle \approx 0.00229 \text{ for } n_\gamma = 1.71, \xi_0 = 0.095, \Upsilon_0 = \Upsilon_{av} = 0.063$$

Summing the above two depolarizations,

the luminosity weighted depolarization is given by $[\Delta P] = 0.273\langle \Delta P \rangle = 3.3\times 10^{-3}$

K.Yokoya, Pisin Chen, AIP Conference Proceedings 187, 938(1989)

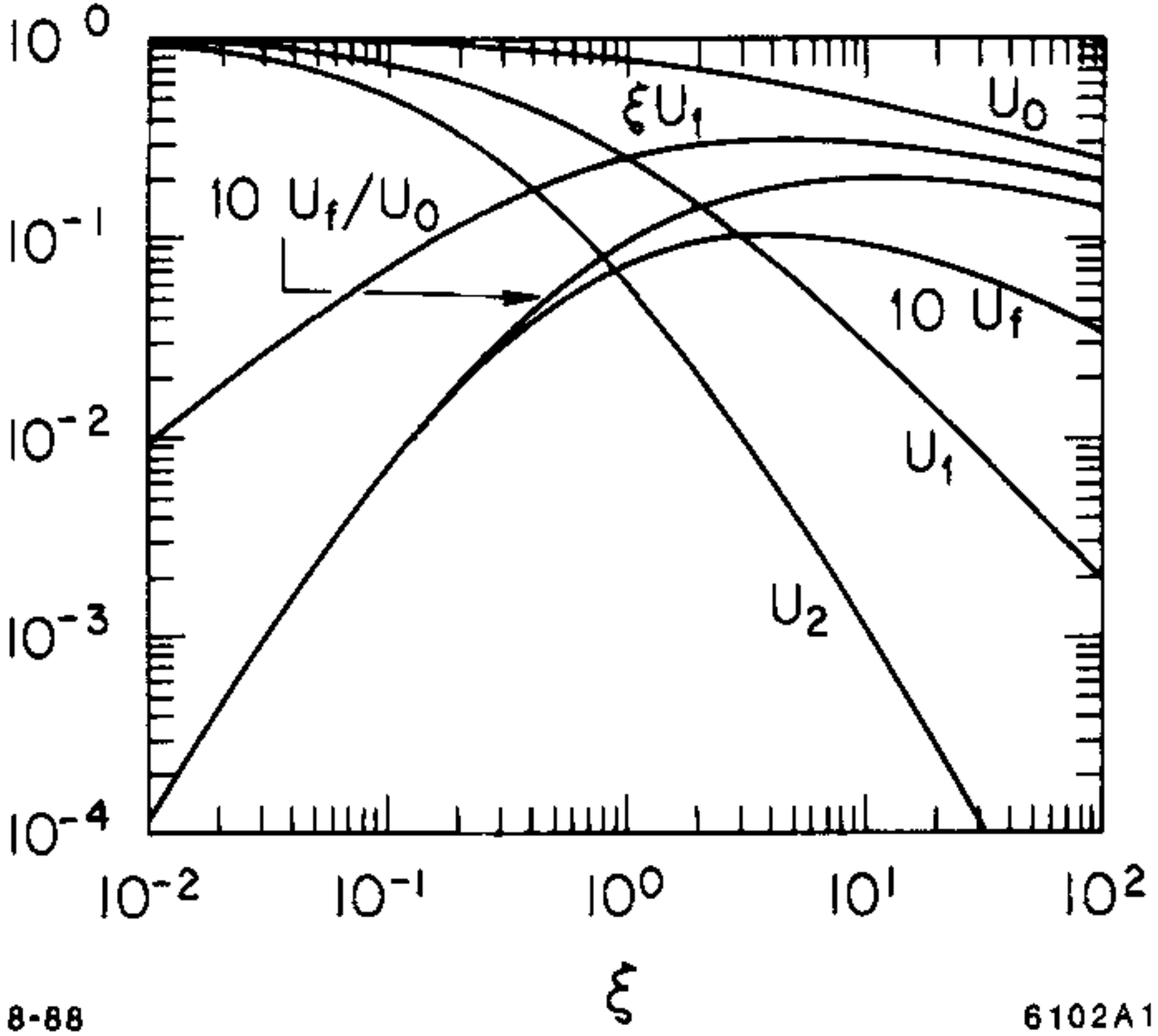

K.Yokoya, Pisin Chen, AIP Conference Proceedings 187, 938(1989)

(2) The luminosity weighted polarization calculated with collisions at IP

for head-on collisions with $D_x << 1$

$$|\vec{\mathcal{P}}^{UP(before)}| - |\vec{\mathcal{P}}^{lum.wgt}| = 0.273\left(|\vec{\mathcal{P}}^{UP(before)}| - |\vec{\mathcal{P}}^{DP(after)}|\right)$$

$$\vec{\mathcal{P}}^{lum.wgt} = \frac{\int \mathcal{L}(t)\vec{\mathcal{P}}^{lum,1}(t)dt}{\int \mathcal{L}(t)dt}, \text{ where } \vec{\mathcal{P}}^{lum,1}(t) \text{ is the one for a single bunch collision}$$

Ref . K. Yokoya and P. Chen, Depolarization Due to Beam-beam Interaction in Electron - Positron Linear Colliders, AIP Conf. Proc. 187 (1989) 938

The difference is due to the Sokolov-Telnov effect in the collisions, e.g. the spins become to be align in parallel to the magnetic field due to the spin flip during synchrotron radiation.

for actual collisions, detailed simulation is needed.

The absolute polarization, i.e. the luminosity weight polarization, can be estimated by the physics events such the measurements of total cross section of fermion pair production for various polarization configurations i.e. so called the Blondel scheme, and the forward W^+W^- production.

Theoretical Limit of the Statistical Precision

Currently implemented processes:

Process	Channel
single $W^{\pm}$	$e\nu l\nu$, $e\nu q\bar{q}$
WW	$q\bar{q}q\bar{q}$, $q\bar{q}l\nu$, $l\nu l\nu$
ZZ	$q\bar{q}q\bar{q}$, $q\bar{q}ll$, $llll$
$ZZWW$Mix	$q\bar{q}q\bar{q}$, $l\nu l\nu$
Z	$q\bar{q}$, ll

- Same processes as for physics analysis (DBD)
  - → Classification
  - → Cross section
- Any combination of processes can be used
- Further Process can easily added

Consider best case scenario using σ_{tot}:

- Assumption of a perfect 4π detector
- No background
- No systematic uncertainties
- Using all implemented processes

Statistical precision H-20: $\Delta P/P\,[\%]$

E	**500**	**350**	**250**	**500**	**250**
$\mathcal{L}$	**500**	**200**	**500**	**3500**	**1500**
$P^{-}_{e^-}$	0.2	0.3	0.1	0.08	0.09
$P^{+}_{e^-}$	0.05	0.06	0.03	0.02	0.02
$P^{-}_{e^+}$	0.1	0.1	0.06	0.04	0.04
$P^{+}_{e^+}$	0.2	0.3	0.1	0.08	0.08

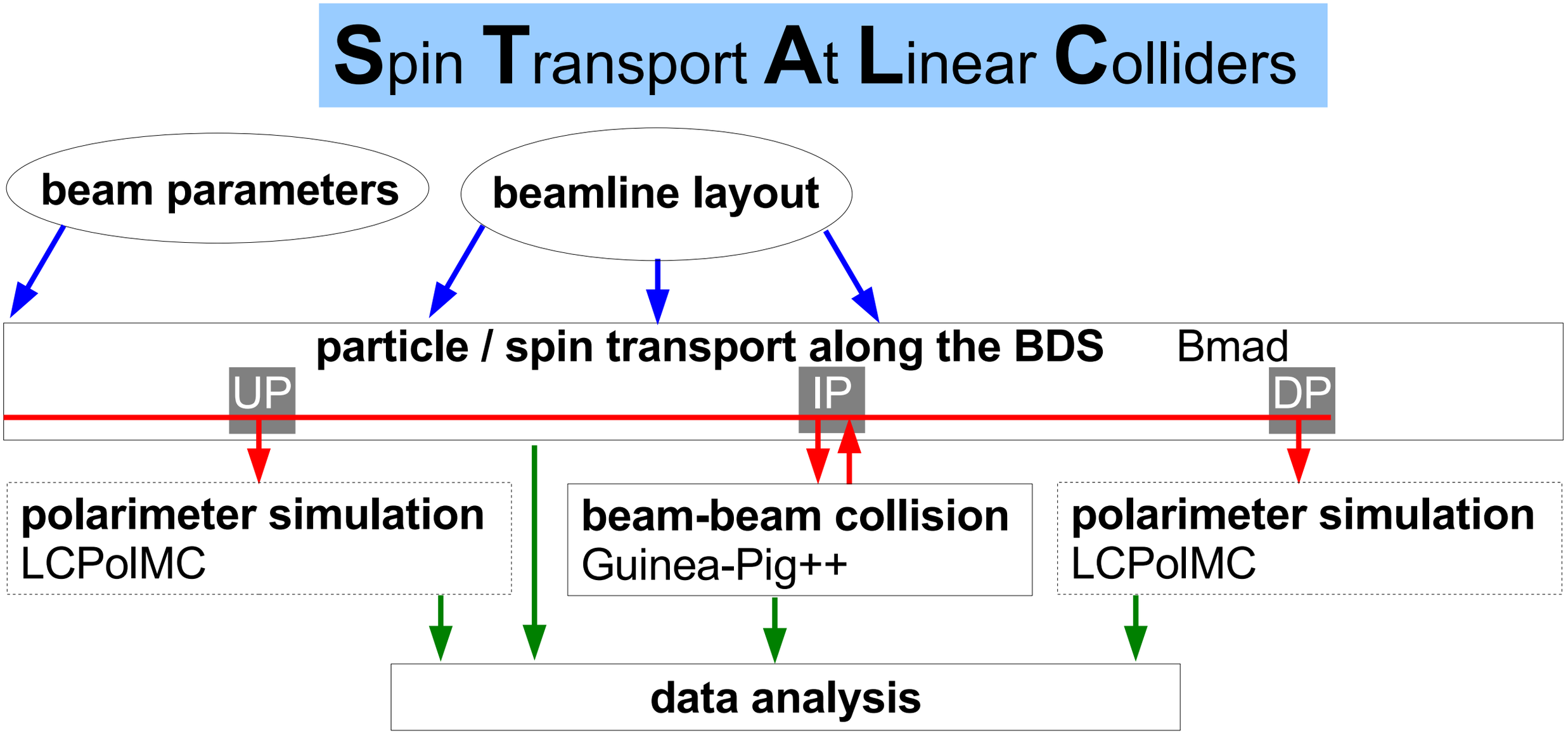

Figure 4. Program flow in `STALC`. UP/DP denotes the up-/downstream polarimeter.

M.Beckmann, J.List, A.Vauth and B.Vormwald, Spin transport and polarimetry in the beam delivery system of the international linear collider, JINST 9 P07003, 2014

In head-on collisions, the already focussed bunches attract each other even further due to their mutual electrical fields (pinch effect [11]). The T-BMT precession due to this mutual focussing of the bunches leads to a spin fan-out like in a quadrupole magnet. For flat, longitudinally polarised beams ($\sigma_{xe} \gg \sigma_{ye}$, $\mathcal{P}_z = |\vec{\mathcal{P}}|$) and a small horizontal disruption parameter ($D_x \ll 1$), the polarisations before ($|\vec{\mathcal{P}}|^{\text{bef}}$) and after ($|\vec{\mathcal{P}}|^{\text{aft}}$) the collision as well as the luminosity-weighted polarisation $|\vec{\mathcal{P}}|^{\text{lumi,1}}$ are related as follows (equation 16 in [23]):

$$|\vec{\mathcal{P}}|^{\text{bef}} - |\vec{\mathcal{P}}|^{\text{lumi,1}} = 0.273 \left(|\vec{\mathcal{P}}|^{\text{bef}} - |\vec{\mathcal{P}}|^{\text{aft}} \right) \tag{3.8}$$

If the angular divergence of the bunches before the collision is negligible in terms of spin fan-out, the spin fan-out during the collision can be related to the angular divergence θ_r^{aft} after the collision (equation 31 in [23], see also equation (3.6)): $\because f(\theta_r) = |\vec{\mathcal{P}}|_{max} \cdot \cos\left((1 + a\langle\gamma\rangle) \cdot \theta_r\right)$ Eq.(3.6)

$$|\vec{\mathcal{P}}|^{\text{bef}} - |\vec{\mathcal{P}}|^{\text{aft}} \approx \frac{1}{2} |\vec{\mathcal{P}}|^{\text{bef}} \cdot (1 + a\gamma)^2 \cdot (\theta_r^{\text{aft}})^2 \tag{3.9}$$

Merging these two equations, one obtains: $\because 0.273 \approx \frac{1}{4}$

$$|\vec{\mathcal{P}}|^{\text{bef}} - |\vec{\mathcal{P}}|^{\text{lumi,1}} \approx \frac{1}{2} |\vec{\mathcal{P}}|^{\text{bef}} \cdot (1 + a\gamma)^2 \cdot \left(\frac{\theta_r^{\text{aft}}}{2} \right)^2 \tag{3.10}$$

As explained in [24] and [25], one can interpret this as about half of the T-BMT precession occurring before the hard interaction. A comparison to equation (3.9) implies that one can reproduce the luminosity-weighted polarisation at a point behind the IP where the angular divergence has to be reduced by a factor $1/2$ with respect to the divergence at the IP after the collision.

3 The Blondel scheme

If a process $e^+e^- \to f\bar{f}$ is mediated by pure s-channel vector-particle exchange the cross section for the different polarization states can be written as

$$\sigma = \sigma_u \left[1 - \mathcal{P}_{e^+}\mathcal{P}_{e^-} + A_{\mathrm{LR}}(\mathcal{P}_{e^+} - \mathcal{P}_{e^-})\right], \tag{1}$$

where $\mathcal{P}_{e^+}$ and $\mathcal{P}_{e^-}$ are the longitudinal polarizations of the positrons and electrons measured in the direction of the particle's velocity. σ_u is the unpolarized cross section and A_{LR} the left-right asymmetry. If the signs of the two polarizations can be switched independently four cross sections can be measured for four unknowns. From these cross sections the polarizations can be obtained, if $A_{\mathrm{LR}} \neq 0$ [3]:

$$\mathcal{P}_{e^\pm} = \sqrt{\frac{(\sigma_{+-} + \sigma_{-+} - \sigma_{++} - \sigma_{--})(\mp\sigma_{+-} \pm \sigma_{-+} - \sigma_{++} + \sigma_{--})}{(\sigma_{+-} + \sigma_{-+} + \sigma_{++} + \sigma_{--})(\mp\sigma_{+-} \pm \sigma_{-+} + \sigma_{++} - \sigma_{--})}}$$

where in σ_{ij} i denotes the sign of the positron- and j the sign of the electron-polarization. This method has some clear advantages. There are no intrinsic limitations by polarimeter systematics and the polarization is measured for the colliding particles, so some effects like the depolarization due to beamstrahlung are accounted for and the measurement is automatically luminosity weighted. However, since cross section products are involved also this measurement is affected by correlation effects. As a drawback of this method some luminosity needs to be spent with same helicities for both beams which is not very interesting for most physics processes.

“Spin fan-out” due to non-uniform spin precession

for beams with spatial, angular and energy spreads

For the angular divergence

$$f(\theta_x) = |\vec{\mathcal{P}}_{max}| \cos\left((1 + a\langle\gamma\rangle)\,\theta_x\right) \text{ for the longitudinal polarization}$$

$$a \equiv (g-2)/g \approx 0.001159652$$

for ILC, θx = 43.1 μrad at IP, $\sqrt{s}$=500GeV with the electron beam polarization of 80%

$$0.8 - f(\theta_x) = 0.24 \times 10^{-3}$$

Beam Polarisation and Crossing Angle & antiDID

incoming beams not parallel to solenoid field:

- spin precession - longitudinal polarisation changes:
  only solenoid: 0.05%
  with antiDID: 0.6%

- *vertical* “kick” on beam
  => σ(y) at IP increases by factor 3-4
  (only solenoid, 50 with antiDID)
  => “anti-solenoids” required

Anti-solenoids will eliminate spin precession at the same time!

(Alternative: skew quadrupoles - would be bad for polarisation!)

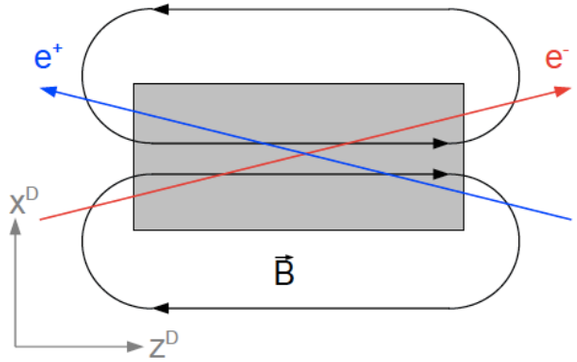

only solenoid

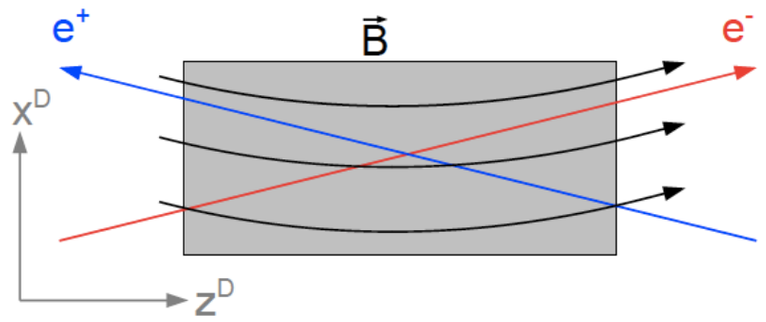

with antiDID

[PhD Thesis M.Beckmann, Hamburg 2013]

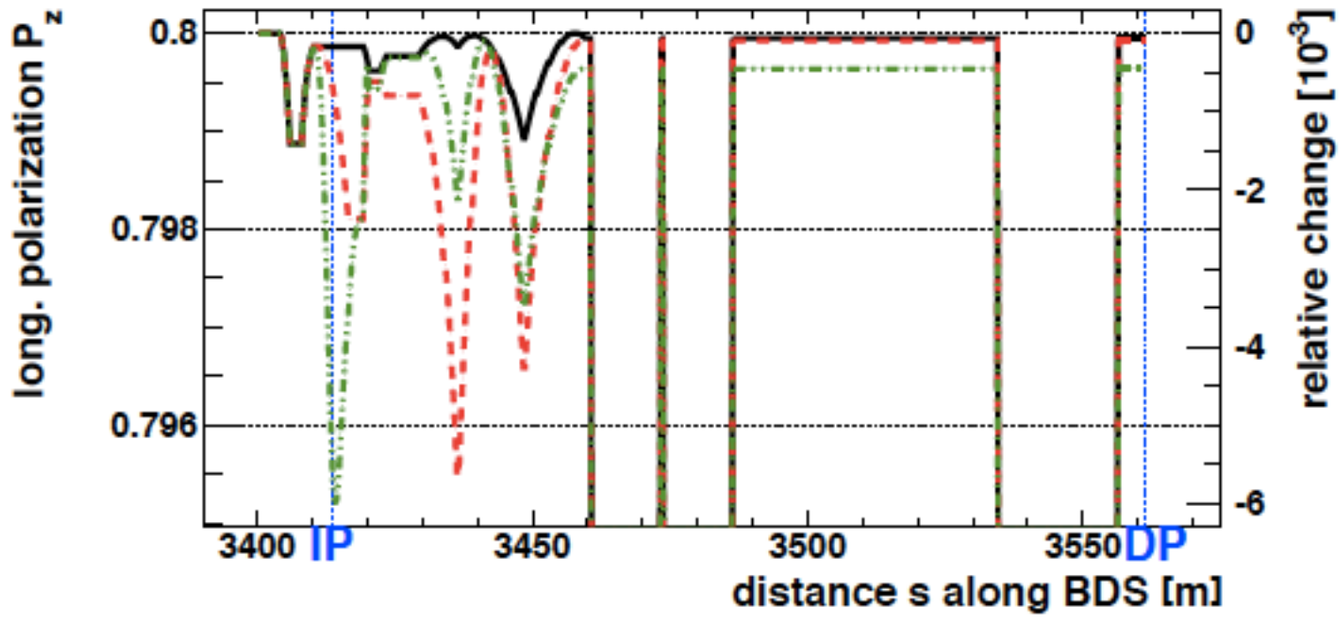

Simulation results with mis-alignments of magnets in the BDS, where M5 (10) : alignment errors (RMS) 5(10)μm and 5(10)μrad for magnets

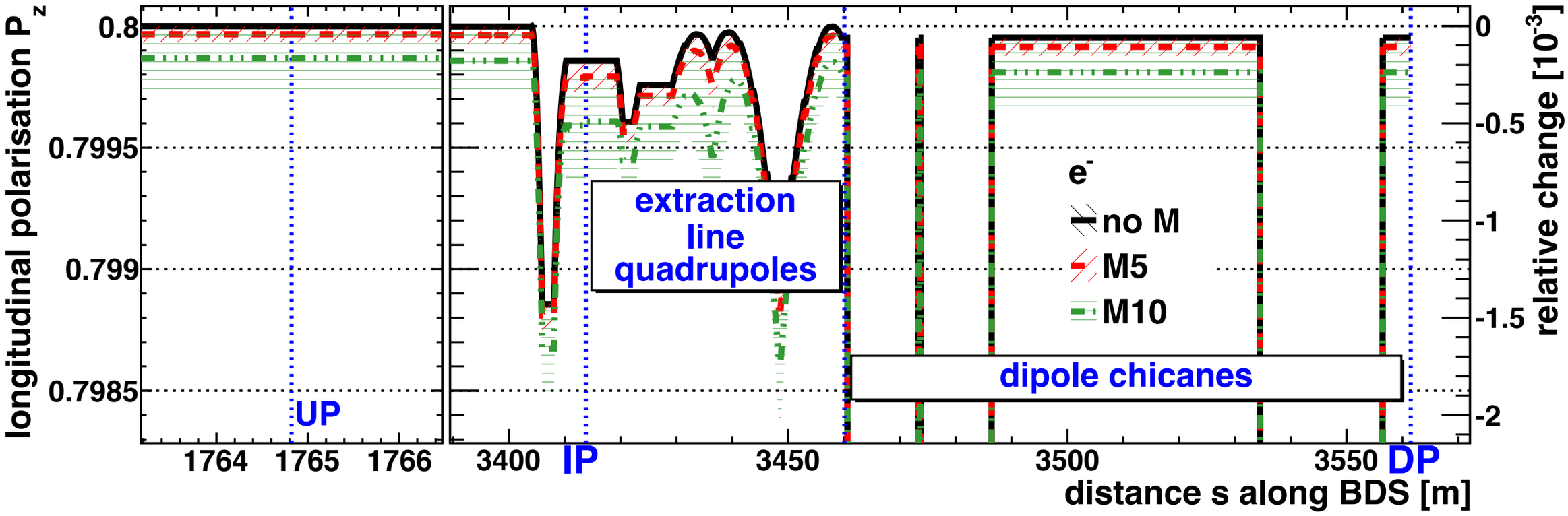

Figure 6. Longitudinal polarisation $\mathcal{P}_z$ of the electron beam at the upstream polarimeter (UP, left part) and between e^+e^- IP and downstream polarimeter (DP, right part) for the data samples listed in table 8. The uncertainty bands correspond to the RMS spread of all runs. For the perfectly aligned case, the band is too small to be visible. SB2009_Nov10 lattice , no detector solenoid, no crab cavity

Results of ΔPz(UP-DP) : uncertainty of 0.09(035)x10^{-3} for “M5(M10)"

M.Beckmann, J.List, A.Vauth and B.Vormwald, Spin transport and polarimetry in the beam delivery system of the international linear collider, JINST 9 P07003, 2014

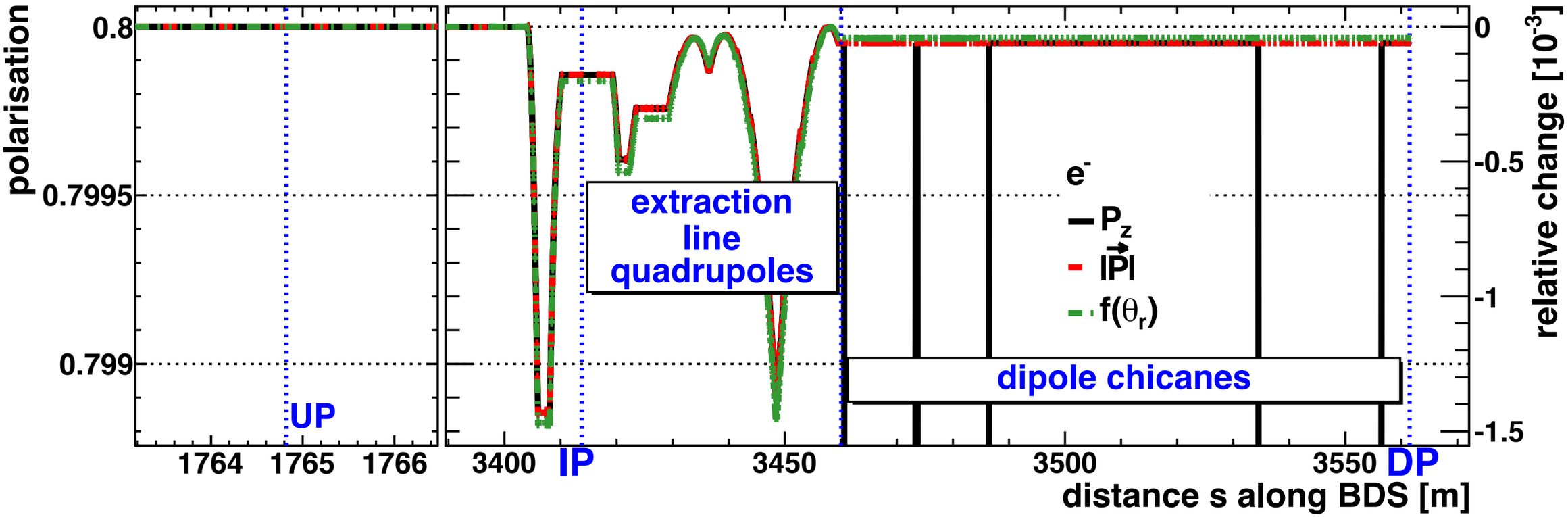

Figure 5. Longitudinal polarisation $\mathcal{P}_z$ (black, solid), magnitude of the polarisation vector $|\vec{\mathcal{P}}|$ (red, dashed) and the function $f(\theta_r)$ of the angular divergence defined in equation (3.6) (green, dash-dotted) of the electron beam at the upstream polarimeter (UP, left part) and between e^+e^- IP and downstream polarimeter (DP, right part).

SB2009_Nov10 lattice , perfect alignment, no detector solenoid, no crab cavity

Table 10. Contributions to the uncertainty of the spin transport from the upstream to the downstream polarimeter for a beam energy of 250 GeV in the absence of collisions.

Contribution	$\delta\mathcal{P}_z/\mathcal{P}_z\,[10^{-3}]$
Beam and polarisation alignment at polarimeters (assuming $\Delta\vartheta_{\text{bunch}} = 50\,\mu$rad, $\Delta\vartheta_{\text{pol}} = 25\,$mrad)	0.72
Random misalignments ($10\,\mu\text{m}/\mu\text{rad}$) with beam orbit correction	0.35
Variation in beam parameters (10 % in the emittances)	0.03
Longitudinal precession in detector magnets	0.01
Bunch rotation to compensate the beam crossing angle	< 0.01
Emission of synchrotron radiation	0.005
Total	0.80

M.Beckmann, J.List, A.Vauth and B.Vormwald, Spin transport and polarimetry in the beam delivery system of the international linear collider, JINST 9 P07003, 2014

Polarization measurement by the Compton scattering

Collisions between the beam and the laser, QED process

(a)

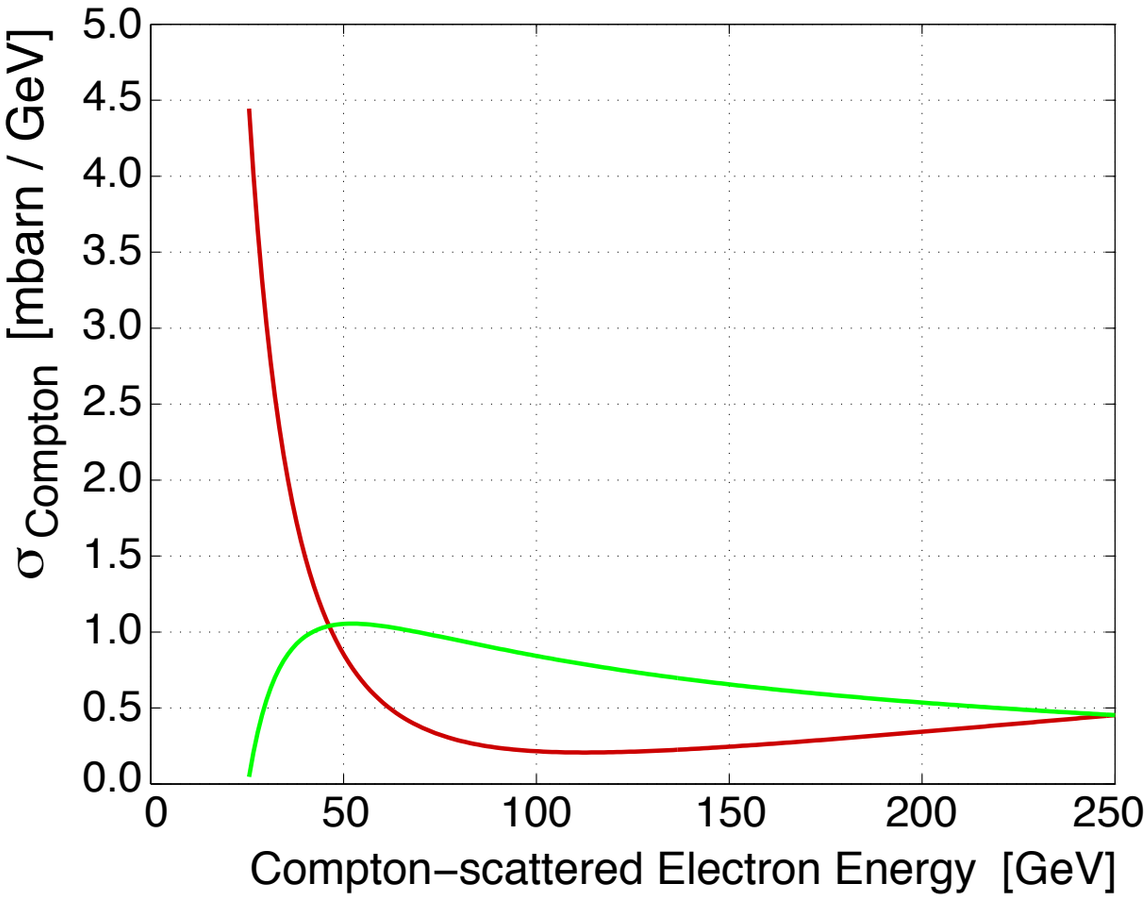

(b)

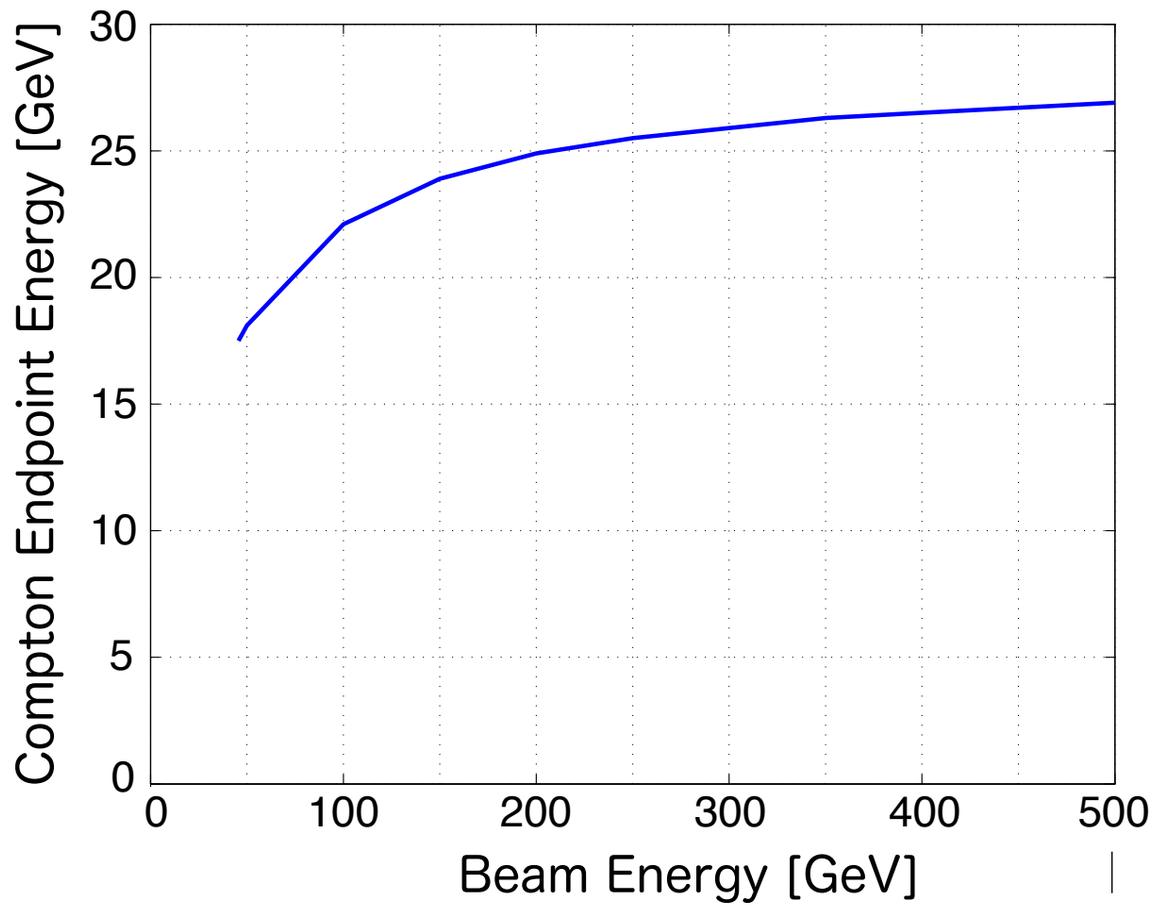

Figure 2. (a) Compton differential cross section versus scattered electron energy for same (black/red curve) and opposite (grey/green curve) helicity configuration of laser photon and beam electron. The beam energy is 250 GeV and the laser photon energy is 2.3 eV. (b) Compton edge energy dependence on the beam energy.

S. Boogert et al., “Polarimeters and energy spectrometers for the ILC Beam Delivery System” , 2009 JINST 4 P10015

Polarimeter principle

The opposite sign helicity configuration ($P\lambda$=-1), which has parallel spins (m_j=3/2) , dominates at the Compton edge over the other helicity and spin orientation ($P\lambda$=+1 and m_j=1/2).

σ=154(118)mb for $P\lambda$=-1 (+1)

E_0 (GeV	λ (nm)	ω_0 (eV)	x	ω_{max} (GeV)	E_{min} (GeV)
45.6	1064	1.165	0.813	20.4	25.2
	532	2.33	1.63	28.3	17.3
	266	4.66	3.25	34.9	10.7
250	1064	1.165	4.46	204	46
	532	2.33	8.92	225	25
	266	4.66	17.8	237	13

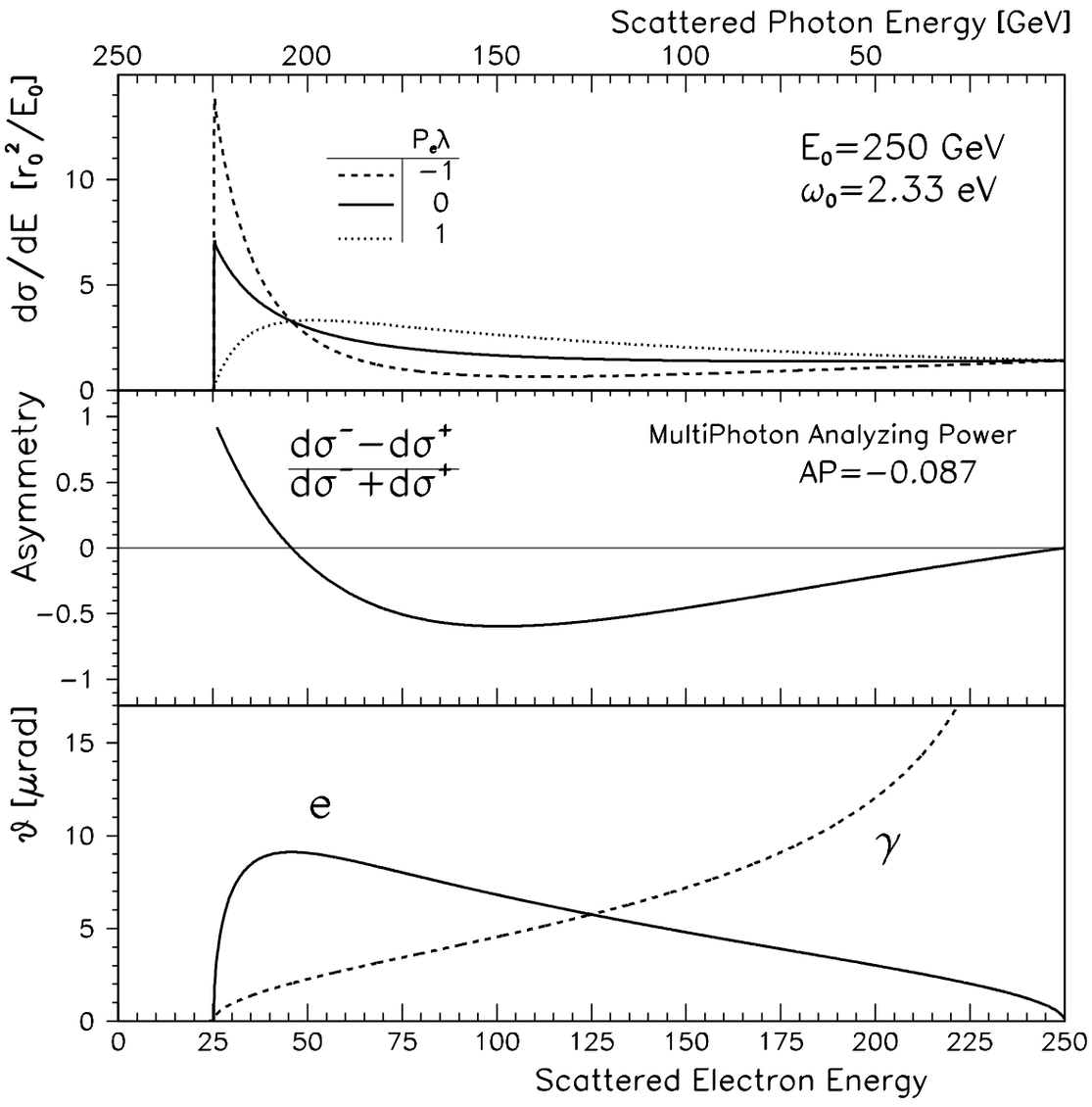

Figure 4. Energy spectra (top), spin asymmetry (middle) and scattering angles (bottom) of Compton scattered electrons and photons, for a beam energy of 250 GeV and a green laser.

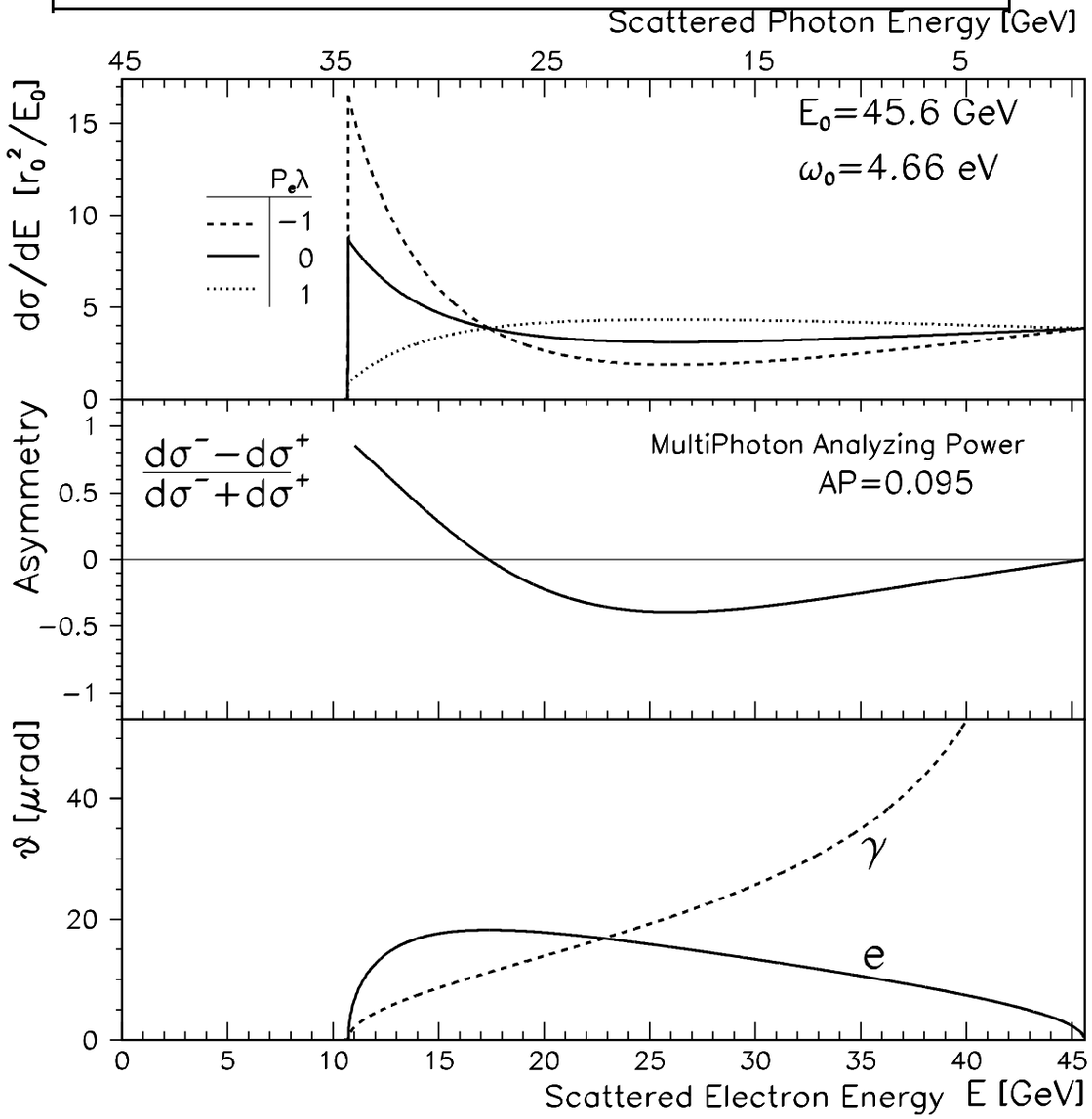

Figure 6. Energy spectra (top), spin asymmetry (middle) and scattering angles (bottom) of Compton scattered electrons and photons, for a beam energy of 45.6 GeV and an ultraviolet laser.

V. Gharibyan, N. Meyners and P. Schuler, “The TESLA Compton polarimeter,” LC-DET-2001-047

Table 3. Selected parameters of the electron and laser beams at the up- and downstream polarimeter.

	e^+/e^- beam	Laser beam	
		Upstream	Downstream
Energy	45.6 - 500 GeV	2.33 eV	2.33 eV
Bunch charge/energy	$2 \cdot 10^{10}\, e$	35 μJ	100 mJ
Bunches per train	1312 - 2625	1312 - 2625	1
Bunch length σ_t	1.3 ps	10 ps	2 ns
Average power		0.2-0.5 W	0.5 W

x 3 with three lasers

Laser intensity must be increased for S/N at DP with larger backgrounds

Table 4. Size and energy spread of electron and positron beams at the up- and downstream polarimeter locations obtained from `STALC`.

		UP		DP		DP with collisions
		e^+	e^-	e^+	e^-	e^+/e^-
Horizontal bunch size σ_{xe}	[μm]	24	32	7	15	~ 3000
Vertical bunch size σ_{ye}	[μm]	3	3	33	39	~ 1200
Beam energy spread σ_E/E	[10^{-3}]	0.7	1.2	0.7	1.3	~ 44

disrupted beam at DP
(Downstream polarimeter)

M.Beckmann, J.List, A.Vauth and B.Vormwald, Spin transport and polarimetry in the beam delivery system of the international linear collider, JINST 9 P07003, 2014

Table 5. Selected parameters of the up- and downstream polarimeters. For the downstream polarimeter, the luminosities are based on the electron beam parameters in absence of collisions at the e^+e^- IP.

		Upstream	Downstream
Beam crossing angle α	[mrad]	10	15.5
Crossing plane		horizontal	vertical
Laser beam size $\sigma_{x\gamma} = \sigma_{y\gamma}$	[μm]	50	100
Luminosity / bunch	[$10^4\,\mathrm{b}^{-1}$]	1.0	18
Luminosity	[$10^{29}\,\mathrm{cm}^{-2}\mathrm{s}^{-1}$]	630	9.1
$\delta\mathcal{P}_z/\mathcal{P}_z$ (stat)		$< 1\,\%/\,\mathrm{s}$	$< 1\,\%/\,\mathrm{min}$
$\delta\mathcal{P}_z/\mathcal{P}_z$ (sys)		0.25 %	0.25 %

Both measurements are expected to be systematically limited after a very short time.

Table 6. Uncertainty budget for the Compton polarimeters.

Source of uncertainty	$\delta\mathcal{P}_z/\mathcal{P}_z$
Detector analysing power	0.15 – 0.2 %
Detector linearity	0.1 %
Laser polarisation	0.1 %
Electronic noise and beam jitter	0.05 %
Total	0.25 %

alignment error w.r.t. the beam

M.Beckmann, J.List, A.Vauth and B.Vormwald, Spin transport and polarimetry in the beam delivery system of the international linear collider, JINST 9 P07003, 2014

Table 1. Magnetic chicane parameters for the BDS Compton polarimeters. The magnet labels given in parenthesis refer to figures 6 and 7.

Chicane Parameters	Upstream	Polarimeter	Downstream	Polarimeter
Chicane Length [m]		74.6		72.0
Number of magnets		12		6
Magnet Length [m]		2.4		2.0
Magnetic Field [T]	0.0982	(1P–12P)	0.4170 0.6254 0.4170	(1P, 2P) (3P, 4P) (1G, 2G)
Magnet 1/2-gap [cm]	1.25	(1P–12P)	11.7 13.2 14.7	(1P–3P) (4P) (1G, 2G)
Magnet pole-face width [cm]	10.0 20.0 30.0	(1P–3P) (4P–9P) (10P–12P)	40.0 54.0 40.0	(1P–3P) (4P) (1G, 2G)
Dispersion at mid-chicane for 250 GeV [mm]		20		20

Upstream Polarimeter

~1650m upstream from IP

$\delta P/P \sim 0.25\%$ averaging over 2 entire trains with opposite helicity

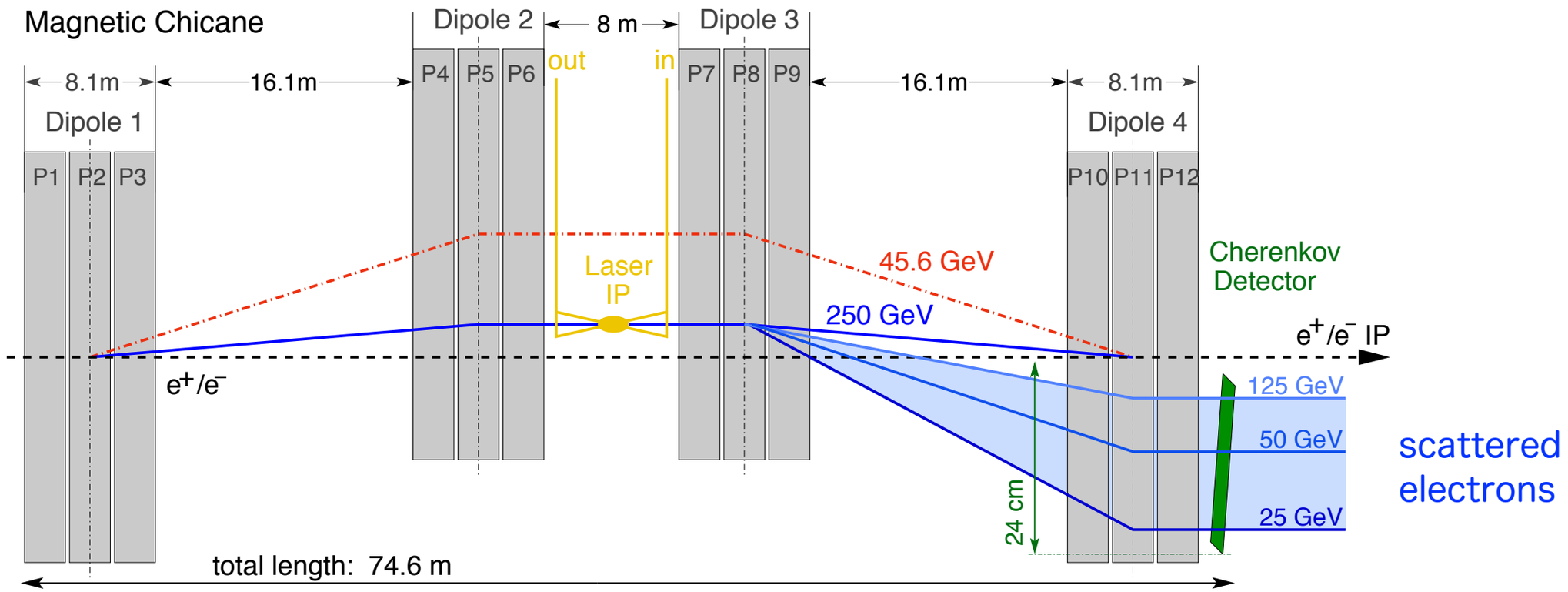

Figure 2.4.3: *Schematic of the upstream polarimeter chicane.*

It is capable to monitor the polarization in bunch by bunch since the laser beam can have the same bunch train structure in principle.

S. Boogert et al., "Polarimeters and energy spectrometers for the ILC Beam Delivery System" , 2009 JINST 4 P10015

Downstream Polarimeter and Energy Spectrometer

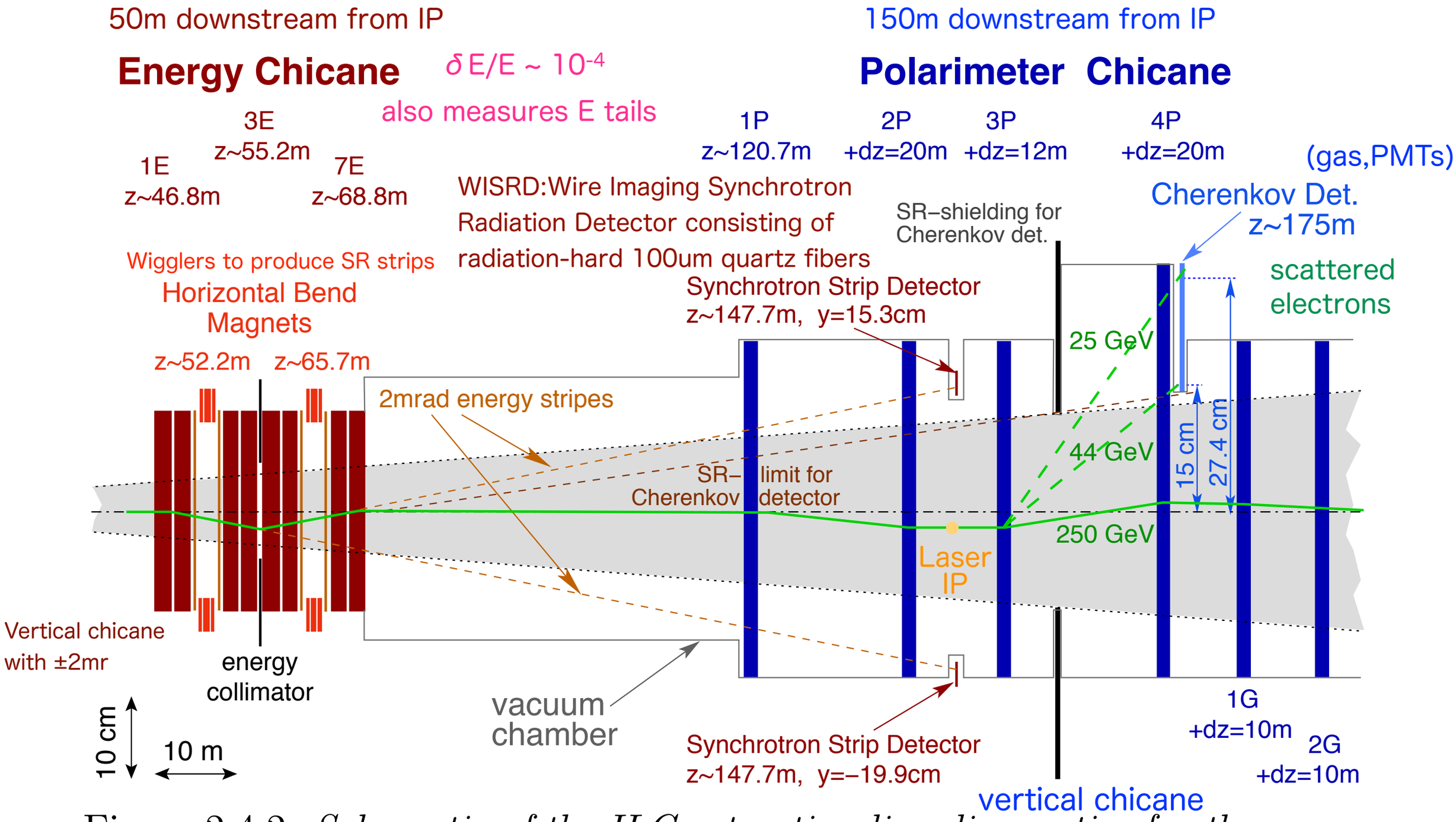

Figure 2.4.2: *Schematic of the ILC extraction line diagnostics for the energy spectrometer and the Compton polarimeter.*

S. Boogert et al., "Polarimeters and energy spectrometers for the ILC Beam Delivery System" , 2009 JINST 4 P10015

Downstream Polarimeter

Plan view: Config. of surface laser room, penetration shaft and extraction line tunnel

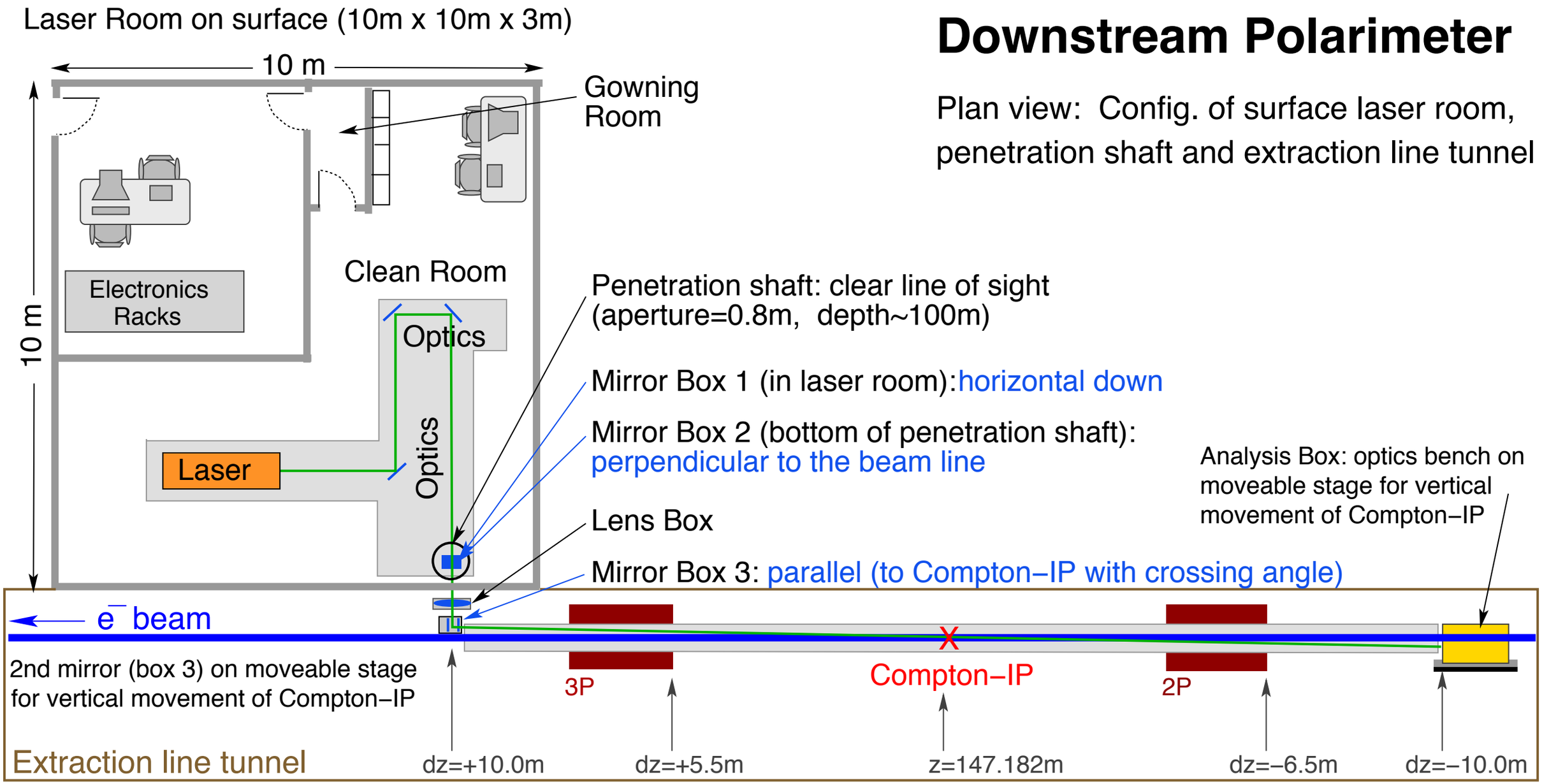

Figure 3. Proposed configuration of laser room, penetration shaft and extraction line layout for the downstream Compton polarimeter.

S. Boogert et al., "Polarimeters and energy spectrometers for the ILC Beam Delivery System" , 2009 JINST 4 P10015

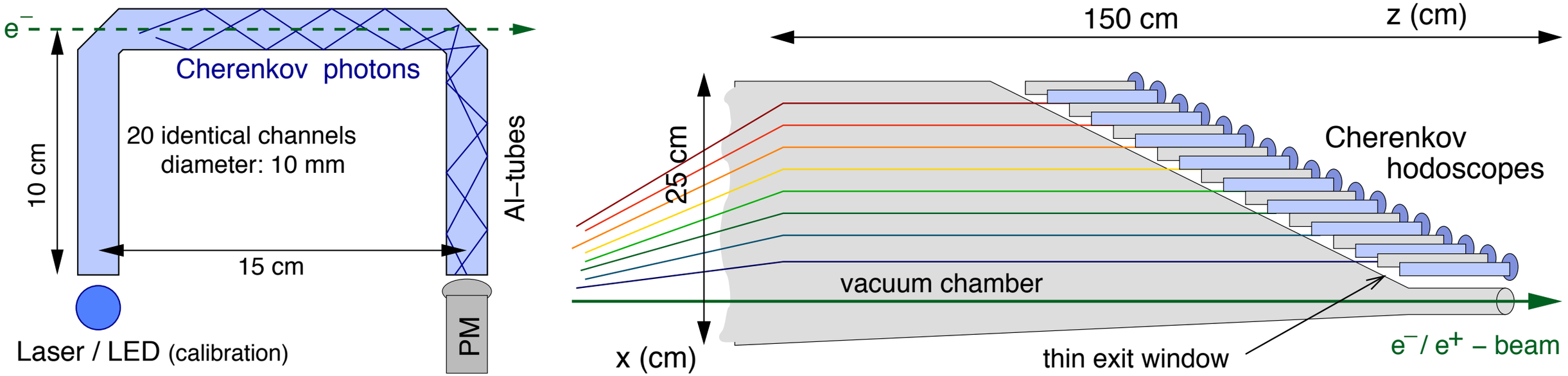

Figure 5. Schematic of a single gas tube (left) and the complete hodoscope array covering the tapered exit window (right) as foreseen for the Cherekov detectors of both polarimeters.

Candidate of Cherenkov gases is perfluorobutane (C_4F_{10}) for a high Cherenkov threshold of 10 MeV

S. Boogert et al., "Polarimeters and energy spectrometers for the ILC Beam Delivery System" , 2009 JINST 4 P10015

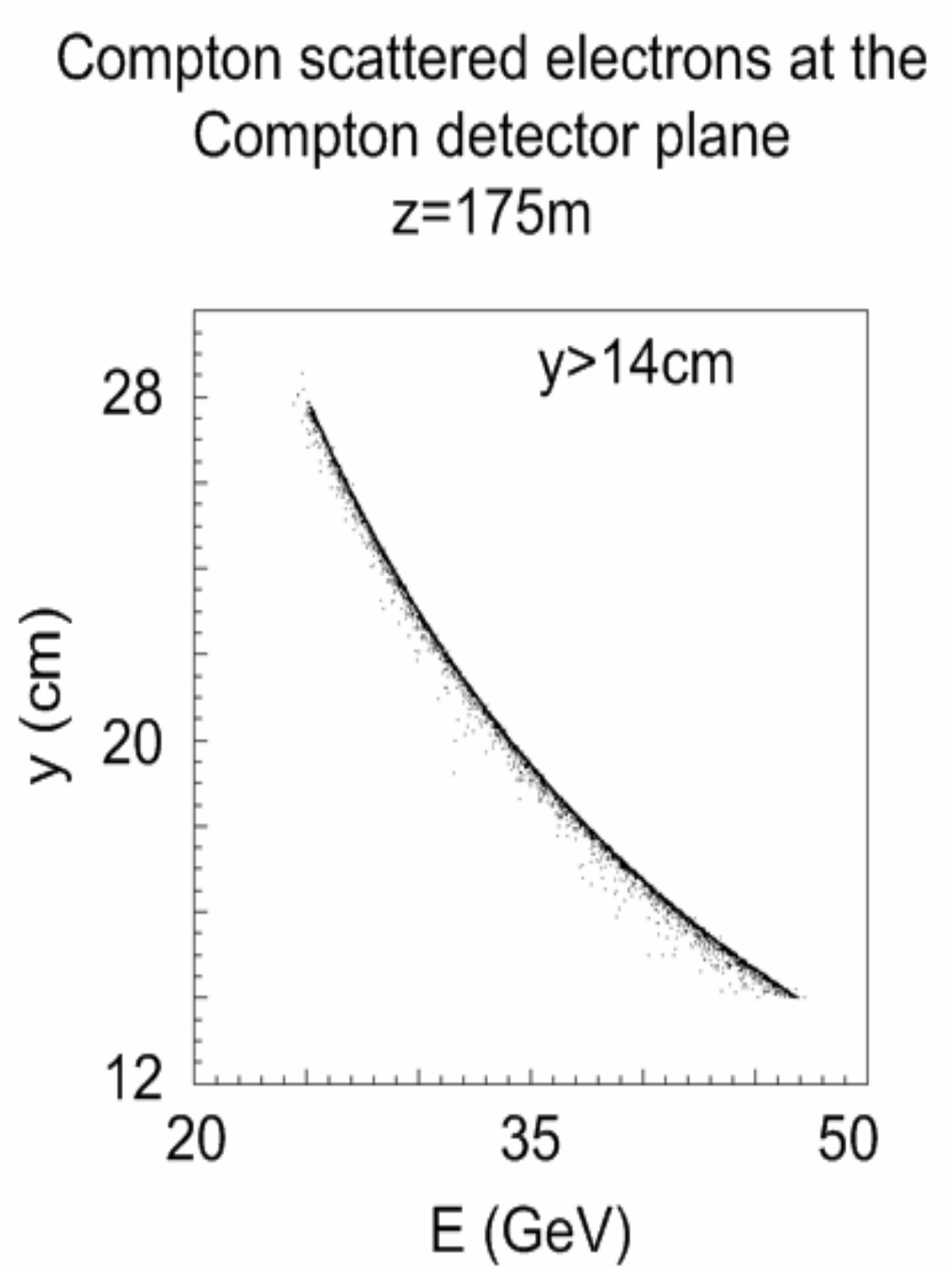

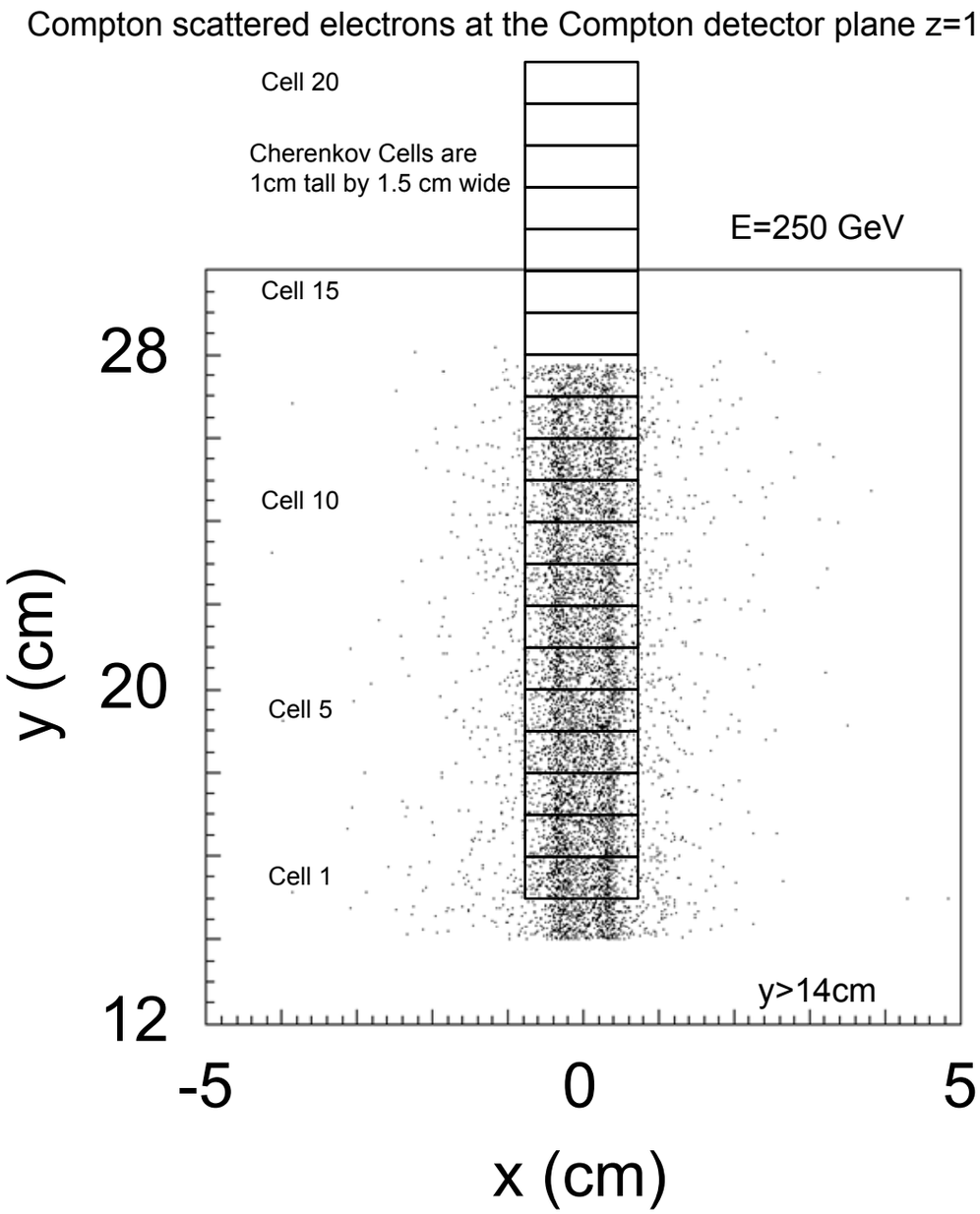

Energy versus y for the Compton scattered electrons at the Compton Detector plane (z = 175m) for beam energy of 250 GeV.

K. Moffeit, Workshop on polarization and energy measurements at ILC, 4/9-11, 2008, DESY, Zeuthen

Systematic Errors

- The physics of the Compton scattering process is well understood in QED, with radiative corrections less than 0.1%
- Detector backgrounds are easy to measure and correct for by using laser off pulses;
- Polarimetry data can be taken simulatanously with physics data;
- The Compton scattering rate is high and small statistical errors can be achieved in a short amount of time (sub-1% precision in one minute is feasible);
- The laser helicity can be selected on a pulse-by-pulse basis;
- The laser polarization is readily determined with 0.1% accuracy.

Expected Polarimeter Systematic Errors

Uncertainty	**δP/P**
Detector Analyzing Power	0.2%
Detector Linearity	0.1%
Laser Polarization	0.1%
Electronic Noise and Background Subtraction	0.05%
TOTAL	0.25%

K. Moffeit, Workshop on polarization and energy measurements at ILC, 4/9-11, 2008, DESY, Zeuthen

Precise Beam Energy measurements for E = 45.6GeV to 500GeV

Upstream Energy Spectrometer

700m upstream from IP

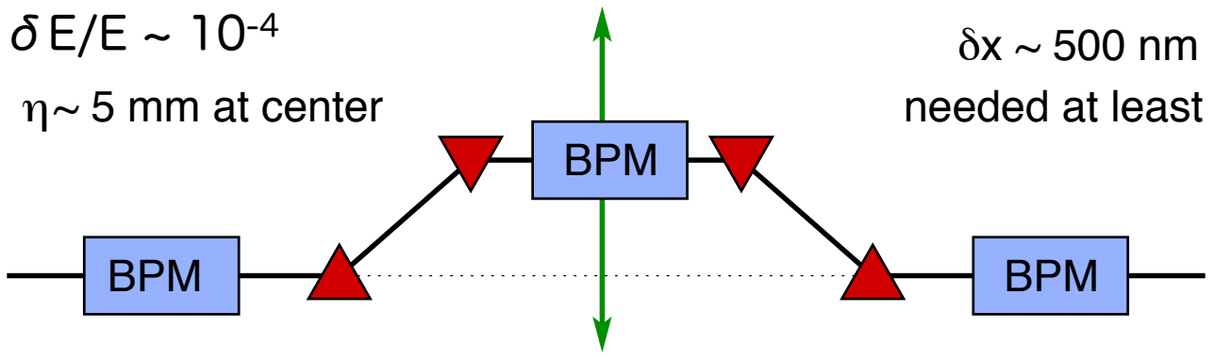

cavity type BPM can have the 20nm resolution which is enough for 45.6GeV beam energy measurements with 100ppm at the same magnetic fields of the chicane.

Figure 2.4.1: *Schematic for the upstream energy spectrometer using BPMs.*

Downstream Energy Spectrometer

50m downstream from IP

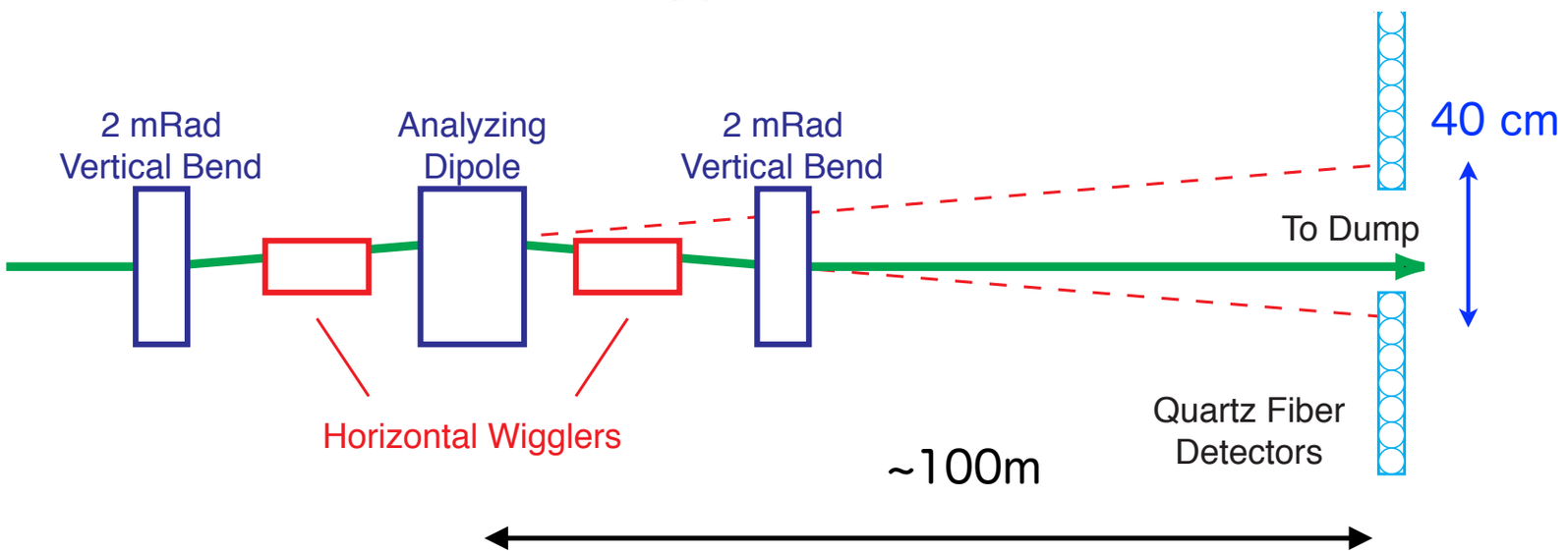

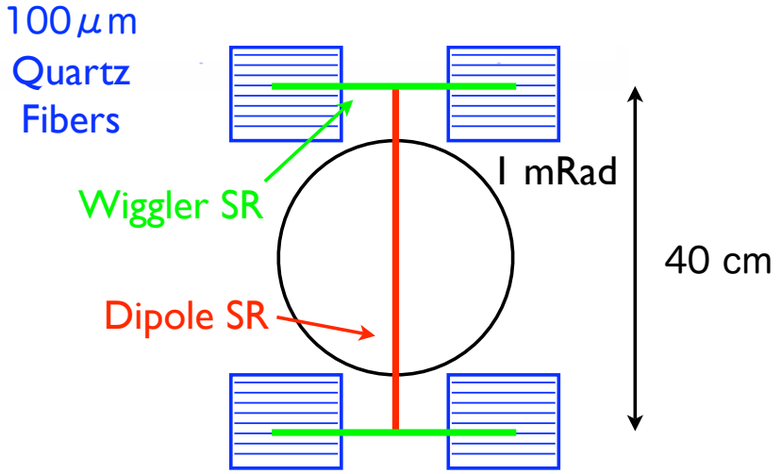

125MeV / 100μm for 500GeV beam
100ppm with 40μm accuracy

It is also capable to measure the beam energy distribution with the disruption down to 50% of the nominal beam energy.

S. Boogert et al., "Polarimeters and energy spectrometers for the ILC Beam Delivery System" , 2009 JINST 4 P10015

E. Torrence, Workshop on polarization and energy measurements at ILC, 4/9-11, 2008, DESY, Zeuthen

IR

2 detectors with Push-pull

Concept of single IR with two detectors

accessible during run

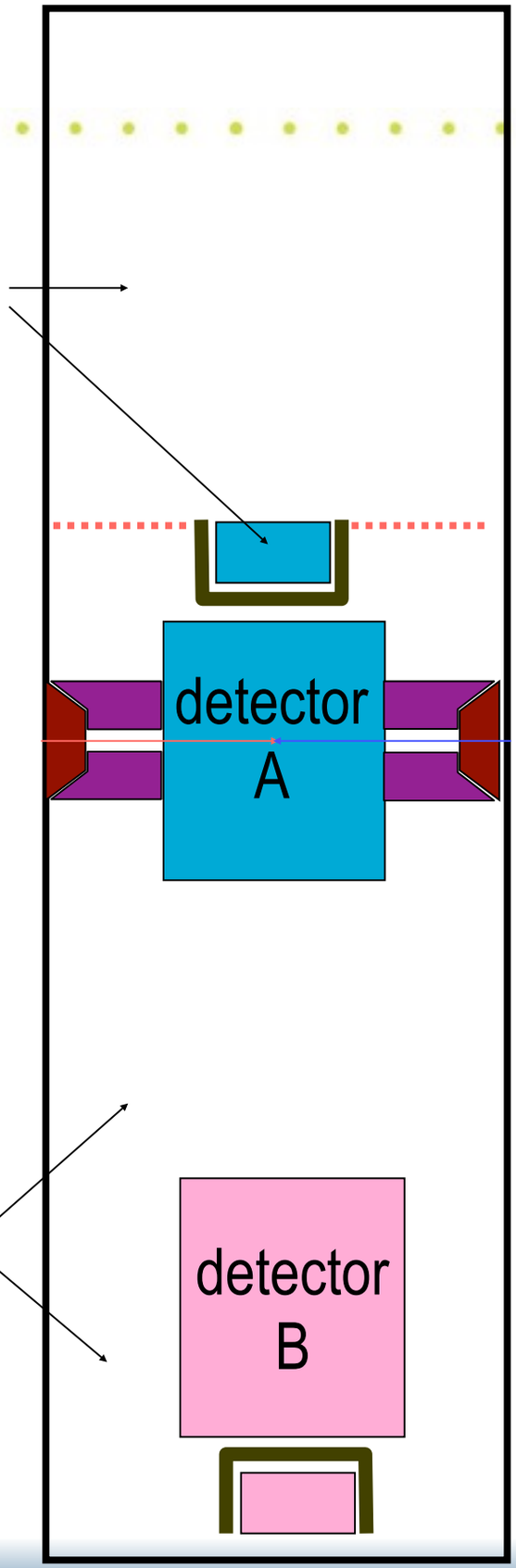

accessible during run

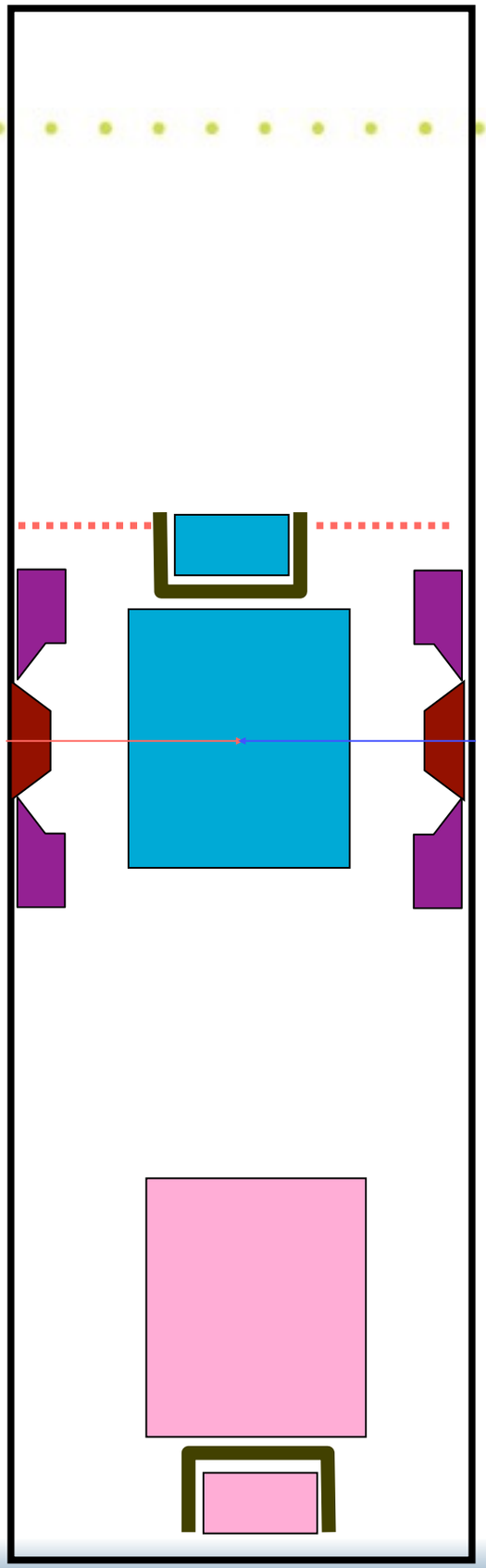

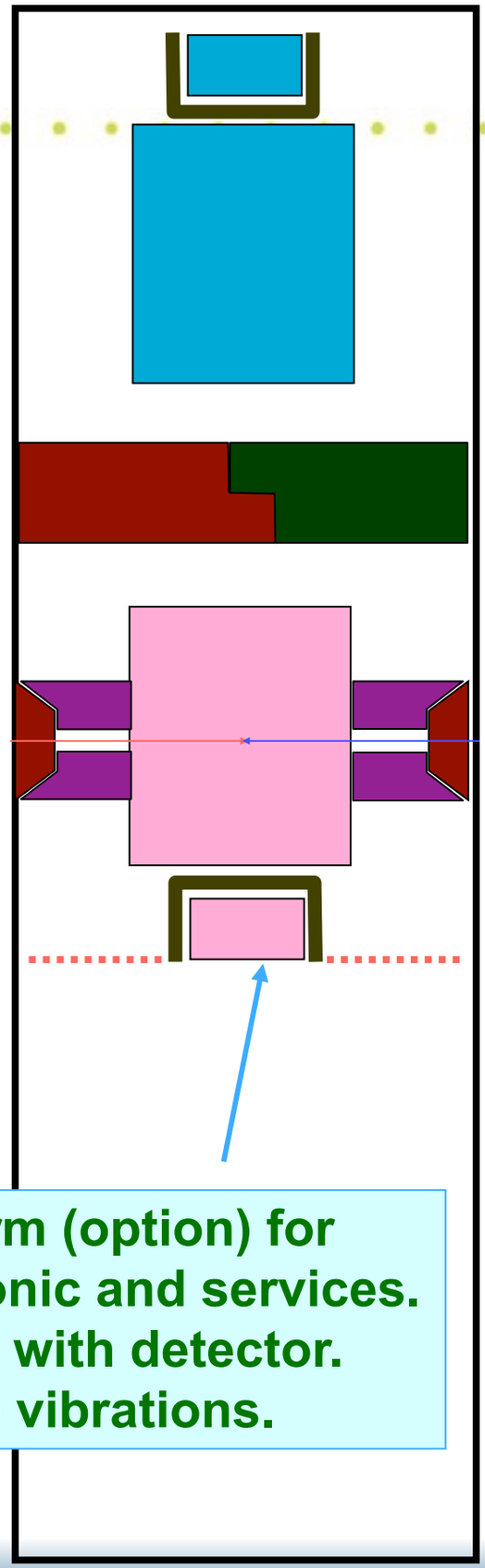

Platform (option) for electronic and services. Moves with detector. Isolate vibrations.

DBD : Push pull on the platform

ILD

SiD

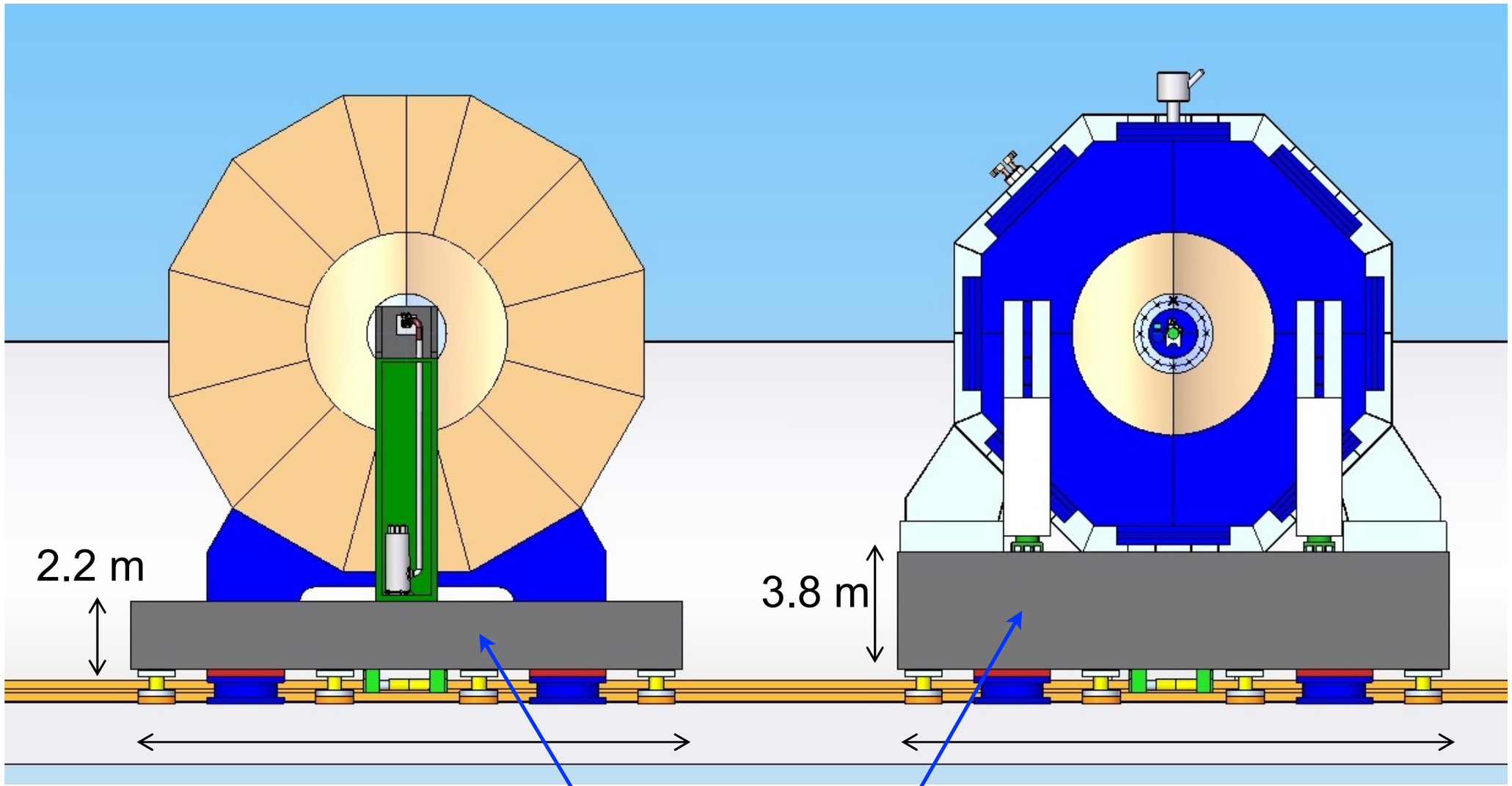

Platform
(cost included in BDS/accelerator)

ILD and SID moving on platforms

Agreed at ALCPG11, March 19-23,2011, Eugene, OR, USA,

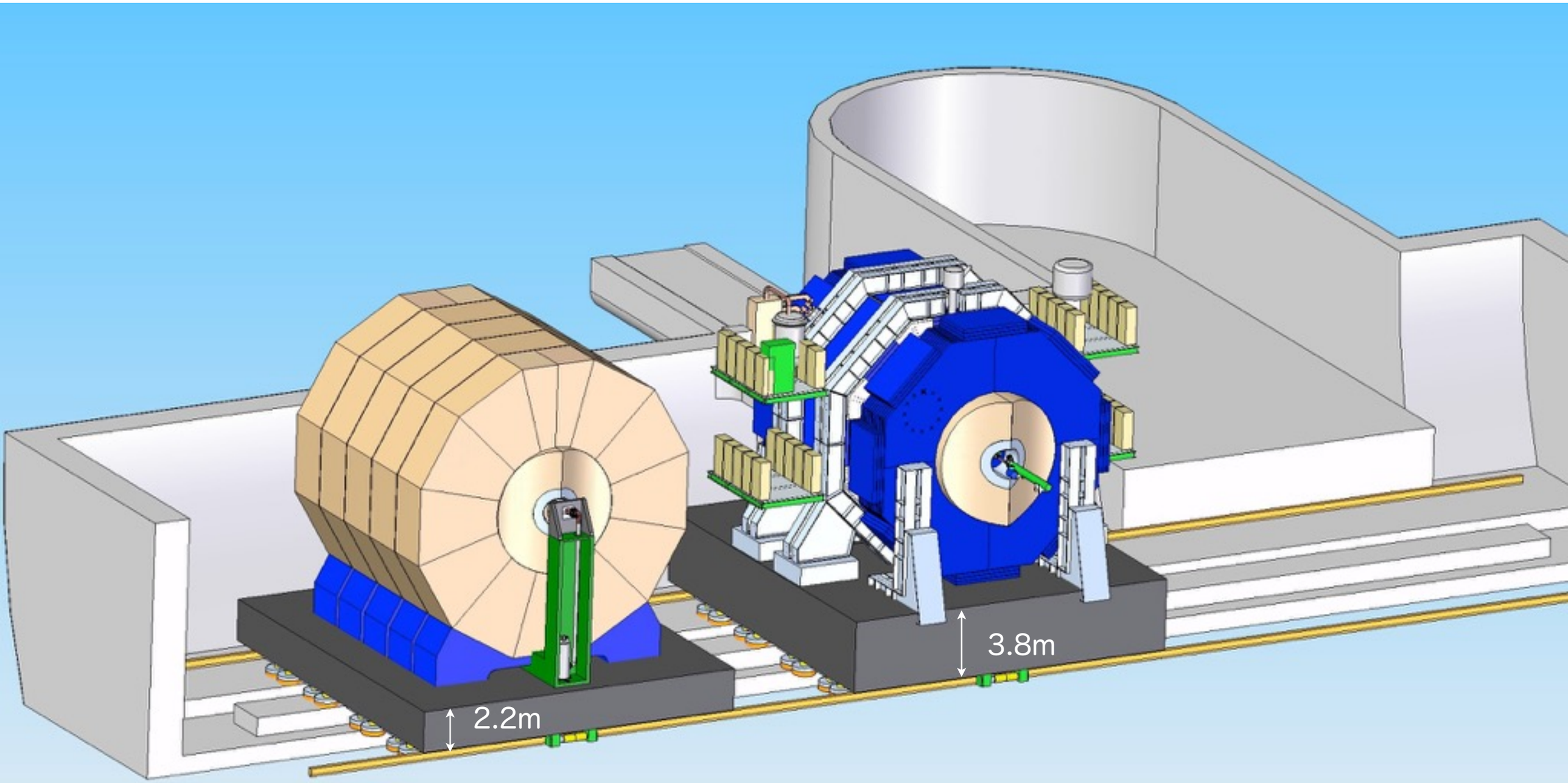

Preliminary ANSYS analysis of Platform

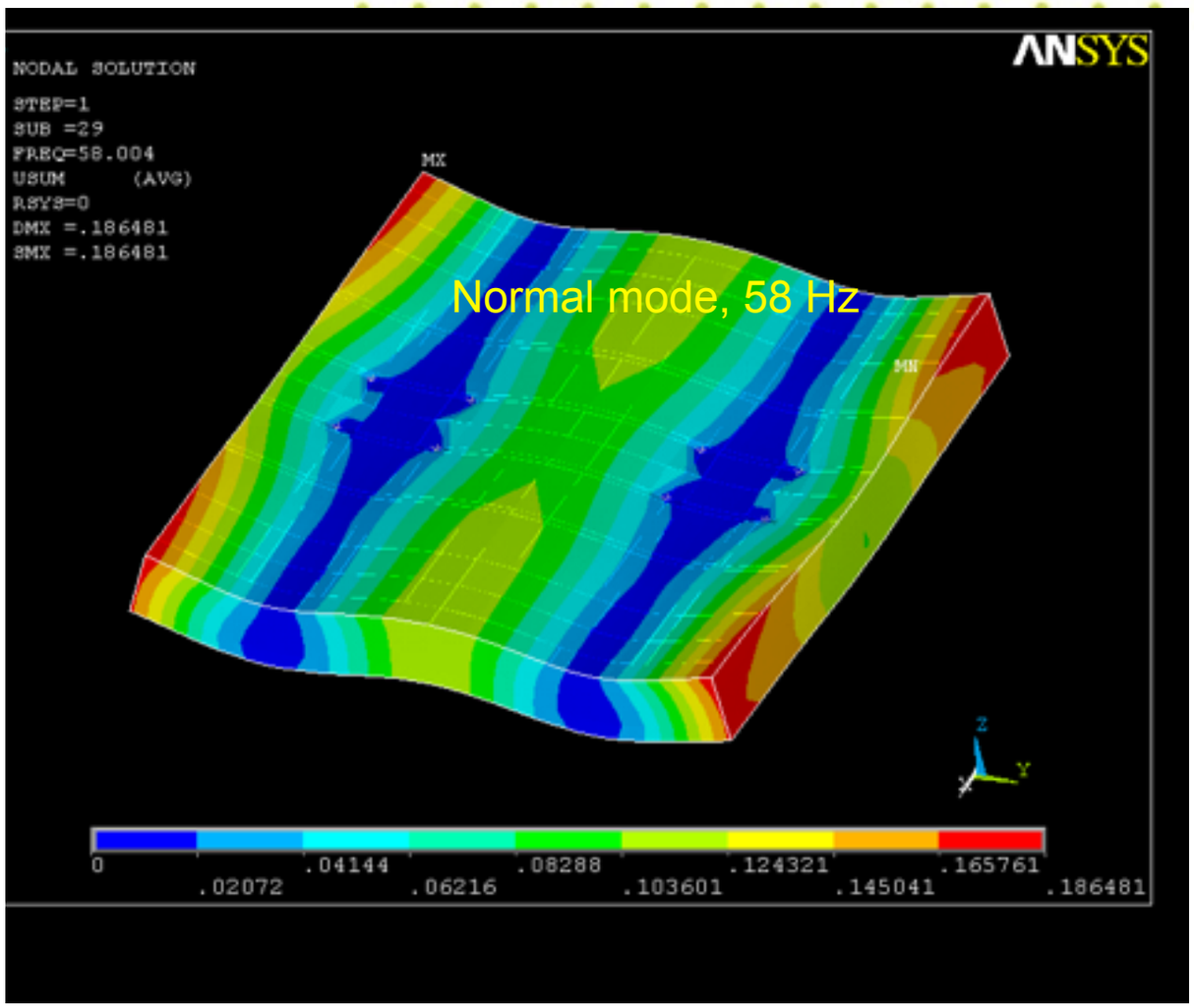

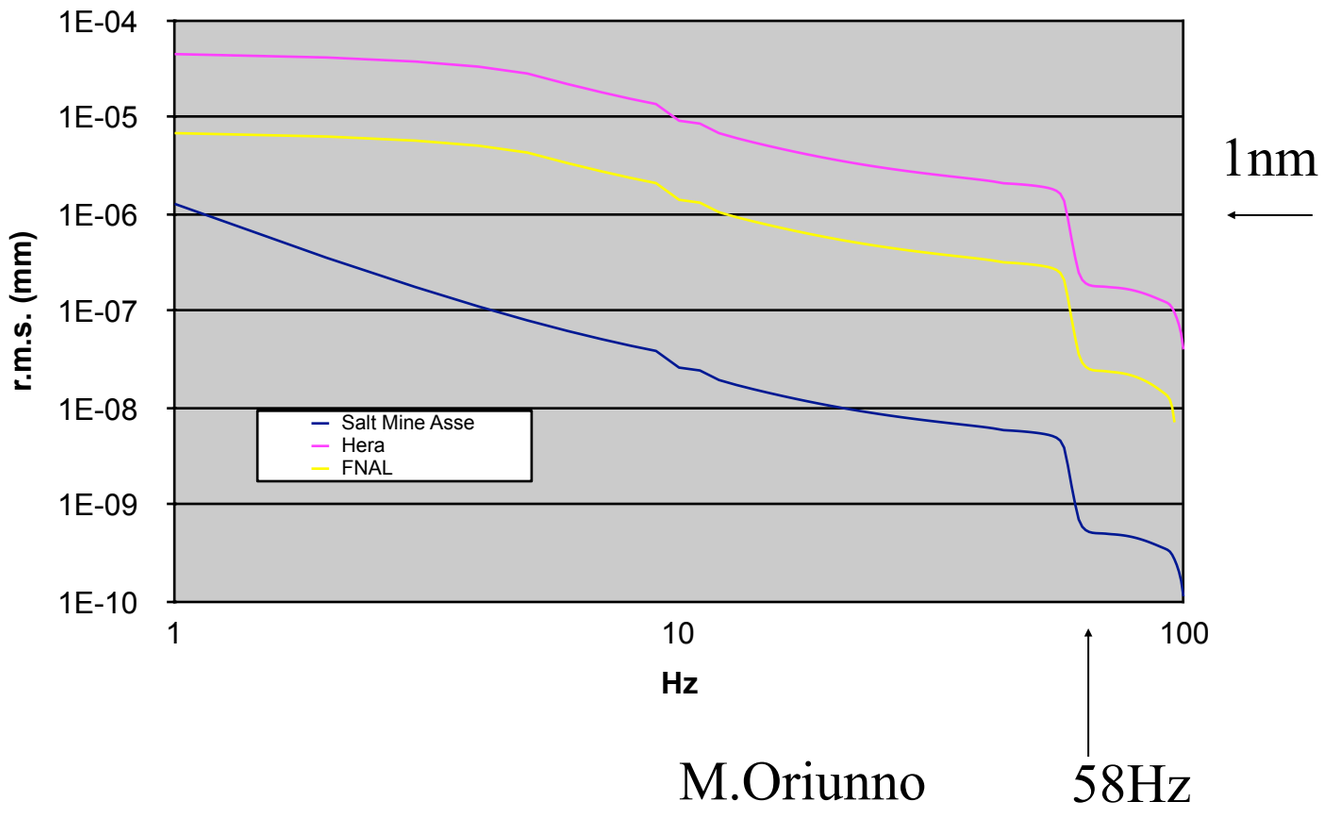

- First look of platform stability look rather promising: resonance frequencies are rather large (e.g. 58Hz) and additional vibration is only several nm

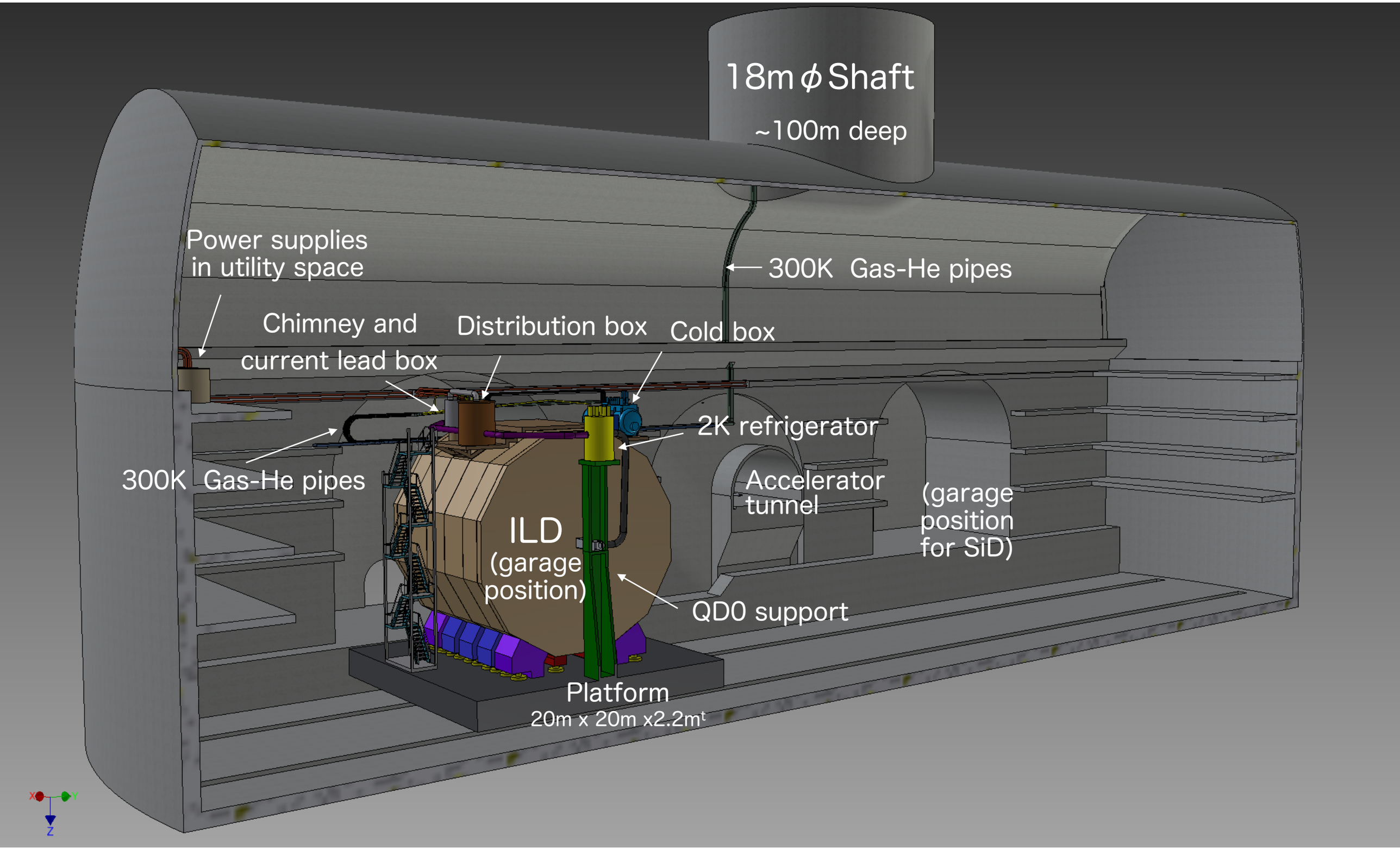
18mϕ Shaft
~100m deep
Power supplies
in utility space
300K Gas-He pipes
Chimney and
current lead box
Distribution box
Cold box
2K refrigerator
300K Gas-He pipes
Accelerator
tunnel
(garage
position
for SiD)
ILD
(garage
position)
QD0 support
Platform
20m x 20m x2.2m^t

Self-shielding of the detector (ILD0) at IR

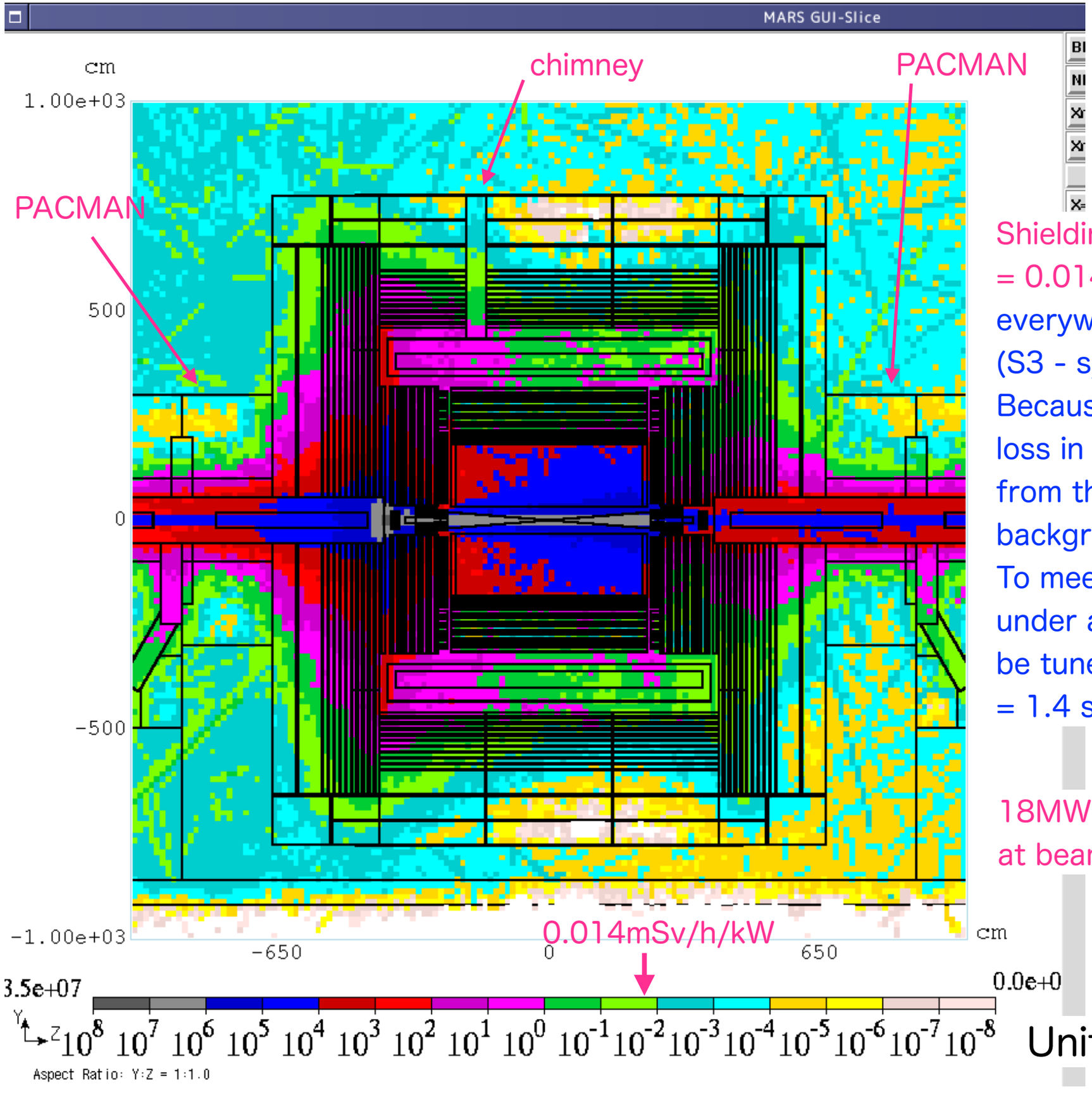

Shielding capability of 250 mSv/h/18MW = 0.014mSv/h/kW is required everywhere to meet SLAC requirement (S3 - system failure).

Because of detector design, total beam loss in the IR hall must be below 1 W from the requirement to reduce detector background.

To meet KEK guideline for integral dose under accidental beam loss, beam should be tuned off within 0.1 mSv / 250mSv/h = 1.4 seconds.

18MW 500GeV beam loss at beam calorimeter

Unit: mSv/hr/kW

Radiation Rules at KEK

- Normal operation
  - **0.2 μSv/h for Non-designated area (K1)**
  - **1.5 μSv/h for Supervised area (K2)** **experimental hall**
  - **20 μSv/h for Simple controlled area (K3)**
  - **100mSv/h for access restricted**
- Shielding **100 μSv/event(K2)**
  1mSv/event (K3)
- Mis-steering beam loss
  - **1 hour integration of dose rate should not exceed 1.5 μSv/h using radiation monitor.**

    (Terminate injection and wait 1 hour)

In the KEK regulation, there is no explicit description of ambient dose limit for beam operation conditions and beam loss classification such as SLAC-RSS

SiD and ILD : Shielding capability of 250 mSv/h / 18 MW = 0.014 mSv/h/kW is required everywhere to meet SLAC requirement

Area classification : SLAC rule

- Normal operation (S1) including screen, wire-scanners
  - **0.5 μSv/h for GERT (General Employ Radiation Training)**
  - **5 μSv/h for Radiation Worker (RW)**

- Mis-steering (S2) hardware failures, operator errors,..
  - **4 mSv/h**
- Annual dose should be less than 10mSv/year (S1,S2).
- System failure (S3) beam stopper failure and/or electric power failure of important bending magnet
  - **250 mSv/h and 30 mSv/event**

(from SLAC-I-720-0A05Z-002-R001 Radiation Safety Systems (Technical Basis Document, April 2006))

Area classification : LHC design

- Normal operation
  - **0.1 μSv/h for Non-designated area**
  - **1 μSv/h for Supervised area**
  - **3 μSv/h for Simple controlled area**
- Total beam loss
  - **0.3 mSv/h for Non-designated area**
  - **2.5 mSv/h for Supervised area**
  - **50 mSv/h for Simple controlled area**

(from http://indico.cern.ch/conferenceDisplay.py?confId=1561 talk of D. Forkel-Wirth)

FD
ILC QD0 : SCQ

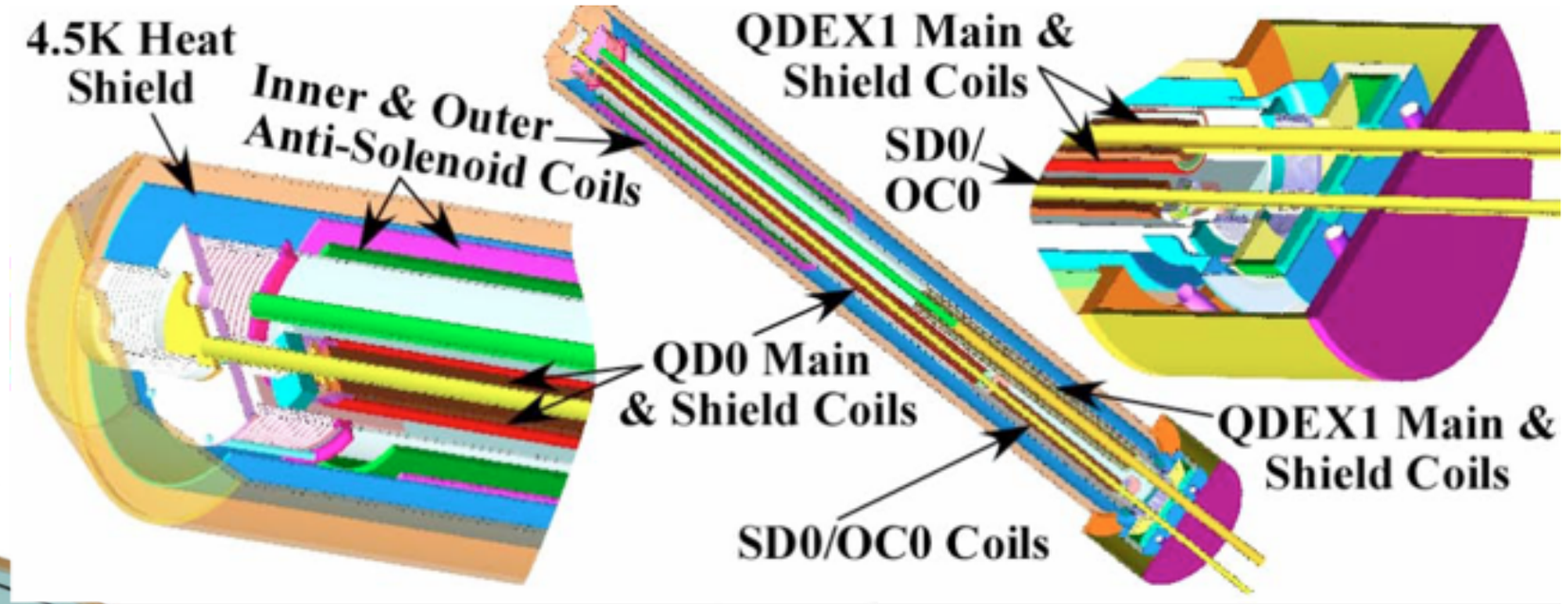

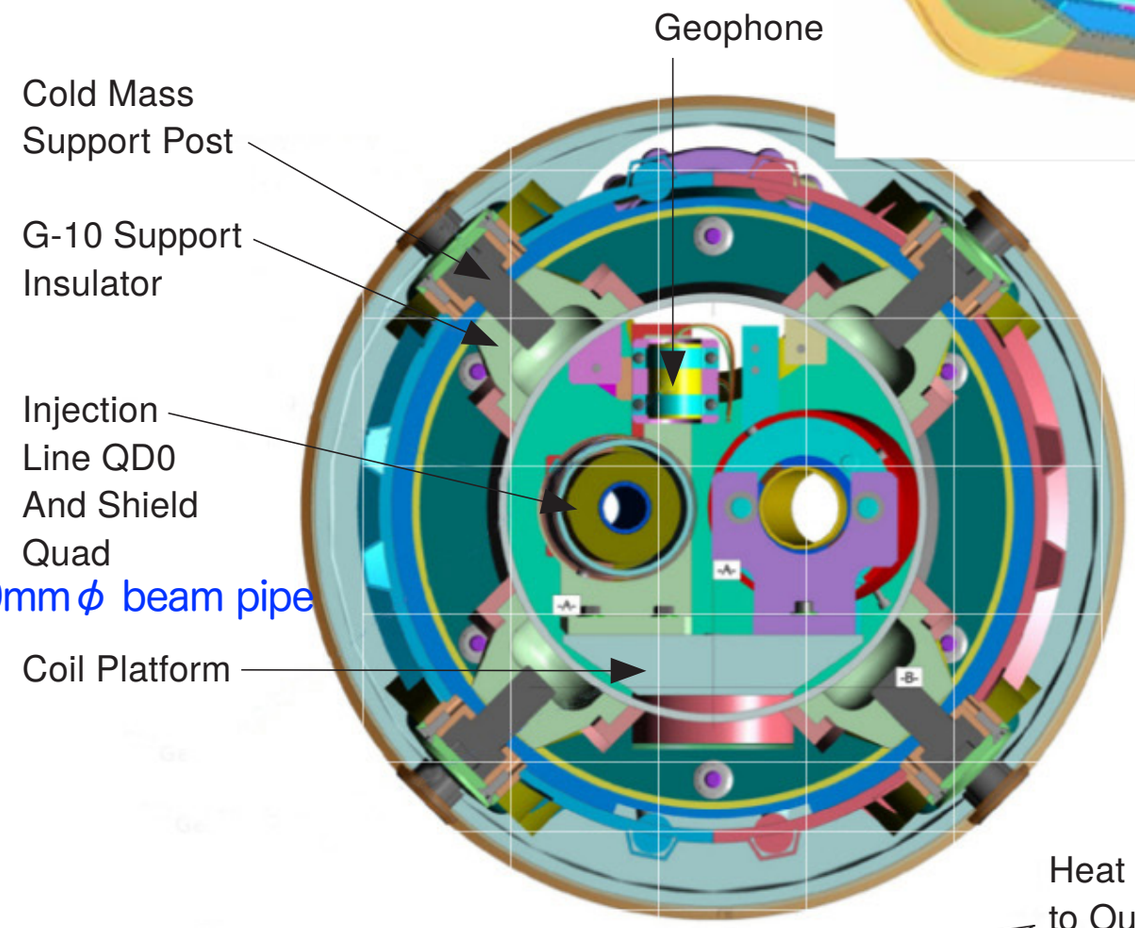

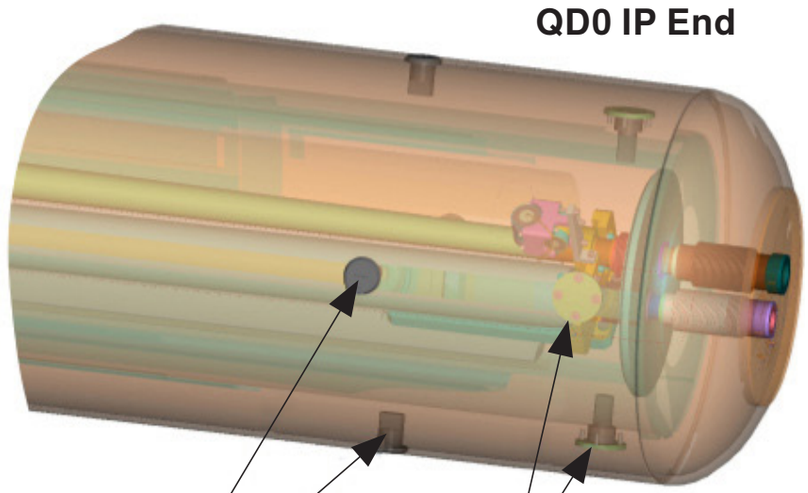

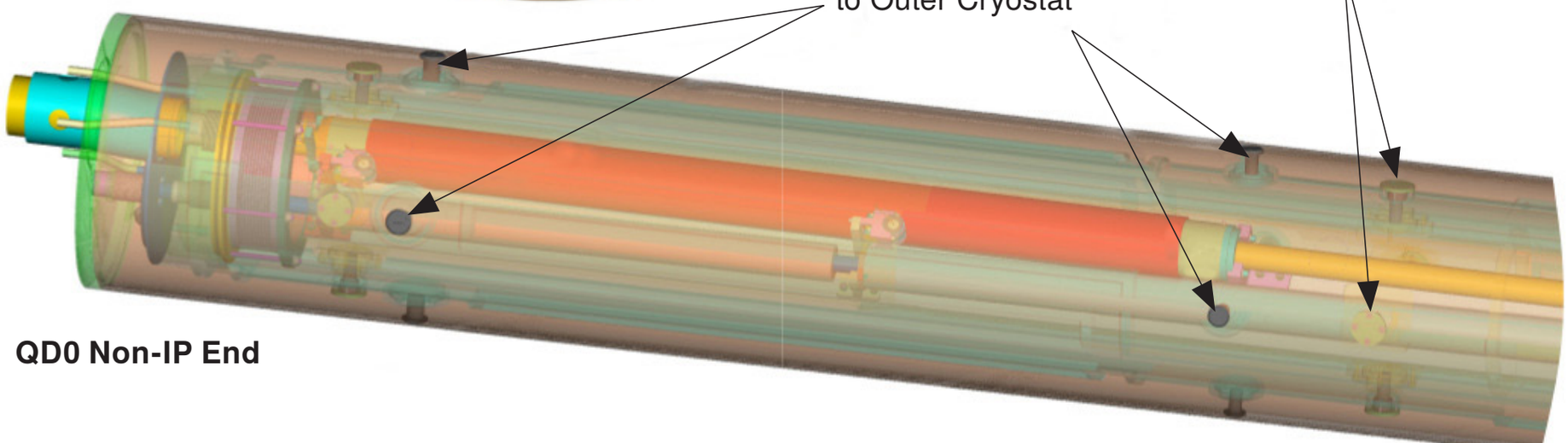

CLIC QD0 : Hybrid magnet

with tenability of 80 - 100%

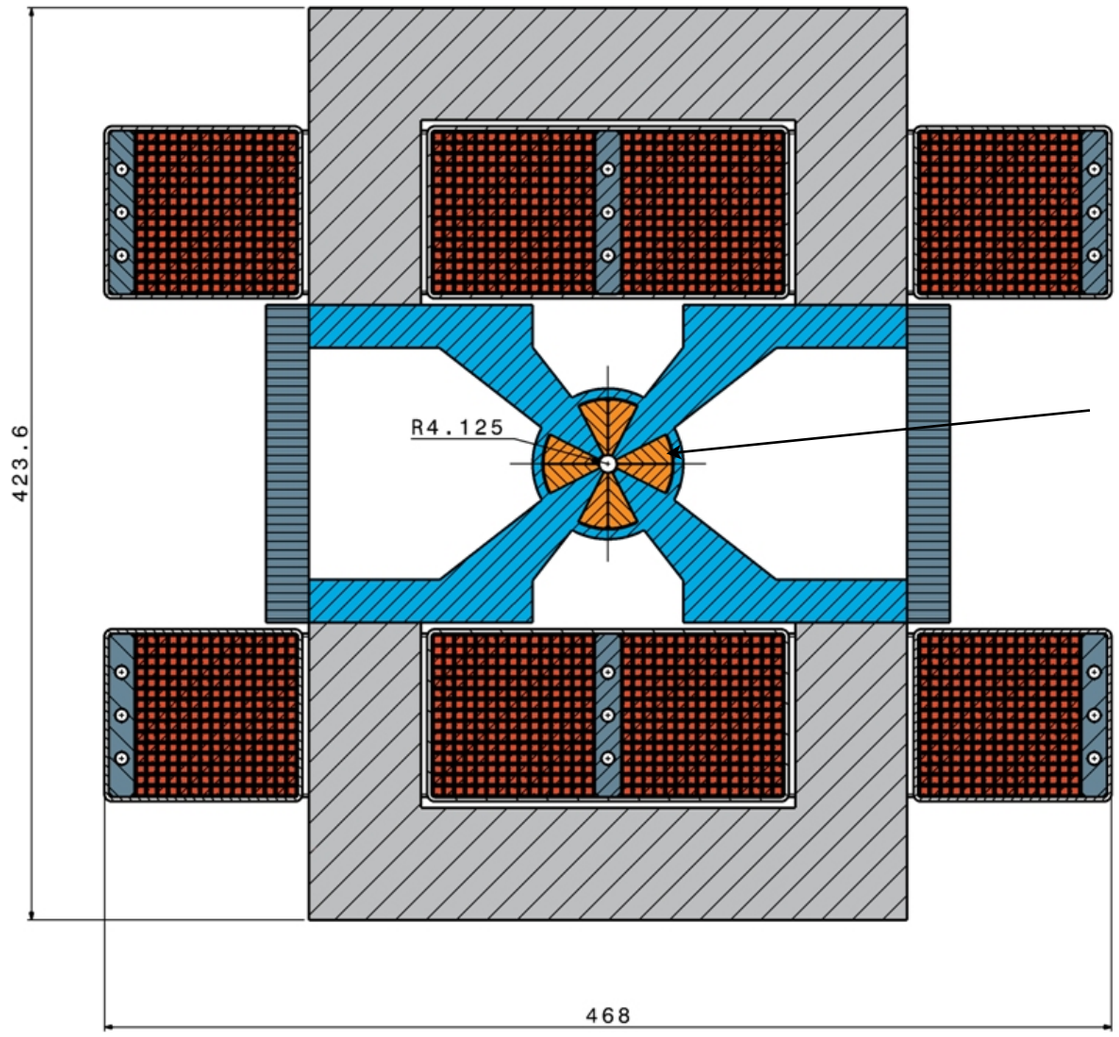

permanent magnets

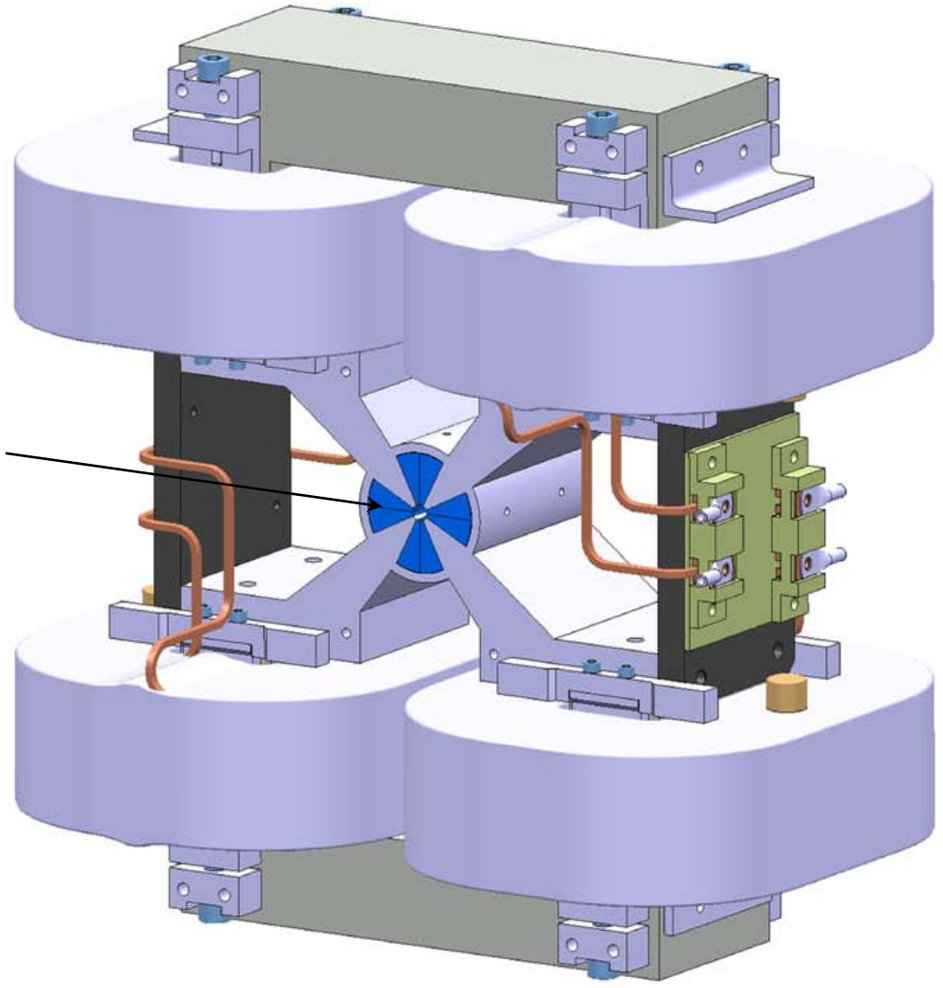

Fig. 5.289: Hybrid QD0 short prototype

with the same cross section but shorter length, which performs close to the specifications

Table 4: Specifications of the FD QD0 quadrupole for the different L* cases.

L*	m	3.5	4.3	6.0	8.0
Gradient	T/m	575	382	200	211
Length	m	2.7	3.3	4.7	4.2
Beam aperture	(r) mm	3.8	6.7	8	8.5
Jitter tolerance	nm	0.15	0.15	0.2	0.18
Gradient tol	10^{-6}	5	5	-	3
Octupolar error	10^{-4}@1mm	7	7	-	3
Prealignment	μm	10	10	8	2

QD0 supports in ILD and SiD

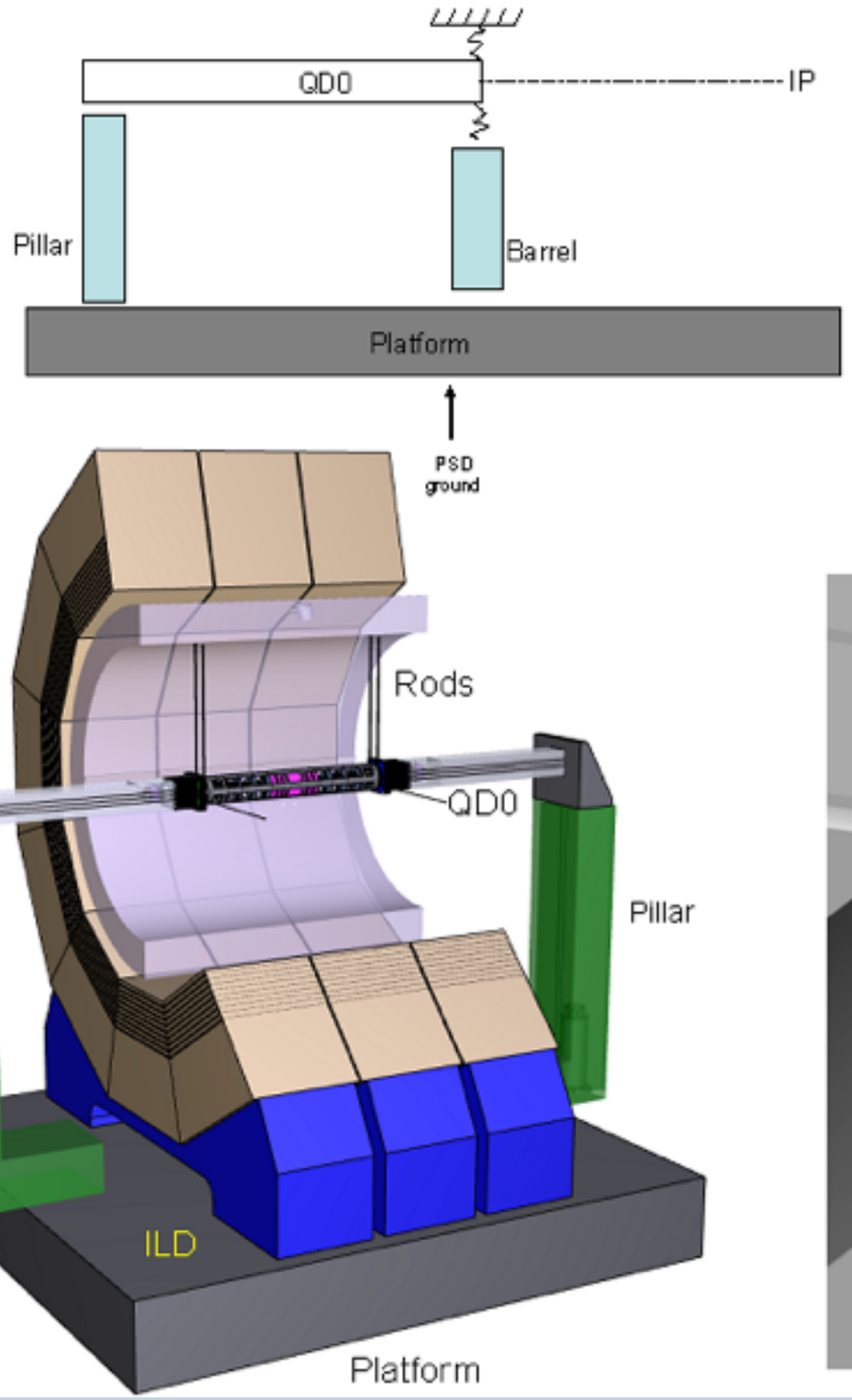

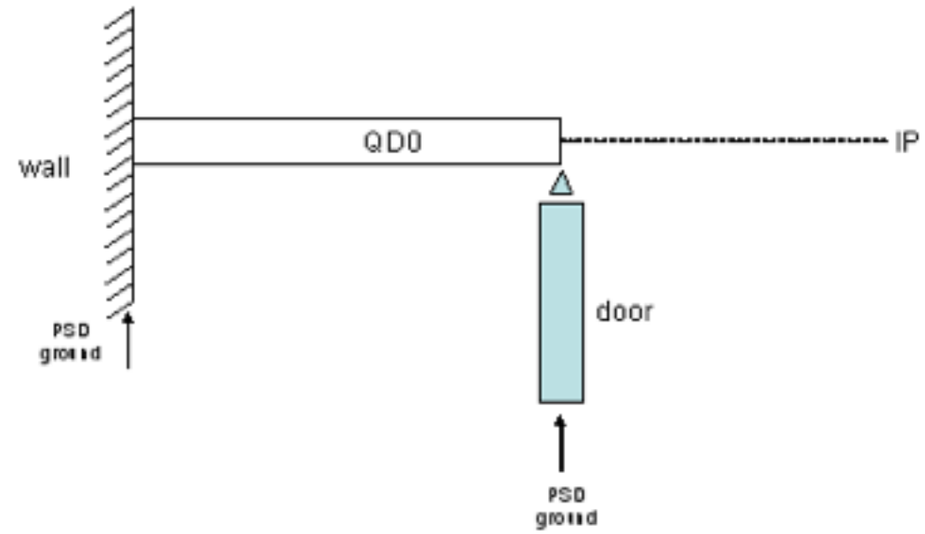

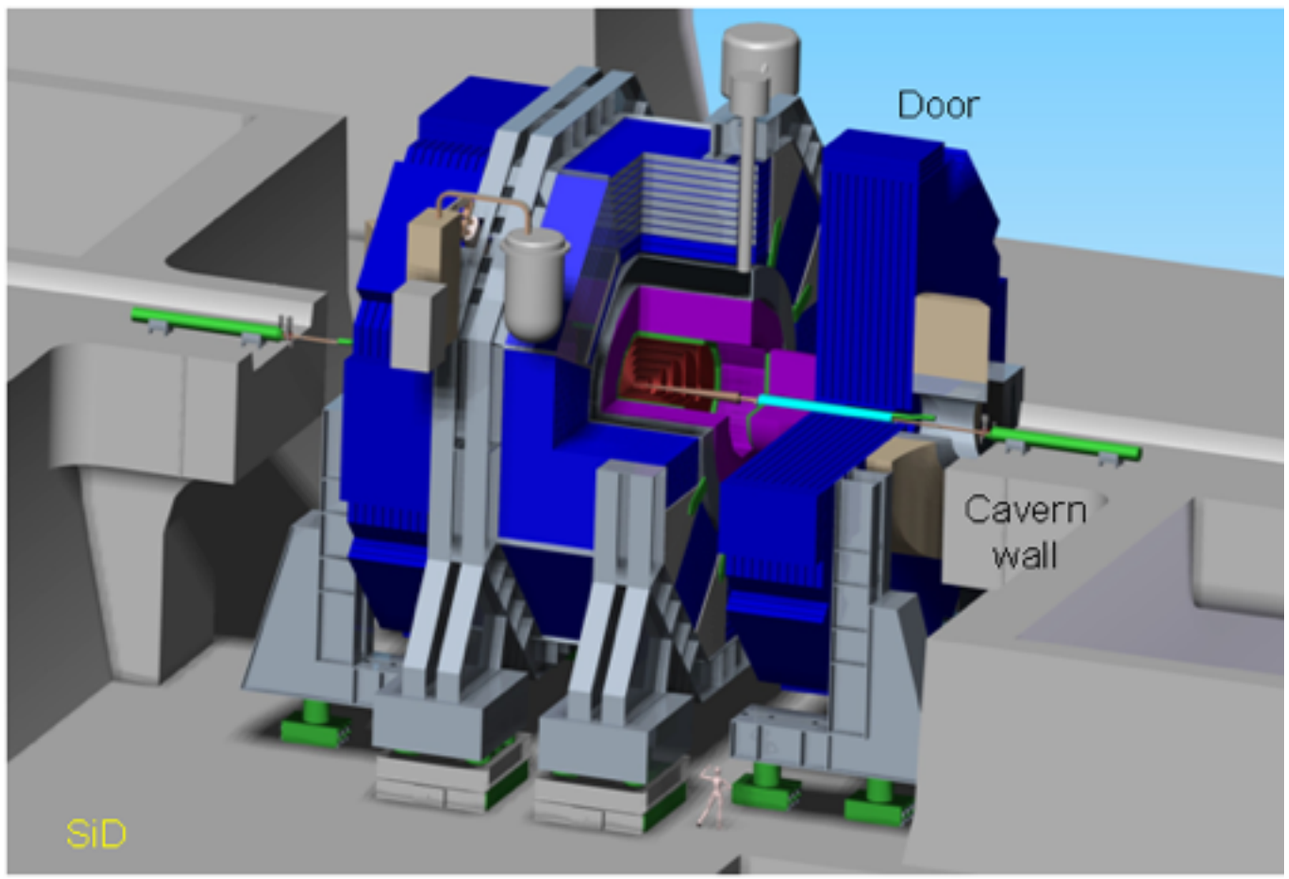

Vibration Study (C.Collette, D.Thsilumba,ULB)

SLAC

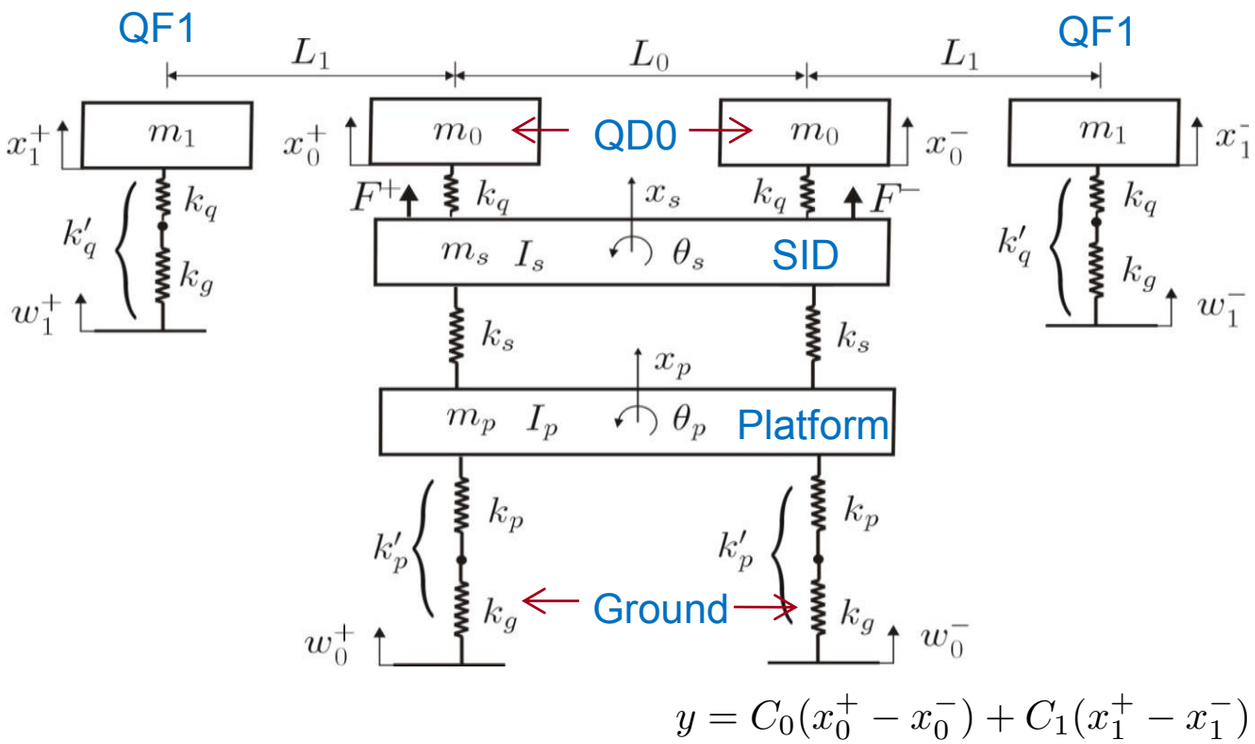

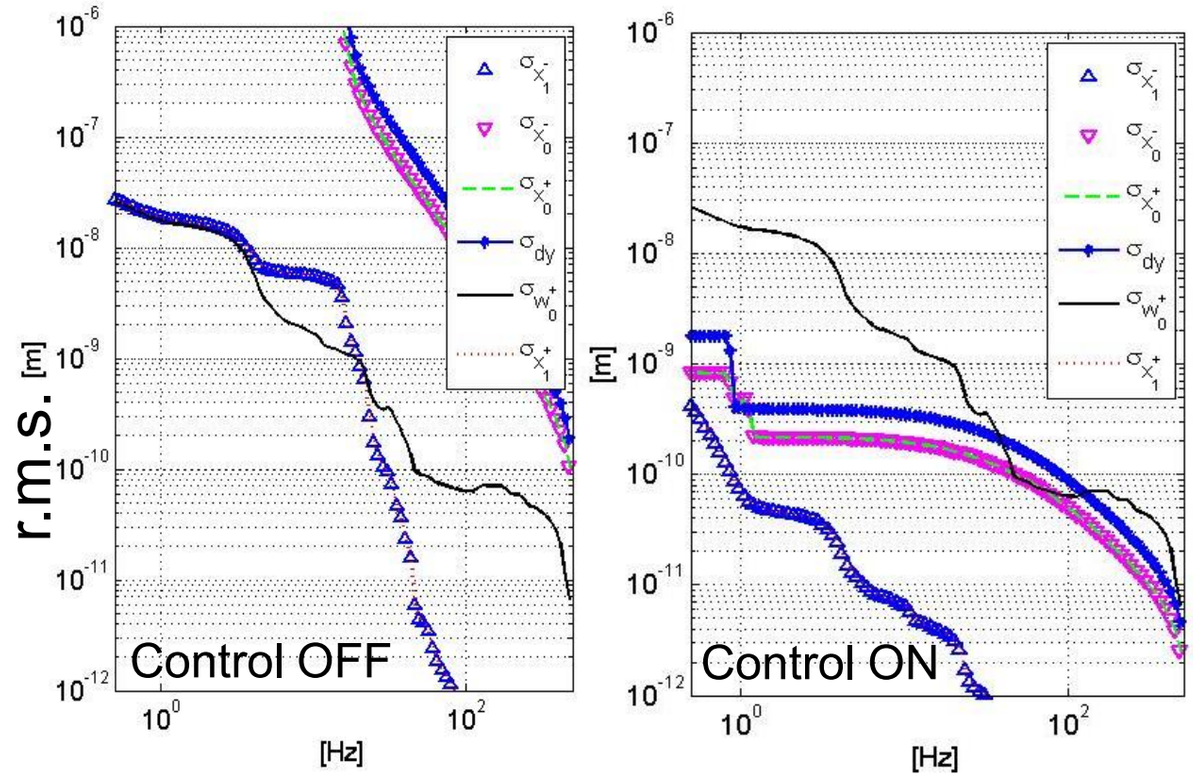

1. Ground Motions measured at the SLD detector hall
2. Conservative spectrum of the technical noise on the detector.
3. The model predicts that the maximum level of *r.m.s.* vibration seen by QDO is well below the capture range of the IP feedback system available in the ILC. With the addiction of an active stabilization system on QD0, it is also possible to achieve the stability requirements of CLIC.
4. Experimental measurements of the technical noise instrumenting CMS during LS1 with permanent vibration sensors

ILD QD0 support, by H. Yamaoka, LCWS2010, Beijing

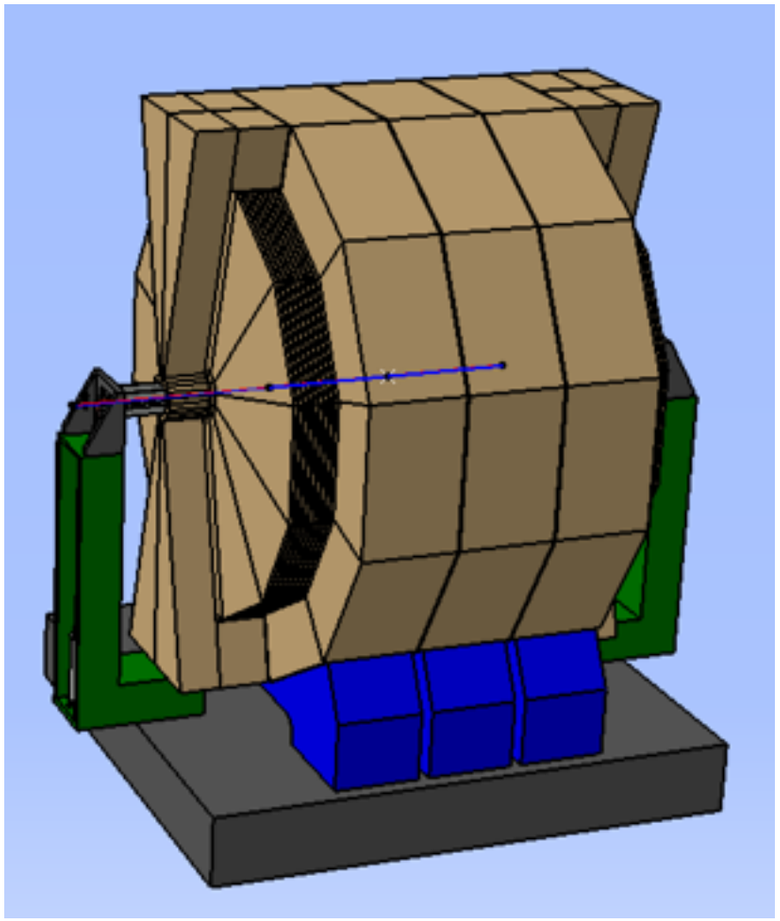

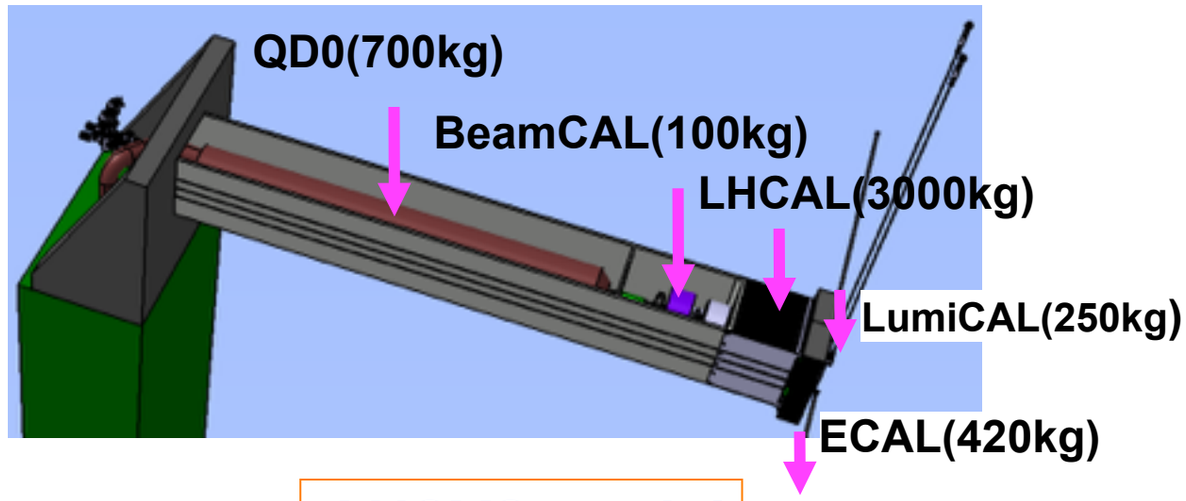

ANSYS model

fixed or support bracket

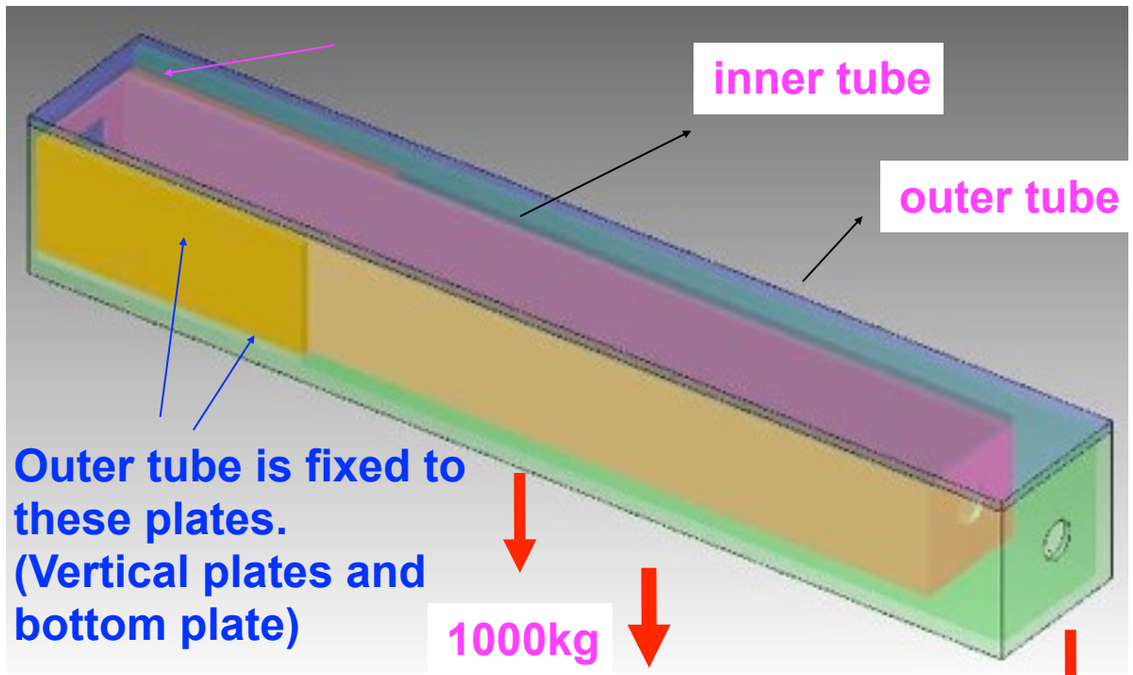

3D CAD model

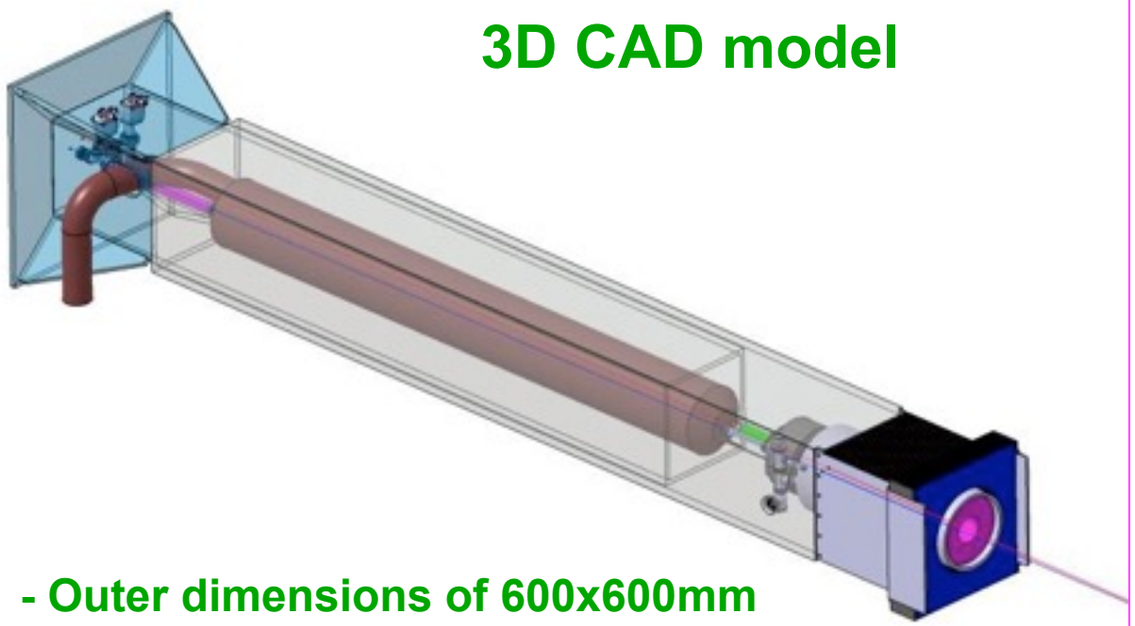

- Outer dimensions of 600x600mm
- 25mm thick

ILD QD0 support, by H. Yamaoka, LCWS2010, Beijing

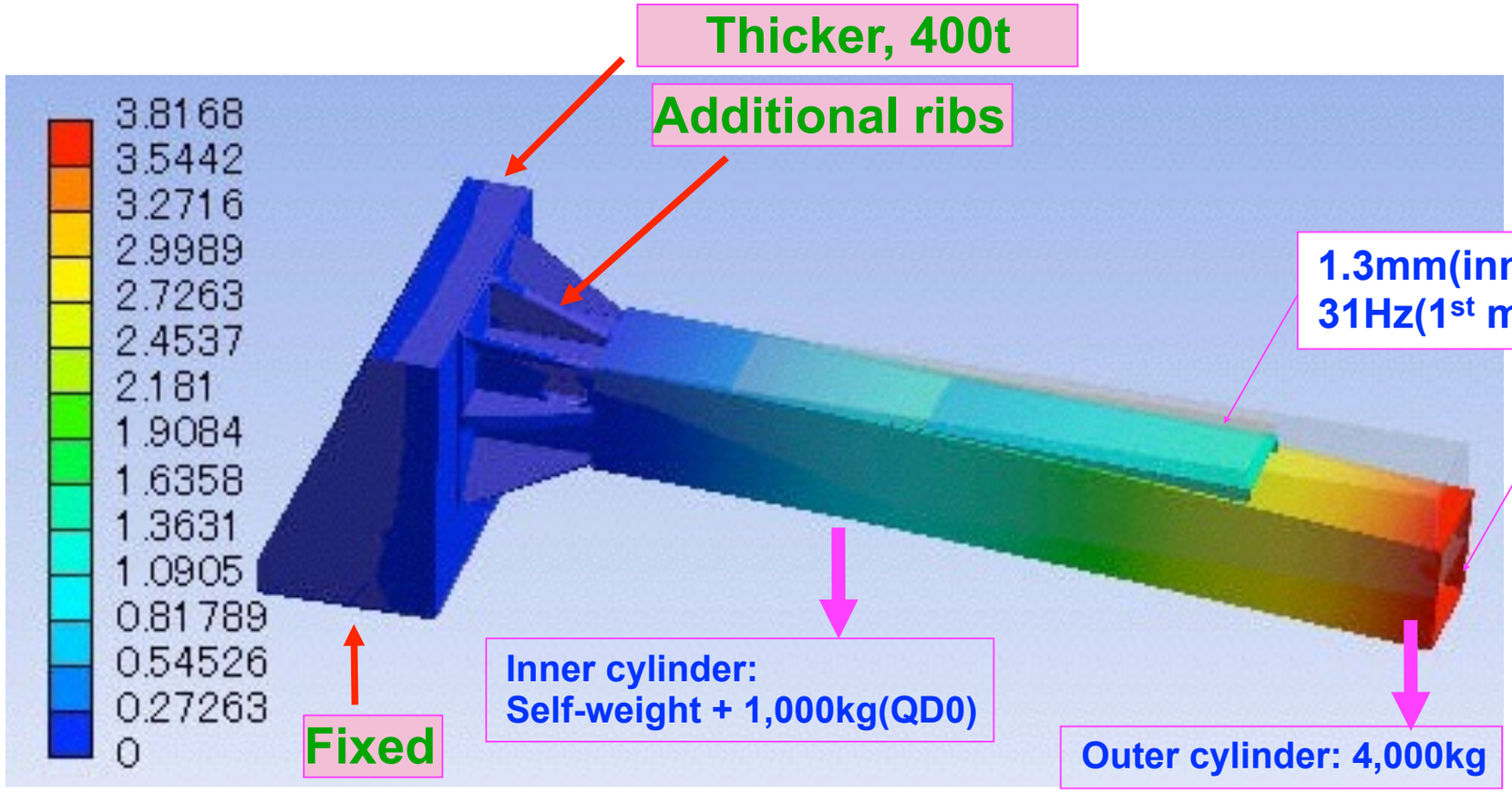

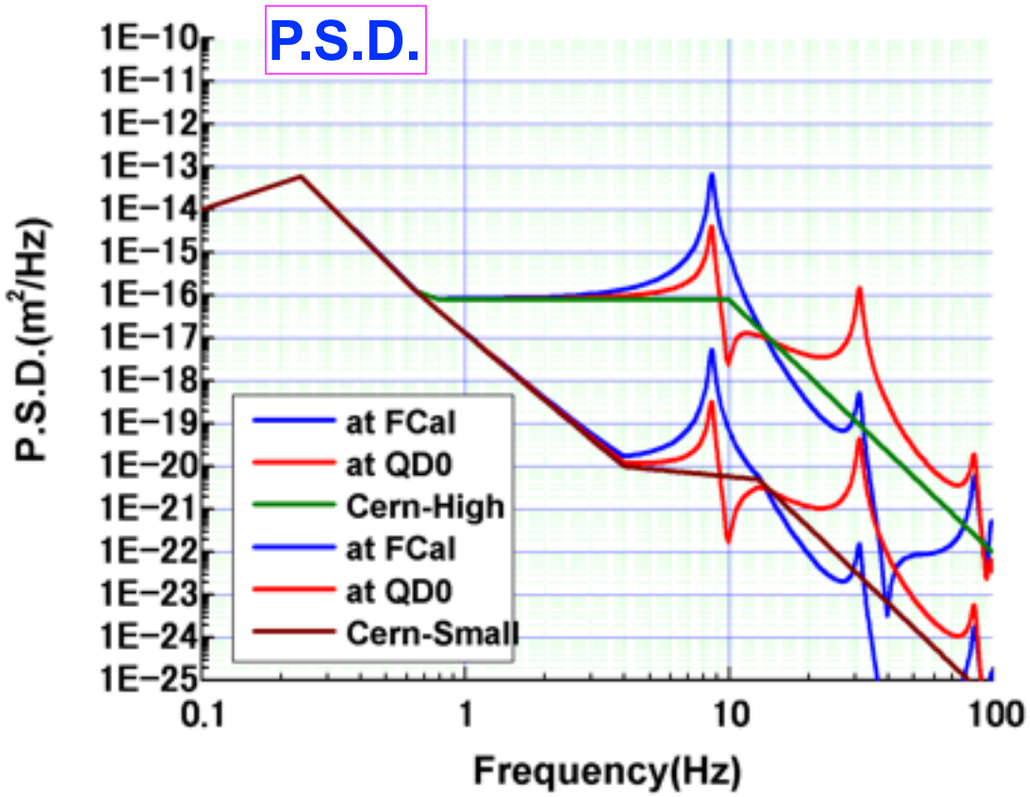

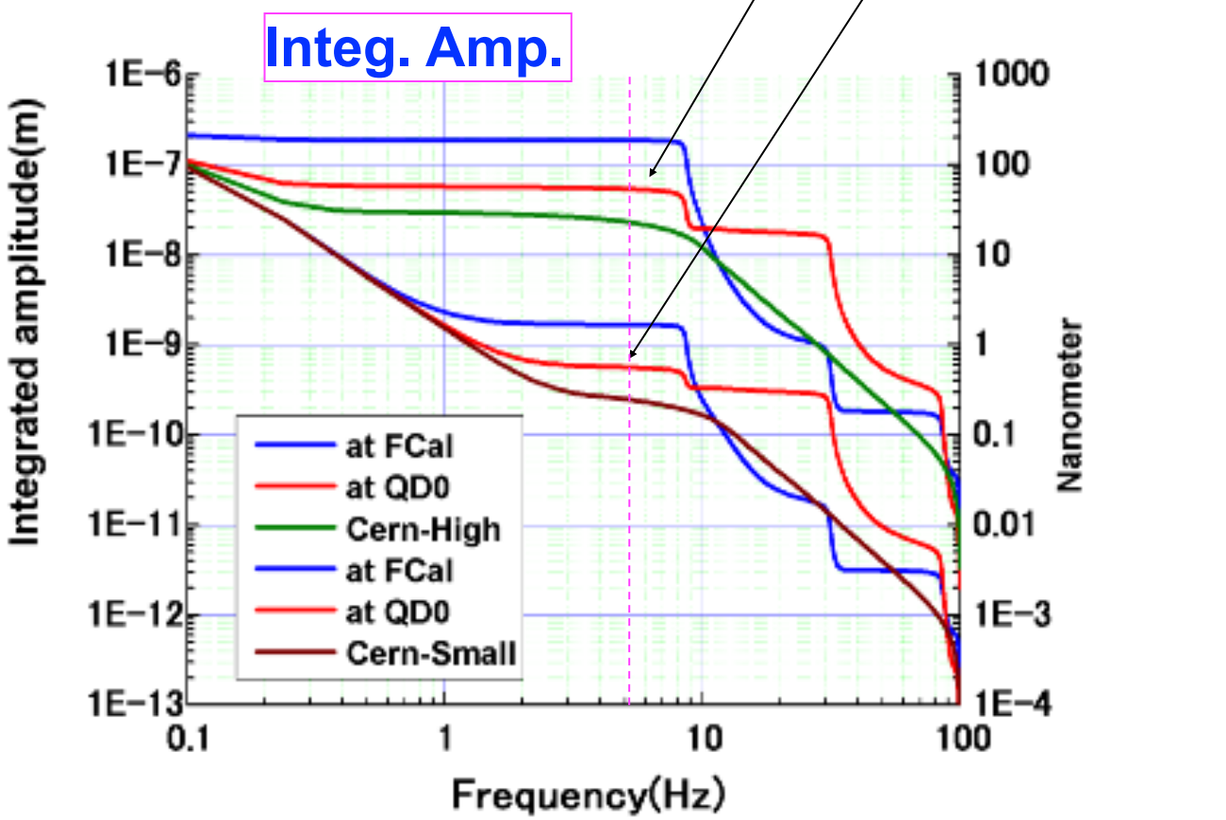

"Parameters for the Linear Collider"

Update November 20, 2006

The Parameters Subcommittee of ILCSC
Asia: Sachio Komamiya, Dongchul Son
Europe : Rolf Heuer (chair), Francois Richard
North America: Paul Grannis, Mark Oreglia

For LC operation at less than maximum energy, we assume that the luminosity scales as L ~ √s.

Baseline machine

"Luminosity and reliability of the machine should allow the collection of approximately L_{eq} = 500 fb^{-1} in the first four years of running, not counting year zero which is assumed to mainly serve for machine commissioning and short pilot physics run(s). ..... the full luminosity of $2x10^{34}$ $cm^{-2}s^{-1}$ at 500 GeV....

It is assumed here that the design luminosity and the efficiency/reliability of the machine will only be reached gradually within the first years of operation (10, 30 and 60% in years 1,2 and 3, resp.) and that the design luminosity and reliability will be reached in year four (i.e. 100% in year 4) of physics running, not counting year 0.

I.) A scenario suggested by R.Settles and modified by T.Tauchi,

--Notation: BPL=best possible luminosity.

--Assumption: two detectors acquire BPL in 1.25×10^7 sec each year.
That is, 0.62×10^7 sec per detector.

--Assumption: 1.25×10^7 sec = 145 days = 20 weeks running at BPL.
That is, 10 weeks per detector per year.

--Assumption: Yearly long shutdown for yearend holidays and
machine work/detector work = 12 weeks (week 51 to week 10).

--Scenario: -start week 11, det-1 on beam.

-det-1 BPL running 2 weeks + 1 week contingency
for machine study
and inefficiency

-push-pull+calib 1 week

-det-2 BPL running 2 weeks + 1 week contingency
for machine study
and inefficiency

-push-pull+calib 1 week

--Therefore 1 cycle = 8 weeks.

--Need 5 cycles so that each detector gets 10 weeks of BPL running.

--Total running time = 40 weeks, meaning from week 11 to week 50.

II.) Evolution of BPL from “Parameters for the Linear Collider”, November 2006:

For 1.25 x10^7 sec of running in a year and L_{goal}=2x10^{34}cm^{-2}sec^{-1},

--Yr 0: commissioning of machine and detectors, i.e. no BPL running.

--Yr 1: BPL = 10% of L_{goal} = 25 fb^{-1} : 2.5 fb^{-1}/push-pull

--Yr 2: BPL = 30% of L_{goal} = 75 fb^{-1} : 7.5 fb^{-1}/push-pull

--Yr 3: BPL = 60% of L_{goal} = 150 fb^{-1} : 15 fb^{-1}/push-pull

--Yr 4: BPL =100% of L_{goal} = 250 fb^{-1} : 25 fb^{-1}/push-pull

---

total = 500 fb^{-1} (250 fb^{-1} each for two detectors)

This model involves 10 push-pulls per year while for precision-physics measurements, we may need fewer push-pulls.

Do we need Gentleman's agreement between the two detectors for common publication of experimental results ?

“Discovery papers” with all members of two collaborations plus accelerator physicists as authors